The structural and functional significance of lipid-binding properties of human Notch ligands



Xinyi Feng

Department of Biochemistry and St Edmund Hall

University of Oxford

Michaelmas Term 2024

A thesis submitted for the degree of Doctor of Philosophy, University of Oxford

The structural and functional significance of lipid-binding properties of human Notch ligands

Xinyi Feng, Department of Biochemistry and St Edmund Hall, University of Oxford

A thesis submitted for the degree of Doctor of Philosophy, Michaelmas Term 2024

Abstract

The Notch receptor and its canonical ligands Jagged/Serrate and Delta-like form part of a core metazoan juxtacrine signal transduction pathway crucial for development and tissue homeostasis. An N-terminal phospholipid-binding C2 domain on JAG1 has previously been shown to be required for optimal *trans*-activation of the Notch receptor. The putative membrane-interaction site, formed by the C2 apical loops, and located distal from the Notch-binding surface, varies considerably between canonical ligands and confers different lipid-binding properties *in vitro*. This project has investigated C2 apical loops in Delta-like 4 (DLL4) to assess the functional importance of membrane binding in a representative member of the other main Notch ligand family.

A series of DLL4 variants containing either somatic missense mutations identified from cancer databases, or engineered C2 loop deletions, were constructed by mutagenesis and expressed as soluble N-terminal ectodomain (NE3) proteins in HEK293F. Out of seventeen DLL4 variants constructed, three cancer database variants showed defective secretion, as did the three protein-engineered loop deletions, indicating the loops may play a role in C2 domain folding. The remaining eleven variants were all secreted into the extracellular medium, similarly to WT-DLL4. Following protein purification, six variants showed functional effects when tested on engineered Notch reporter cell lines. These results ranged from a reduction to an enhancement in Notch activation and were in contrast to the more severe loss of activities associated with previously studied JAG1 C2 variants, suggesting a more nuanced effect of DLL4 loop substitutions. A similar

range of effects were also observed in primary human umbilical vein endothelial cells, where qPCR was used to measure ephrinB2 gene expression, a downstream marker of DLL4-mediated signalling. In particular, variants E40K and R41S (β1-2), R100G (β3-4), and D128N (β5-6) showed consistent statistically significant differences in both cell lines. Notch binding to C2 DLL4 variants, measured either using a plate assay with limited fragments encompassing core binding regions, or a cellular assay where soluble ligand fragments were presented to cell surface expressing Notch receptors, was shown to be unaffected by apical loop substitutions, which suggests DLL4 C2 membrane binding has a distinct function in the activation process. Molecular dynamics simulations provided plausible mechanistic insight, by showing that DLL4 C2-membrane interactions could be influenced by lipid composition or by the sequence of apical loops.

In parallel to these studies, further analysis of the role of the N-glycan located on N143 of the β5-6 C2 apical loop of JAG1 demonstrated that N-glycan removal, either by mutagenesis or by PNGase F digestion, significantly reduced Notch activation. JAG1 expressed from GnTI^{-} HEK293S, which had high-mannose in place of the complex-type glycan on N143, showed similar levels of Notch activation to HEK293T purified protein, suggesting that activity was not affected by these changes in the glycan structure. Lipid binding to JAG1 constructs, measured using a FACS-based liposome binding assay, was shown to be impaired by removal of this site-specific N-glycan, suggesting membrane binding is important for optimal Notch activation. Overall, these data provide evidence for a distinct contribution made by apical loops of Notch ligand C2 domains to the process of Notch activation. These effects are more pronounced in JAG1, but the enhanced or reduced activity shown by DLL4 variants can be explained by subtle changes in membrane orientation. Finally, the altered Notch activation profiles associated with many cancer database variants studied suggests ligand mutations may contribute to the tumorigenic potential of cells.

Acknowledgements

First and foremost, I would like to express my deepest gratitude to my supervisor, Professor Penny Handford, for providing invaluable guidance, encouragement, patience, and insightful advice throughout my DPhil programme. Her unwavering support and expertise are indispensable to my thesis writing and growth as a researcher. I would also like to thank my co-supervisor Professor Christina Redfield, my thesis committee members Professor Martin Cohn and Professor Catherine Pears, and my college advisor Professor Lars Jansen for their thoughtful feedback and mentorship. And I would like to thank my viva examiners Professor Alan Berry and Professor Simon Newstead for sparing their time and expertise to assess my thesis.

Secondly, I am deeply thankful to the past and present members of the Handford lab for their constant support, and for creating a friendly, collaborative, and thought-provoking work environment. In particular, I would like to extend my heartfelt thanks to my senior Dr. Yao Meng for guiding me on experimental skills and mentoring me with patience and kindness during my DPhil. Another special acknowledgement goes to my lab mate Zhihan Bo, whose kindness, support, and dedication have been invaluable throughout the journey. Our many insightful discussions about data, troubleshooting sessions, and shared moments of encouragement have not only enriched my research but also made this experience truly memorable. Many thanks also go to Dr Shruti Mittal, Dr Hilman Nurmahdi, Isabel Dowling, Imogen Treger, Grace Kirman for creating an enjoyable atmosphere in the lab. I am also profoundly grateful to our collaborators, Dr Andreas Larsen and Professor Weston Struwe's lab, who contributed their expertise to key aspects of my research. Their inspiring and instrumental support is crucial in shaping and validating key findings of this work.

Additionally, this research would not have been possible without the key resources and facilities provided by the department and the university. I am deeply appreciative to Dr Robert Hedley and Dr Vasiliki Tsioligka from the Flow Cytometry Facility, Dr Deirdre Kavanagh from the Micron Bioimaging Facility, Dr Helen Sheldon from the Department of Oncology, the Barr lab and Zitzmann lab from the Department of Biochemistry for their technical assistance and generosity to share their equipment. I am also sincerely grateful to my college, St Edmund Hall, for their generous support in the form of travel grants and other resources, which allowed me to present my work at international conferences and engage with the broader scientific community.

On a personal note, I am deeply grateful to my family for their love, understanding and belief in me throughout the journey. The unwavering support, constant encouragement, and unconditional love I received from my mom have been the cornerstone of my strength and the greatest source of inspiration. I am also sincerely thankful to my friends, Heidy Chen, Ishin Tee, Mengyuan Wu, Rachel Zhou, Zoe Huang, Zhiyan Bo, Zhiyue Gao, and many others, both near and far, for standing by me, lifting me up during challenging times, and celebrating each milestone along the way. A special thank goes to the first friend I met in Oxford, Zhihan Bo, and her family, who welcomed me into their home, included me in their festival celebrations, and always took care of me. Their warmth and care made my time away from home so much brighter.

Completing this thesis has been both a challenging and rewarding experience, and I am incredibly grateful to everyone who have supported me along the way.

Xinyi Feng

16th January 2025

Table of Contents

List of Abbreviations xii

1 Chapter 1: Introduction 1

1.1 Overview of the Notch signalling pathway 2

1.1.1 History of Notch signalling 2

1.1.2 Molecular mechanisms of Notch signalling 5

1.1.2.1 Surface expression of Notch molecules 5

1.1.2.2 *Trans*-activation 6

1.1.2.3 *Cis*-inhibition 9

1.1.2.4 *Cis*-activation 10

1.1.2.5 Noncanonical Notch signalling 11

1.1.3 Spatiotemporal patterning guided by Notch signalling 11

1.2 Notch signalling in health and disease 14

1.2.1 Physiological roles of Notch signalling 14

1.2.1.1 Angiogenesis 15

1.2.1.2 Myogenesis 17

1.2.2 Insights from genetic disorders 18

1.2.2.1 Diseases associated with JAG1: ALGS/EHBA 21

1.2.2.2 Disease associated with DLL4: AOS 22

1.2.3 Pathological relevance of Notch signalling in cancer 23

1.3 Notch pathway components 24

1.3.1 Structure of Notch receptors 25

1.3.1.1 Notch extracellular domain 25

1.3.1.2 Notch intracellular domain 29

1.3.2 Structure of Notch ligands 29

1.3.2.1 C2 domain: an N-terminal module conferring both receptor and lipid binding properties 31

1.3.2.2 DSL domain: an indispensable Notch binding unit 31

1.3.2.3 EGF repeats in Notch ligands 33

1.3.2.4 Cysteine-rich domain 33

1.3.3 Notch/ligand complexes 34
1.3.3.1 Jag1 and Dll4 receptor binding affinities 35
1.3.3.2 Dll1 and Dll4 receptor binding affinities 36
1.3.3.3 Novel potential extracellular receptor/ligand interactions 37
1.4 Regulation of Notch pathway 38
1.4.1 Roles of glycosylation 40
1.4.1.1 Notch receptor O-glycosylation 41
1.4.1.2 Notch receptor N-GlcNAcylation 43
1.4.1.3 Notch Ligand O-glycosylation 44
1.4.2 Roles of ubiquitination 44
1.4.2.1 Ubiquitination operative at the receptor level 44
1.4.2.2 Ubiquitylation operative at the ligand level 45
1.4.3 Regulatory roles of mechanical forces 46
1.4.3.1 Pulling force generated by endocytosis 46
1.4.3.2 Catch bond formation 47
1.5 C2 domain 48
1.5.1 The C2 domain superfamily 49
1.5.2 Calcium-dependent C2-membrane interactions 50
1.5.3 Calcium-independent C2-membrane interactions 55
1.5.4 Functionally important C2 domain in Notch ligands 59
1.6 Project Aims 62
2 Chapter 2: Materials and Methods 63
2.1 Mutagenesis 63
2.1.1 Primer design 63
2.1.2 Site-directed mutagenesis using overlap extension PCR 64
2.1.3 Restriction enzyme digestion and ligation 65
2.1.4 Agarose gel electrophoresis and gel extraction 66
2.1.5 DNA/RNA concentration measurement 67
2.1.6 Transformation 67
2.1.7 Plasmid purification and DNA sequencing 67
2.2 Tissue culture 68
2.2.1 HEK293T/HEK293S cells 68

2.2.1.1 Maintenance and subculture 68
2.2.1.2 Thawing and cryopreservation 68
2.2.2 HEK293F cells 69
2.2.2.1 Maintenance and subculture 69
2.2.2.2 Thawing and cryopreservation 69
2.2.3 HEK293 mN1/2-NLuc/CLuc-RBPJ reporter cells 70
2.2.4 CHO hN1G4^{esn} reporter cells 70
2.2.5 Schneider-2 (S2) *Drosophila* cell line 70
2.2.5.1 Maintenance and subculture 70
2.2.5.2 Thawing and cryopreservation 71
2.2.6 Primary Human Umbilical Vein Endothelial Cells (HUVECs)..... 71
2.3 Protein synthesis and purification 72
2.3.1 JAG1/2 constructs from HEK293T/S 72
2.3.1.1 Large scale transfection of HEK293T/S 72
2.3.1.2 Culture medium collection 73
2.3.2 DLL4 constructs from HEK293F 73
2.3.2.1 Large scale transfection of HEK293F..... 73
2.3.2.2 Culture medium collection 74
2.3.3 NOTCH constructs from S2 74
2.3.3.1 Protein expression from S2 stable lines..... 74
2.3.4 Chromatography..... 75
2.3.4.1 Immobilised metal affinity chromatography (IMAC) 75
2.3.4.2 Size exclusion chromatography (SEC) 75
2.3.5 Protein concentration measurement..... 76
2.3.6 SDS-PAGE 76
2.3.7 Western Blot 76
2.3.8 PNGase F digestion of Notch ligands..... 77
2.4 Notch activation assays..... 77
2.4.1 Split-luciferase assay by HEK293 mN1/2-NLuc/CLuc-RBPJ cells 77
2.4.2 YFP-expression based assay by CHO-K1 hN1G4^{esn} reporter cells 78
2.4.3 ELISA-based ligand immobilisation assay..... 79

2.4.4 Quantitative reverse transcription PCR (RT-qPCR) assay by HUVECs 80
2.4.4.1 HUVECs culture for RT-qPCR assay 80
2.4.4.2 RNA extraction and reverse transcription 81
2.4.4.3 Real-time quantitative PCR (qPCR) 81
2.4.5 Coculture assay 83
2.4.5.1 Transient transfection 83
2.4.5.2 Coculture and split-luciferase Notch activation assay 83
2.4.5.3 Evaluation of mRNA expression level 84
2.4.5.4 Evaluation of ligand surface expression level 84
2.5 Binding assay 85
2.5.1 Plate-based Notch receptor-ligand binding assay 85
2.5.2 Bead-based liposome aggregation assay 86
2.5.2.1 Lipid stock preparation 86
2.5.2.2 Liposome preparation and characterisation 86
2.5.2.3 FACS-based liposome aggregation assay 86
2.5.3 FACS-based ligand binding assay 88
2.5.4 FACS-based receptor binding assay 89
2.6 Statistical Analysis 90
3 Chapter 3: Studying the functional importance of the DLL4 C2 domain using cancer database variants 91
3.1 Introduction 92
3.2 Cancer database search 93
3.3 Preparation of ligand protein constructs 97
3.3.1 Target site mutagenesis and secretion tests 97
3.3.1.1 NE3 constructs of cancer database variants 97
3.3.1.2 NE3 constructs of C2 loop shortening variants 101
3.3.2 Protein purification 102
3.4 Testing Notch activation capacity of the purified DLL4$_{NE3}$ cancer database variants 105
3.5 Full-length DLL4 variants cell surface expression 109

3.5.1 Plasmids preparation and RNA expression tests 109
3.5.2 Cell surface expression of FL-DLL4 variants 111

3.6 Testing Notch activation capacity of the FL-DLL4 variants using a coculture assay 114

3.7 Conclusion 116

4 Chapter 4: Studying the functional importance of the DLL4 C2 domain in physiologically relevant HUVECs 121

4.1 Introduction 121

4.2 Development of an RT-qPCR assay to measure DLL4-induced signalling 127

4.2.1 Expression of Notch target genes in HUVECs 127
4.2.2 Optimisation of assay conditions 128

4.3 Testing Notch activation capacity of the purified DLL4 cancer database variants 131

4.3.1 Quality check of RNA and cDNA templates 131
4.3.2 Analysis of qPCR raw data 132
4.3.3 Expression of Notch target genes induced by DLL4 variants 135

4.4 Conclusion 137

5 Chapter 5: Investigating the Notch-binding and membrane-interacting properties of DLL4 variants 140

5.1 Introduction 141

5.2 Preparation of receptor protein constructs 142

5.2.1 Expression of recombinant Notch receptors in S2 insect cells .. 142
5.2.2 Purification of recombinant Notch receptors 143

5.3 Binding of purified $DLL4_{NE3}$ variants to purified Notch receptors 145

5.3.1 Optimisation of plate-based Notch binding assay 145
5.3.1.1 Saturation tests on Maxisorp plate 145
5.3.2 Notch binding assay of $DLL4_{NE3}$ cancer database variants 148
5.3.2.1 $DLL4_{NE3}$ cancer database variants 148

5.3.2.2 Titration tests of $DLL4_{NE3}$ variants 149

5.4 Ligand binding of purified $DLL4_{NE3}$ variants by cells expressing FL-Notch receptors 151

5.4.1 Ligand binding by HEK293-mN1 cells 151

5.4.2 Ligand binding by HUVECs 152

5.5 Receptor binding of recombinant NOTCH1 receptors by HEK293T cells expressing FL-DLL4 variants 153

5.5.1 Titration test 153

5.5.2 Receptor binding by HEK293T cells expressing FL-DLL4 155

5.5.2.1 Cancer database variants 155

5.5.2.2 C2-loop-shortening variants 157

5.6 Liposome binding 157

5.7 Mechanistic insight from Molecular Dynamics Simulations 159

5.7.1 Binding modes of WT-DLL4-C2 interacting with different membranes 160

5.7.2 Binding modes of E40K and R41S variants 163

5.8 Conclusion 166

6 Chapter 6: Studying the functional importance of a conserved N-glycan in JAG1 C2 domain 176

6.1 Introduction 177

6.2 Conservation of the N-glycosylation site on C2 β5-6 loop in the Jagged/Serrate family 179

6.3 Preparation of protein constructs 182

6.3.1 Target site mutagenesis and secretion tests 182

6.3.2 Protein purification 183

6.3.2.1 $JAG1_{NE3\text{-}Fc\text{-}His}$ N143Q from HEK293T 183

6.3.2.2 $JAG1_{NE\text{-}Fc\text{-}His}$ from HEK293S 186

6.3.3 PNGase F digestion of ligand constructs 187

6.3.3.1 PNGase F digestion of $JAG1_{NE3}$ and $DLL4_{NE3}$ 187

6.3.3.2 PNGase F digestion of FL-J1 189

6.3.4 Glycoproteomic analysis of JAG1 N-glycan structure 189

6.4 Testing native fold with 65D monoclonal antibody 191
6.4.1 Optimising ligand immobilisation 191
6.4.2 Epitope recognition of N143Q$_{NE3}$ variant and PNGase digested JAG1$_{NE3}$ and FL-J1 192
6.5 Testing Notch activation capacity of the JAG1 constructs 194
6.5.1 NOTCH1 activation by N143Q$_{NE3}$ variant 194
6.5.2 NOTCH1 activation by deglycosylated JAG1$_{NE3}$ and DLL4$_{NE3}$ .. 195
6.5.3 N-glycan structure requirements for activity 197
6.5.4 NOTCH1 activation by deglycosylated FL-J1 198
6.6 Investigating lipid-binding properties of deglycosylated JAG1$_{NE3}$ 200
6.7 Conclusion 202
7 Chapter 7: Discussion and future work 207
7.1 Objective of the thesis 208
7.2 Expression and secretion of DLL4 variants 208
7.3 The effects of DLL4 cancer database variants on Notch activation 210
7.4 The effects of DLL4 C2-loop-shortening variants on Notch activation 218
7.5 The effects of DLL4 variants on Notch receptor binding and lipid binding 219
7.6 Possible implications of the C2-membrane mediated regulatory mechanism of Notch signalling 220
7.7 Future directions 223
Bibliography 226

List of Abbreviations

A	ACC	Aplasia cutis congenita
	ALGS	Alagille syndrome
	ANK	Ankyrin repeats region
	AOS	Adam-Oliver syndrome
	APC	Allophycocyanin
	Ax	Abruptex region
C	cb	Ca^{2+}-binding
	CADASIL	Cerebral autosomal dominant arteriopathy with subcortical infarcts and leukoencephalopathy
	CBL	Calcium-binding loops
	cDNA	Complementary deoxyribonucleic acid
	CD46	Complement regulator protein 46
	CHO	Chinese hamster ovary cells
	CMD	Congenital muscular dystrophy
	CME	Clathrin-mediated endocytosis
	CMT2	Charcot-Marie-Tooth disease type 2
	Co-A	Coactivator
	Co-R	Corepressor
	COSMIC	Catalogue of somatic mutations in cancer
	CRD	Cysteine-rich domain
	Cryo-EM	Cryogenic electron microscopy
	Cryo-ET	Cryo-electron tomography
	CSL	CBF1/Su(H)/Lag-1
D	Dlk	Delta-like non-canonical Notch ligand 1
	Dll/DLL	Delta-like
	DLS	Dynamic light scattering
	DOS	Delta/OSM-11 motif
	dsDNA	Double-stranded deoxyribonucleic acid
	DSL	Delta/Serrate/LAG-2
	DTX4	Deltex 4
E	EC	Endothelial cell
	ECD	Extracellular domain
	EFNB2	Ephrin B2

	EGF	Epidermal growth factor
	EHBA	Extrahepatic biliary atresia
	ELISA	Enzyme-linked immunosorbent assay
	EMT	Epithelial-mesenchymal transition
	EOGT	EGF domain-specific O-GlcNAc transferase
	ER	Endoplasmic reticulum
	EV	Empty vector
F	FACS	Fluorescence-activated cell sorting
	FPKM	Fragments per kilobase of transcript per million mapped reads
	FPLC	Fast protein liquid chromatography
G	GAPDH	Glyceraldehyde-3-phosphate dehydrogenase
	GDC	Genomic data commons
	GEO	Gene expression omnibus
	GlcNAc	N-acetylglucosamine
	GnT-I/II/III	Mannoside acetylglucosaminyl-transferase 1/2/3
	GOF	Gain-of-function
	GSI	Gamma-secretase inhibitor
H	HD	Heterodimerisation domain
	HEK	Human embryonic kidney cells
	HES1	Hairy and enhancer of split-1
	HRP	Horseradish peroxidase
	HSC	Hematopoietic stem cell
	HUVEC	Human umbilical vein endothelial cell
I	ICD	Intracellular domain
	IgG	Immunoglobulin G
	IMAC	Immobilised metal affinity chromatography
	iPSC	Induced pluripotent stem cells
J	Jag/JAG	Jagged
L	LBR	Ligand-binding region
	LC-MS	Liquid chromatography-mass spectrometry
	LFng/LFNG	Lunatic Fringe
	LNR	Lin12-Notch repeats
	LOF	Loss-of-function
M	MAb/MAB	Monoclonal antibody
	MAML	Mastermind-like
	MD	Molecular dynamics
	MFI	Median fluorescence intensity

	MFng/MFNG	Manic Fringe
	MGAT1/3	Mannoside acetylglucosaminyl-transferase 1/3
	Mib	Mindbomb
	MNNL	Module at the N-terminus of Notch ligand
	mN1/2	Mouse Notch1/2
	MS	Mass spectrometry
	MSC	Mesenchymal stem cells
	MuSC	Muscle stem cell
	MW	Molecular weight
N	NE3	N-terminus to EGF3 fragment
	NECD	Notch extracellular domain
	NEDBAS	Neurodevelopmental disorder with nonspecific brain abnormalities and with or without seizures
	Neur	Neuralised
	NEXT	Notch extracellular truncation region
	NICD	Notch intracellular domain
	NLS	Nuclear localisation sequence
	NMR	Nuclear magnetic resonance
	NRR	Negative regulatory region
	NTC	Notch transcription complex OR no template control
	NTM-ICD	Notch transmembrane and intracellular domain
P	PCR	Polymerase chain reaction
	PDZ	PSD-95/Dlg/ZO-1 motif
	PEST	Proline/glutamic acid/serine/threonine-rich motif
	PNGase F	Peptide-N-glycosidase F
	POFUT1	Protein O-fucosyltransferase 1
	POGLUT1	Protein O-glucotransferase 1
	PTM	Post-translational modification
Q	qPCR	Quantitative polymerase chain reaction
R	RAM	RBPJ association module
	RE	Restriction enzyme
	RFng/RFNG	Radical Fringe
	RPKM	Reads per kilobase of transcript per million mapped reads
	RQ	Relative quantity
	RT-PCR	Reverse transcription PCR
S	SAXS	Small angle X-ray scattering
	SCC	Squamous cell carcinoma

	SD	Standard deviation
	SDS-PAGE	Sodium dodecyl sulphate polyacrylamide gel electrophoresis
	SEC	Size-exclusion chromatography
	SPR	Surface plasmon resonance
	ssDNA	Single-stranded deoxyribonucleic acid
	Syt1	Synaptotagmin 1
	S1/2/3	Site 1/2/3
	S2 cell	Schneider-2 cell
T	TAD	Transactivation domain
	T-ALL	T-cell acute lymphoblastic leukaemia
	TC	Tissue culture
	T_m	Melting temperature
	TMD	Transmembrane domain
	TOF	Tetralogy of Fallot
V	VDW	Van der Waals interactions
	VEGF	Vascular endothelial growth factor
	VEGFR	VEGF receptor
	VWFC	von Willebrand factor type C
W	WT	Wild type
X	XL-MS	Cross-linking mass spectrometry
Y	YFP	Yellow fluorescent protein

Amino acid abbreviations

A	Ala	Alanine
C	Cys	Cysteine
D	Asp	Aspartic acid
E	Glu	Glutamic acid
F	Phe	Phenylalanine
G	Gly	Glycine
H	His	Histidine
I	Ile	Isoleucine
K	Lys	Lysine
L	Leu	Leucine
M	Met	Methionine

N	Asn	Asparagine
P	Pro	Proline
Q	Gln	Glutamine
R	Arg	Arginine
S	Ser	Serine
T	Thr	Threonine
V	Val	Valine
W	Trp	Tryptophan
Y	Tyr	Tyrosine

Lipid abbreviations

LPC	Lysophosphatidylcholine
LPE	Lysophosphatidylethanolamine
PA	Phosphatidic acid
PC	Phosphatidylcholine
PE	Phosphatidylethanolamine
PE-CF	Phosphatidylethanolamine-carboxyfluorescein
PG	Phosphatidylglycerol
PI	Phosphatidylinositol
PIP2	Phosphatidylinositol-4,5-bisphosphate
PS	Phosphatidylserine
SM	Sphingomyelin

Metric prefixes

n	10^{-9}
µ	10^{-6}
m	10^{-3}
k	10^{3}

Chapter 1: Introduction

1.1 Overview of the Notch signalling pathway

1.1.1 History of Notch signalling

In 1914, the Notch phenotypes in *Drosophila melanogaster* were first identified by John S. Dexter, who noticed a heritable abnormality in fruit flies consisting of small notches in their wing tips (Dexter, 1914). Three years later, Thomas Hunt Morgan identified the first mutant allele of the *Notch* gene (Morgan, 1917). By 1920s, multiple *Notch* mutant alleles were identified, associated with phenotypic responses, such as lethality, notched wings, or in abnormal hair bristles in female flies (Bridges, C.B., 1916, 1919; J. C. Li, 1927; Morgan, T. H., 1923). In the 1930s, Donald Poulson described the effects of *Notch* deficiency on the development of *Drosophila* embryos by removal of entire chromosomes. Fly embryos lacking *Notch* were found to develop normally through the first four hours of embryogenesis but then failed to develop the mesoderm and endoderm, suggesting the important role of *Notch* in embryonic development (Poulson, 1937). Subsequently, *Notch* in *Drosophila melanogaster* was extensively studied, from its developmental effects (Poulson, D. F., 1967), its inducibility via X-ray treatment (Lefevre, 1955), and its nature as a complex locus (Welshons, 1958a, 1958b; Welshons, W. J., 1965; Welshons & Von Halle, 1962). From these early studies prior to 1980s, mutational responses of *Notch* were associated with *Drosophila* morphogenesis and embryogenesis, although the specific developmental function of this gene was not yet elucidated.

The molecular studies of the *Notch* locus in *Drosophila melanogaster* began in the 1980s, when cDNA analysis allowed description of the nucleotide sequence of the *Notch* gene and the amino acid sequence of the Notch protein (Artavanis-Tsakonas et al., 1983). Transcriptional analysis strengthened the earlier notion of *Notch* as a single genetic unit, despite the complex interallelic complementation patterns and phenotypic interactions observed (Grimwade et al., 1985; Shellenbarger & Mohler, 1975). By sequencing the

overlapping cDNA clones of *Notch* and aligning the predicted amino acid sequence with other known proteins, it was hypothesised that Notch is a membrane-spanning protein that contains an extracellular epidermal growth factor (EGF) repeat region and an intracellular domain (Kidd et al., 1986; Wharton et al., 1985). Deletion analysis of *Drosophila* Notch together with aggregation assays subsequently found that two of the EGF repeats, 11 and 12, were necessary and sufficient to mediate interactions with both *Drosophila* Notch ligands Delta and Serrate (Rebay et al., 1991). Furthermore, overexpression of Notch lacking the extracellular domain led to dominant gain-of-function (GOF) phenotypes whereas overexpression of Notch lacking the intracellular domain led to dominant loss-of-function (LOF) phenotypes, suggesting that whilst the extracellular domain contained the primary ligand-interacting region, the cytoplasmic domain was essential for signal transduction (Rebay et al., 1993). Researchers then characterised and resolved the sequences for other members of the Notch pathway, such as the ligands Delta, Serrate in *Drosophila* and LAG-2 in *C.elegans* (Fleming et al., 1990; Tax et al., 1994; Vässin & Campos-Ortega, 1987). Similar to the Notch receptor, the ligands were also found to be single pass transmembrane proteins with an extracellular EGF-repeat region. These results supported the hypothesis that Notch was a core component of a contact-dependent mechanism that communicates molecular signals between neighbouring cells.

Since the 1980s, researchers began to recognise the important roles of Notch signalling in many cellular contexts and various model organisms. Studies of *Notch* in *Drosophila melanogaster* suggested that the Notch protein was involved in controlling the accurate differentiation of specific tissues during development, including the embryonic nervous system; and *Notch* mutations were found to cause defects in the central nervous system, further supporting that *Notch* is an important neurogenic gene (Lehmann et al., 1983; Spyros Artavanis-Tsakonas, 1988; T. Xu et al., 1990). The *C. elegans* Notch homologues,

LIN-12 and GLP-1, were also discovered to function in cell fate decision by controlling the differentiation of anchor cells and ventral uterine precursor cells via intercellular communication, and both receptors require the LAG family ligands for function with certain degree of biochemical interchangeability during embryogenesis (Austin & Kimble, 1989; Greenwald & Seydoux, 1990; Lambie & Kimble, 1991; Seydoux & Greenwald, 1989; Yochem et al., 1988). Meanwhile, researchers started to dissect the detailed molecular mechanism of these structurally related Notch proteins, showing that the truncated forms containing only the intracellular domain of *Drosophila* Notch, *C. elegans* LIN-12, and their vertebrate homologues were sufficient to initiate constitutive activity that led to GOF cell fate transformations in respective organisms (Struhl et al., 1993). These results suggested that the Notch intracellular domain had an intrinsic activity, whereas the extracellular domain played a main regulatory role.

So far, the Notch pathway has been discovered in all metazoans, such as *Drosophila* (Morgan, 1917), *Hydra* (Käsbauer et al., 2007; Prexl et al., 2011), *Xenopus* (Coffman et al., 1990), rat (Weinmaster et al., 1991), mouse (Del Amo et al., 1992), zebrafish (Bierkamp & Campos-Ortega, 1993), chicken (Lardelli et al., 1995), and Sea Urchin (Sherwood & McClay, 1997). Compared to the *Drosophila* Notch family, which consists of a single Notch receptor and two Notch ligands (Delta and Serrate), the mammalian Notch family has an expanded repertoire consisting of four Notch paralogues (Notch1-4) and at least five Notch ligands—classified as either Delta-like (Dll1, Dll3 and Dll4) or Serrate/Jagged (Jag1 and Jag2) family. The variety of Notch receptors and ligands implies the pleiotropic role of the Notch pathway in mammalian development, including neuron differentiation (neurogenesis), somite formation (somitogenesis), muscle formation (myogenesis), heart development (cardiogenesis), blood formation (haematopoiesis), and the formation and maturation of blood vessels (vasculogenesis and angiogenesis). Furthermore, the importance of Notch signalling in human health was

first revealed by Leif Ellisen, who found that a human homologue of *Drosophila Notch*, when broken by chromosomal translocation, was closely associated with T lymphoblastic neoplasms (Ellisen et al., 1991). A few years later, *NOTCH3* mutations on chromosome 19 were found to be pathogenic in CADASIL (cerebral autosomal dominant arteriopathy with subcortical infarcts and leukoencephalopathy) patients, establishing the first link between Notch and human congenital disease (Joutel et al., 1996). Thereafter, defects in Notch signalling have been implicated in a diverse range of acquired and genetic diseases.

1.1.2 Molecular mechanisms of Notch signalling

The Notch pathway is a short-range signal transduction system where its activity is usually induced by direct interactions between receptor and ligand expressed on opposing cell surfaces, leading to *trans*-activation. Notch signalling is transmitted through core components comprising receptors, ligands, transcription factors and target genes to regulate various developmental and homeostatic processes, such as cell fate determination, cell survival and stem cell maintenance (Duvall et al., 2022; Gozlan & Sprinzak, 2023; Kobia et al., 2020; Logeay et al., 2022; Porcheri et al., 2020; Seymour et al., 2020). When ligands and receptors are expressed on the same cell surface, Notch pathway can be inhibited, a process known as *cis*-inhibition (Sprinzak et al., 2010). Recently, *cis*-activation has also been observed (Nandagopal et al., 2019).

1.1.2.1 Surface expression of Notch molecules

The Notch receptor is synthesised as a 300-350 kDa glycoprotein at the ribosomes imparted into the endoplasmic reticulum (ER), after which it undergoes various post-translational modifications (PTMs) to its extracellular domain (ECD) before being translocated to the plasma membrane (Figure 1-1). Most Notch receptors are cleaved by a furin-like convertase at site 1 (S1) in the *trans*-Golgi network, which yields a

heterodimer held together by non-covalent interactions (Blaumueller et al., 1997; Kopan & Ilagan, 2009; Logeat et al., 1998). The heterodimer consists of two fragments with masses around 120 kDa and 200 kDa, corresponding to the Notch transmembrane and intracellular domain (NTM-ICD; 120 kDa) and the Notch extracellular domain (NECD; 200 kDa), respectively (Blaumueller et al., 1997; Sanchez-Irizarry et al., 2004). Unlike mammalian Notch, *Drosophila* Notch maturation was found not to require the S1 cleavage, with the majority of receptors present as full-length uncleaved versions on the cell surface (Kidd & Lieber, 2002). The NECD also undergoes various O-glycosylation modifications, which can affect receptor stability and its maturation and trafficking, and modulate ligand binding (Figure 1-1) (Ogawa et al., 2020; Okajima et al., 2008; Takeuchi et al., 2017).

1.1.2.2 *Trans*-activation

When canonical ligands from the signal-sending cell bind via specific sites to Notch receptors on the signal-receiving cell extracellularly in *trans*, Notch is *trans*-activated. Furthermore, evidence suggests that JAG1 also binds to the cell membrane via its N-terminal C2 domain, forming a receptor-ligand-membrane ternary complex that is required for optimal Notch signalling (Suckling et al., 2017). Like the receptors, Notch ligands undergo various PTMs including O-linked and N-linked glycosylation of their ECD, and ubiquitylation of their intracellular domain (ICD) which mediates ligand trafficking (Figure 1-1). Upon ligand engagement, the receptor-ligand complex is internalised by ubiquitylation-dependent clathrin-mediated endocytosis within the signal-sending cell, which generates a mechanical pulling force that promotes a conformational change of Notch and exposes a proteolytic site 2 (S2) for enzymatic cleavage (Figure 1-1). Cleavage of the S2 site, buried within the receptor's membrane-proximal negative regulatory region (NRR), by the ADAM family metalloprotease leads to dissociation of NECD from the transmembrane and intracellular domains (also known as the Notch

extracellular truncation (NEXT) region), thereby exposing an intramembrane proteolytic site (S3) (Groot & Vooijs, 2012). This ligand endocytosis-induced dissociation of Notch heterodimer and NECD internalisation into ligand-bearing cells were observed in both *Drosophila* and mammalian systems, suggesting a mechanism shared by canonical ligands (Klueg & Muskavitch, 1999; Nichols et al., 2007; Parks et al., 2000).

NEXT is subsequently cleaved by ɣ-secretase, releasing the transcriptionally active Notch intracellular domain (NICD) from the inner face of cell membrane (Figure 1-1). Loss of ɣ-secretase activity leads to accumulation of Notch receptors at the cell surface, suggesting that S3 cleavage takes place primarily on the cell membrane (Chyung et al., 2005; Kaether et al., 2006; Sorensen & Conner, 2010). However, mutations which impair Notch endosomal trafficking or endosomal acidification were observed to reduce NICD levels and Notch signalling (Vaccari et al., 2008; Valapala et al., 2013; Y. Yan et al., 2009), suggesting that S3 cleavage is not entirely limited to cell surface but may also take place in endocytic compartments. Recent study using time-resolved proximity labelling showed that, when S3 cleavage is blocked by GSI (gamma-secretase inhibitor) after ligand stimulation, the S2-truncated NOTCH2 (NEXT) was found proximal to proteins associated with vesicles or endosomes, suggesting that NOTCH2 was internalised after S2, but before S3 cleavage (Martin et al., 2023).

NICD, once released, then translocates to the nucleus and forms a complex with the RBPJ family DNA-binding protein (also known as CSL or CBF1/Su(H)/Lag-1) (Bray & Gomez-Lamarca, 2018; Falo-Sanjuan et al., 2019). The RBPJ family of proteins act in the canonical Notch pathway as transcription factors, which, when bound to the NICD, converts the transcriptional repression complex to transcriptional activation complex by displacing corepressors and recruiting coactivators such as Mastermind proteins (MAML1-3) (Figure 1-1). Resolution of the ternary structure of the active transcription complex consisting of CSL/RBPJ, the NICD domains, and MAML-1, bound to *HES-1*

promoter DNA sequence, reveals a sequential binding process of the activatory complex assembly (S. H. Choi et al., 2012). The NICD/CSL/MAML complex further recruits co-activators such as p300 and the mediator complex, ultimately loading RNA polymerase II and activating the expression of appropriate Notch target genes such as *HES* and *HEY* (Henrique & Schweisguth, 2019; Kopan & Ilagan, 2009; Kuang et al., 2021; Oswald & Kovall, 2018; Sprinzak & Blacklow, 2021). In the absence of NICD, RBPJ associates with several different co-repressors, such as FHL1 or SHARP in mammals and Hairless in *Drosophila*, to inhibit downstream gene expression (Borggrefe & Oswald, 2009; Liefke et al., 2010).

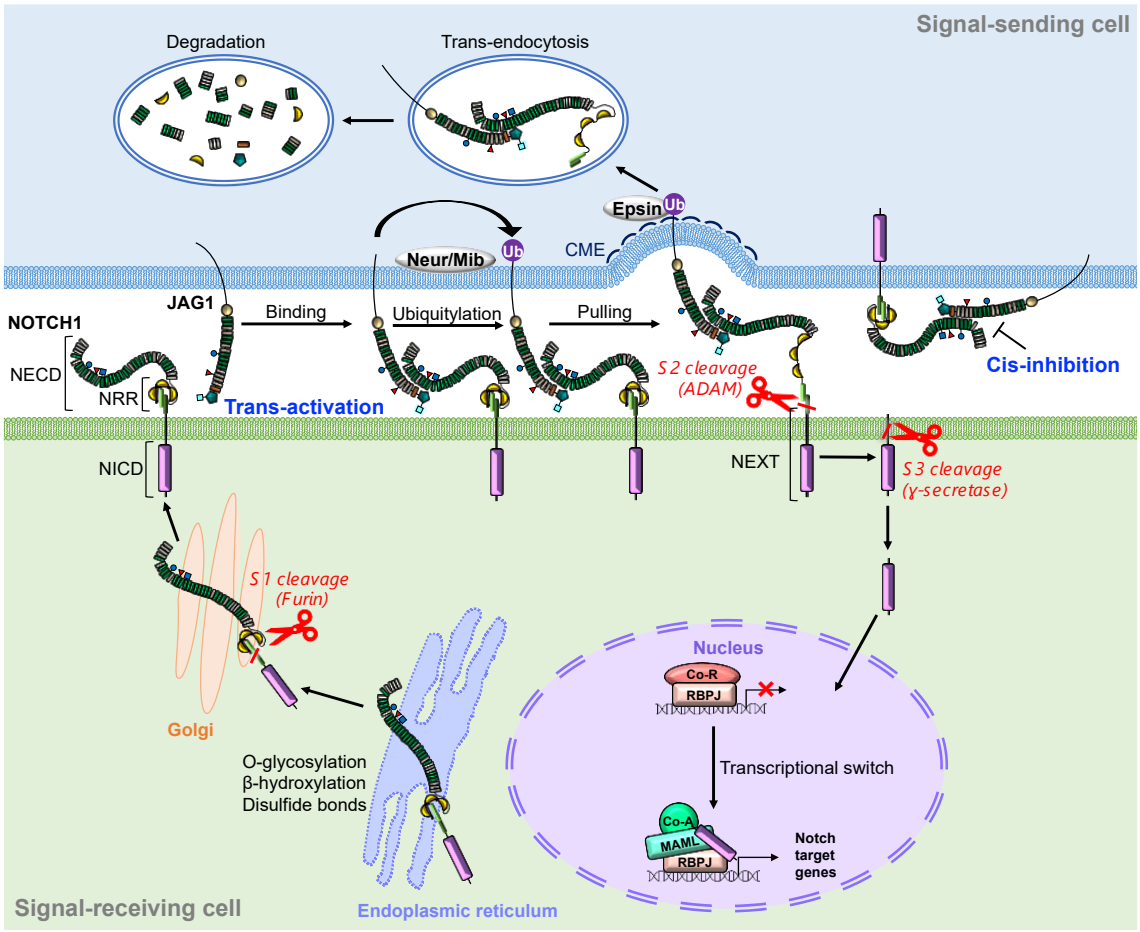


Figure 1-1. Overview of the canonical Notch signalling pathway (Adapted from (Meng et al., 2023)). Core steps in the Notch pathway are shown using human NOTCH1 and JAG1 as examples. Both Notch receptors and ligands undergo various PTMs before translocation to the plasma membrane. These include proteolytic cleavage at site 1 (S1) by furin (scissors), as well as O- and N-glycosylation, where O-fucose (red triangle), O-glucose (blue circle), O-GlcNAc (blue square), and N-glycan (light blue square) additions are found on specific

domains. At the cell surface, the Notch receptor is *trans*-activated upon binding by the ligand expressed from a neighbour cell. Ubiquitylation-mediated *trans*-endocytosis of the ligand-receptor complex generates a pulling force and exposes additional proteolytic sites for S2 and S3 cleavage by ADAM metalloprotease (scissors) and ɣ-secretase (scissors), respectively. The NICD liberated from the membrane translocates to the nucleus and interacts with RBPJ (wheat) to displace corepressors (Co-R; deep salmon) and recruit Mastermind-like (MAML; blue) and additional coactivators (Co-A; green), thereby inducing transcription of Notch target genes. A *cis*-inhibition complex of receptor and ligand expressed on the same cell surface is also shown.

1.1.2.3 *Cis*-inhibition

Cis-inhibition occurs when Notch receptors and ligands are present on the same cell surface. Like *trans*-activation, receptor-ligand interactions at the cell surface also appear to be required for *cis*-inhibition. *Cis*-inhibition plays important roles in cell fate specification and boundary formation, such as those regulating wing development and patterning, sensory organ precursor emergence and sensory bristles development, and photoreceptor specification during eye development in *Drosophila* (Cooper & Bray, 2000; De Celis & Bray, 1997; Jacobsen et al., 1998; Klein et al., 1997; Micchelli et al., 1997; Miller et al., 2009; Simpson, 1990; Troost et al., 2023). Likewise, *cis*-inhibition regulates various physiological processes in vertebrates, such as neurogenesis and somitogenesis during embryonic development, epidermal stem cell maintenance, and tip stalk cell differentiation during sprouting angiogenesis (Benedito et al., 2009; Chitnis et al., 1995; Cordes et al., 2004; Del Álamo et al., 2011; Franklin et al., 1999; Henrique et al., 1997; Lowell et al., 2000; Marchetto et al., 2020; Negri et al., 2019). Additionally, a recent study suggested that Jag1-Notch1 *cis*-inhibition maintains the native state of embryonic hematopoietic stem cell (HSC) by downregulating genes associated with lineage differentiation (Thambyrajah et al., 2024).

Although the exact mechanism of *cis*-inhibition has not been delineated, it is generally believed that the *cis*-complex is removed from the cell surface by endocytosis and then degraded, leading to mutual inactivation of *cis*-bound Notch receptors and ligands (Becam et al., 2010; Matsuda & Chitnis, 2009; Sprinzak et al., 2010). Experimental data and mathematical modelling identified distinct signalling dynamics of *trans*-activation and *cis*-inhibition, where the former shows graded-response to *trans*-ligand levels, whereas the latter has a sharp, switch-like response to a threshold level of *cis*-ligands (Sprinzak et al., 2010). A simplified Notch-Delta modelling system suggests an ultrasensitive switch between signal- sender and receiver states, whilst inclusion of Jagged into this system generates an additional hybrid state that has the potential to be either signal- sending or receiving (Boareto et al., 2015; Sprinzak et al., 2010). At a cellular level, *trans*-activation appears to compete with *cis*-inhibition, making Notch signalling particularly sensitive to the relative levels of Notch molecules available on the cell surface (Del Álamo et al., 2011). Moreover, the strength of *cis*-inhibition varies widely depending on the combination of receptor, *cis*-ligand and *trans*-ligand identity (Kuintzle et al., 2023).

1.1.2.4 *Cis*-activation

Cis-activation has recently been shown to occur between various receptor (NOTCH1, NOTCH2)-ligand (DLL1, DLL4) pairs in the same cell types (Nandagopal et al., 2019). Addition of soluble recombinant Notch receptors that blocked surface ligands was shown to inhibit both *trans*- and *cis*- activation, suggesting that both mechanisms require receptor-ligand interactions at the cell surface (Klose et al., 2015; Nandagopal et al., 2019). Likewise, the activity level of *cis*-activation is also affected by receptor-ligand affinity. Both increased binding affinity induced by Fringe-modification of receptors or use of a higher-affinity ligand for Notch such as DLL4 were shown to lead to enhanced *cis*-activation (Nandagopal et al., 2019).

1.1.2.5 Noncanonical Notch signalling

The noncanonical Notch pathway is known to be RBPJ/CSL-independent, and is activated either in a ligand-independent manner or by binding to noncanonical ligands (reviewed by (Kopan & Ilagan, 2009)). Notch is activated by ɣ-secretase- dependent or independent mechanisms, therefore can exert functions using its membrane-bound form (NTM-ICD). Since the noncanonical Notch signalling is RBPJ/CSL-independent, the signalling response is usually elicited by interplay with other signalling pathways, such as PI3K-AKT, mTOR, Wnt and NF-κB pathways. For instance, Notch signalling can inhibit the PI3K/AKT/mTOR pathway to induce apoptosis and autophagy, and inhibitors of these pathways were found to have synergistic effect on T-cell Acute Lymphoblastic Leukaemia (T-ALL) cell lines (Khoshamooz et al., 2020; X.-M. Wang et al., 2014; K. Zhang et al., 2021). Furthermore, Notch can be modulated by non-canonical ligands that are structurally diverse from the canonical ligands (reviewed by (D'Souza et al., 2010)). For instance, the Delta-like non-canonical Notch ligand 1 (Dlk1) which appeared to interact with Notch only in *cis*, was found to play various developmental and cancer-related roles through Notch-dependent mechanisms (Finn et al., 2019; Pittaway et al., 2021). The Notch canonical ligands can also act on non-Notch receptors, such as the noncanonical role of JAG1 as physiological ligand for CD46 in T helper type 1 cells (Le Friec et al., 2012).

1.1.3 Spatiotemporal patterning guided by Notch signalling

The Notch pathway not only regulates cell-fate decisions at an individual cell level, but also drives spatiotemporal pattern formation in tissues at a multicellular level. Notch signalling can give rise to convergent cell fates (lateral induction) or divergent cell fates (lateral inhibition) among neighbouring cells to drive pattern formation. Lateral inhibition was initially characterised in *Drosophila*, where the cell first adapts a sender phenotype (low Notch, high Delta) or a receiver phenotype (high Notch, low Delta) in a stochastic

manner (De Celis & Bray, 1997; De Celis & Garcia-Bellido, 1994; Huppert et al., 1997; Simpson, 1997). Upon engagement of Delta from the sender cell, Notch signalling is activated in the receiver cell, which in turn activates its downstream transcriptional targets to downregulate Delta, allowing the initial sender cell to force its neighbours into opposite cell states (Bocci et al., 2020; Collier et al., 1996; Huppert et al., 1997; Manderfield et al., 2012; Sprinzak et al., 2010) (Figure 1-2A). For example, lateral inhibition modulated synergistically by Dll1-Notch signalling and Jag1 *cis*-inhibition allows the alternate pattern of hair cells and supporting cells to be established during inner ear development (Daudet & Lewis, 2005; Petrovic et al., 2014).

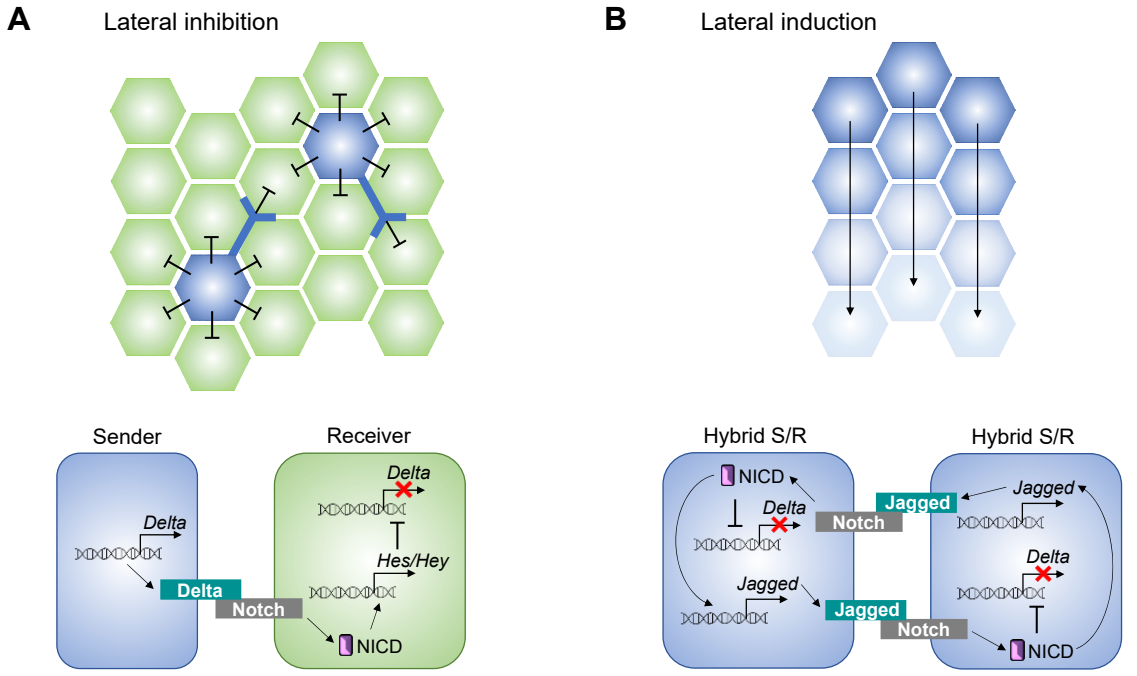


Figure 1-2. Notch signalling feedback mechanisms mediate lateral inhibition and lateral induction. (A) Top: During lateral inhibition, a high-Delta sender cell (blue) suppresses Delta expression in neighbouring cells, thereby enforcing a low-Delta receiver phenotype (green). This typically results in patterns of sender cells (blue) inhibiting several neighbours (green) and driving them to adapt an opposite cell state. The range of inhibition can be extended by filopodia extensions. Bottom: Detailed Delta-Notch circuit in lateral inhibition, where Delta on the sender cell activates Notch receptor in the receiver cell, releasing NICD that activates expression of *Hes/Hey*, which in turn supresses Delta production. (B) Top: During lateral induction, Notch activation in the initial cells (darker blue) induces a pool of neighbours (lighter blue) to adapt a common fate, which can then activate

Notch signalling in further contacting cells (light blue) to adapt a similar fate. Bottom: Detailed Jagged-Notch circuit in lateral induction, where upon Notch activation, NICD transcriptionally activates Jagged expression and represses Delta expression, therefore establishing and maintaining a hybrid Sender/Receiver (S/R) state.

Lateral induction occurs when Notch signalling modulates a similar cell state among neighbours by positive feedback, whereby upregulating ligand expression in the signal-receiving cells (Figure 1-2B). During inner ear development, lateral induction of JAG1 expression specifies the pro-sensory domains, and during cardiac development, Notch functions via lateral induction to promote epithelial-mesenchymal transition (EMT) to form endocardial cushion and heart valves (Hartman et al., 2010; Petrovic et al., 2014; Timmerman et al., 2004). A hybrid Sender/Receiver (S/R) phenotype, maintained by Notch-Jagged signalling, was reported (Boareto et al., 2015; Manderfield et al., 2012). The hybrid S/R state expresses intermediate levels of receptors and ligands, arising from the asymmetric effects of NICD on ligand production that represses Delta but stimulates Jagged production, hence allowing cells to both send and receive Notch signal (Figure 1-2B). The interplay of lateral inhibition and lateral induction plays important roles in pattern formation, leading to emergent multi-cellular dynamics in different biological contexts, such as inner ear development and EMT (for review see (Bocci et al., 2020)).

1.2 Notch signalling in health and disease

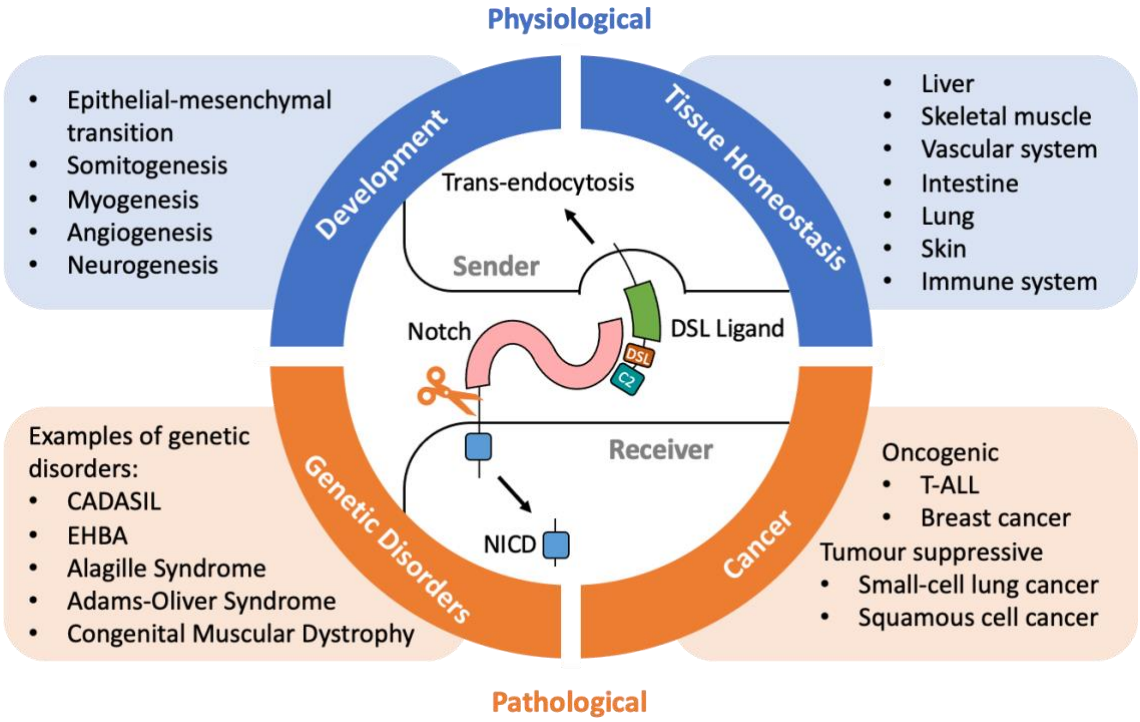


Figure 1-3. Physiological and pathological roles of Notch signalling with examples (adapted from (Siebel & Lendahl, 2017)). Notch signalling plays important roles in many developmental and homeostasis processes, mutations and dysregulations in the pathway lead to various cancer and developmental phenotypes in different tissues and organs. CADASIL: Cerebral Autosomal Dominant Arteriopathy with Subcortical Infarcts and Leukoencephalopathy; EHBA: Extrahepatic Biliary Atresia; T-ALL: T-cell Acute Lymphoblastic Leukaemia.

1.2.1 Physiological roles of Notch signalling

As a highly conserved and ubiquitously expressed signalling pathway, Notch haploinsufficiency leads to serious embryonic lethality (see Appendix 8.1.1 for the phenotypic consequences of deleting specific Notch pathway members in mouse models). Notch signalling is constitutively active during embryonic development (high level) and in the mature stage of body development (low level) and is upregulated in response to conditions of injury or stress. With regulatory roles in the differentiation and function of stem cells, Notch signalling maintains the stemness of progenitor cells by

promoting their self-renewal and dedifferentiation (Dong et al., 2010; Dray et al., 2021; Hilton et al., 2008). Based on temporal and spatial expression of Notch components, Notch signalling also regulates cell fate decisions by controlling the differentiation of progenitor cells (Sparks et al., 2010; Zong et al., 2009). In addition, Notch signalling is vital for maintaining tissue homeostasis, mainly through lateral inhibition or induction of transformation of mature cells, to modulate normal tissue regeneration and damage repair (Alabi et al., 2018; Minnis-Lyons et al., 2021).

1.2.1.1 Angiogenesis

Angiogenesis, the formation of new blood vessels from a pre-existing vasculature, is regulated by the Notch pathway. The two Notch ligands, Dll4 and Jag1, appear to have opposite effects on sprouting, and their interplay is crucial for balancing angiogenesis. During sprouting, endothelial cells (ECs) differentiate into distinct morphologies and functional properties, known as tip and stalk phenotypes (Gerhardt et al., 2003). Notch signalling is known to be important for the tip-stalk cell fate decision, wherein the tip cell has low Notch activity and the stalk phenotype is maintained by a high level of Notch signalling (Hellström et al., 2007; Lobov et al., 2007; Suchting et al., 2007). The tip phenotype is initiated by vascular endothelial growth factor (VEGF), which signals through VEGF receptor (VEGFR)-2 to enhance Dll4 expression in the tip cell via a Notch-dependent mechanism (Figure 1-4A) (Caolo et al., 2010; Gerhardt et al., 2003; Phng & Gerhardt, 2009). Dll4 presented by the tip cell then signals through Notch1 in the adjacent ECs to maintain their stalk phenotype. Dll4-induced Notch activation downregulates VEGFR-2 whilst upregulates VEGFR-1, resulting in reduced VEGF sensitivity in stalk cells, hence preventing VEGF-induced tip phenotype in these cells (Suchting et al., 2007). In addition, the Dll4-mediated Notch signalling can further upregulate the expression of Dll4 and the Rho GTPase, RHOQ, which in turn promotes Notch signalling in ECs (Bridges et al., 2020; Caolo et al., 2010). Hence, a positive feed-

forward pathway is established, through which Dll4 could propagate its own expression to synchronise Notch signalling between ECs and maintain the stalk phenotype.

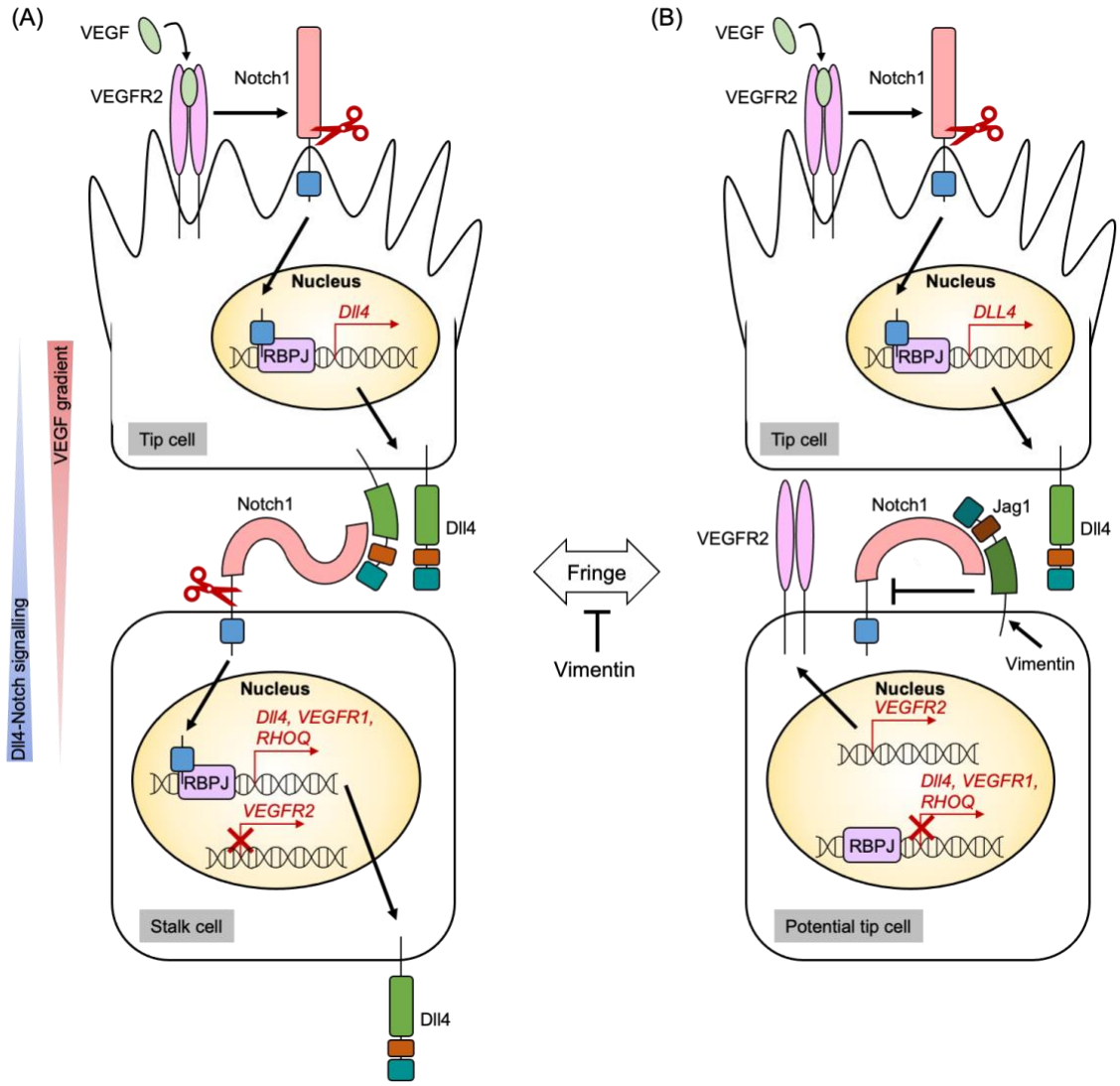


Figure 1-4. Notch signalling in sprouting angiogenesis. Signalling between endothelial cells (ECs) through the Notch pathway regulates sprouting angiogenesis in response to angiogenic stimulus. (A) In the tip cell, VEGF stimulus induces Dll4 expression through VEGFR-2 and Notch1 signalling. In the stalk cell, activation of Notch1 by Dll4 downregulates VEGFR-2 expression and upregulates VEGFR-1 expression, thereby suppressing tip cell phenotype. *Dll4* and *RHOQ*, whose expression is also induced by Dll4/Notch signalling, further propagate Notch signalling in ECs to maintain the stalk phenotype, establishing a positive feed-forward mechanism. (B) Sprouting is promoted when Jag1 in the stalk cell antagonises Dll4/Notch signalling to maintain a potential tip cell phenotype that is responsive to VEGF. Notch glycosylation by Fringe enzymes enhances Dll4/Notch1 signalling and inhibits Jag1/Notch signalling, hence modulating the interplay between the two ligands.

Vimentin binds to Jag1-ICD to enhance Jag1/Notch signalling and suppresses Fringe expression, providing additional regulatory potential.

The tip-stalk phenotypic specification is also reversible, depending on the Dll4-Notch signalling strength and the presence of proangiogenic factors such as VEGF and Jag1. Whilst expression of Dll4 in tip cells prevents neighbouring cells from adapting the tip phenotype, Jag1 expressed in stalk cells antagonises Dll4-Notch signalling via *cis*-inhibition to promote new sprouting (Figure 1-4B) (Benedito & Hellström, 2013; Hellström et al., 2007; Herbert & Stainier, 2011; Jakobsson et al., 2010; Suchting et al., 2007). The interplay between these two ligands is modulated by Fringe, a Notch glycotransferase known to potentiate the Delta/Delta-like induced Notch signalling, and has an opposite effect on the Serrate/Jagged ligands (Kuintzle et al., 2023; Panin et al., 1997; L.-T. Yang et al., 2005). In the ECs, Fringe modifications of Notch enhance Dll4-induced Notch activation, thereby strengthening the tip cell signalling capacity, but inhibit Notch1 activation by Jag1, rendering Jag1 into an antagonist ligand (Benedito et al., 2009). Furthermore, the equilibrium between anti-sprouting Dll4 signalling and proangiogenic Jag1 signalling could also be shifted by the intermediate filament vimentin, which binds to Jag1- but not Dll4- ICD, to block Jag1 recycling and amplify Jag1 signalling strength by promoting efficient transendocytosis (Antfolk et al., 2017). Vimentin also downregulates Fringe expression, whereby further potentiating Jag1-Notch interactions.

1.2.1.2 Myogenesis

Notch signalling is required for regulating myogenesis and self-renewal of skeletal muscle stem cells (MuSCs) in both embryonic development and adult stages (reviewed by (Gioftsidi et al., 2022)). Upon MuSC activation, Notch signalling rapidly declines to allow MyoD expression, driving the cells towards the proliferation phase. Blockade of Notch signalling, in either embryonic or adult MuSCs, leads to ectopic differentiation and

depletion of progenitor cells, resulting in muscle hypotrophy or dystrophy in mice models (Bjornson et al., 2012; Fukada et al., 2011; S. Lin et al., 2013; Mourikis et al., 2012; Schuster-Gossler et al., 2007). Dll1 appeared to be the prevalent Notch ligand in both embryonic and adult myogenesis (Schuster-Gossler et al., 2007; Yartseva et al., 2020). The oscillatory expression of *Hes1*, and thereon *MyoD* and *Dll1* oscillations, in activated MuSCs was shown to be required for sustaining their proliferative phase and self-renewal, whereas dampened *MyoD* or *Dll1* oscillations promoted MuSCs differentiation (Lahmann et al., 2019; Y. Zhang et al., 2021).

1.2.2 Insights from genetic disorders

As a core pathway conserved in all metazoans, the Notch pathway is associated with a number of developmental disorders and cancer caused by inherited and somatic mutations (Table 1-1). Dysregulation of the pathway results in disease phenotypes affecting various tissues, such as liver, muscle, skin, and vasculature. The mechanisms of different diseases, such as Alagille syndrome (ALGS), Adams-Oliver syndrome (AOS), and Tetralogy of Fallot (TOF), provide molecular insights for the spatiotemporal-specific expression of Notch pathway members and dependence of specific receptor-ligand pairs under different circumstances. Moreover, identification of various types of mutations and their association with specific disease phenotypes highlight the functionally important regions in Notch pathway proteins and their dose-dependent effects.

Disease	Related genes	Mutations	Phenotypes
ALGS	*JAG1, NOTCH2*	Missense/frameshift/splice site leading to decay/retention of JAG1	Hepatic, skeletal, cardiac, renal developmental disorders.
EHBA	*JAG1*	Missense site leading to reduced ability of activating Notch	Partial or total absence of bile duct.
TOF	*JAG1, NOTCH1*	Missense/frameshift mutation, most reported missense mutations cluster at the extreme N-terminus	Hole in septum of heart.
Congenital Muscular Dystrophy (CMD)	*JAG2, POGLUT1*	Missense, frameshift, nonsense, in-frame deletion, and a larger deletion encompassing *JAG2*	Progressive muscle weakening.
Charcot-Marie-Tooth disease type 2 (CMT2)	*JAG1*	Missense mutations in *JAG1*	Partial paralysis of vocal fold and peripheral neuropathy.
CADASIL	*NOTCH3*	Predominantly cysteine-related missense mutations in EGF domains	Impaired differentiation and maturation of vascular smooth muscle cells, accumulation of proteins in matrix around vascular smooth muscle cells.
AOS	*NOTCH1, DLL4, EOGT*	Addition/deletion of a cysteine residue in EGF domains	Terminal limb-reduction defects, skin/skull absence and cardiovascular anomalies.
Bicuspid aortic valve disease	*NOTCH1*	Missense/frameshift mutation	Abnormal aortic valve leaflets and aorta.
Dowling-Degos Disease	*POFUT1, POGLUT1*	Non-sense, frameshift and missense mutations contributing to haploinsufficiency of POFUT1 and POGLUT1	Lacy/net-like pattern of abnormally darkened skin.
Spondylocostal Dysostosis	*LFNG, DLL3*	Missense mutation, in-frame deletion of *LFNG* leading to loss of the enzyme activity; in-frame deletion/insertion of *DLL3* leading to truncations of ECD or missense mutations disrupt EGF repeats of DLL3	Fused/deleted/uneven/ severe curvature spine, truncal shortening.

Table 1-1. Summary of genetic diseases caused by gene mutations affecting Notch ligands and receptors and glycosyltransferases.

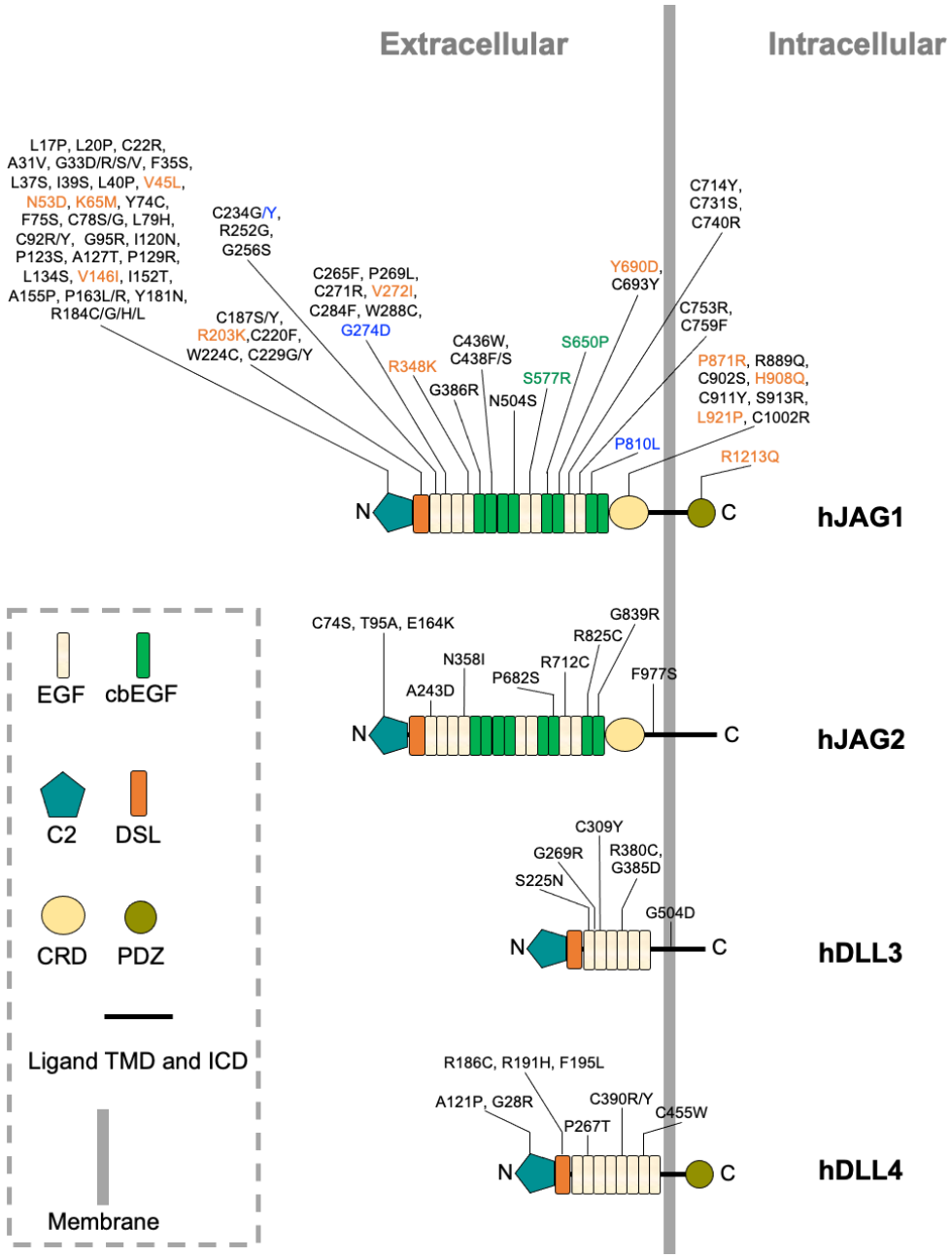


Figure 1-5. Map of Notch ligand missense mutations associated with genetic diseases (adapted from (Meng et al., 2023)). Disease-associated mutations in Notch ligands are mapped onto their domain organisation schematics. ALGS (black), TOF (blue), CMT2 (green) and EHBA (orange) missense mutations are labelled in hJAG1. CMD, SD and AOS-associated missense mutations are labelled in hJAG2, hDLL3 and hDLL4 respectively. Haploinsufficiency of *hDLL1* is disease-causing in neurodevelopmental disorder with nonspecific brain abnormalities and with or without seizures (NEDBAS) (Fischer-Zirnsak et al., 2019).

1.2.2.1 Diseases associated with JAG1: ALGS/EHBA

The autosomal dominant ALGS is cause by mutations in either ligand (*JAG1*) or receptor (*NOTCH2*), with majority (94%) of the cases dominated by mutations in *JAG1* (Birtel et al., 2018; Fischetto et al., 2019; Gilbert et al., 2019; Kamath et al., 2013; L. Li et al., 1997; Maya Kamath et al., 2012) (Table 1-1, Figure 1-5). As a multi-system disorder, ALGS has been recognised to cause cardiac, vertebral, hepatic, biliary, facial, pulmonary and renal defects (Fabris et al., 2007, 2019; Hankeova et al., 2021, 2022; Meester et al., 2019). Reduced Notch signalling caused by haploinsufficiency is identified as the main disease mechanism (Penton et al., 2012). Whole gene deletion as well as protein truncation mutations, including frameshift, nonsense and splice site, account for more than 80% of the cases, whereas missense mutations which spread across the entire *JAG1* lead to similar functional outcome that is consistent with haploinsufficiency (Bauer et al., 2010; Lu et al., 2003; Morrissette et al., 2001). Following structure determination of the N-terminal fragment of JAG1, a subset of ALGS missense mutations mapping to the JAG1 C2 domain were found to typically affect the hydrophobic core of the domain, leading to misfolding and ER retention of JAG1 and hence functional haploinsufficiency (Chillakuri et al., 2013). *JAG1* mutations are also recognised in some isolated cases of EHBA, a progressive fibro-inflammatory disorder characterised by absence of all or a portion of the bile duct between porta hepatis and the duodenum (Kohsaka et al., 2002) (Table 1-1, Figure 1-5). The majority of the mutations identified are sporadic and missense, including a subset that typically affects the loop structures of the JAG1 C2 domain (Chillakuri et al., 2013). Unlike JAG1-C2 mutations associated with ALGS which cause protein misfolding and non-secretion, EHBA-associated JAG1-C2 mutations in the apical loop regions lead to reduced C2-mediated lipid-binding and reduced Notch activation in reporter cells without affecting JAG1 secretion or its Notch binding affinity (Suckling et al., 2017). The results suggest an important role of JAG1 in biliary tract development that requires ligand-membrane interactions.

1.2.2.2 Disease associated with DLL4: AOS

Several Notch pathway members have been implicated in AOS, a rare developmental disorder characterised by congenital scalp defects known as aplasia cutis congenita (ACC) and terminal transverse limb defects. The pathogenesis of AOS can be associated with either autosomal dominant mutations in *NOTCH1*, *DLL4*, and *RBPJ*, or autosomal recessive mutations in *EOGT* which codes for EGF domain-specific O-GlcNAc transferase (EOGT) (Table 1-1, Figure 1-5) (Adams & Oliver, 1945; Meester et al., 2015). Symptoms may include cutaneous lesion on the scalp, heart defects, limb anomalies such as hypoplastic or absent distal phalanges, lesions on abdomen and neurological concerns (Rashid et al., 2022). Nonsense, frameshift and missense mutations in *DLL4* have been identified, which spread across the protein with no mutational hotspot (Table 1-1, Figure 1-5) (Meester et al., 2015; Nagasaka et al., 2017; Rojnueangnit et al., 2022; Stittrich et al., 2014). The disease-causing mechanism is hypothesised to be LOF since missense mutations identified in DLL4 either map to its receptor-ligand binding interface (p.G28R, p.R186C) that could impair receptor-ligand interactions or are found within the hydrophobic core of the C2 domain (p.A121P) that may lead to misfolding and ER retention (Meester et al., 2015; Rojnueangnit et al., 2022). Similarly, nonsense, frameshift and missense mutations are identified in *NOTCH1* with a subset in the latter group which maps to the ligand-binding region (LBR) and have implications in protein misfolding (Southgate et al., 2015; Stittrich et al., 2014). The divergent phenotypes observed for *DLL4/NOTCH1*-associated AOS suggest that additional genetic modifiers and environmental factors could play a role, but the prevalence of cardiovascular and skeletal features highlights the importance of DLL4-NOTCH1 pathway in these two systems (Meester et al., 2015).

1.2.3 Pathological relevance of Notch signalling in cancer

The Notch pathway plays key roles in regulating cell differentiation, proliferation, and homeostasis during both embryonic and adult stages, hence aberrant signalling is closely associated with cancer development and progression (Aster et al., 2017). Hyperactive Notch signalling is implicated to be oncogenic in various types of cancer, such as T-ALL, colorectal cancer, breast cancer, and glioma, leading to poor prognosis, lower survival rates and poor life expectancy (Bernasconi-Elias et al., 2016; Bonfiglio et al., 2022; J. H. Choi et al., 2008; Gao et al., 2011; Guo et al., 2009; Ho et al., 2013; Jubb et al., 2012; Kim et al., 2015; Lim et al., 2017; Reedijk et al., 2005; Santagata et al., 2004; Stephens et al., 2013; Strati et al., 2017; Sugiyama et al., 2016; Vaish et al., 2017; Weng et al., 2004; Westhoff et al., 2009; Yuan et al., 2015; Zheng et al., 2015; Zhu et al., 2021). The oncogenic effect of Notch signalling could result from upregulated expression of Notch receptors or ligands, but the disease mechanism could also be linked to mutations that produce a hyperactive Notch protein with constitutive activity (Aster et al., 2017).

Several studies on squamous cell carcinomas (SCC) unravelled the tumour-suppressive role of Notch signalling in various tissues (Agrawal et al., 2011; Alcolea et al., 2014; Boukhatmi et al., 2020; Hammerman et al., 2012; Sawangarun et al., 2018; Stransky et al., 2011). Various types of LOF mutations have been identified in *NOTCH1*, 2 and *3*, whose functionally important regions such as LBR could be affected (Agrawal et al., 2011; Nowell & Radtke, 2017; Stransky et al., 2011; N. J. Wang et al., 2011). However, oesophageal SCC presents a paradoxical example, as *NOTCH1* LOF mutations could also be found in normal aging human oesophagus, and in some disease models, downregulation of Notch1 was identified as a protective mechanism to inhibit tumourigenesis (Abby et al., 2023; Martincorena et al., 2018). These results contradict earlier studies, suggesting that the role of NOTCH1 as a tumour suppressor warrants further analysis.

1.3 Notch pathway components

Canonical Notch receptors and ligands have highly conserved modular arrangement of domain architecture in metazoans from *Drosophila* to humans (Figure 1-6). They are mostly type I transmembrane proteins with a large ECD and a relatively shorter ICD. A typical exception is *C. elegans*, whose receptor/ligand ECDs are much shorter and among its Delta/Serrate/LAG-2 (DSL) ligands, five out of ten are transmembrane (cARG-1, cLAG-2, cAPX-1, cDSL-2/6) whereas the rest are soluble (cDSL-1/3/4/5/7) (Komatsu et al., 2008). The NECD consists of multiple EGF repeats and a membrane proximal NRR region harbouring the S2 proteolytic cleavage site (Figure 1-6). The S3 cleavage site resides in the Notch transmembrane domain (TMD), followed by the NICD, which generally contains a RBPJ association module (RAM), several nuclear localisation sequences (NLS), an ankyrin repeats region (ANK), a transactivation domain (TAD) and a proline/glutamic acid/serine/threonine-rich motif (PEST). Exceptions such as NOTCH3/4 lack the TAD, and dNotch has an additional glutamine-rich repeat (OPA) in its ICD (Bellavia et al., 2008; James et al., 2014; Kopan & Ilagan, 2009). The Jagged/Serrate and Delta-like families of ligands also share a common modular domain organisation of their ECD, which includes the core receptor binding site comprising an N-terminal C2 domain and a contiguous DSL domain. This is followed by a variable number of EGF repeats and a Jagged/Serrate-specific cysteine-rich domain (CRD) that is absent in the Delta-like family (Figure 1-10). Additionally, some ligands (JAG1, DLL1, DLL4) contain a PSD-95/Dlg/ZO-1 (PDZ) motif in their ICD which plays a role independent of Notch signalling (Ascano et al., 2003; D'Souza et al., 2010).

1.3.1 Structure of Notch receptors

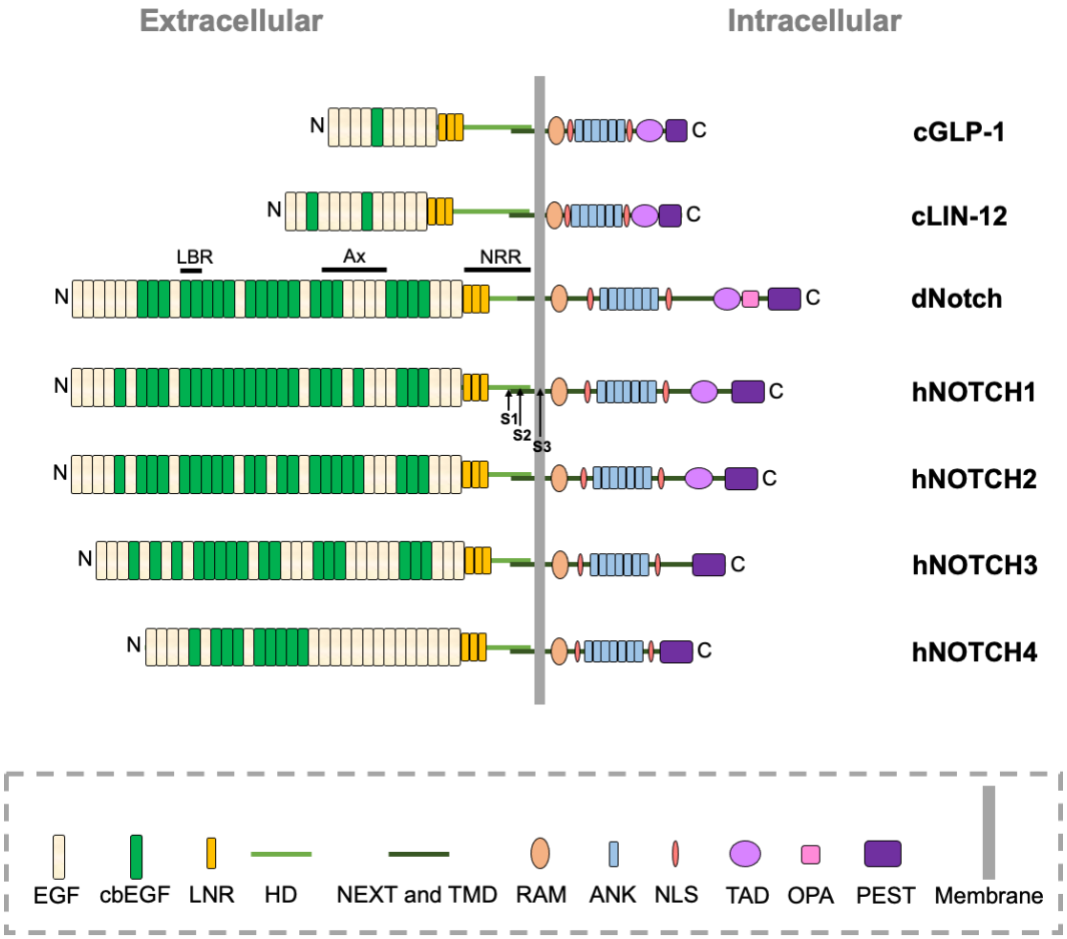


Figure 1-6. Domain architecture of Notch receptors. Notch receptors are type I transmembrane proteins containing multiple EGF-like domains, either non-Ca^{2+} binding (wheat) or Ca^{2+} binding (green), in their ECDs. *Drosophila* Notch (dNotch), the four human Notch paralogues (hNOTCH1-4), and the *C. elegans* Notch paralogues (cGLP-1 and cLIN-12) have similar domain organisation but differ in their number of EGF domains. The core ligand-binding region (LBR, EGF11-12), the Abruptex region (Ax, EGF24-29), and the negative regulatory region (NRR) are indicated on dNotch. The proteolytic cleavage sites (S1-3) are indicated on hNOTCH1.

1.3.1.1 Notch extracellular domain

Most surface expressed Notch receptors are furin-processed and exist as a heterodimer following S1 cleavage, except dNotch, which is furin-independent during its maturation (Kidd & Lieber, 2002; Logeat et al., 1998). The NECD is predominated by multiple EGF tandem repeats comprising both Ca^{2+} binding-EGFs (cbEGF) and non-cbEGFs, in which

the cbEGF harbours a Ca^{2+} binding consensus [D/E/N]-X-[D/N]-[D/E/N/Q]-Xm-[D/N/Q]*-Xn-[Y/F] (where * indicate possible β-hydroxylation, and m/n are variables) (Handford et al., 1991; Meng et al., 2023; Rees et al., 1988) (See Appendix 8.1.2 for detailed sequence analysis). Each EGF is a ~40 residue motif containing six conserved cysteines that are oxidised in the ER to form three disulfide bonds in a canonical 1-3, 2-4, 5-6 pattern to stabilise the native fold (Cooke et al., 1987).

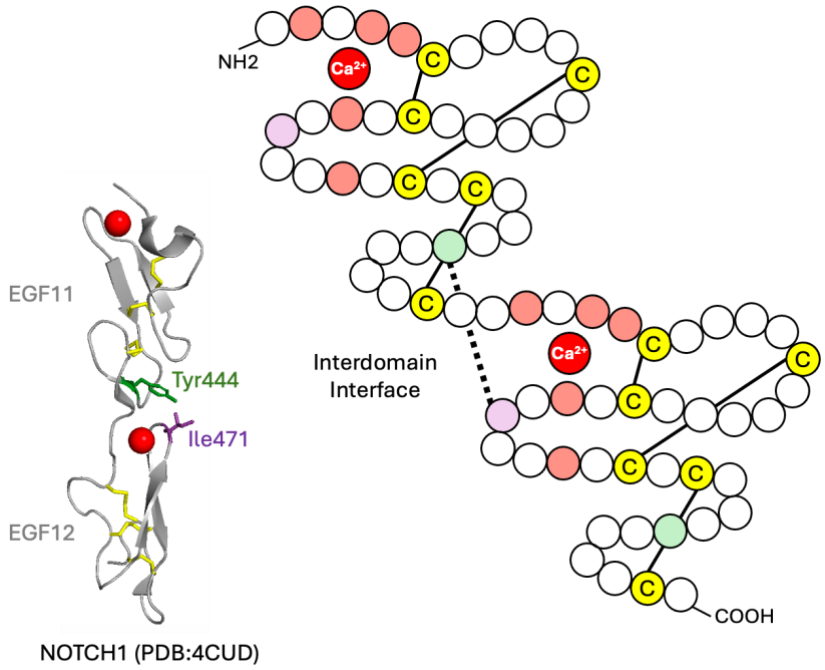


Figure 1-7. cbEGF-cbEGF domain pair in Notch. (Right) Schematic secondary structure illustration of the prototypical cbEGF-cbEGF domain pair. Calcium ions are coloured in red, and residues involved in the Ca^{2+} binding consensus [D/E/N]-X-[D/N]-[D/E/N/Q]-Xm-[D/N/Q]*-Xn-[Y/F] are coloured in pink. The aromatic (green) and hydrophobic (purple) residues involved in interdomain hydrophobic packing are highlighted, where hydrophobic interactions are illustrated with a black dotted line. Intradomain disulfide bonds are drawn as black solid lines, and the cysteine residues involved are coloured yellow. (Left) Crystal structure of hNOTCH1 EGF11-12 (PDB:4CUD) is shown as an example of cbEGF domain pair in Notch. Ca^{2+} ions (red spheres), disulfide bonds (yellow sticks), and residues involved in interdomain hydrophobic packing (Tyr444 in EGF11: green, Ile471 in EGF12: purple) are highlighted. Note the near linear arrangement of the cbEGF domains.

cbEGF domain pairs adapt a near linear tertiary structure, where the interdomain interface is stabilised by hydrophobic interactions between an aromatic residue in the N-

terminal EGF domain and a hydrophobic residue in the C-terminal EGF domain as well as Ca^{2+} ligation (Figure 1-7) (Cordle et al., 2008; Downing et al., 1996; Hambleton et al., 2004). The structure of the EGF11-12 region, previously shown to be the main LBR in *Drosophila* studies, was resolved by NMR and X-ray crystallography of Notch EGF11-13 fragments (Cordle et al., 2008; Hambleton et al., 2004; Suckling et al., 2017; Taylor et al., 2014). Structural data from *Drosophila* Notch and human NOTCH1/2 show that this region, consisting of three consecutive cbEGF domains, has a rigid and linear conformation under Ca^{2+}-saturating conditions (Figure 1-8) (Cordle et al., 2008; Suckling et al., 2017; Taylor et al., 2014). Moreover, our recent SAXS and NMR data showed that NOTCH1 EGF20-27 also has a rigid and elongated structure with most cbEGF domains having high Ca^{2+} affinity, except the EGF20-21 interface which showed Ca^{2+}-dependent flexibility due to a weaker Ca^{2+} affinity (Bo et al., 2024).

The interdomain interfaces involving cbEGF-non-cbEGF pairs are more variable compared to the rod-like cbEGF pairs, making the full-length Notch structure difficult to predict. X-ray crystallography data showed that the EGF4-7 region of NOTCH1 has a rigid, bent conformation with a tilt angle ~90° between cbEGF5 and non-cbEGF6, whereas interdomain orientations determined from residual dipolar couplings suggested a flexible interface between cbEGF9 and non-cbEGF10 (Figure 1-8) (Weisshuhn et al., 2016). Combining structural information from this study, with the LBR structure determined earlier, has led to a model for the NOTCH1 EGF4-13 region (Figure 1-8) (Cordle et al., 2008; Hambleton et al., 2004; Weisshuhn et al., 2016). In a more recent study, SAXS analysis of a full-length NOTCH1 ectodomain fragment performed under physiologically relevant conditions (2mM Ca^{2+}, pH7.4) revealed that the NECD is not simply a linear rod, supporting the earlier structural data for EGF4-7 and EGF9-10 (Zeronian et al., 2021). The maximum dimension (~38nm) observed for the ectodomain

from SAXS is much shorter than the expected length of a fully extended model (36 x 3nm = ~108nm), suggesting that additional flexible or bent regions exist.

The Notch negative regulatory region (NRR) comprising three cysteine-rich Lin12-Notch repeats (LNR) and a membrane-proximal heterodimerisation domain (HD) functions as the mechanosensor in the Notch activation pathway. The X-ray crystal structure of the NRR revealed an autoinhibited conformation where the three Ca^{2+}-bound LNR repeats wrap around the HD domain to protect the S2 cleavage site from protease access (Figure 1-8) (Gordon et al., 2007). Autoinhibition can be overcome by application of a mechanical pulling force or use of Ca^{2+} chelators, both of which make the S2 site available for ADAM protease-mediated cleavage (Gordon et al., 2007; Rand et al., 2000).

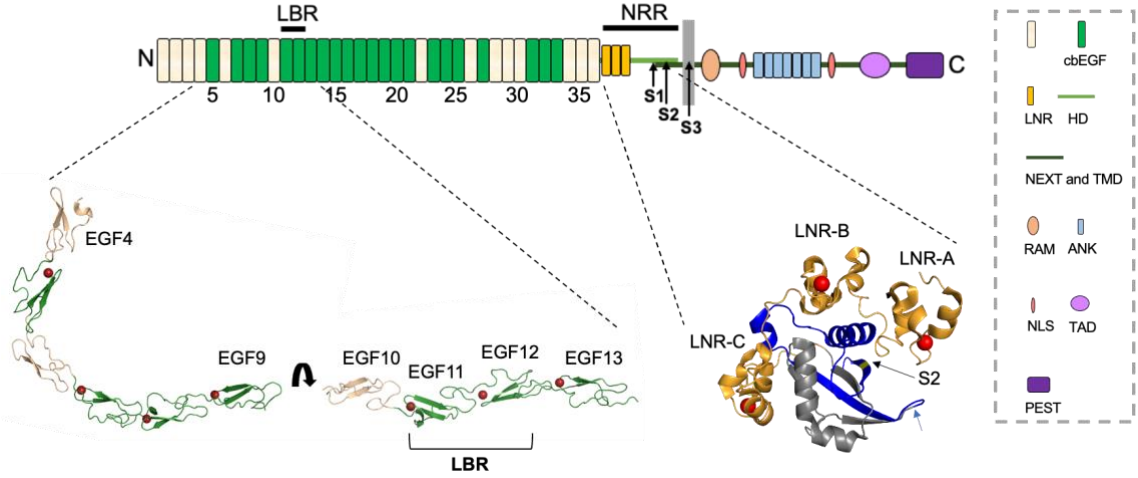


Figure 1-8. Notch extracellular domain structural features. Model of EGF4-13 region of the hNOTCH1 ECD (adapted from (Weisshuhn et al., 2016)). The models for the EGF4-9 and EGF10-13 regions (left) of NOTCH1 are based on the X-ray structures (PDB: 5FMA, 2VJ3) and residual dipolar coupling measurements (Weisshuhn et al., 2016). The structure of furin-cleaved NOTCH1 NRR (PDB: 3ETO) (right) (Gordon et al., 2009) is shown with the LNR modules in yellow, the region of the HD domain preceding the S1 cleavage site in grey, and the region after in blue. The S2 cleavage site, between the residues A1721 and V1722, (coloured grey) is indicated by a black arrow. The position of a deleted loop (residues 1623-1669) containing the S1 cleavage site is indicated by a blue arrow.

1.3.1.2 Notch intracellular domain

Notch signalling is mediated by tightly regulated proteolytic cleavage events that lead to liberation of the NICD and assembly of a nuclear Notch transcription complex (NTC), which in turn drives the expression of downstream target genes. Resolution of the ternary structure of the active transcription complex consisting of RBPJ, the NICD ANK and RAM domains, and MAML-1, bound to HES-1 promoter DNA sequence, delineates a sequential binding process to assemble the activatory complex (S. H. Choi et al., 2012). Within the core NTC, only RBPJ directly binds DNA and targets the NTC to specific gene loci. The NICD/RBPJ/MAML complex further recruit co-activators such as p300, ultimately loading RNA polymerase II and activating the expression of Notch target genes. In the absence of NICD, RBPJ associates with co-repressors, such as FHL1 or SHARP in mammals and Hairless in *Drosophila*, to inhibit gene expression (Borggrefe & Oswald, 2009; Liefke et al., 2010). Using live imaging approaches to probe the behaviours of NICD, CSL and MAML, a dynamic Notch 'ON' transcription hub was revealed, where proteins involved in the Notch transcription complex concentrate at a regulated gene locus to promote transcription in a probabilistic manner, resulting in only one third of the Notch 'ON' hubs being actively transcribing (Baloul et al., 2024; DeHaro-Arbona et al., 2024). This dynamic protein hub was shown to have changeable composition and confer transcriptional memory to target enhancers that allows rapid reactivation.

1.3.2 Structure of Notch ligands

From *Drosophila* to human, the Jagged family ligands (Jag1, Jag2) and Delta-like family ligands (Dll1, Dll3, Dll4), which are homologues of the *Drosophila* Serrate and Delta, constitute the canonical Notch ligand repertoire. Apart from Dll3, which has its expression restricted to intracellular compartments, and some soluble forms in *C.elegans*, the other canonical ligands are all expressed on the cell surface and function in either a *trans*-activatory or *cis*-inhibitory way (Figure 1-9) (G. Chapman et al., 2011). Notch ligands

share a common modular arrangement of their domain architecture, consisting of a relatively small ICD, a TMD, and a large ECD. The ectodomain of the DSL ligands comprises four functional regions, including a signal peptide, an N-terminal C2 domain, a highly conserved DSL domain, followed by a variable number of EGF repeats. The Jagged family ligands are larger and contain an additional Jagged-specific CRD (Figure 1-9) that distinguishes them from Delta-like ligands.

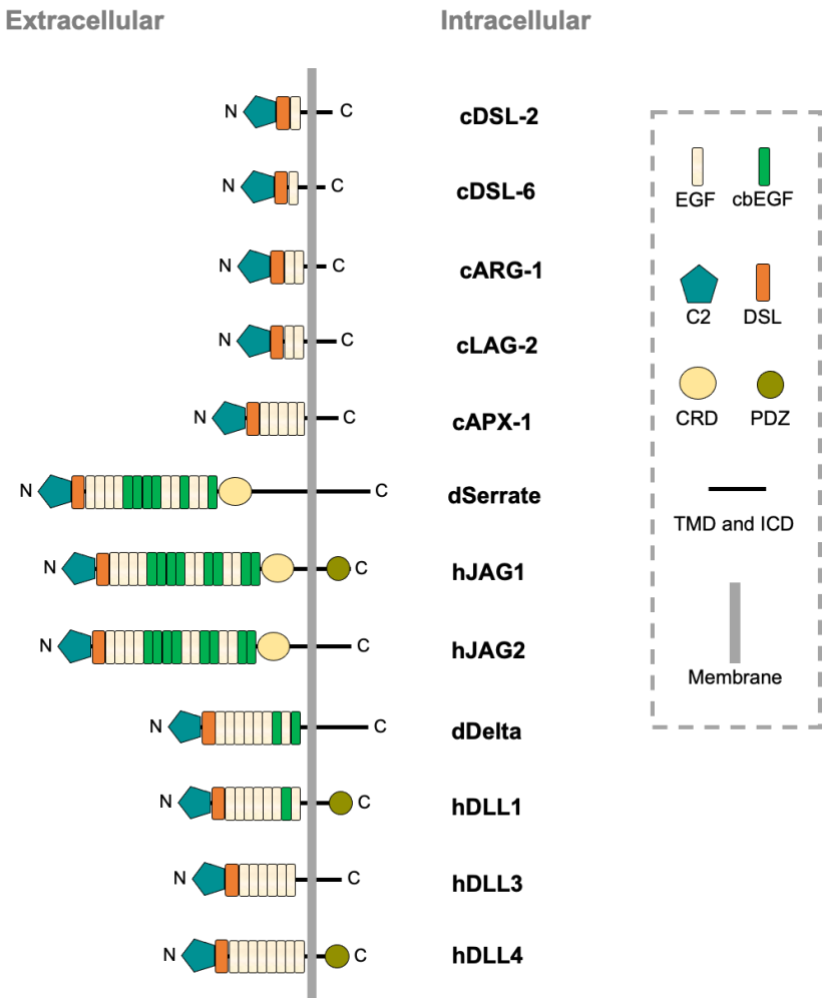


Figure 1-9. Domain architecture of Notch ligands. Notch ligands are type I transmembrane proteins containing multiple EGF-like domains, either non-Ca^{2+} binding (wheat) or Ca^{2+} binding (green), in their ECDs. The canonical Notch ligands have similar domain arrangement of their ECDs, consisting of an N-terminal C2 domain (teal), a DSL domain (orange), and a variable number of EGF repeats, but the Jagged/Serrate family differs from the Delta-like family by having an additional CRD (light yellow). Different ligand types show distinct cytoplasmic tails such that their ICDs vary largely in length and sequence homology (Pintar et al., 2007). Some ligands contain a C-terminal PDZ motif.

1.3.2.1 C2 domain: an N-terminal module conferring both receptor and lipid binding properties

The N-terminal region of the canonical Notch ligands contains a conserved ~100 amino acid module N-terminal to the DSL domain (Figure 1-9&1-10). This domain, formerly known as the MNNL (Module at the N-terminus of Notch ligand), was found to have significant homology among *Drosophila* and vertebrate Notch ligands, and is required for optimal Notch binding (Parks et al., 2006). The MNNL in human JAG1 was then structurally characterised as a C2 domain (Chillakuri et al., 2013), a common phospholipid-recognition domain identified in many membrane-targeting proteins (Corbalan-Garcia & Gómez-Fernández, 2014; Law et al., 2010; D. Zhang & Aravind, 2010). Based on structural and functional analyses, this C2 domain was shown to be a conserved N-terminal domain in all canonical Notch ligands, with the lipid-binding element suggested to be required for optimal Notch signalling (Suckling et al., 2017). Moreover, later determination of crystal structures of Notch ligand N-terminal fragments bound to the Notch1 LBR provide structural evidence of a receptor binding site located at the base of the C2 domain (Luca et al., 2015, 2017). Therefore, the ligand C2 domain confers additional complexity to the Notch signalling pathway due to its dual receptor- and lipid- binding properties.

1.3.2.2 DSL domain: an indispensable Notch binding unit

Following the N-terminal C2 domain is a disulfide-stabilised module termed DSL domain (Henderson et al., 1997). Early functional experiments identified a cysteine-to-tyrosine LOF substitution within this domain, and deletion mutagenesis showed that the DSL domain was a minimal requirement for receptor binding (Henderson et al., 1994; K. Shimizu et al., 1999). From X-ray crystal structures of the *in vitro* refolded Jag1 DSL-EGF3 fragment and HEK293S-expressed natively folded Jag1 C2-EGF3 fragment, the DSL domain was shown to consist of double-stranded anti-parallel β-sheets that is

structurally similar to the EGF domain but has a non-canonical 1-2, 3-4, 5-6 disulfide pattern (Figure 1-10) (Chillakuri et al., 2013; Cordle et al., 2008). Based on the structure, the DSL domain was proposed to have evolved from the truncation of two tandemly connected short EGF domains (Cordle et al., 2008). The DSL domain contains a highly conserved positively charged cluster on one of its surface loops bounded by two aromatic residues, which is important for Notch binding (Cordle et al., 2008; Kopan & Ilagan, 2009). Functional analysis of *Drosophila* Serrate suggested that the same DSL loop is required for Notch binding in both *trans*-activation and *cis*-inhibition (Cordle et al., 2008). More recently, analysis using cross-linking mass spectrometry (XL-MS) suggested further DSL interaction possibilities as Jagged1 DSL-EGF1 domains were shown to interact with Notch1 NRR in solution (Zeronian et al., 2021).

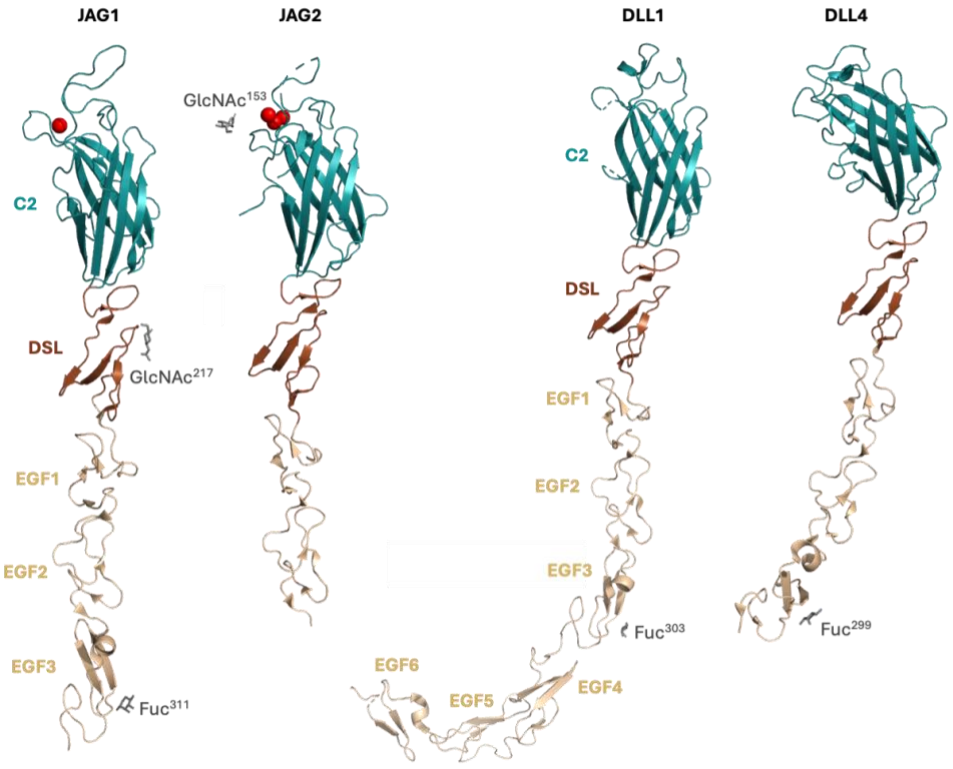


Figure 1-10. Structural features of Notch ligands. Crystal structures of $JAG1_{C2\text{-}EGF3}$ (PDB: 4CC1), $JAG2_{C2\text{-}EGF2}$ (PDB: 5MWF), $DLL1_{C2\text{-}EGF6}$ (PDB: 4XBM), and $DLL4_{C2\text{-}EGF3}$ (PDB: 5MVX) are shown (C2: teal, DSL: brown, EGF: wheat). Sugar modifications including N-linked GlcNAc and O-linked fucose are shown as grey sticks. The Jagged/Serrate family C2 domains bind Ca^{2+} (red sphere), unlike the Delta family ligands.

1.3.2.3 EGF repeats in Notch ligands

Both cbEGFs and non-cbEGFs are identified in Jagged/Serrate family ligands, dDelta and Dll1, whereas Dll3 and Dll4 ectodomains comprise entirely non-cbEGFs (Figure 1-9) (See Appendix 8.1.2 for detailed sequence analysis). Apart from disulfide bonds, other PTMs, such as O-fucosylation, O-glucosylation and β-hydroxylation were also found at unique locations on ligand EGF domains (Dinchuk et al., 2002; Haines & Irvine, 2003). In Notch ligands, the two non-cbEGF domains C-terminal to the DSL domain also contribute to receptor binding (Fleming, 2020; K. Shimizu et al., 1999). The EGF1 and 2 in Notch ligands exhibit an unusual domain conformation with shorter loop sequences, which resembles the Delta/OSM-11 (DOS) motif seen in *C.elegans* (Chillakuri et al., 2012; Komatsu et al., 2008). The other EGFs have more orthodox sequences, forming the canonical secondary structure with a central β-hairpin (Figure 1-10). The X-ray structure of DLL1 C2-EGF6 is the longest ligand ectodomain resolved, which revealed an extended conformation (Kershaw et al., 2015). Whilst EGF1-2, EGF2-3, EGF3-4, and EGF5-6 domain pairs have a rod-like conformation, EGF4 and 5 have a bent interdomain interface with a turn of ~90° (Figure 1-10). In addition, a recent XL-MS study performed on soluble fragments suggested that Jag1 EGF8-11 domains can potentially interact with Notch1 EGF33-NRR (Zeronian et al., 2021).

1.3.2.4 Cysteine-rich domain

The CRD, which is found exclusively in the Jagged/Serrate family, is a membrane-proximal region that is partially homologous to the von Willebrand factor type C-like (VWFC) domain but lacks the terminal CCX8C spacing (D'souza et al., 2008). Structure of the CRD has not yet been resolved, but deleting CRD in *Xenopus* Serrate caused abnormal expression of N-tubulin in primary neurons via the Notch/Su(H) pathway,

suggesting that CRD is involved in Notch signalling and regulates neurogenesis of *Xenopus* embryos (Kiyota & Kinoshita, 2002).

1.3.3 Notch/ligand complexes

The Notch receptor/ligand co-crystallisation structures were obtained using an affinity maturation technique, which resolved the complex of Dll4 C2-EGF1 bound to Notch1 EGF11-13 and the complex of Jag1 C2-EGF3 bound to Notch1 EGF8-12 (Figure 1-11A&B) (Luca et al., 2015, 2017). Structural data of the complexes showed that the bound receptor and ligand are arranged in an antiparallel organisation, which could underlie both *cis*- and *trans*- interactions. Two core binding sites were identified in both complexes, including 'site 1' between receptor EGF12 and ligand C2 domain, and 'site 2' between receptor EGF11 and ligand DSL domain (Figure 1-11A&B). Specifically, EGF12 of Notch1 is shown to interact with a disulfide-tethered (Cys61-Cys74) loop (β2-β3) at the base of the Dll4 C2 domain (Luca et al., 2015). Key residues involved in the receptor/ligand interface are consistent with previous observations made in mutagenesis and structural studies (Cordle et al., 2008). The O-fucose on Thr466 in Notch1 EGF12 was shown to participate directly in ligand binding (Figure 1-11A&B) (Luca et al., 2015, 2017). The O-glucose identified on Ser435 in Notch EGF11 could also potentially modulate binding (Figure 1-11B) (Luca et al., 2015).

Compared to the Dll4/Notch1 complex, the Jag1/Notch1 complex contains an additional binding site between Notch1 EGF8 and Jag1 EGF3, which has a conserved valine buried in the interface (Figure 1-11A) (Luca et al., 2017). This supports earlier experimental results, where the *Notch* ^{jigsaw} mutation V361M selectively affected Serrate-dependent Notch activation and reduced Notch binding (S. Yamamoto et al., 2012). The site 3 interface is stabilised by an O-fucose on Thr311 of Notch1 EGF8, which binds directly via hydrogen bonding to Asn298 in Jag1 EGF3 (Figure 1-11A). The O-fucose on Thr311

of Jag1 EGF3 interacts via a minor Van der Waals (VDW) contact with His313 in Notch1 EGF8, suggesting another potential O-fucose-mediated interaction.

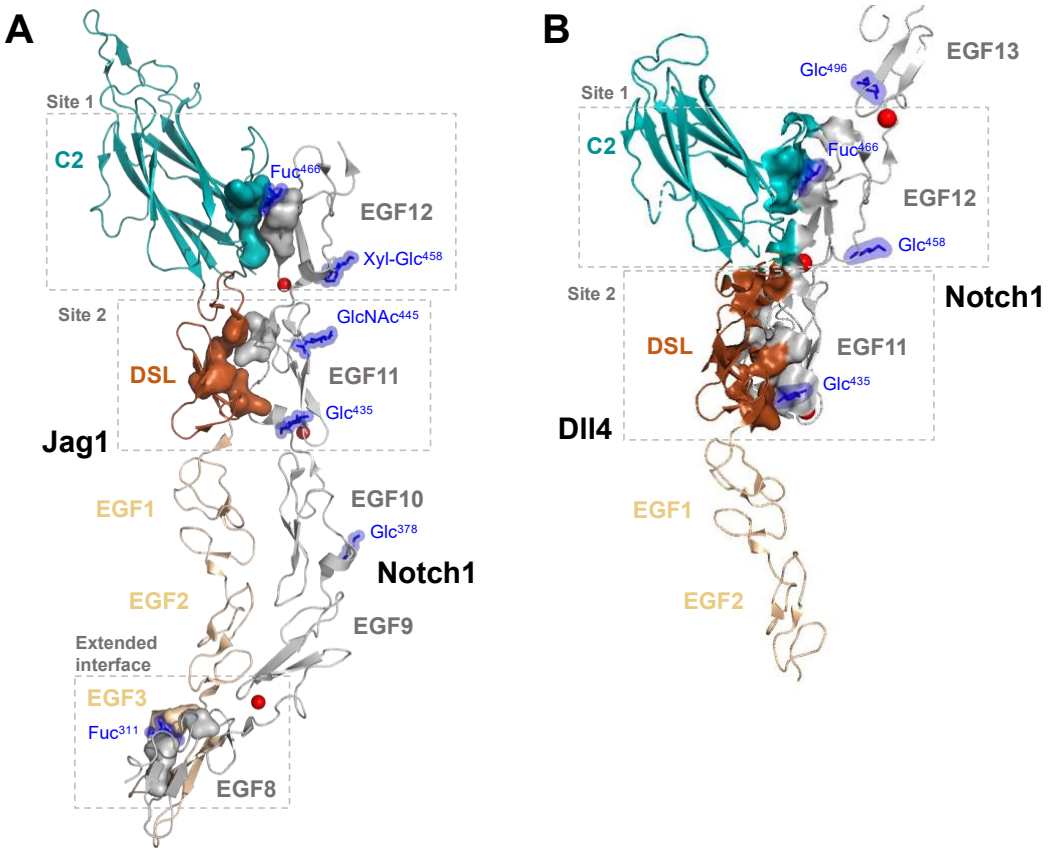


Figure 1-11. Structures of Notch receptor-ligand complexes (adapted from (Meng et al., 2023)). (A) X-ray structure of Notch1 EGF8-12 in complex with Jag1 C2-EGF3 (PDB: 5UK5). Jag1 C2 and DSL domains are shown in teal and orange respectively. The non-cbEGF domains are shown in wheat. Notch1 fragment is shown in grey. The Ca^{2+} ions are shown as red spheres. Key residues involved in binding are shown as surface representations. O-glycans are coloured blue. Fuc: fucose; Glc: glucose; GlcNAc: N-acetylglucosamine; Xyl: xylose. (B) X-ray structure of Notch1 EGF11-13 in complex with Dll4 C2-EGF2 (PDB: 4XLW) using the same colour scheme in (A).

1.3.3.1 Jag1 and Dll4 receptor binding affinities

Structural and biophysics data both suggest that Dll4 has higher binding affinity for Notch1 compared to other Notch ligand paralogues, possibly owing to differences in the orientations and buried surface areas of their binding interface (Luca et al., 2015, 2017). Comparison of $Notch1_{EGF11\text{-}13}$-$Dll4_{N\text{-}EGF1}$ and $Notch1_{EGF8\text{-}12}$-$Jag1_{N\text{-}EGF3}$ co-crystallisation

complexes shows that the binding interface area of the Notch1-Dll4 complex is ~200 Å^2 larger than the Notch1-Jag1 analogous interface, which could be partially compensated the additional binding site (site 3) between Jag1-EGF3 and Notch1-EGF8 (Luca et al., 2017). Surface plasmon resonance (SPR) measurements showed that, even with this additional site 3 interaction, Jag1$_{N\text{-}EGF3}$ still had a lower binding affinity for Notch1$_{EGF8\text{-}12}$ compared to Dll4$_{N\text{-}EGF3}$. Moreover, although site 3 was demonstrated to contribute substantially to Jag1/Notch1 interactions, SPR measurements using equivalent fragments showed a minimal effect of this additional site on Dll4/Notch1 binding affinity (Luca et al., 2017). However, these binding experiments lacked the pulling force element used in the actual biological receptor-ligand engagement. Biomembrane force probe force-clamp spectroscopy was used to demonstrate catch bond formation by intradomain rearrangements that may extend the Jag1/Notch1 bond lifetime and alter their binding interface (Luca et al., 2017). By using a site-directed mutant library to select for DLL4 variants that recapitulate the site 3 interaction between Jag1 and Notch1, a higher binding-affinity version of DLL4, referred to as 'DLL4.v2' (N-EGF5), was produced which displayed increased signalling capacity (Gonzalez-Perez et al., 2023). When combining DLL4.v2, which harbours structure-guided site 3 changes, with previously reported affinity-enhancing substitutions, a synthetic Delta^{MAX} ligand was engineered with a binding affinity that was 500- to 1000-fold higher than wild-type human DLL4 (Gonzalez-Perez et al., 2023).

1.3.3.2 Dll1 and Dll4 receptor binding affinities

Early binding assays using Dll1/4$_{N\text{-}EGF3}$ recombinant proteins showed that Dll4 had about 10-fold higher binding affinity for Notch1 compared to Dll1 (Andrawes et al., 2013). Although there is no co-crystallisation structure available for the Dll1/Notch1 complex, structure-based sequence analysis comparing their core receptor binding sites show highly conserved residues in both the C2-EGF12 and the DSL-EGF11 interfaces

(Suckling et al., 2017). Nevertheless, using flow-cytometry based binding assays with soluble Notch proteins and co-culture assays with stromal cells, two unique proline residues identified in the loop β2-β3 of Dll1 C2 domain were shown to account for its lower Notch binding affinity and activation potential (K.-I. Hirano et al., 2020). In addition, molecular dynamics (MD) simulation data suggest that this β2-3 loop, which is stabilised by a disulfide bridge, has restricted structural mobility in Dll1 due to its proline-rich region (K.-I. Hirano et al., 2020). On the other hand, the β2-3 loop in Dll4, which was more flexible in MD simulations, was suggested to allow Notch1 binding at a lower interaction energy, and when this loop was mutated to the same proline-rich sequence, similar interaction energy and limited movement as that of Dll1 were observed (K.-I. Hirano et al., 2020). These *in silico* analysis results were supported by *in vitro* experimental data, which showed that a protein-engineered Dll4 variant containing the β2-3 loop double proline substitutions had reduced Notch1 binding and activation capacities.

1.3.3.3 Novel potential extracellular receptor/ligand interactions

A recent study based on cross-linking mass spectrometry (XL-MS), which utilised a lysine-targeted PhoX reagent, has identified previously undetected intra- and inter-molecular interactions mediated by receptor and ligand ectodomains in solution (Figure 1-12) (Zeronian et al., 2021). Three Jag1 fragments, C2-EGF3, EGF10 and CRD, were found to contact with the membrane-proximal Notch1 EGF29-NRR region. However, no interactions were identified for the previously known core receptor-ligand binding sites, attributed to the lysine residues being buried in the interface and/or the presence of O-glycans which may interfere the cross-linking reactions. Subsequent analysis using SPR and microscale thermophoresis identified a specific interaction with moderately high affinity (K_d = 0.6 mM) between Notch1 NRR and Jag1 C2-EGF3, and some low affinity sites between Jag1 EGF8-11/CRD fragments and Notch1 EGF33-NRR (Figure 1-12). Moreover, intramolecular interactions between Jag1 C2-EGF1, EGF5-6, EGF9-12, and

CRD were observed, with weak binding between C2-EGF3 and EGF8-11 and CRD confirmed in quantitative interaction assays. Low affinity intramolecular interactions between Notch EGF8-13 and EGF33-NRR were also detected. These results, together with the SAXS analysis of Notch1 full-ectodomain and dynamics data for EGF9-10 (section 1.3.2.3), suggest that additional interactions are possible apart from those observed in the core receptor/ligand-binding sites (Weisshuhn et al., 2016; Zeronian et al., 2021). However, further functional analysis of membrane bound Notch is required to determine the physiological relevance.

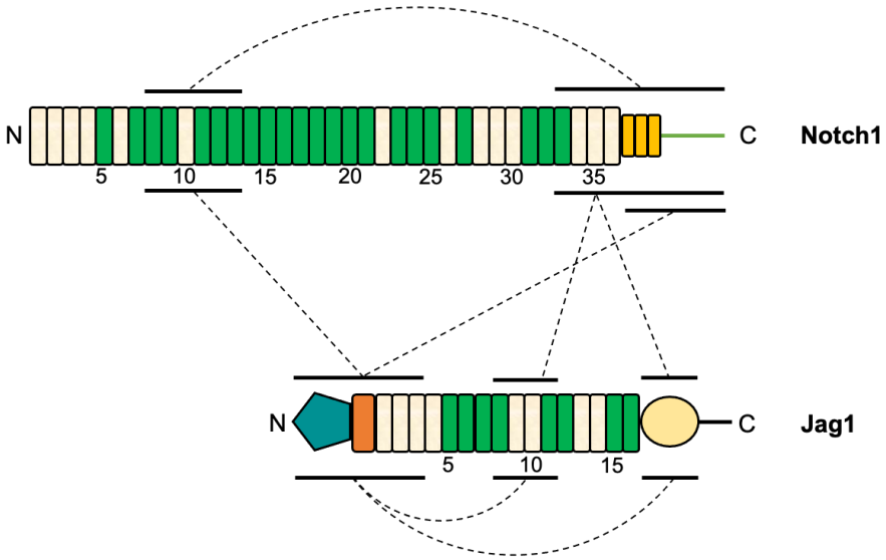


Figure 1-12. Notch1-Jag1 interaction network in solution (adapted from (Zeronian et al., 2021)). Schematics of the reported inter- and intra- molecular interactions in the Notch1-Jag1 full ectodomain complex based on XL-MS data, verified by quantitative interaction assays. Direct interactions between different constructs (solid black lines) are shown as dotted lines (intermolecular: straight dotted lines; intramolecular: curved dotted lines).

1.4 Regulation of Notch pathway

The Notch pathway relays extracellular signals from the cell surface to the genome in a direct, linear mechanism without signal amplification. The signalling outcome is usually transient due to the one-off usage of each receptor and the short lifetime of NICD, rendering Notch signalling intrinsically dynamic and highly sensitive to changes in its

core components and modifiers. The ability to signal depends upon the receptor and ligand identity and expression levels, which can vary with cell types and developmental states (Henrique & Schweisguth, 2019). However, the receptor/ligand variety is not sufficient to explain the broad range of different physiological responses observed, suggesting additional regulatory mechanisms. Notch activation is regulated by multiple factors, such as PTMs of Notch molecules in terms of ubiquitination and glycosylation, and biophysical components. Other factors such as transcriptional control mechanisms modulating NICD stability also play a role (Table 1-2) (Carrieri et al., 2019; Falo-Sanjuan et al., 2019; Giaimo et al., 2021; Nandagopal et al., 2018).

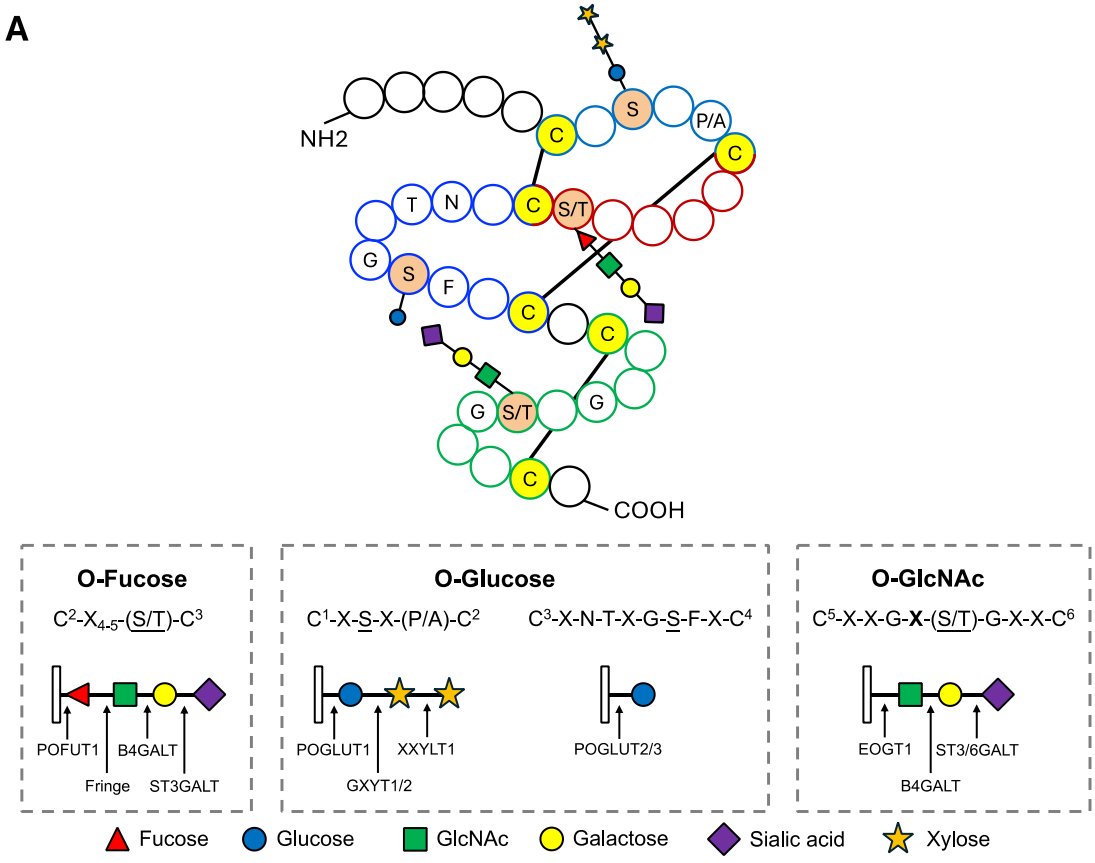
Type	***Drosophila melanogaster***	***Caenorhabditis elegans***	**Mammals**
Receptor	dNotch	cGLP-1, cLIN-12	hNOTCH1/2/3/4
Ligand	dDelta, dSerrate	cARG-1, cLAG-2, cAPX-1, cDSL-1/2/3/4/5/6/7	hDLL1/3/4
Glycosyltransferase	OFUT-1, Fringe, RUMI, EOGT	OFUT-1	POFUT-1, Lunatic Fringe, Radical Fringe, Manic Fringe, POGLUT-1/2/3, EOGT-1
S1 cleavage			PC5/6, Furin
S2 cleavage	Kuzbanian (TACE)	SUP-17, ADM-4	ADAM-10 (Kuzbanian), ADAM-17 (TACE)
S3 cleavage	Presenilin (Aph-1), Nicastrin (Pen-2)	SEL-12, HOP-1, APH-1/2, PEN-2	Presenilin-1/2, APH-1, Nicastrin, PEN-2
E3 Ubiquitin ligase	Mindbomb-1/2, Neuralised, Deltex, Nedd4, Su(Dx), Archipelago, d-cbl	WWP-1, SEL-10	Mindbomb-1/2 (skeletrophin), NEDD4, Neuralised-1/2, Deltex-1/2/3/4, Itch (AIP4), Cbl, FBXW-7 (SEL-10), Mdm2
Deubiquitinating enzyme (DUB)	USP12, eIF3-S5		USP12, eIF3f
CSL DNA-binding protein	Su(H)	LAG-1	CBF1/ RBPJ
Co-activator	Mastermind	LAG-3, SEL-8	Mastermind-like 1/2/3
Co-repressor	Hairless, SMRTR		SMRT
Target bHLH repressor genes	*E(spl)*	*REF-1*	*HES, HEY, ESR*

Table 1-2. Notch pathway components in different species. The Notch pathway contains a repertoire of receptor and ligand paralogues, which pair up differently depending on the biological contexts. Notch activation requires sequential proteolytic

events catalysed by the cleavage enzymes. The activation strength and outcome are modulated by various PTMs, such as glycosylation and ubiquitination. There are additional proteins that can modify the signalling output, which are listed.

1.4.1 Roles of glycosylation

Two main classes of sugar modification, O- and N-linked glycosylation, have been identified on Notch receptors and ligands, which play crucial regulatory roles in Notch signalling. Mutations affecting glycosyltransferases involved in the Notch pathway have been implicated in several human diseases with distinct phenotypes (Algaze et al., 2013; Basmanav et al., 2014; D. Choi et al., 2017; Servián-Morilla et al., 2016; Shaheen et al., 2013; Sparrow et al., 2006; Takeuchi et al., 2017). Figure 1-13 summarises potential O-glycosylation sites throughout the NECD, based on available glycoproteomic data and consensus sequence analysis (See Appendix 8.1.3 for more details).



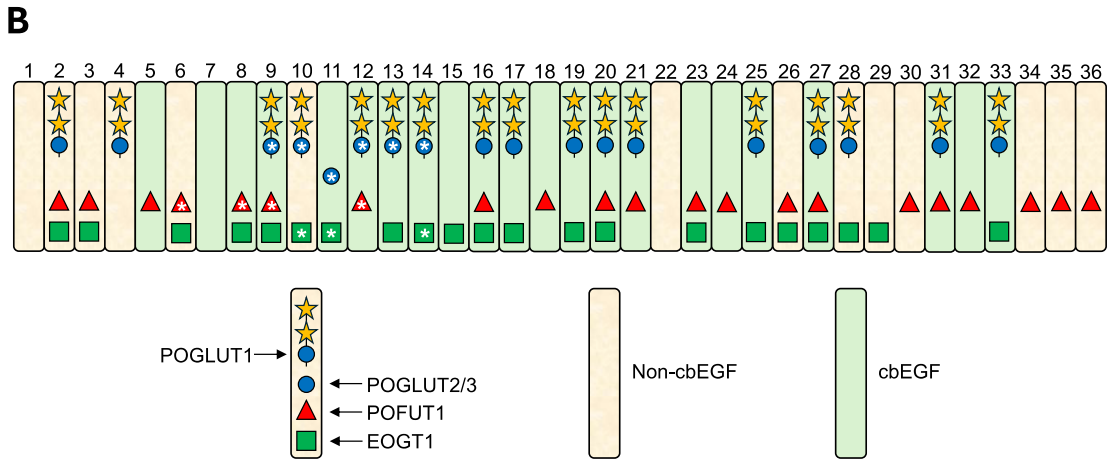


Figure 1-13. Structural basis of Notch O-glycosylation. (A) Schematic illustration of a typical EGF domain showing the O-glycosylation sites with glycan structures. Residues of the POFUT1, POGLUT1, POGLUT2/3, and EOGT1 consensus sequences are depicted as red, dark blue, light blue, and green circles respectively, with the modified S/T residue shaded in orange. Cysteine residues forming the intradomain disulfide bonds (black solid lines) are shaded in yellow. The mammalian enzymes involved in O-glycan modifications are shown below. (B) Illustration of the O-glycosylation sites found on human NOTCH1 EGF repeats as predicted by consensus sequences. The cbEGF and non-cbEGF domains are shown in green and wheat respectively. O-glycan modifications that have been confirmed experimentally are highlighted by asterisks (Andrawes et al., 2013; Pennarubia et al., 2022; Takeuchi et al., 2018; Taylor et al., 2014; Yokoi & Nishimura, 2020).

1.4.1.1 Notch receptor O-glycosylation

The multifaceted regulation of Notch signalling by O-glycosylation of the Notch receptor has been extensively studied (for review see (Harvey & Haltiwanger, 2018; Pandey et al., 2021; Saiki et al., 2021; Varshney & Stanley, 2018)). O-fucosylation, catalysed by 'protein O-fucosyltransferase 1' (POFUT1) (Figure 1-14) (Y. Wang et al., 1996, 2001), mainly plays a structural role in receptor-ligand binding, although some O-fucose sites may also affect Notch folding and trafficking (Kakuda et al., 2020; Okamura & Saga, 2008; Takeuchi et al., 2017; Yao et al., 2011). O-fucosyltransferase LOF typically downregulated Notch signalling, shown later to be due to a severe reduction in ligand binding (Luca et al., 2015, 2017; Okajima et al., 2003; Sasamura et al., 2003; Taylor et

al., 2014). Removal of specific O-fucose site on functionally important regions, such as Notch LBR EGF12, led to *Notch*-null-like phenotypes and embryonic lethality in animal models (Ge & Stanley, 2008; Pandey et al., 2019; Varshney et al., 2019). Incorporation of synthesised O-fucose analogues into Notch1 EGF8 was found to reduce Notch signalling induced by Delta-, but not Jagged- family ligands, suggesting ligand dependent differences (M. Schneider et al., 2018).

O-fucose can be further extended by Fringe, which adds a GlcNAc sugar using a β-1,3-linkage (Brückner et al., 2000; Moloney, Panin, et al., 2000). *Drosophila* has a single protein Fringe whereas mammals have three Fringe paralogues, namely manic (MFng), radical (RFng), and lunatic Fringe (LFng) (Cohen et al., 1997; Johnston et al., 1997). Fringe-modified *Drosophila* Notch had enhanced binding affinity for Delta and decreased affinity for Serrate, leading to upregulated Delta-induced Notch signalling during wing vein development and reduced *cis*-inhibition of Serrate by Notch during wing margin formation (Brückner et al., 2000; Irvine & Wieschaus, 1994; LeBon et al., 2014; Pandey et al., 2019; A. Xu et al., 2007). The three mammal Fringe paralogues have more diverse functions for different Notch receptor-ligand pairs. Whilst Dll1-mediated Notch activation was enhanced by all three Fringes, LFng and MFng downregulated Jag1-mediated Notch activation, whereas RFng increased Jag1-Notch1 signalling (Kakuda et al., 2020; Kakuda & Haltiwanger, 2017; LeBon et al., 2014). Flow cytometry and SPR analyses showed that the affinity of O-fucosylated Notch1 EGF11-13 for both Jag1 and Dll1 N-terminal fragments was enhanced upon modification by LFng, whereas the affinity for Dll4 did not increase further, likely because Dll4 already has substantially higher binding affinity without the modification (Taylor et al., 2014). Moreover, structural analysis of the Notch1-Jag1 and Notch1-Dll4 binding interfaces suggested that the elongated GlcNAc could serve as a molecular bridge (Luca et al., 2015, 2017).

O-glucose sites identified from structural work are usually located more peripherally and not directly involved in the receptor-ligand binding interface (Luca et al., 2015, 2017). The only exception is on Dll4/Notch1 interface, which has a non-consensus glucose modification of Ser435 on Notch EGF11 that could potentially modulate binding (Andrawes et al., 2013; Luca et al., 2015). O-glucosylation was suggested to act downstream of ligand-binding and upstream or at the level of S2 cleavage, likely by maintaining the autoinhibited conformation of NECD to protect the S2 site in the absence of ligand binding (Acar et al., 2008; Fernandez-Valdivia et al., 2011; Leonardi et al., 2011). Downregulated O-glucosylation were observed to reduce Notch cleavage and activation without affecting its surface expression level or ligand-binding capacity (Acar et al., 2008; Chu et al., 2013; Fernandez-Valdivia et al., 2011, 2011; Leonardi et al., 2011; Ma et al., 2011; Ramkumar et al., 2015; Servián-Morilla et al., 2016, 2020). Similar to O-fucose and O-glucose, O-GlcNAc also contributes to the proper folding and trafficking of Notch but has a more nuanced effect (Müller et al., 2013; Ogawa et al., 2020; Sawaguchi et al., 2017).

1.4.1.2 Notch receptor N-GlcNAcylation

Both *Drosophila* Notch and mouse Notch1 were previously suggested to be N-glycosylated, but the role of N-glycosylation was less well studied (Johansen et al., 1989; Moloney, Shair, et al., 2000). The enzyme ‘mannoside acetylglucosaminyl-transferase 3’ (MGAT3 or GnT-III) is known to add a β-1,4-linked GlcNAc to N-glycans to generate a bisecting GlcNAc structure on Notch receptors (Narasimhan, 1982; Nishikawa et al., 1992). By supressing the *MGAT3* mRNA levels, the expression and activity levels of *NOTCH1* and *NOTCH3* were shown to be downregulated, and altered receptor localisation was observed, suggesting a potential regulatory role in Notch trafficking (Allam et al., 2017).

1.4.1.3 Notch Ligand O-glycosylation

Compared to Notch receptors, glycosylation in Notch ligands is less well studied. Structural data and mass spectrometric analyses have identified O-glycan modifications on a number of EGF domains in ligands (Luca et al., 2015, 2017; Müller et al., 2013; Panin et al., 2002; Thakurdas et al., 2016). In particular, an O-fucose on Jag1 facilitates the formation of the third ligand-receptor binding site (see section 1.3.3) (Luca et al., 2017). Unlike the observed downregulated signalling for Notch receptors, incorporation of O-fucose analogues into ligands did not affect Notch activation in reporter cells, suggesting an elusive functional link (M. Schneider et al., 2018). However, an early study showed that the liver development in *Jag1*$^{+/-}$ animals is sensitive to the gene dosage of *fringe*, suggesting that *fringe* could potentially mediate the phenotypic variability of ALGS (Ryan et al., 2008). Moreover, in a *Jag1*$^{+/-}$ mouse model, removal of a single copy of *Poglut1* suppressed the defect seen in bile duct development, implying that a reduction in O-glucosylation could compensate for the reduced Jag1 level (Thakurdas et al., 2016). More recently, mutations impairing JAG1 O-glycosylation were observed to reduce JAG1 surface expression and associated with autosomal dominant peripheral nerve disease (CMT2) (Sullivan et al., 2020). In general, Notch signalling mediated by ligand-glycosylation was shown to be dosage-sensitive in pathological contexts (Pandey et al., 2021).

1.4.2 Roles of ubiquitination

1.4.2.1 Ubiquitination operative at the receptor level

The *Drosophila*-derived Dx and Su(dx), and their vertebrate homologues, are the most well characterised E3 ligases involved in Notch ubiquitylation (Le Bras et al., 2011; Moretti & Brou, 2013). Both families of E3 ligases primarily interact with NICD to modify the PEST and TAD domains (Moretti & Brou, 2013), except a few unusual sites, such as K29 in Notch1 which is targeted by the mammalian Su(dx) orthologue Itch/AIP4 to control

Notch degradation (Chastagner et al., 2008). *Drosophila* studies show that both Dx and Su(dx) interact with NICD and regulate endocytic trafficking of Notch through a clathrin-dependent route (Cornell et al., 1999; Matsuno et al., 1995; H. Shimizu et al., 2014; Wilkin et al., 2004, 2008). Dx/Dx-related proteins differ from Su(dx)/Su(dx)-related proteins by exhibiting a mixture of upregulated and downregulated effects on Notch signalling, whereas data so far have only displayed downregulated effects of Su(dx)-related proteins on Notch signalling (for review see (Dutta et al., 2022; Revici et al., 2022)). Ubiquitination also modulates the half-life of Notch molecules via phosphorylation-dependent degradation (for review see (H.-J. Lee et al., 2015)). Notch transactivation-induced transcriptional activation is usually coupled to NICD degradation by recruiting the Cyclin C-CDK8 complex that phosphorylates the PEST domain, followed by FBW7-mediated NICD ubiquitylation and proteasomal degradation (Fryer et al., 2004; O'Neil et al., 2007; Thompson et al., 2007). Notch1 signalling was also shown to be downregulated by an integrin-linked kinase, which phosphorylated the TAD domain, followed by FBW7-mediated ubiquitination, to destabilise the active NICD (Mo et al., 2007).

1.4.2.2 Ubiquitylation operative at the ligand level

Ubiquitylation of Notch ligands is catalysed by two E3 ubiquitin ligases, Neuralised (Neur) and Mindbomb (Mib), which play critical roles in Notch signalling by regulating ligand processing, maintenance, and activation. Cells lacking Neur or Mib are unable to activate the Notch signalling cascade even if there is a successful ligand-receptor interaction (Deblandre et al., 2001; Itoh et al., 2003; E. C. Lai et al., 2001, 2005; Le Borgne et al., 2005). In *Drosophila* Delta-Notch signalling, these E3 ligases appeared to recognise different lysine residues and docking sites within the ligand ICD for ubiquitylation in different development contexts (Kang et al., 2013; Le Borgne et al., 2005). In mammals, Neur-1 ubiquitinates Jag1 whereas Neur-2 ubiquitinates Dll1, suggesting specific pairing

of different ligases and ligands (Koutelou et al., 2008; Song et al., 2006). Ubiquitylation-mediated ligand endocytosis modulates Notch signalling via two mechanisms—downregulation of *cis*-inhibition by ligand internalisation and maintenance of a controlled surface ligand expression level by recycling a functional pool of ligands (Del Álamo et al., 2011; Emery et al., 2005; Palmer et al., 2014).

1.4.3 Regulatory roles of mechanical forces

1.4.3.1 Pulling force generated by endocytosis

Early studies found that the secreted forms of *Drosophila* ligands containing only the ectodomain had an antagonistic nature (X. Sun & Artavanis-Tsakonas, 1996, 1997), and LOF mutations of Notch pathway members involved in endocytosis led to signalling-deficient phenotypes (Meloty-Kapella et al., 2012; Poodry, 1990), suggesting that mechanical forces generated at the cell surface are essential for Notch activation. A classical model of *trans*-activation proposed that transendocytosis of the ligand and the bound NECD generates a mechanical pulling force essential for Notch activation. In the classical 'pulling force' model, the ICD of Notch ligands is ubiquitinated by Neur and Mib1 (see section 1.4.2.2 for details) and recognised by epsin, which then interacts with clathrin to create the clathrin-coated pit (Figure 1-14), leading to clathrin-dependent transendocytosis (Deblandre et al., 2001; Itoh et al., 2003; W. Wang & Struhl, 2004, 2005; Xie et al., 2012). Ligand-endocytosis-induced dissociation of Notch heterodimer promotes a conformational change of the NRR that exposes the S2 cleavage site (Nichols et al., 2007), which is autoinhibited by the interdomain interactions within the NRR (Gordon et al., 2007, 2009, 2015). A more recent bilateral endocytosis model suggested that ubiquitination of Notch at the plasma membrane by Deltex 4 (DTX4) could induce *cis*-endocytosis of receptors in the signal-receiving cell, which may also contribute to the mechanical pulling force (Figure 1-14) (G. Chapman et al., 2016; Chastagner et al., 2017).

On the other hand, recent studies have also suggested a pulling force independent model, which proposed that prolonged and clustered receptor-ligand interactions might be sufficient to elicit signal activation without *trans*-endocytosis or its associated pulling-force (Morsut et al., 2016; Smyrlaki et al., 2024).

1.4.3.2 Catch bond formation

Biophysics data showed that transendocytosis during Notch activation generates a pulling force in the range of 5-10 pN, which is sufficient to alter the NRR conformation from autoinhibitory to activatory, allowing S2 cleavage (Gordon et al., 2015; Luca et al., 2017; Meloty-Kapella et al., 2012; X. Wang & Ha, 2013). The stability of the Notch-ligand complexes, indicated by their dissociation lifetime, was demonstrated to increase as a function of applied force and reach a maximum at ~10 pN for the Notch-Jag1 complex (Luca et al., 2017). This property termed ‘catch-bond’ stabilises the *trans*-activating complex under tension and transmits force to the NRR (Figure 1-14). Catch-bond formation can be explained by a predicted conformational change in the Notch ligand induced by the mechanical force, which enlarges the receptor-ligand contact interface and strengthens binding (Luca et al., 2017).

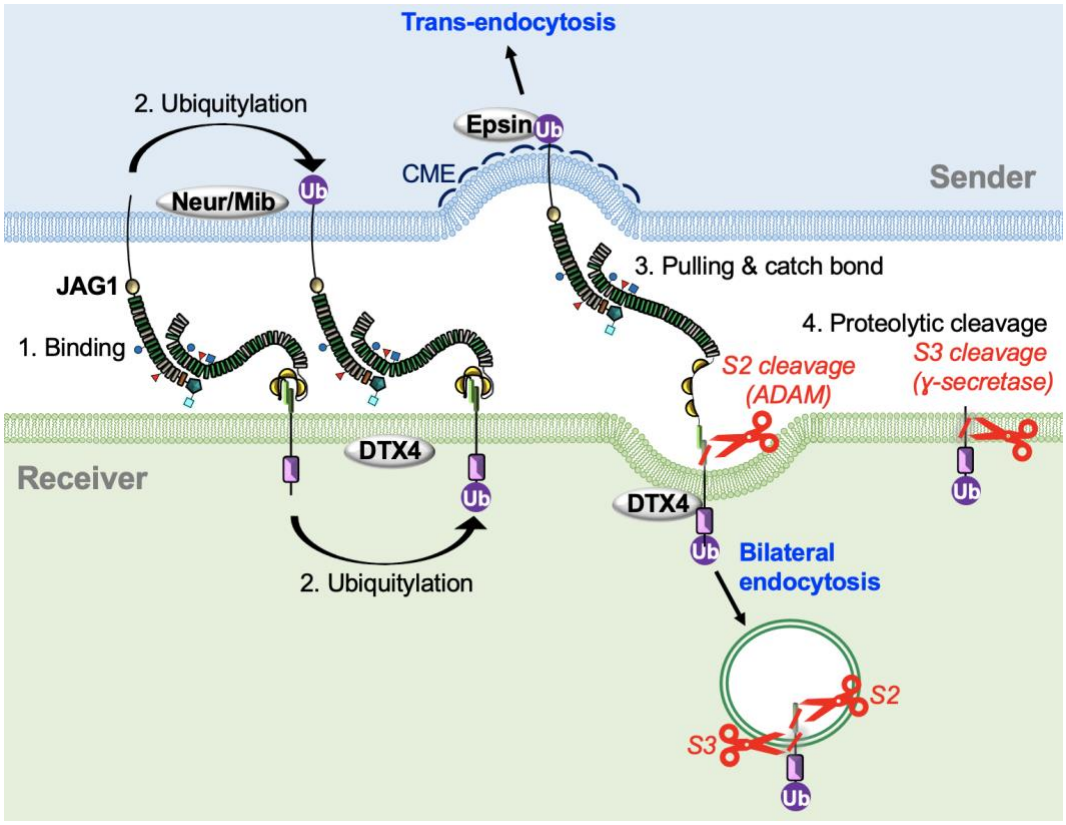


Figure 1-14. Proposed mechanical forces in canonical Notch signalling. Schematic of the sequential events during the bilateral endocytosis Notch signalling model: 1. binding of Notch receptors to DSL ligands, likely facilitated by ligand C2-membrane binding; 2. ligand ubiquitylation by Neur or Mib and receptor ubiquitylation by DTX4; 3. clathrin mediated endocytosis (CME) of the ligand and ligand-bound NECD into the sender cell, and possible internalisation of the membrane-anchored fragment of Notch and DTX4 by the receiver cell. These may create a pulling force that promotes conformational changes whereby the catch bond behaviour is engaged. 4. S2 and S3 cleavage takes place presumably after the dissociation of Notch heterodimer (Nichols et al., 2007). ADAM10-mediated S2 cleavage is suggested to occur both at the cell surface and in the endocytic vesicles to process Notch (Chastagner et al., 2017).

1.5 C2 domain

The N-terminal domain in human JAG1 was first identified as a C2 phospholipid recognition module in 2013, and later it was found that the C2 domain confers novel lipid-binding properties to all canonical Notch ligands *in vitro* (Chillakuri et al., 2013; Suckling

et al., 2017). *In vitro* assays suggested that the interaction of Notch ligands with lipid membranes was required for optimal Notch activation (Suckling et al., 2017), proposing novel regulatory potential of the Notch pathway.

1.5.1 The C2 domain superfamily

The extensive repertoire of structurally distinct lipid-binding domains shed light on the diverse functional contexts of the elaborate eukaryotic membrane system. The C2 domain is one of the most prevalent lipid-binding domains identified in several distinct protein families, forming the C2 domain superfamily. This domain type, which confers both lipid-binding and protein-binding properties, has roles in a variety of cellular processes involving membranes, such as vesicular trafficking, actin/tubulin anchorage, localisation of small GTPases, as well as phosphoinositide-mediated signalling (Corbalan-Garcia & Gómez-Fernández, 2014; D. Zhang & Aravind, 2010). The C2 domain is mostly found in intracellular membrane targeting proteins, such as synaptotagmin and cPLA2α, but an exception prior to identification within the canonical Notch ligands is perforin, which is extracellular (Corbalan-Garcia & Gómez-Fernández, 2014; Law et al., 2010). All C2 domains share a common structure of a β-sandwich configuration consisting of eight antiparallel β-strands, and can be classified into two topologies, type I (formerly known as the synaptotagmin-like variants or the S-family) or type II (formerly known as the PLC-like variants or the P-family), depending on the circular permutation they adopt (Figure 1-15A&B) (Corbalan-Garcia & Gómez-Fernández, 2014). Notch ligands typically adopt the type II C2 topology. Since Ca^{2+}-mediated lipid-binding plays an important role in many C2 domain-containing proteins, especially the PKC-C2 family (Figure 1-15C), C2 domains can be further classified into Ca^{2+}-dependent or -independent types, in which the latter class, despite having lost the Ca^{2+}-binding residues, can still bind lipids (Larsen & Sansom, 2021).

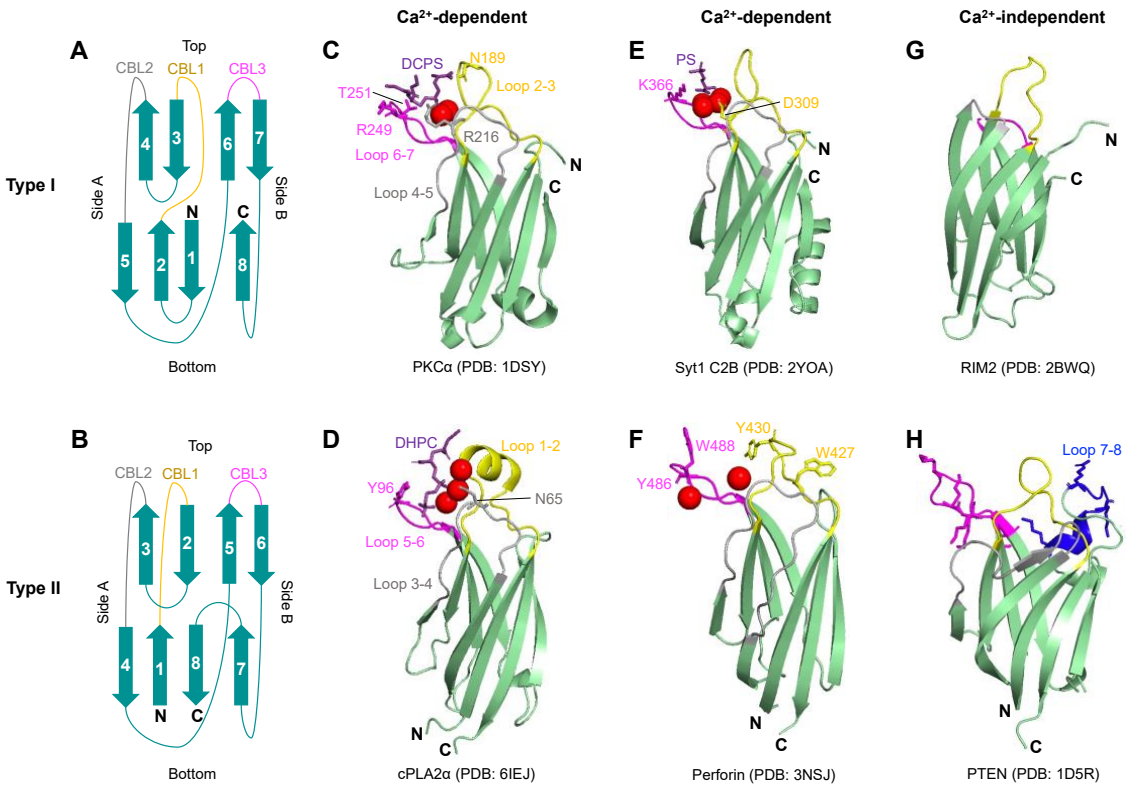


Figure 1-15. Classification of the C2 domain superfamily based on topologies and Ca^{2+}-dependence. (A, B) Schematics of the type I and type II topologies. β strands are numbered and connected with loops, where the putative calcium-binding loops (CBL1, CBL2, CBL3) are highlighted in yellow, grey and magenta respectively. The β-sheet containing the N- and C- termini is denoted as "front" and the other β-sheet is denoted as "back". All canonical Notch ligands adopt the type II C2 topology. (C-H) Examples of Ca^{2+}- dependent and independent C2 domains in each topology (Ca^{2+} ions: red spheres). The bound phosphatidylserine (DCPS) in PKCα (PDB: 1DSY), the bound phosphatidylcholine (DHPC) in cPLA2α (PDB: 6IEJ), and the bound phosphoserine (PS) in synaptotagmin-1 (Syt1) C2B domain (2YOA) are coloured in purple. Key residues directly involved in lipid binding are shown in stick representations. The aromatic residues critical for membrane binding in perforin-C2, and the solvent-exposed positively charged residues in PTEN-C2 are also shown in stick representation. DCPS = 1, 2-dicaproyl-sn-phosphatidyl-L-serine. DHPC = 1,2-dihexanoyl-sn-glycero-3-phosphocholine.

1.5.2 Calcium-dependent C2-membrane interactions

In both type I and type II C2 domain topologies, Ca^{2+} binding is modulated by loops on one side of domain, denoted as the top/apical side (Figure 1-15A&B), as this is where Ca^{2+}-mediated lipid-binding takes place. These Ca^{2+}-binding loops (CBLs) coordinate

with metal ions using highly conserved aspartate residues and some additional residues (Corbalan-Garcia & Gómez-Fernández, 2014). In many cases, apart from an increased structural stabilisation, Ca^{2+} binding does not cause any significant conformational changes to the native fold, as suggested by comparing the Ca^{2+}-bound forms of synaptotagmin-1 (Syt1)-C2A, PLCδ1, PKCα and PKCβ with their Ca^{2+}-free forms (Grobler et al., 1996; Shao et al., 1996, 1998; Verdaguer et al., 1999). On the other hand, Ca^{2+}-mediated structural stabilisation seems to play a more extended role in perforin proteostasis, since an engineered Ca^{2+}-stabilising perforin becomes functionally hyperactive with significantly enhanced thermal stability (Brennan et al., 2018). Perforin contains both high-affinity Ca^{2+}-binding sites that can be constitutively occupied at low intracellular Ca^{2+} levels (limited availability of Ca^{2+} in lytic granules (Ham et al., 2022)), as well as low-affinity Ca^{2+}-binding sites that only respond to high Ca^{2+} concentrations either from the extracellular fluid ($[Ca^{2+}]$ = 2~5mM) or the ER ($[Ca^{2+}]$ = 100μM~1mM).

Depending on the intrinsic Ca^{2+} affinity of the C2 domain, the membrane docking of different C2 domains can be selectively triggered by the Ca^{2+} concentration. Therefore, calcium binding in perforin has important regulatory roles: i) promoting protein folding in the ER, ii) activating extracellular perforin to favourite binding to target cell membranes, and iii) facilitating oligomerisation to form pores (Brennan et al., 2018; J. A. Lopez et al., 2013; Traore et al., 2013). On the other hand, selective occupancy of only high-affinity sites in the secretory granules keeps perforin functionally inert to prevent premature membrane insertion (Ham et al., 2022; Kataoka et al., 1997). Moreover, unlike other examples where Ca^{2+}-binding to C2 loops induces no major conformational changes, Ca^{2+}-binding in perforin C2 domain was found to trigger significant movement of its CBL1, which is in a suboptimal membrane-binding orientation without Ca^{2+}-binding and switches to a membrane-binding active form in the presence of Ca^{2+} (Yagi et al., 2015). Comparison between the apo- and holo- C2 crystal structures of perforin revealed a Ca^{2+}-dependent conformational rearrangement that brings its CBL1 and CBL3 into close

proximity to form a hydrophobic lipid-interacting groove, which consists of four key solvent-exposed aromatic residues (Figure 1-15F) that are critical for membrane binding but do not directly coordinate Ca^{2+}-binding (Traore et al., 2013; Yagi et al., 2015).

Meanwhile, Ca^{2+}-binding can dramatically alter the electrostatic properties of the C2 domain CBLs, providing an electrostatic switch that drives the association of some C2 domains to the membrane (Corbalan-Garcia & Gómez-Fernández, 2014; Murray & Honig, 2002; Shao et al., 1997). Without Ca^{2+}-binding, the CBL region in Ca^{2+}-dependent C2 domains is negatively charged due to the presence of conserved aspartate residues. Upon Ca^{2+}-binding, the CBLs become either overall neutral (e.g., cPLA2α) or positively charged (e.g., PKCβ, Syt1), enabling the C2 domain to associate with phospholipids and act as a Ca^{2+}-activated membrane module (Cho & Stahelin, 2006; Corbalán-García & Gómez-Fernández, 2006; Guerrero-Valero et al., 2009; Larsen & Sansom, 2021; Rizo & Südhof, 1998). Different C2 domains show lipid-binding preferences based on their chemical nature—whilst cPLA2α-C2 which has enriched solvent-exposed hydrophobic side chains preferentially docks to zwitterionic membranes (e.g., phosphatidylcholine/PC) via hydrophobic interactions, the highly basic CBLs of Syt1-C2A and PKCβ-C2 maintain their binding to anionic membranes (e.g., phosphatidylserine/PS) via electrostatic interactions (Murray & Honig, 2002; Nalefski et al., 2001). The hydrophobic nature of the cPLA2α CBLs also allows its deeper penetration into the membrane, where the Ca^{2+}-binding facilitates membrane penetration through reducing the free energy required for inserting charged groups into the phospholipid bilayer (Y. Hirano et al., 2019; Murray & Honig, 2002). Compared to intracellular C2 domains, the apical loops of Notch ligands C2 are less hydrophobic, suggesting that they are not deeply buried in the membrane bilayer irrespective of whether or not they bind Ca^{2+} (Suckling et al., 2017).

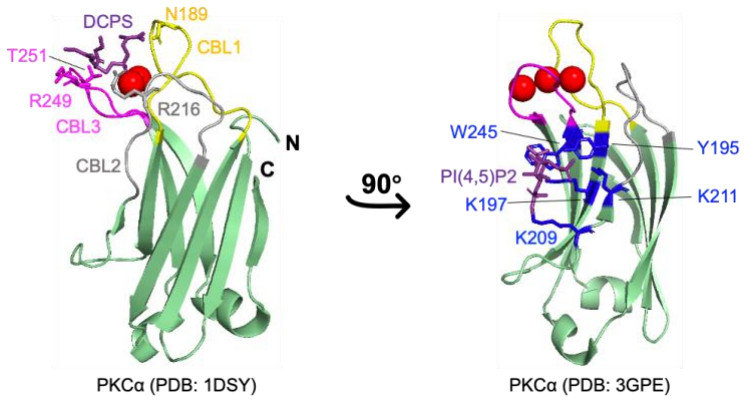


Figure 1-16. Different Ca^{2+}-binding sites in PKCα C2 domain. PKCα-C2 bound to DCPS (PDB: 1DSY) or $PI(4,5)P_2$ (PDB: 3GPE) are shown in cartoon representations, where key residues involved in each phospholipid binding are shown in stick representations, suggesting very distinct binding sites consisting of completely different lipid-binding residues. The C2 domains are coloured in pale green, the Ca^{2+} ions bound at the apex of the C2 domain are shown as red spheres. CBL1 is shown in yellow, CBL2 in grey and CBL3 in magenta. The bound phospholipids are coloured in purple. DCPS=1,2-dicaproyl-sn-phosphatidyl-L-serine. PI(4,5)P2 = [(2R)-1-octadecanoyloxy-3-[oxidanyl-[(1R,2R,3S,4R,5R,6S)-2,3,6-tris(oxidanyl)-4,5-diphosphonooxy-cyclohexyl]oxyphosphoryl]oxy-propan-2-yl](8Z)-icosa-5,8,11,14-tetraenoate.

Crystal structures of the protein-Ca^{2+}-lipid ternary complexes (Figure 1-15C/D/E), including the PKCα-C2 in complex with phosphatidylserine (PS) (Verdaguer et al., 1999), the Syt1-C2B in complex with phosphoserine (Honigmann et al., 2013), and the cPLA2α-C2 in complex with PC (Y. Hirano et al., 2019), showed that Ca^{2+} directly bridged these C2 domains to the bound phospholipid. Structural and sequence analysis showed that PC recognition by the cPLA2α-C2 is very different from PS recognition by the PKCα-C2 and Syt1-C2B, that cPLA2α-C2 has a much longer CBL1 and none of the residues involved in PS recognition are conserved in cPLA2α (Figure 1-15) (Y. Hirano et al., 2019). In addition, PKCα-C2 (PDB: 3GPE) was shown to be able to interact with $PI(4,5)P_2$ through a different motif that requires residues located on the β3 and β4 strands (Figure 1-16) (Guerrero-Valero et al., 2009).

cPLA2α-C2 was shown to bind phospholipids selectively, with the PC binding affinity being ~5-fold greater than that for PS, phosphatidic acid (PA), phosphatidylglycerol (PG), or phosphatidylinositol (PI) (Y. Hirano et al., 2019). Early study shows that Syt1 C2A domain, which natively has a PS binding preference, can become capable of binding PC after grafting the cPLA2α CBLs onto its C2 domain (Gerber et al., 2001). This loop swopping approach only works when all three CBLs are grafted, suggesting that all three CBLs are required for PC recognition and these apical loops are essential and sufficient to confer C2 domain lipid-binding specificity. Further analysis suggested that this lipid-binding selectivity is mainly determined by the Tyr96 on CBL3, which specifically targets lipids containing a phosphorylcholine headgroup (contains a positively charged choline group and negatively charged phosphate and carbonyl groups, and is a neutral molecule as a whole), such as PC and sphingomyelin (SM) (Y. Hirano et al., 2019). Interestingly, whilst binding of phosphatidylcholine (DHPC) to cPLA2α-C2 causes no significant change in the protein conformation, the binding is implicated to induce membrane structural changes by promoting membrane curvature and tubulation, since selective binding and oligomerisation of cPLA2α-C2 on membranes with positive curvature were observed (Cai et al., 2012; Grimmer et al., 2005; San Pietro et al., 2009; Ward et al., 2012, 2020). The capacity to induce membrane deformation could be accounted for by the deeper membrane penetration (~78-85% of a fluid bilayer) by the cPLA2α-C2.

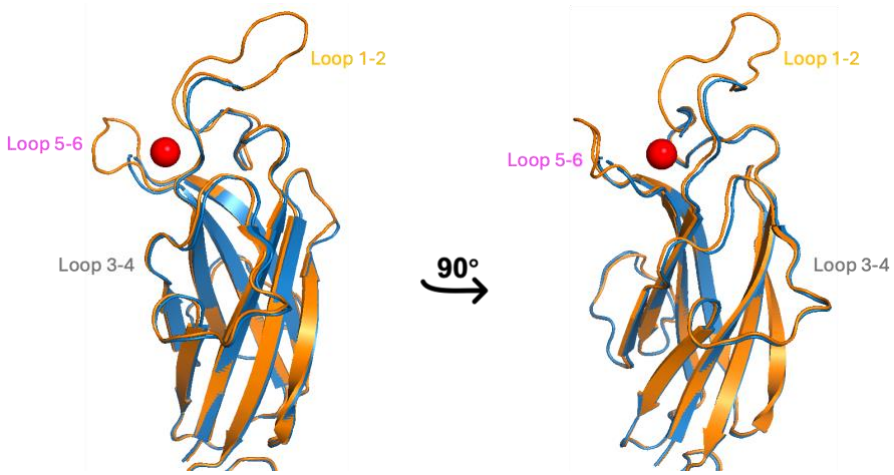


Figure 1-17. Superimposed crystal structures of the Ca^{2+}-free (4CBZ, blue) and Ca^{2+}-bound (4CC1, orange) JAG1-C2 domains (adapted from (Chillakuri et al., 2013)). Some

residues in loops β1-2 and β5-6 in the Ca^{2+}-free C2 were not modelled into the final apo-structure. Ca^{2+} ion (red sphere) is shown to be bound in a cleft between the apical loops β1-2 and β5-6. The conformation of all three apical loops (β1-2, β3-4, and β5-6) has no distinguishable change upon Ca^{2+} binding.

In most cases, the C2 domain acts as a form of membrane docking for soluble proteins (e.g., PKCs, PLCδ, cPLA2) or additional membrane docking for integral proteins (e.g., synaptotagmins) (Corbalan-Garcia & Gómez-Fernández, 2014; Davletov et al., 1998; Davletov & Sudhof, 1993; Guerrero-Valero et al., 2009). Since canonical Notch ligands are single-pass transmembrane proteins, their C2 domain provides potential for peripheral membrane binding in addition to their transmembrane region (Chillakuri et al., 2013; Suckling et al., 2017). The Jagged family Notch ligands are integral proteins containing an N-terminal Ca^{2+}-dependent C2 domain, where mutations (D140A/D144A) abolishing Ca^{2+}-binding in their CBL regions led to both defective liposome binding and reduced Notch activation (Chillakuri et al., 2013; Meng et al., 2022; Suckling et al., 2017). Similar to the above-mentioned intracellular C2 domains, the crystal structure of the Ca^{2+}-bound JAG1-C2 superimposed with its Ca^{2+}-free apo-structure showed structurally undistinguishable apical loop region (Figure 1-17), suggesting that Ca^{2+} binding caused no significant conformational change to the domain native fold (Chillakuri et al., 2013). Hence, findings from other Ca^{2+}-dependent C2 domains can provide molecular insight into how C2-mediated membrane binding in Notch ligands is regulated in a Ca^{2+}-dependent manner.

1.5.3 Calcium-independent C2-membrane interactions

Some Ca^{2+}-independent C2 domains, such as PTEN, bind membrane via electrostatic interactions. C2 domains of the Delta-like family Notch ligands are Ca^{2+}-independent, thus may share structural and functional features with this type of C2. Moreover, some Ca^{2+}-dependent C2 domains, such as PKCα-C2 and Syt1-C2B, have both Ca^{2+}-

dependent and -independent membrane binding modes, providing additional insight for Jagged family Notch ligands (Guerrero-Valero et al., 2009; Kuo et al., 2009; Nyenhuis et al., 2021).

PTEN has a type II C2 domain with an electrostatic profile similar to that of the other Ca^{2+}-bound form of Ca^{2+}-dependent C2 domains, thus enabling constitutive binding of PTEN-C2 to the membrane (Murray & Honig, 2002). Five solvent-exposed lysine residues (Lys260, Lys263, Lys266, Lys267, and Lys269) reside on the CBL3 of PTEN (Figure 1-15H), resulting in a net positive charge that increases its affinity for the phosphoryl groups in phospholipids and mimics the electrostatic property resulting from Ca^{2+}-binding to the CBL3 region in the Ca^{2+}-dependent C2 domains. The PTEN CBL3 also contains two solvent-exposed hydrophobic residues (Met264 and Leu265) at the apical region, which are residues implicated in membrane insertion in Syt1-C2A and cPLA2α-C2 (Bittova et al., 1999; E. R. Chapman & Davis, 1998; Y. Hirano et al., 2019). Additionally, PTEN has a basic patch on its β7-8 loop consisting of solvent-exposed positively charged residues (Lys327, Lys330, Lys332, and Arg335), which makes this region similar to the membrane-interacting helix in the CBL1 of cPLA2α (Figure 1-15D&H) (Perisic et al., 1998). Mutations of these basic residues in the canonical CBLs of PTEN were shown to weaken its phospholipid-binding affinity, suggesting that the membrane interactions are strongly influenced by ionic strengths (J.-O. Lee et al., 1999).

Apart from the CBL regions, it is also suggested that some C2 domains can adopt alternative modes of membrane interactions. The observation was initially made in PKCα, where the crystal structure of the PKCα-Ca^{2+}-PS-PI(4,5)P_2 quaternary complex showed that the C2 domain can bind both PS and PI(4,5)P_2 using distinct sites of interactions (Figure 1-16). The latter requires a cationic concave surface (or β-groove) encompassing two aromatic residues (Tyr195 and Trp245) and three lysine (Lys197, Lys209, Lys211) located on the C2 β-strands, hence this interaction appears Ca^{2+}-

independent. Mutagenesis analysis supports this deduction, showing that mutations abolishing Ca^{2+}-binding only affected PS recognition, whereas mutations abolishing this polybasic β-groove region only affected $PI(4,5)P_2$ interactions (Guerrero-Valero et al., 2009). Later on, the cationic β-groove was identified as a common feature in many C2 domain families (e.g., PKC, PTEN, PI3K) (D. Zhang & Aravind, 2010).

Using vesicle sedimentation assays, the Syt1-C2B was shown to bind anionic membranes containing PS in a purely electrostatic manner in the absence of Ca^{2+} (Kuo et al., 2009). This membrane binding is mediated via a polybasic strand, which contains consecutive lysine residues (Lys324, Lys325, Lys326, Lys327) forming a positively charged, Ca^{2+}-independent membrane binding surface (Figure 1-18). Models generated from the electron paramagnetic resonance depth parameters showed that, unlike the Ca^{2+}-dependent membrane binding mode of Syt1-C2B, which penetrated ~10Å below the phosphate plane of the bilayer, its Ca^{2+}-independent lipid binding had significantly lower affinity for the PC/PS membrane without penetrating the bilayer (Herrick et al., 2006; Kuo et al., 2009). Furthermore, isothermal titration calorimetry experiments showed that this polybasic patch on Syt1-C2B also binds membrane containing PIP_2 in the absence of Ca^{2+}, and the protein-membrane interaction was also enhanced in the presence of Ca^{2+} (Pérez-Lara et al., 2016). The interaction of the polybasic face with monovalent PS, which has a net charge of -1, is weaker compared to with multivalent PIP_2, which has a net charge near -4 at neutral pH (McLaughlin et al., 2002; Suh & Hille, 2008), suggesting the importance of ionic strength in determining lipid-binding affinity. A more recent study revealed another lipid-binding ‘arginine apex’ on Syt1-C2B, which consists of two highly conserved arginine residues (Arg398, Arg399) at the bottom loop opposite to the CBLs (Figure 1-18) (Nyenhuis et al., 2021). Previously, this arginine apex was proposed to facilitate the C2B domain to contact opposing bilayers as a bridge (Herrick et al., 2009; Xue et al., 2008). Recent data from site-directed spin labelling and

mutagenesis analysis confirmed the association of the 'arginine apex' with negatively charged membranes (contain PS or PIP_2) (Nyenhuis et al., 2021).

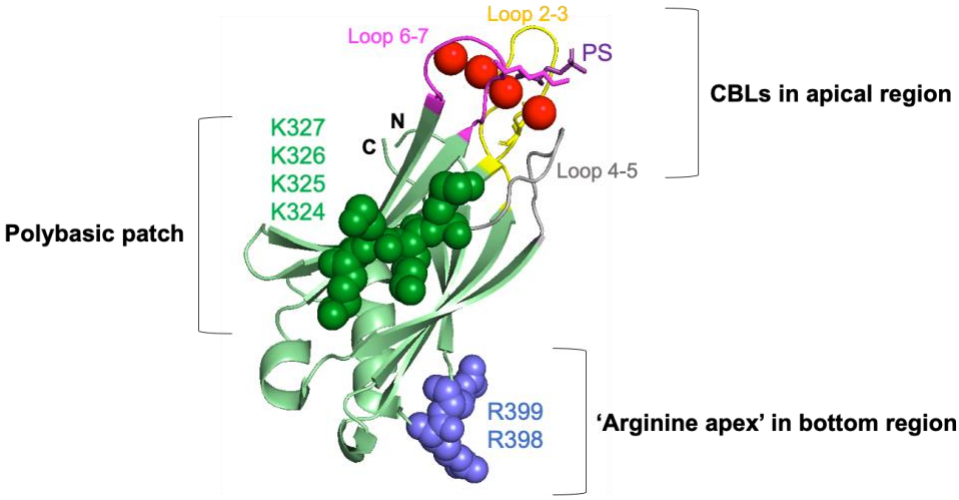


Figure 1-18. Model of Synaptotagmin-1 C2B domain (PDB: 2YOA). The apical CBLs (Loop 2-3: yellow, loop 4-5: grey, loop 6-7: magenta) are bound to Ca^{2+} ions (red spheres) and phosphoserine (PS, purple sticks). The arginine apex is on the opposite face of the CBLs, and contains two conserved Arg398, Arg399 residues shown in sphere representations (blue). The polybasic patch is located on the side face, consistent with the polybasic β-groove region reported in other C2 proteins (D. Zhang & Aravind, 2010). Consecutive lysine residues (Lys 324-327) forming this polybasic face are shown in sphere representations (green).

Whilst three independent lipid binding sites have been identified in Syt1-C2B, only the apical CBLs region has been experimentally confirmed to play a role in lipid-binding in canonical Notch ligands (Chillakuri et al., 2013; Suckling et al., 2017), although we cannot rule out the possibility of additional membrane-interacting sites. In addition, molecular dynamics analysis suggested that, whereas type II Ca^{2+}-independent C2 domains (e.g., PTEN, SHIP2, Smurf2) predominantly bind membranes via their apical loops (i.e., the CBLs), the type I counterparts (e.g., KIBRA, PI3KC2α, RIM2) tend to interact with the membrane noncanonically, using either the side, front, or back of their C2 β-sandwich (Larsen & Sansom, 2021). Thus, unlike Syt1-C2B, which has a type I topology, the type II C2 domains in Notch ligand are more likely to interact with the membrane predominantly using their apical loops.

1.5.4 Functionally important C2 domain in Notch ligands

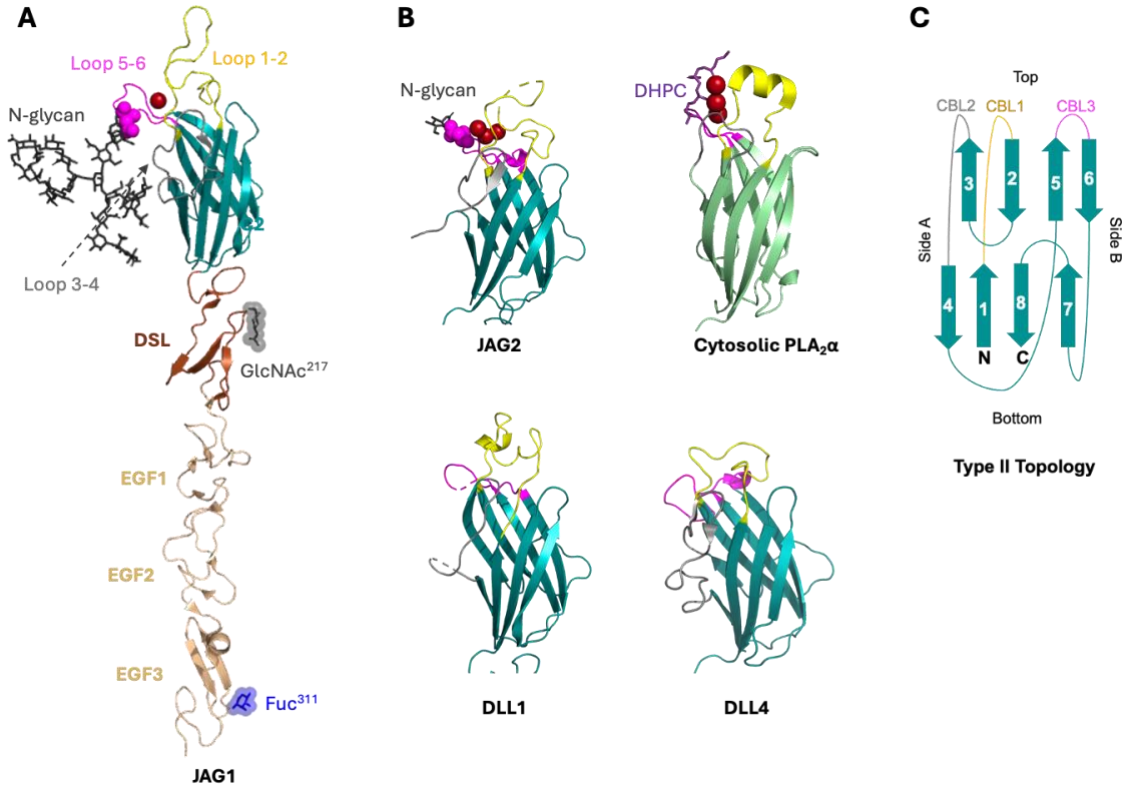


Figure 1-19. Structural features of the C2 domain in Notch ligands. (A) The structure of JAG1 C2-EGF3 (PDB: 4CC1) is shown in ribbon representation (C2: teal, DSL: orange, EGF: wheat). The Ca^{2+} ion bound at the apex of the C2 domain is drawn as a red sphere. A tetra-antennary form of a complex N-glycan on the C2 N143 residue (pink spheres) is modelled based on JAG2 (PDB: 5MWF) and *Drosophila* Delta structure (PDB: 7ALK) and functional experiments (Martins et al., 2021; Meng et al., 2022; Suckling et al., 2017). Loop β1-2 is shown in yellow, loop β3-4 in grey and loop β5-6 in magenta. Additional glycans are indicated including an N-glycan on N217 in the DSL domain and a O-fucose on T311 in the EGF3. (B) Structures of C2 domains of different Notch ligands are shown alongside cPLA2α-C2 (PDB: 6IEJ) which is in complex with DHPC lipid (purple) (Y. Hirano et al., 2019). The apical loops differ in length and conformation (JAG2 PDB: 5MW5, DLL1 PDB: 4XBM, DLL4 PDB: 5MVX), which may affect lipid-binding preferences. Loop β3-4 in Notch ligands are generally more sideways, as compared to the apical loops β1-2 and β5-6. The JAG1 and JAG2 C2 domains bind Ca^{2+} (red), unlike Delta family ligands. An N-glycan on loop β5-6 of JAG2 C2 domain is shown in dark grey. DHPC = 1,2-diheptanoyl-sn-glycero-3-phosphocholine. (C) C2 type II topology adopted by all canonical Notch ligands and cPLA2α. The putative lipid binding loops (CBL1, CBL2, CBL3) are highlighted in yellow, grey and magenta respectively.

The N-terminal C2 domain of Notch ligands (section 1.3.2.1), which was suggested to play a modulatory role in Notch signalling, has been found in canonical Notch ligands in all metazoan species studied so far (*Drosophila*, human, rat), with a type II topology consisting of eight antiparallel β-strands that form a β-sandwich conformation, whose folding is stabilised by a hydrophobic core (Figure 1-19) (Chillakuri et al., 2013; Kershaw et al., 2015; Luca et al., 2015, 2017; Martins et al., 2021; Suckling et al., 2017). The Serrate/Jagged family C2 domains bind Ca^{2+} (one Ca^{2+} in Jag1 and three Ca^{2+} in Jag2), whereas the Delta-like family C2 is Ca^{2+}-independent (Figure 1-19). Substitutions (D140/144A) removing the Ca^{2+}-binding ligands on the apical loop of JAG1 C2 resulted in reduced liposome binding and Notch signalling without affecting the binding affinity for Notch1 fragment (N-EGF14) (Chillakuri et al., 2013). In addition, a subset of human JAG1 variants associated with the genetic disease EHBA which have substitutions mapping to the C2 lipid-binding region, were found to cause a loss of membrane recognition, but not a loss of Notch binding (Suckling et al., 2017). These data suggest that C2 mediates lipid- and receptor- binding independently, likely through distinct interaction sites on the same domain.

Sequence alignments show that the β-strands of the C2 domain are relatively conserved among all ligands, whilst the three inter-strand connecting loops (equivalent to CBLs) at the apex of C2 domain (β1-β2, β3-β4, β5-β6), which form the putative lipid-binding region, are highly variable in length and conformation, suggesting membrane-binding properties may vary among ligands (Figure 1-19 &1-20). Intriguingly, whilst loops β1-β2 and β5-β6 are apparently pointing towards the apex, loop β3-β4 is located more sideways, suggesting that these loops may modulate different C2 binding orientations at the membrane (Figure 1-19). In addition, all Jagged family ligands (Jag1, Jag2, Serrate) but not Delta-like family ligands, except for *Drosophila* Delta, contain a conserved N-glycosylation site in their C2 apical loop β5-β6, which has been confirmed to be modified by structural data and PNGase F digestion analysis (Figure 1-19) (Martins et al., 2021;

Meng et al., 2022; Suckling et al., 2017). The different sugar modifications on the ligand C2 loop region may reflect different lipid-binding specificities for Notch ligands. *In vitro* assays have demonstrated different binding preferences of JAG1 and DLL4, which have variable C2 apical loops, for SM- or ganglioside- rich liposomes respectively (Suckling et al., 2017). *In vivo* experiments have previously shown that glycosphingolipids, one of the main components of lipid rafts, play important roles in Notch signalling in both *Drosophila* and *C.elegans*, suggesting physiological relevance of the binding preference observed (Hamel et al., 2010; Katic et al., 2005). Further functional analyses of the Notch ligands C2 domain showed that Notch addition to liposome/ligand assays promoted association, suggesting that a C2-mediated ternary complex may be formed by receptor, ligand, and membrane to allow optimal Notch signalling (Suckling et al., 2017). In Notch1/Dll4 complex, the receptor binding site on C2 is formed by an inter-strand loop (β2-β3) at the base of the domain, stabilised by a disulfide bridge between Cys 61 and Cys 74 (Luca et al., 2015). Likewise, in Notch1/Jag1 complex, the long loop between β2 and β3 forms the binding site for Notch, interacting directly with an O-fucose on EGF12 (Luca et al., 2017).



Figure 1-20. Sequence alignment of human and *Drosophila* canonical Notch ligands C2-domain. Regions in grey (numbered) indicate the eight anti-parallel β-strands forming the C2 domain, which are relatively well-conserved across Notch ligands compared to the loop regions. Residues in loop β1-2 are shown in yellow, in loop β3-4 are coloured in light grey, and in loop β5-6 are coloured in magenta. The Serrate/Jagged family ligands generally have a longer β1-2 loop and a shorter β5-6 loop compared to the Delta/Delta-like family ligands. The β3-4 loop in JAG2 is notably longer than in other ligands. Pairs of Cys residues that form disulfide bonds are highlighted in yellow and connected by yellow brackets. Symbols: an asterisk (*) indicates a fully conserved residue, a colon (:) indicates conservation between groups of strongly similar properties, a period (.) indicates conservation between groups of weakly similar properties.

1.6 Project Aims

This research project focuses on investigating the functional significance of the C2 lipid-binding properties of human Notch ligands in health and disease. Specifically, the research will: 1) create and purify DLL4 C2-loop variants using COSMIC database and protein-engineering; 2) use biochemical assays and high-throughput methods (ELISA, flow cytometry, etc.), complemented by *in silico* analysis (MD simulations), to assess the Notch receptor binding affinities and lipid membrane interactions of these ligand variants; 3) measure the capacity of WT, protein-engineered, and COSMIC-variant ligands to activate Notch, in reporter cell lines; 4) investigate Notch activation capacity of these variants in physiologically relevant cell types (HUVECs). In addition, following on from an analysis of the JAG1 C2 domain (work by Dr Yao Meng), further study of a functionally important N-glycan site on JAG1 C2 β5-6 loop was performed using similar approaches, which allows comparison of properties between JAG1 and DLL4 C2 domains. Overall, the project aims to provide insight into the molecular basis of how Notch signalling is modulated by C2-mediated membrane interactions in a ligand-dependent manner.

Chapter 2: Materials and Methods

2.1 Mutagenesis

2.1.1 Primer design

Oligonucleotide primers used for mutagenesis and sequencing were designed using SnapGene and ordered from Thermo Fisher Scientific. Primer pairs used for qPCR were

designed based on commercially available primer sequences (OriGene). The primer sequences are in general within 18-30 nucleotides with 40-60% GC content and no strong secondary structure, evaluated by Sigma-Aldrich OligoEvaluator™. The melting temperature (T_m) of the primers was calculated by SnapGene, which uses a nearest neighbour thermodynamic algorithm to account for internal mismatches, loops and dangling ends (SantaLucia & Hicks, 2004). See Appendices 8.2 for the full list of primers used in this project.

2.1.2 Site-directed mutagenesis using overlap extension PCR

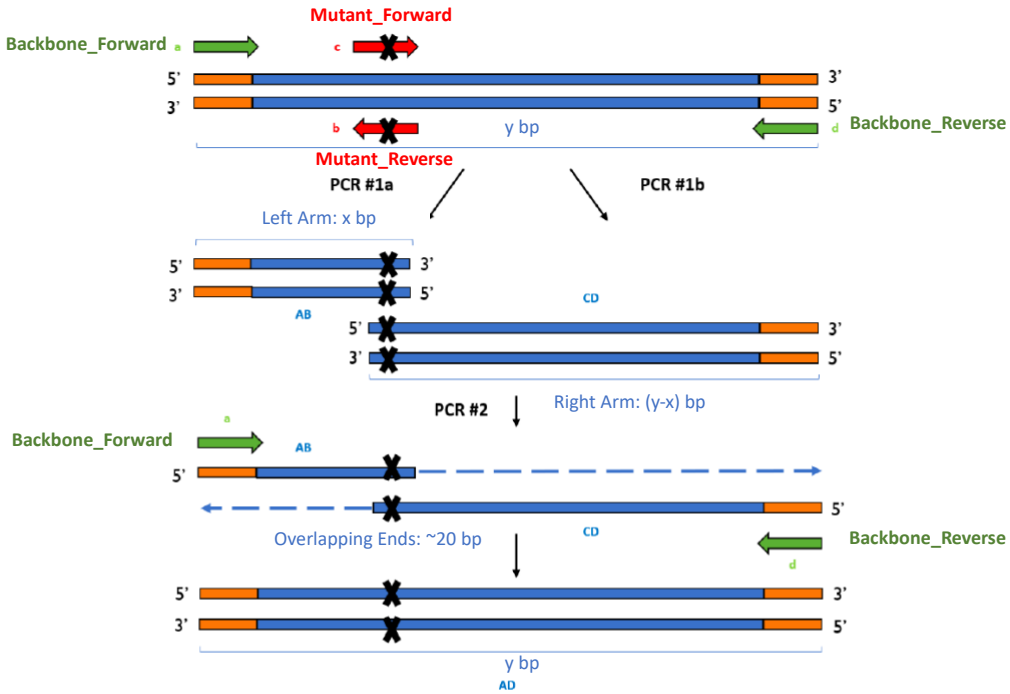


Figure 2-1. Overlap extension PCR. The open reading frame is shown in blue, and DNA from the plasmid is shown in orange. Backbone primers are depicted as green arrows (a and d), mutagenesis primers are depicted as red arrows (b and c). The first round of PCR uses the primer pair a and b to produce the left arm fragment (AB), whilst the primer pair c and d produces the right arm fragment (CD). These two fragments have a ~20bp overlapping region, which allows them to anneal during the second round of PCR. Using the backbone primers a and d, as well as extending their own 3' overlap to make the complementary sequence, fragments AB and CD act as both templates and primers in PCR #2 to produce the complete insert (AD) with the specific mutation (black cross) incorporated.

$JAG1_{N\text{-}EGF3\text{-}Fc\text{-}His}$ was expressed from plasmid *pHL-sec*, whereas $DLL4_{N\text{-}EGF3\text{-}Fc\text{-}His}$ was expressed from plasmid *pcDNA-3.1(+)*. Desired mutations were introduced to these plasmids using overlap extension PCR (Figure 2-1), which consists of two rounds of PCR. Mutagenesis primers (Appendix 8.2.1) were designed containing specific mismatch base pair(s) to produce left arm and right arm sequences with the desired substitution or deletion after the first round of PCR. Target bands in the left arm and right arm products were visualised on and extracted from an agarose gel, and subsequently subjected to a second round of PCR to produce the complete insert sequence containing the desired mutation. PCR reactions were performed using the KOD Hot-Start Polymerase kit (Merck) following the protocol suggested by the manufacturer (Appendix 8.2.3).

2.1.3 Restriction enzyme digestion and ligation

The mutant insert sequence obtained from the overlap extension PCR as well as the wildtype plasmid were double-digested using appropriate restriction enzymes, such as *EcoRI-HF* and *XhoI* in the case of *pcDNA3.1(+) hDLL4-NE3-Fc-His* plasmid (Figure 2-2), otherwise *EcoRI-HF* and *KpnI* in the case of *pHL-sec hJAG1/2-NE3-Fc-His* plasmid. Digestion was performed using restriction enzymes and CutSmart buffer from New England Biolabs (NEB) following the protocol as suggested by the manufacturer (Appendix 8.2.4). The reaction mix was incubated at 37°C for at least 1hr, and then the digested DNA fragments were visualised on an agarose gel where the target bands were extracted from. DNA products containing complementary sticky ends from restriction digestion were subsequently subjected to ligation using the Rapid DNA Ligation kit (Roche) and the protocol recommended by the manufacturer (Appendix 8.2.4). The ligation mix was incubated at room temperature for 1hr. After incubation, 5µL of ligation product was subsequently transformed into 50µL of NEB 5-alpha Competent *E. coli* cells.

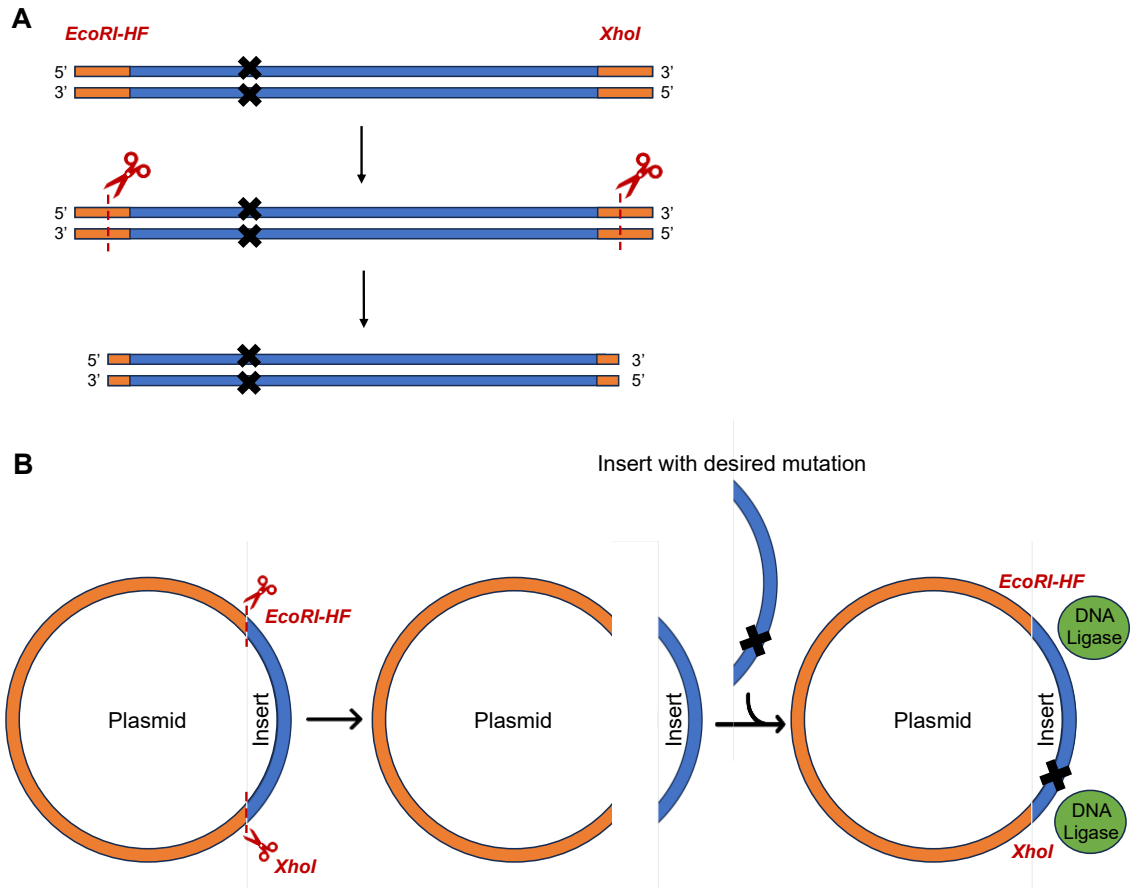


Figure 2-2. Restriction digestion and ligation. (A) Digestion of the insert DNA produced from overlap extension PCR using restriction enzymes, which gives a shorter insert DNA with sticky ends. (B) Digestion of the plasmid using the same restriction enzymes cleaves out the wildtype insert DNA, producing an 'empty' vector with complementary sticky ends ready for ligation. Mixing the mutant insert DNA with 'empty' vector in the presence of DNA ligase produces full-length plasmid containing the desired mutation.

2.1.4 Agarose gel electrophoresis and gel extraction

Agarose gels were prepared using TBE buffer (Appendix 8.2.2A) and SYBR™ Safe DNA gel stain (Invitrogen™) diluted to a final concentration of 1µL dye per mL gel (Appendix 8.2.5). DNA samples were mixed with 6x DNA loading dye (NEB) in a 5:1 ratio and run alongside a 100bp or 1kb DNA ladder (NEB). Gel casting and electrophoresis were carried out in a DNA electrophoresis tank (Bio-Rad) at 80V for 1hr, followed by DNA bands visualisation using a UV transilluminator (Bio-Rad Gel Doc XR+ System) and photo-taking on a gel documentation system (Bio-Rad Image Lab software). For gel

extraction, target bands were excised using a single edge razor blade and transferred to Eppendorf tubes, thereon the DNA fragments were extracted using a QIAquick Gel Extraction kit (QIAGEN) and the manufacturer's suggested protocol.

2.1.5 DNA/RNA concentration measurement

The concentration of DNA and RNA samples was determined by measuring absorbance at 260nm using a NanoDrop spectrophotometer (Thermo Scientific™). The ratio of absorbance at 260nm and 280nm (260/280) was used to assess the purity of DNA and RNA, which generally should have a ratio ~1.8 for 'pure' DNA or ~2.0 for 'pure' RNA.

2.1.6 Transformation

High efficiency transformation was performed using NEB 5-alpha Competent *E. coli* cells (NEB) and following the manufacturer's recommended protocol (Appendix 8.2.6). 20-50µL of transformation mix was plated onto selection plates containing appropriate selection reagent and incubated at 37°C overnight. For *E. coli* expansion, a single colony was transferred into 100mL 2xYT Broth medium (MP Biomedicals) containing appropriate selection reagent and incubated overnight at 37°C with shaking at 150rpm.

2.1.7 Plasmid purification and DNA sequencing

Plasmids were extracted from expanded *E. coli* culture using QIAGEN Plasmid Mini, Midi and Maxi Kits, following the protocols suggested by the manufacturer. Purified plasmid DNA was sent for Sanger sequencing using the service provided by Source BioScience. The sequencing data were read using SnapGene Viewer (version 7.0.3), the open reading frames were identified using ExPASy Translate tool (https://web.expasy.org/translate/) and the desired polypeptide sequences were verified

using EMBL-EBI's EMBOSS Needle Pairwise Sequence Alignment tool (https://www.ebi.ac.uk/Tools/psa/emboss_needle/).

2.2 Tissue culture

2.2.1 HEK293T/HEK293S cells

2.2.1.1 Maintenance and subculture

Human embryonic kidney (HEK) 293T or HEK293S cells and their derivatives were grown on tissue-culture treated filter-cap polystyrene flasks (Greiner Bio-One) in Dulbecco's modified Eagle's Medium (DMEM, Gibco™), supplemented with 10% fetal bovine serum (FBS, Gibco™), 50 U/mL penicillin and 0.05 mg/mL streptomycin (Sigma), and 2mM L-glutamine (Gibco™). Cells were maintained in a 37°C humidified incubator supplied with 5% CO_2. When cell confluence was reaching 80-100%, which usually took 3-4 days, cells were subcultured, usually at a 1:10 ratio (Appendix 8.2.7). The viability and density of the cells can be determined using the trypan blue exclusion method.

2.2.1.2 Thawing and cryopreservation

Frozen cells were stored in liquid nitrogen until ready to use. A cryovial containing ~1E7 cells in 1mL of freezing medium was removed from liquid nitrogen and immediately thawed in a 37°C water bath. Just before the cells were completely thawed, the vial surface was decontaminated using 70% ethanol and the cells were transferred to a sterile 50mL falcon tube containing 9mL complete medium, which has been prewarmed to 37°C. The cells were centrifuged at 1000 rpm for 3 minutes, resuspended in ~10mL complete medium, and transferred to a T75 flask. After incubation overnight at 37°C, which allows viable cells to attach to the bottom of the flask, the old medium was aspired on the next day and replaced with fresh complete medium. The cells were maintained to 80-90% confluency and then proceeded to subculture. Generally, the cell viability should be >80%, and if the viability is below 60%, a new batch of cells should be thawed. For

cryopreservation, desired quantity of 293T/S cells were cultured to 80-90% confluency, harvested, and resuspended in appropriate volume of ice-cold freezing medium to yield a final density of ~1E7 cells/mL. The freeze medium was made of FBS containing 10% (v/v) DMSO (Sigma), sterilised by filtration through a 0.22μm pore size membrane (Millex-GP syringe filter, Millipore). The freeze medium cell suspension was dispensed into cryotubes as 1mL aliquots, after which the cells were put into an automated, controlled-rate freezing apparatus (Corning® CoolCell™) and kept at -80°C overnight, and subsequently transferred to liquid nitrogen storage.

2.2.2 HEK293F cells

2.2.2.1 Maintenance and subculture

HEK293F (FreeStyle™) cells were cultured in Freestyle™ 293 Expression Medium (Gibco™) using a 37°C humidified orbital shaking incubator (135rpm) supplied with 8% CO_2. The cells were maintained up to 3E6 cells/mL in a volume of 25-40mL using a 125mL polycarbonate Erlenmeyer flask with vented cap (Corning®) or a volume of 80mL using a 250mL Erlenmeyer flask (Corning®). HEK293F cells were subcultured typically every 48-72hr, when the cell density was between 1-3E6 viable cells/mL. Cell density and viability were determined using trypan blue exclusion, after which cells were diluted using fresh, prewarmed medium and seeded to a new shaker flask at 0.1-0.2E6 viable cells/mL in the desired final volume. HEK293F suspension culture was split without centrifugation, and the cell viability should be >90%.

2.2.2.2 Thawing and cryopreservation

HEK293F cells were thawed and frozen using methods described in Section 2.2.1.3 with some modifications. Frozen HEK293F cells were stored in a cryovial containing 1mL of cells at ~1E7 viable cells/mL in 90% Freestyle™ 293 Expression Medium and 10% DMSO. Cells were thawed and transferred directly into a 125mL sterile shaker flask

containing 30mL prewarmed medium without centrifugation. After culturing overnight, determine the cell density and viability, which should generally have a viability >70%, and subculture the cells at 0.3E6 viable cells/mL (Section 2.2.2.1).

2.2.3 HEK293 mN1/2-NLuc/CLuc-RBPJ reporter cells

HEK293 mN1/2-NLuc/CLuc-RBPJ reporter cells were initiated, maintained, and frozen using the same methods for HEK293T (Section 2.2.1) with some modifications. Cells were maintained in complete DMEM supplemented with 0.4µg/mL puromycin and 100µg/mL hygromycin and split 1:5 when cell confluence was reaching 80-100%, which usually took 3-4 days.

2.2.4 CHO hN1G4^{esn} reporter cells

CHO hN1G4^{esn} reporter cells were initiated, maintained, and frozen using the same methods for HEK293T (Section 2.2.1) with some modifications. Cells were maintained in complete MEM Alpha (Gibco™) (containing 10% FBS, 50 U/mL penicillin and 0.05 mg/mL streptomycin, and 2mM L-glutamine), supplemented with 10µg/mL blasticidin, 625µg/mL geneticin, and 400µg/mL zeocin.

2.2.5 Schneider-2 (S2) *Drosophila* cell line

2.2.5.1 Maintenance and subculture

S2 cells (EXPRES^{2}ION® Biotechnologies, Denmark) were maintained in EX-CELL® 420 serum-free medium (Sigma) in vented shaker flasks (Corning®) with appropriate culture volume as described in Section 2.2.2.1. The cells were cultured using a 25°C orbital shaking incubator at 100-115 rpm and split every 3-4 days. For subculture, an aliquot of cell suspension was diluted 1:10 with PBS for counting, and the cell density and viability were determined using trypan blue exclusion. Cells were centrifuged at 330xg for 5min

and resuspended in room-temperature, fresh medium at a density of 5E6 cells/mL for FBS-containing media or 8E6 cells/mL for FBS-free media.

2.2.5.2 Thawing and cryopreservation

Frozen S2 cells were stored in a cryovial containing ~2.5E8 cells in 1mL freeze medium consisting of 40% EX-CELL® 420, 50% FBS and 10% DMSO. Cells were thawed and transferred directly into a 125mL sterile shaker flask containing 25mL 25°C medium (EX-CELL® 420 + 10% FBS). After incubation at 25°C and 100rpm for 24-48hr, the cells were split to 8E6 cells/mL in 25mL fresh medium (Section 2.2.5.1). Cell culture initiated from frozen stock should be grown for two passages in FBS-containing media before removing the FBS. S2 cells were frozen using methods described in Section 2.2.1.3 with some modifications. For cryopreservation, S2 cells were split at 5E6 cells/mL in EX-CELL® 420 + 10% FBS and incubated at 110rpm at 25°C for 48hr. Cells were centrifuged at 125xg for 3min and resuspended to 40-250E6 cells/mL in freeze medium.

2.2.6 Primary Human Umbilical Vein Endothelial Cells (HUVECs)

HUVECs (Lonza) were bought at passage 0. Cells were initiated, maintained, and frozen using the same methods for HEK293T (Section 2.2.1) with some modifications. HUVECs were maintained in EGM™-2 BulletKit™ Medium (Lonza, medium supplemented with 2% FBS, 0.04% hydrocortisone, 0.4% hFGF-B, 0.1% VEGF, 0.1% R3-IGF-1, 0.1% ascorbic acid, 0.1% hEGF, 0.1% GA-1000, and 0.1% heparin (v/v)). The growth medium was refreshed 16-24hr after seeding and every 48hr thereafter. Media volume was increased to 1.5mL/5cm^2 when cell confluence is 25-45% and further increased to 2mL/5cm^2 when cell confluence is above 45%. Cells were subcultured at 1:5 ratio when they were 80-100% confluent, and the growth rate would vary for each batch of cells. Trypsinisation was performed at 37°C for 3-5 minutes until ~90% of the cells were rounded up. HUVECs can be used for experiments from passage 2 (p2) to p7 but should

not be used beyond p7. HUVECs were frozen at 2E6 viable cells/mL in cryopreservation media consisting of 80% complete EGM™-2, 10% DMSO and 10% FBS. Cells were thawed and transferred directly into a T75 flask containing 15mL prewarmed medium without centrifugation.

2.3 Protein synthesis and purification

JAG1 constructs were produced using HEK293T cells (Aricescu et al., 2006), JAG1 lacking complex N-glycan modifications was produced using HEK293S GnTI$^-$ cells (Y.-C. Lin et al., 2014), whilst DLL4 proteins were expressed by HEK293F (FreeStyle™) cells, all through a transient transfection system. NOTCH receptors were produced from *Drosophila* Schneider 2 (S2) stable cell lines. See Appendix 8.2.8 for protein sequences.

2.3.1 JAG1/2 constructs from HEK293T/S

2.3.1.1 Large scale transfection of HEK293T/S

For large scale protein purification, an 875 cm^2 5-layer cell culture flask (each layer is 175 cm^2, Falcon®) was used to expand HEK293T/S cells. To track cell confluency, a T175 flask was seeded at the same cell density as the 5-layer flask. Each confluent T175 flask can be split 1:6 into 1x 5-layer flask and 1x T175 flask in 125mL and 25mL complete DMEM (Section 2.2.1.1), respectively. Transient transfection can be conducted when the cells are 80-90% confluent, which usually takes 3-4 days. On the day of transfection, a transfection mix (Table 2-1) was prepared and incubated at room temperature for 20min. Meanwhile, the old medium was removed from the 5-layer flask and replaced with100mL fresh DMEM (no additive) without disturbing the cell layer seeded. The transfection mix was then distributed into flasks and mixed gently with the medium. HEK293T/S cells were incubated for ~90hr before medium collection.

Component	Amount per T175	Amount per 5-layer
DMEM (no additive)	5 mL	25 mL

PEI (1 mg/mL stock)	100 µg	500 µg (500 µL stock)
Plasmids	50 µg	250 µg

Table 2-1.Transfection mix for HEK293T/S cells.

2.3.1.2 Culture medium collection

For harvesting, HEK293T/S culture medium was collected into 50mL falcon tubes and centrifuged at 4°C, 4400rpm (JLA-16.250, Beckman Coulter) for 10min. The supernatant was filtered using a sterile disposable bottle top filter with 0.2µm pore size SFCA membrane (Thermo Scientific™) and diluted with 3x volume of pre-chilled washing buffer (50mM Tris, 200mM NaCl, pH 9.0). A small aliquot of filtered medium and cell pellet resuspended in PBS were reserved for Western blotting check.

2.3.2 DLL4 constructs from HEK293F

2.3.2.1 Large scale transfection of HEK293F

The expression and secretion levels of $DLL4_{NE3}$ fragments in HEK293T cells were generally low, making protein purification from HEK293T challenging. Therefore, HEK293F, which expressed DLL4 better than HEK293T, were used alternatively. HEK293F cells were subcultured for a minimum of 5 passages before use in transfection to allow recovery from thawing. On the day of transfection, the cell density and viability were determined, which should be about 1.2-1.5E6 cells/mL with a viability >90%. Cells were diluted to 1E6 cells/mL using fresh, prewarmed medium in a volume of 80mL in each 250mL flask. A transfection mix (Table 2-2) was prepared using plasmid DNA and FreeStyle™ MAX Reagent (Gibco™) diluted in OptiPro™ SFM (Gibco™), and incubated at room temperature for 10min for complex formation. Plasmids used for HEK293F transfection were sterilised by filtration through a 0.22µm pore size membrane (Millex-GP syringe filter, Millipore). After incubation, 3.2mL of DNA-lipid mixture was added dropwisely to the 250mL flask containing 80mL cell suspension while slowly swirling the

flask. Cells were incubated in an orbital shaking incubator at 37°C and 135rpm with 8% CO_2 for ~96hr before medium collection.

Component	Amount per 80mL	Total volume (in OptiPro)
MAX Reagent	112 µL	1.6 mL
Plasmids	112 µg	1.6 mL

Table 2-2. Transfection mix for HEK293F cells.

2.3.2.2 Culture medium collection

HEK293F culture medium was collected into 50mL falcon tubes and centrifuged at 4°C, 3500rpm (JLA-16.250, Beckman Coulter) for 10min. The supernatant was filtered using a sterile disposable bottle top filter with 0.2µm pore size SFCA membrane (Thermo Scientific™) and diluted with 2x volume of pre-chilled MES buffer (20mM MES, 200mM NaCl, pH 6.5). A small aliquot of filtered medium and cell pellet resuspended in PBS were reserved for Western blotting.

2.3.3 NOTCH constructs from S2

2.3.3.1 Protein expression from S2 stable lines

DNA encoding the Notch receptor constructs was subcloned into expression vector pEXS2-2 to generate S2 cell lines stably expressing human NOTCH receptors (Expres2ion® Biotechnologies, Horsholm, Denmark). S2 stable lines expressing human NOTCH constructs were established and maintained using methods described in Section 2.2.5 and were further expanded to 500mL culture at 8E6 cells/mL in a 2L filter cap cell culture roller bottle (Greiner) without centrifugation. After ~96hr of incubation, the cell suspension was collected and centrifuged at 4°C, 4400xg (JLA-8.1000, Beckman Coulter) for 20min. The supernatant was filtered using a sterile disposable bottle top filter with 0.2µm pore size SFCA membrane (Thermo Scientific™). A small aliquot of filtered medium and cell pellet resuspended in PBS were reserved for Western blotting.

2.3.4 Chromatography

2.3.4.1 Immobilised metal affinity chromatography (IMAC)

Filtered and diluted culture medium (from HEK293T/S/F or S2) was allowed to flow through a 1mL His-Tag Purification Column (Roche) containing immobilised Nickel ions, facilitated by a peristaltic P-1 pump (GE Healthcare) at a 0.4-0.8mL/min flow rate. The column was then washed with ~50mL washing buffer at a 1mL/min flow rate to remove any unbound protein. Protein was eluted from the column by 20mL elution buffer at a 1mL/min flow rate and collected in a 10kDa MWCO polyethersulfone ultrafiltration tube (Vivaspin®, Cytiva). The eluted protein was concentrated down to ~1mL by centrifuging at 3000xg (5702/R, eppendorf) at 4°C, before being purified by size-exclusion chromatography (SEC). Samples of flow-through, wash-through and eluate were reserved for Western Blot analysis using an anti-6X His tag antibody (ab1187, Abcam) to confirm the presence of the protein of interest. See Appendix 8.2.9 for IMAC buffers.

2.3.4.2 Size exclusion chromatography (SEC)

The concentrated protein eluate was injected onto a AKTA Pure FPLC liquid chromatographic system (Cytiva) and purified using a Superdex™ 200 Increase 10/300 GL column (GE Healthcare). The system was pre-washed with filtered MilliQ water and equilibrated with filtered gel filtration buffer. For each run, 500µL protein sample was injected onto the column at 0.6 mL/minute flow rate. The presence of protein in the flow-through was monitored using a 280nm wavelength UV monitor and analysed using UNICORN 7.3 software. The elution peak fractions were collected and analysed using SDS-PAGE to confirm protein presence and purity. Fractions containing the protein of interest were pooled and concentrated at 4°C using an ultrafiltration tube (Vivaspin®, Cytiva). Purified protein was frozen using liquid Nitrogen and stored at -80°C. See Appendix 8.2.9 for buffers used for SEC.

2.3.5 Protein concentration measurement

The concentration of protein samples was determined by measuring absorbance at 280nm (A_{280}) using a NanoDrop spectrophotometer (Thermo Scientific™). The protein concentration was calculated based on the molecular weight (MW) and extinction coefficient (ε) of the specific protein construct using the following equations:

$$\text{Molar concentration} = (A_{280}/\varepsilon)$$

$$\text{Concentration in ng/µL} = (A_{280}/\varepsilon) \times \text{MW } (A_{280}/\varepsilon) \times 1000$$

The theoretical extinction coefficient and MW for each protein can be calculated using ProtParam tool on the ExPASy bioinformatics server.

2.3.6 SDS-PAGE

Gels were poured in two stages in a 1.5mm gel casting stand (Bio-Rad) (Appendix 8.2.10). The resolving gel was poured first and allowed to set under a layer of isopropanol. After the gel had set, the isopropanol was removed and the stacking gel was poured, after which a gel comb was inserted to create sample lanes. Protein samples for analysis were mixed in a suitable volume with either non-reducing or reducing loading dye (Appendix 8.2.2G) and boiled at 100°C for 10 minutes. Gels were run at 150V for 60 minutes in electrophoresis buffer (0.1% SDS, 30mM Tris, 250mM glycine, pH 8.3) and stained using SimplyBlue™ SafeStain (Invitrogen™) overnight. After staining, gels were washed with MilliQ water overnight. Gel images were taken using a scanner.

2.3.7 Western Blot

Samples for Western Blot analysis were first run on an appropriate SDS-PAGE gel (Section 2.3.6). After gel electrophoresis, proteins were transferred by immunoblotting to a nitrocellulose membrane (Amersham™) in ice-cold blotting buffer (Appendix 8.2.2I) at 100V for 90 minutes using the Mini Trans-Blot® Cell blotting electrodes (Bio-Rad). After blotting, the nitrocellulose membrane was transferred to fresh blocking buffer (PBS

containing 5% skimmed milk powder, 0.1% Triton X-100) and blocked at room temperature for 1hr. After blocking, primary antibody (HRP conjugated) was added to fresh blocking buffer at an appropriate dilution and incubated with the membrane for 1hr on a roller mixer (60rpm). The membrane was then washed 5 x 4 minutes with PBST buffer (Appendix 8.2.2J) to remove any unbound antibody. After washing, excess buffer was removed, and 1:1 mixed ECL™ Western Blotting Analysis System reagents (Amersham™) was added to nitrocellulose membrane and left to develop for 1 minute. Excess reagent was removed, and the membrane was gently dried and fixed by cling film on a cassette before exposing with chemiluminescence film (Amersham™) in a dark room. The film was developed using an OPTIMAX® 2010 X-Ray Automatic Film Processor (PROTEC X-ray technology).

2.3.8 PNGase F digestion of Notch ligands

Deglycosylation of ligand proteins was performed under nondenaturing reaction conditions using PNGase F (500,000 U/mL, P0704, NEB). 2µg of purified Notch ligand was combined with 2µL of 10X GlycoBuffer 2 (0.5M Sodium Phosphate, pH 7.5, NEB) and H_2O to make a 20µL total reaction volume. 0.2µL PNGase F was added per reaction and incubated at 37°C for 4-24hr. A positive control was included alongside, which was an aliquot of protein subjected to incubation under the nondenaturing reaction conditions without adding PNGase F. After incubation, the extent of deglycosylation was assessed by mobility shifts on SDS-PAGE gels (Section 2.3.6 & 2.3.7).

2.4 Notch activation assays

2.4.1 Split-luciferase assay by HEK293 mN1/2-NLuc/CLuc-RBPJ cells

Split-luciferase Notch activation assay was performed using HEK293 mNotch1/2-NLuc/CLuc-RBPJ reporter cells as previously described (Figure 2-3) (Ilagan et al., 2011). Purified ligand Fc-tagged constructs (10ng/µL, 50µL/well) in HBS buffer (Appendix

8.2.2K) were immobilised on 96-well tissue culture plates (Corning® flat clear bottom black TC-treated polystyrene microplates) overnight at 4°C two days prior to assay. One day prior to assay, the plates were washed once with 200µL/well HBS buffer, and Notch split-luciferase reporter cells were seeded onto the immobilised ligand (4E4 cells in 200µL complete DMEM per well). Luciferin signal of Notch luciferase reporter cells was measured 24hr after culture at 37°C. On the day of signal detection, the cells were gently washed once with 200µL/well HBS buffer. 100µL/well luciferin substrate solution (150µg/mL D-luciferin, 1mM $MgCl_2$, 0.1% glucose in HBS buffer) was then added, followed by 10 times pipetting mix, and the luminescence signal was measured immediately by a PHERAstar *FS* microplate reader (BMG LABTECH).

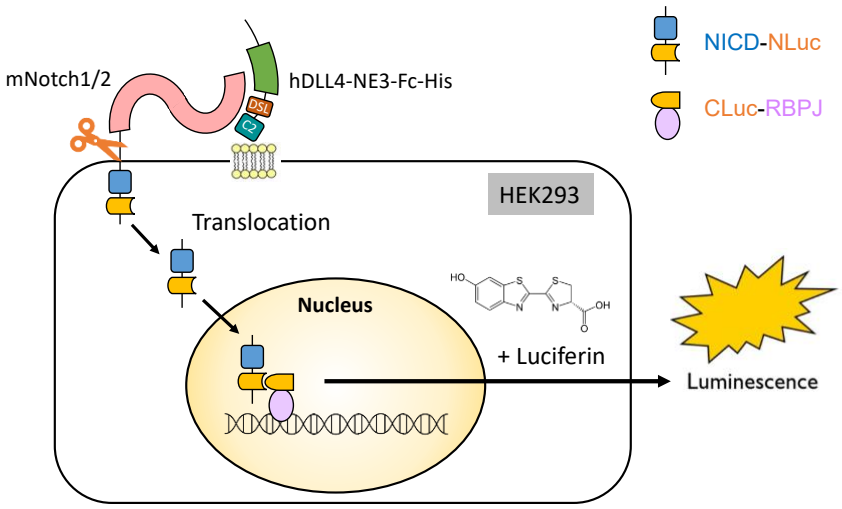


Figure 2-3. Notch activation reported by HEK293 mNotch1/2-NLuc/CLuc-RBPJ reporter cells. Cartoon illustrating the luciferase complementation imagining reporter system, which utilises the association between NICD and RBPJ to reform the enzymatically active luciferase from NLuc and CLuc.

2.4.2 YFP-expression based assay by CHO-K1 hN1G4^{esn} reporter cells

YFP-expression based Notch activation assay was performed using CHO-K1 hN1G4^{esn} reporter cells as previously described (Figure 2-4) (Sprinzak et al., 2010). CHO-K1 cells stably expressing hNOTCH1(ECD)-Gal4 and H2B-YFP controlled by an upstream UAS promoter were established and maintained as described in Section 2.2.4. Cells were split

1:3 into complete MEM Alpha three days prior to assay. Ligand coating and cell seeding into 96-well microplates were performed as described in Section 2.4.1. For PNGase F digested ligand proteins (Section 2.3.8), 96-well plates were pre-coated with 10ng/μL recombinant protein G (21193, Pierce, Thermo Scientific™) overnight at 4°C for protein adhesion. YFP signal of CHO-YFP reporter cells was measured 48hr after culture at 37°C. Cells were trypsinised and resuspended in 100μL/well PBS and kept on ice. YFP signal was measured by analysis of 10,000 single cells using the BD LSRFortessa X20 flow cytometer (excitation/emission 488/530nm).

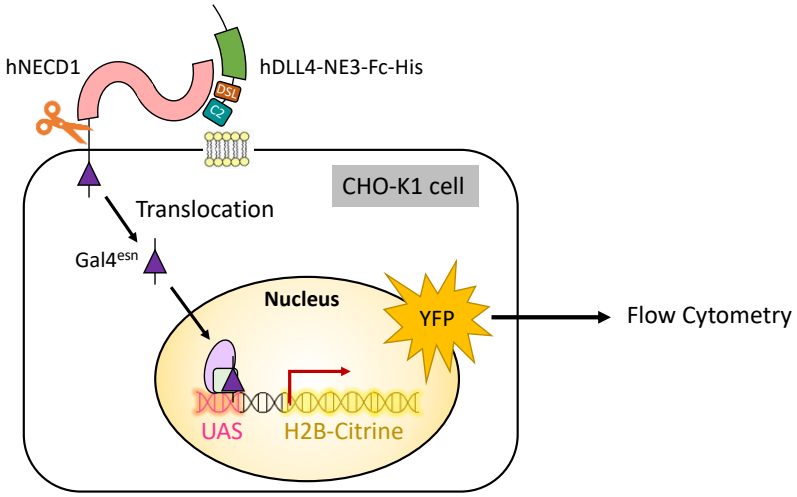


Figure 2-4. Notch activation reported by CHO-K1 hN1G4^{esn} reporter cells. Cartoon illustrating the YFP-expression based assay, which monitors the transcriptional response of the H2B-Citrine reporter upon ligand-induced Notch activation using a chimeric hNECD1-Gal4^{esn} receptor. The YFP reporter gene is downstream of a UAS promoter that is targeted by the Gal4^{esn} activator.

2.4.3 ELISA-based ligand immobilisation assay

Ligand immobilisation on 96-well tissue culture plates was assessed by an ELISA-based assay. 96-well tissue culture plates were coated with purified His-tagged ligand constructs as described in Section 2.4.1. After coating at 4°C overnight, the plate was washed once with HBS buffer (Appendix 8.2.2K) and blocked with 200μL/well 4% (w/v) BSA (Sigma-Aldrich) in the same buffer for 1hr. All incubation steps were done on a rocking shaker (~40rpm) at room temperature. After the plate blocking step, HBS buffer

washes were performed three times to remove remaining BSA. An HRP-conjugated anti-His tag antibody (ab1187, Abcam) with a 1:2000 dilution (0.5ng/μL) in HBS buffer was added (50μL/well) and incubated for 1hr, after which four washes with washing buffer and two subsequent washes with HBS buffer were performed. 100μL/well freshly prepared HRP substrate solution (Appendix 8.2.2P) was added and the absorbance signal at a wavelength of 415nm (A_{415}) was measured immediately by a PHERAstar *FS* microplate reader (BMG LABTECH).

2.4.4 Quantitative reverse transcription PCR (RT-qPCR) assay by HUVECs

2.4.4.1 HUVECs culture for RT-qPCR assay

HUVECs (to passage 7, Lonza) were maintained as described in Section 2.2.6. Cells were grown to near 100% confluency and EGM-2 medium was refreshed to allow growth for another 24hr. Meanwhile, 6-well tissue culture plates (flat bottom, Corning® Costar®) were coated with BSA (as a reference sample) or purified Fc-tagged ligand constructs (10ng/μL, 350μL/well) at 4°C overnight. After protein coating, extra liquid was aspired and HUVECs were seeded onto the immobilised ligand (1E5 cells/mL, 2.5mL/well). Cells were harvested for RNA extraction 24hr after culture at 37°C (Figure 2-5).

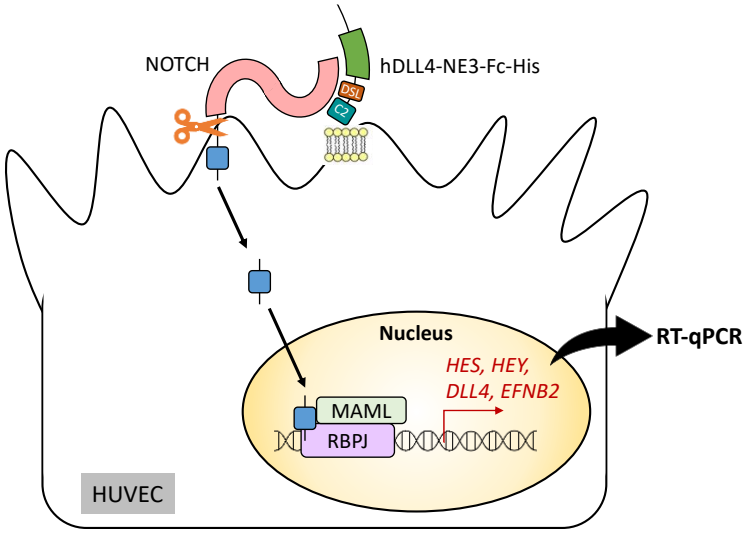


Figure 2-5. Notch activation reported by HUVECs. Cartoon illustrating the RT-qPCR assay, which monitors the transcriptional response of Notch target genes, especially the DLL4-

selective marker *EFNB2*, upon ligand-induced Notch activation (Iso et al., 2006). HUVECs are known to express all four Notch paralogues (NOTCH1-4), four ligands (JAG1/2, DLL1/4), and some HES/HEY family members (Patel et al., 2005).

2.4.4.2 RNA extraction and reverse transcription

RNA extraction was performed using RNeasy Mini Kit (QIAGEN) following the manufacturer's suggested protocol. HUVECs grown in a monolayer in the 6-well plates were lysed directly and homogenised. On-column digestion of DNA during RNA purification was performed using RNase-Free DNase Set (QIAGEN) and following the manufacturer's suggested protocol to prevent genomic DNA contamination. Concentrations of purified RNA samples were measured (Section 2.1.5). RNA samples were immediately subjected to reverse transcription and reserved for purity check. cDNA synthesis by reverse transcriptase was performed using Omniscript RT Kit (QIAGEN), Recombinant RNasin® Ribonuclease Inhibitor (Promega) and Oligo-dT primer (QIAGEN) following the manufacturer's suggested protocol. 2µg template RNA was added per 20µL reaction. RNA samples from the previous step and cDNA samples were proceeded directly with PCR (Section 2.1.2) using *hGAPDH* primers (Appendix 8.2.1F) as a quantitative control and analysed using agarose gel electrophoresis (Section 2.1.4).

2.4.4.3 Real-time quantitative PCR (qPCR)

qPCR was carried out using the QuantiTect® SYBR® Green PCR Kit (QIAGEN) on a 7500/7500 Fast Real-Time PCR System (Applied Biosystems®) following the manufacturer's suggested protocol (Table 2-3). qPCR reaction mix was prepared in MicroAmp® Fast 96-well reaction plates (0.1mL, PCR compatible DNA/RNA/RNase free, Applied Biosystems®), which were then sealed with MicroAmp™ Optical Adhesive Film (Applied Biosystems®) and placed in the real-time cycler to run the cycling programme. The real-time cycler was programmed (Table 2-4) and the raw data was analysed using

the Applied Biosystems 7500 Real-Time PCR Software (v2.3). Relative quantification was done using the $\Delta\Delta C_T$ method normalising to relevant house-keeping gene (*GAPDH*) and using BSA-treated cells as the reference sample. After qPCR, the specificity of PCR products was further checked by gel electrophoresis (Section 2.1.4).

Component	Amount/reaction
Reaction mix	
2x QuantiTect SYBR Green PCR Master Mix (include the ROX passive reference dye)	12.5 µL
Primer A	0.3 µM
Primer B	0.3 µM
RNase-free water	Variable
Template cDNA	4 µL (≤500 ng/reaction)
Total reaction volume	25 µL

Table 2-3. qPCR reaction setup. cDNA was synthesised from equal amount starting RNA (2µg RNA per 20µL RT reaction mix) and generally had a concentration of 800-1000 ng/µL after RT reaction. The cDNA samples were then diluted 1:8 using RNase-free water to generate a final concentration of 100-125 ng/µL. No more than 500 ng template cDNA was added per qPCR reaction. A no template control (NTC) omitting any cDNA template from the reaction was included for each primer pair, which served as a general control for extraneous nucleic acid contamination and a control for primer dimer formation. See Appendix 8.2.1F for detailed information of qPCR primers.

Step	Time	Temperature
Holding Stage		
PCR initial heat activation	15 min	95°C
Cycling Stage		
Denaturation	15 s	94°C
Annealing	30 s	60°C
Extension	30 s	72°C
Number of cycles	40	
Melting Curve Stage		
Step 1	15 s	95°C
Step 2	1 min	60°C
Step 3	30 s	95°C
Step 4	15 s	60°C

Table 2-4. qPCR reaction conditions. A melting curve analysis was performed after the cycling programme to verify the specificity and identity of the PCR products.

2.4.5 Coculture assay

2.4.5.1 Transient transfection

HEK293T cells were seeded onto Corning® 6-well tissue culture plates (4.5E5 cells/mL, 2.5mL/well in complete DMEM) three days prior to assay. After no more than 24hr incubation at 37°C, cells were transfected with either empty vector or vector expressing full-length Notch ligand using TransIT®-293 transfection reagent (Mirus Bio®) and Opti-MEM™ reduced serum medium (Gibco™) (Table 2-5). The transfection mix was incubated at room temperature for 20min and added dropwisely to cells in the 6-well plate directly. Cells were incubated for at least 24hr at 37°C before use. Transfection could also be performed in 12-well plate, using 1.8E5 cells/well (1mL/well).

Component	Amount/well (12w plate)	Amount/well (6w plate)
pcDNA3.1(+) wtDLL4-FL	1.6 µg	4 µg
TransIT-293	4.8 µL	12 µL
Opti-MEM	100 µL	250 µL

Table 2-5. Transfection mix for coculture.

2.4.5.2 Coculture and split-luciferase Notch activation assay

HEK mNotch1-NLuc/CLuc-RBPJ cells were seeded to 96-well tissue culture plates (white bottom, TC surface, Thermo Scientific™) two days prior to assay (2E4 cells in 125µL complete DMEM per well). After incubation at 37°C for 24hr, HEK293T cells expressing full-length Notch ligands were harvested and gently seeded onto split-luciferase reporter cells in the same 96-well plate at 1:1 cell density (2E4 cells in 125µL complete DMEM per well) for coculture. An aliquot of transfected HEK293T cells was reserved to check surface ligand expression level. After 24hr of coculture at 37°C, luciferin signal was detected as described in Section 2.4.1, but without pipetting mix.

2.4.5.3 Evaluation of mRNA expression level

Transient transfection of HEK293T cells was performed as described in Section 2.4.4.1 and cells were harvested for RNA extraction after 24hr incubation at 37°C. RNA extraction and reverse transcription were performed as described in Section 2.4.3.2. RNA and cDNA samples were proceeded with PCR using *hGAPDH* and *hDLL4* primers (Appendix 8.2.1F) and analysed using gel electrophoresis (Section 2.1.4).

2.4.5.4 Evaluation of ligand surface expression level

Ligand expression levels on the surface of transfected HEK293T cells were tested using flow cytometry. 5-10E5 cells were harvested, centrifuged at 2500 rpm at 4°C for 5min (Sorvall™ Heraeus #3328), and resuspended in ice-cold FACS buffer (Appendix 8.2.2Q). Samples were kept at 4°C or on ice for the rest of steps. Another two washes with FACS buffer were performed (400µL/sample), and cells were resuspended in 100µL/sample FACS buffer containing 10ng/µL anti-hJAG1 (65D mAb, (Masiero et al., 2019)) or 5ng/µL anti-hDLL4 primary antibody (MAB1506, R&D) and incubated for 1hr. Cells were washed twice with FACS buffer to remove unbound primary antibody, resuspended in 200µL/sample FACS buffer containing 1:500 dilution of PE (R-phycoerythrin)-conjugated F(ab')2-Goat anti-Mouse IgG (H+L) Cross-Adsorbed Secondary Antibody (A10543, Thermo Scientific™), and incubated for 1hr in the dark. Cells were washed twice with FACS buffer to remove unbound secondary antibody, resuspended in 400µL/sample DAPI staining solution (1ng/µL DAPI in PBS), and incubated for 10-15 minutes. PE signal was measured by analysis of 30,000 cells using CytoFLEX LX flow cytometer (excitation/emission 561/585nm, Beckman Coulter). Data were analysed using FlowJo 10 software.

2.5 Binding assay

2.5.1 Plate-based Notch receptor-ligand binding assay

Nunc™ MaxiSorp™ ELISA plates (flat-bottom uncoated, Invitrogen™) were coated with purified Notch receptors (400nM, 50µL/well, EGF11-13 or EGF7-13 constructs) in HBS buffer (Appendix 8.2.2L) (Figure 2-6). After incubation at 4°C overnight, the plate was washed thrice with HBS buffer and blocked with blocking buffer (200µL/well, 3% milk and 0.1% gelatin in HBS buffer) for 1.5hr. All incubation steps were done on a rocking shaker (~40rpm) at room temperature. The plate was washed thrice with ELISA washing buffer (Appendix 8.2.2N) before adding purified Fc-tagged Notch ligands (200nM, 50µL/well, N-EGF3 constructs) diluted in HBS buffer. The plate was incubated for 1.5hr and washed thrice with ELISA washing buffer, after which HRP-conjugated Anti-Human IgG Fc antibody (ab97225, Abcam) with a 1:2000 dilution (0.5ng/µL) in HBS buffer was added (50µL/well) and incubated for another 1hr. After incubation, four washes with washing buffer and two subsequent washes with HBS buffer were performed. 100µL/well freshly prepared HRP substrate solution (Appendix 8.2.2P) was added and A_{415} was measured immediately by a PHERAstar *FS* microplate reader (BMG LABTECH).

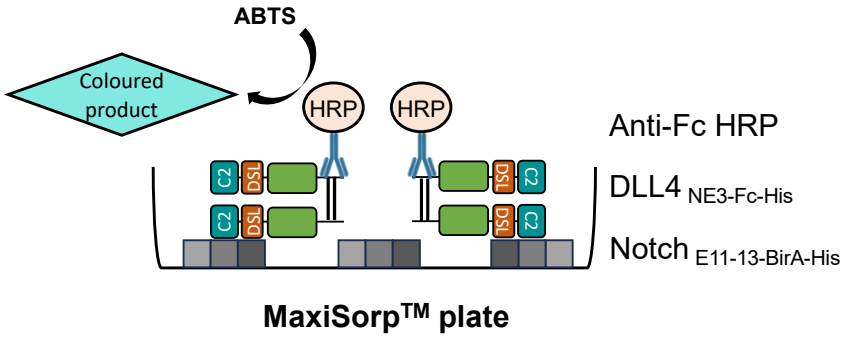


Figure 2-6. Notch binding assay using MaxiSorp™ plate. Plates were coated with $Notch_{EGF11-13}$ (grey) or $Notch_{EGF7-13}$ (not shown) through passive adsorption. Fc-tagged ligand constructs such as $DLL4_{NE3-Fc-His}$ (EGFs: green, DSL: brown, C2: teal) were added. Ligands that bound to receptor LBR were detected by anti-Fc HRP (anti-Fc: blue, HRP: wheat) and the signal was quantified as an absorbance readout (A_{415}) using a plate reader.

2.5.2 Bead-based liposome aggregation assay

2.5.2.1 Lipid stock preparation

Chloroform lipid solutions (Avanti® Polar Lipids) were mixed in desired ratios (Appendix 8.2.11) and dried using nitrogen, and then placed in a freeze dryer for 1hr. All steps were performed in the dark. Dried lipids were resuspended in HBS buffer (Appendix 8.2.2L) at a final concentration of 1mM by shaking at 160rpm at 25°C for 1hr, and then divided to 300µL aliquots. Lipid aliquots were frozen in liquid nitrogen and then thawed in a 37°C water bath for eight freeze-thaw cycles, after which the frozen lipid was stored at -80°C.

2.5.2.2 Liposome preparation and characterisation

One lipid aliquot was thawed and extruded with 21 passes through a polycarbonate Nucleopore filtration membrane (100nm pore width, Whatman®) using a Mini-Extruder (Avanti® Polar Lipids) to produce unilamellar liposomes (Ong et al., 2016). Liposomes were freshly prepared and stored on ice in the dark. The average size and homogeneity of the liposomes were assessed using dynamic light scattering (DLS). Liposomes were diluted 1:20 in HBS buffer to prepare the DLS sample, and the results were analysed using OmniSIZE 2.0 software.

2.5.2.3 FACS-based liposome aggregation assay

Protein G-coated fluorescent beads (particle array kit/PAK Blue, 0.1% w/v, 5.88µm, SPHERO™) were used as solid support to immobilise Fc-tagged purified ligands. Beads were kept on ice in the dark for all steps. Bead solution (10µL/reaction) was washed twice with 10X volumes of HBS/BSA buffer (Appendix 8.2.2M) by centrifugation at 13,000 rpm for 5min and resuspension with vortexing. After washing, beads were resuspended in 5X volumes of HBS/BSA (50µL/reaction). 2µg/reaction purified ligands or mouse IgG (Santa Cruz Biotechnology) was mixed with the beads and incubated for 1hr.

For PNGase-treated samples, digestion was performed on ligands bound to beads by adding 0.2µL/reaction PNGase F (P0704, NEB) and incubating at 37°C for 4hr in the dark. The GlycoBuffer 2 (0.05M Sodium Phosphate, pH 7.5, NEB) used in PNGase F digestion was found to interfere with this experiment (results not shown), likely due to the presence of phosphate ions. Thus, HBS buffer was used instead for on-beads PNGase F digestion. Digestion was quenched by chilling the reaction mix on ice. After ligand coating, beads were washed once with 100µL/reaction of HBS/BSA and resuspended in 50µL/reaction of ice-cold HBS. Freshly prepared liposomes were diluted 1:200 in HBS before adding (50µL/reaction) to beads and incubated for 30min (Figure 2-7). After incubation, sample was diluted with 200µL/reaction HBS before analysing using a BD LSRFortessa X20 flow cytometer (10,000 single events per sample; liposomes: excitation/emission 488/530nm; protein G beads: excitation/emission 640/670nm). Percentage aggregation was analysed using FlowJo 10 software.

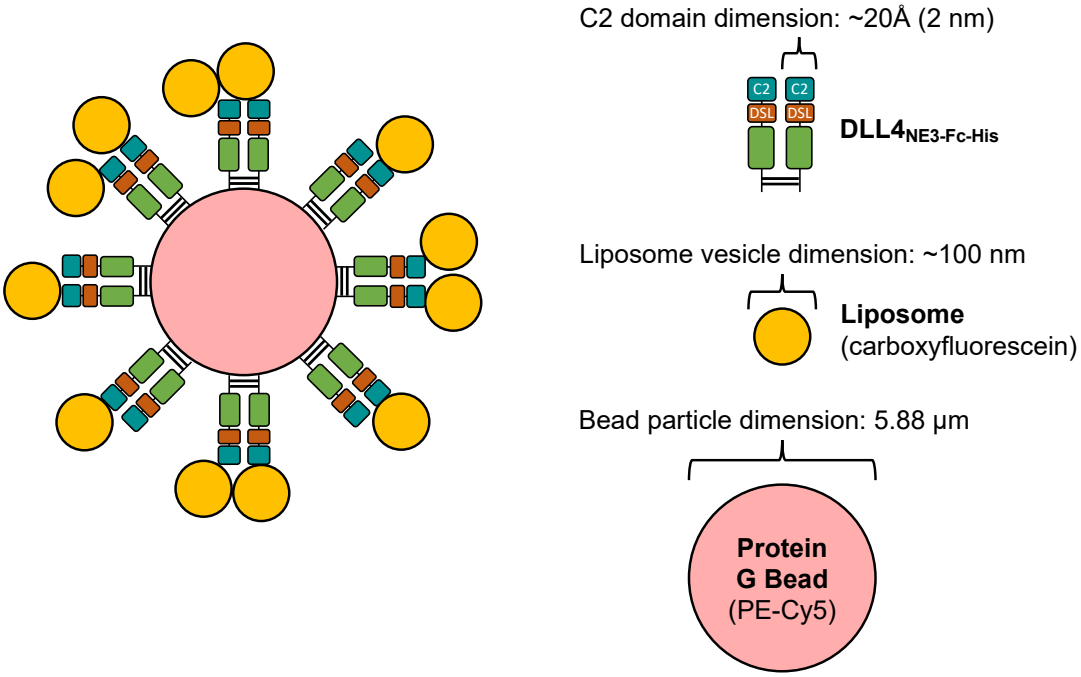


Figure 2-7. Liposome aggregation assay. Cartoon illustrating the bead-protein-liposome complex formed in the liposome aggregation assay. Protein G-coated beads (red) were pre-labelled with a PE-Cyanine®5 (PE-Cy5, red-emitting) fluorophore. Protein G coated on beads bound Fc-tagged ligand dimer with high affinity. The N-terminal C2 domain (teal) of Notch ligands bound liposomes (yellow) via non-covalent interactions. Avidity-driven aggregates

formation was detected by flow cytometry. The cartoon was not drawn in scale, the actual dimensions were labelled on the right.

2.5.3 FACS-based ligand binding assay

Ligand binding experiments were performed with either HEK293 cells expressing full-length mNotch1 or HUVECs expressing all four Notch paralogues (NOTCH1-4) (Patel et al., 2005). HEK293 cells were seeded in 12-well tissue culture plates (flat bottom, Corning® Costar®) at a density of 0.228E6 cells/mL (1mL/well) and incubated for 48hr at 37°C, whereas HUVECs were seeded at a density of 1E5 cells/mL (1mL/well) and incubated for 24hr at 37°C. After incubation, medium was replaced with 400µL/well blocking medium (Appendix 8.2.12) and cells were blocked for 45min at 37°C. Meanwhile, 50nM Fc-tagged Notch ligands and 75nM Alexa Fluor™ 488 (AF488)-conjugated anti-Human IgG (H+L) secondary antibody (A11013, Invitrogen™) were mixed in 100µL/reaction PBS buffer (Appendix 8.2.2C) and incubated at 4°C in the dark on a roller mixer for 1hr. After blocking, the ligand-antibody conjugate solution (100µL/well) was added dropwise to cells to yield a final ligand concentration of 40nM. Cells were incubated with ligands at 37°C for 2hr before being harvested, centrifuged at 3000 rpm at 4°C for 4min, and washed with 300µL/reaction ice-cold HEPES Buffered Saline Solution (HBSS, Lonza) to remove unbound ligands. Samples were kept at 4°C or on ice for the rest of steps. Cells were washed twice with HBSS and resuspended in 300µL/reaction DAPI staining solution (1ng/µL DAPI in HBSS). Ligand binding was quantified by analysis of 30,000 cells using CytoFLEX LX flow cytometer (Beckman Coulter; AF488: excitation/emission 488/525nm; DAPI: excitation/emission 405/450nm) (Figure 2-8). Data were analysed using FlowJo 10 software.

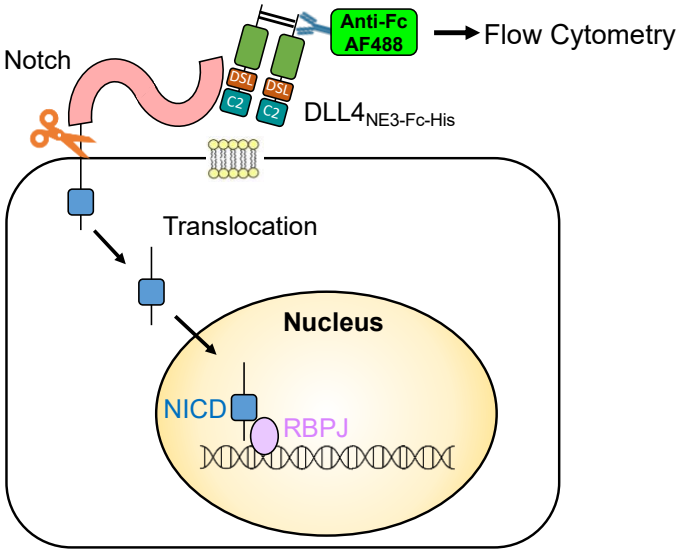


Figure 2-8. Ligand binding by Notch-expressing cells. Cartoon illustrating the ligand binding assay, which monitors ligand binding to full-length Notch receptors presented on the cell membrane using an AF488-conjugated antibody.

2.5.4 FACS-based receptor binding assay

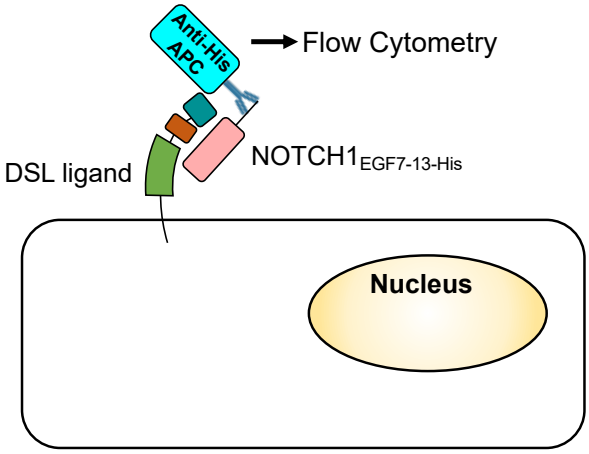


Figure 2-9. Receptor binding by ligand-expressing cells. Cartoon illustrating the receptor binding assay, which monitors binding of purified, His-tagged NOTCH1$_{EGF7-13}$ fragments to full-length ligands presented on the cell membrane using an anti-His APC-conjugated antibody.

Receptor binding experiments were performed using the same methods for ligand binding assay (Section 2.5.3) with some modifications. HEK293T cells transiently transfected to express full-length Notch ligands (Section 2.4.4.1) were used. 200nM His-tagged NOTCH1 constructs (Section 2.3.3) and 10ng/μL APC-conjugated anti-6X His

tag mAb (ab72579, Abcam) were mixed in 100µL/reaction PBS buffer to make the receptor-antibody conjugate solution. The receptor binding signal was measured using the APC fluorescence spectra: excitation/emission 638/660nm.

2.6 Statistical Analysis

Statistical data were analysed with Prism 10 (GraphPad). Data were checked for normality, homogeneity of variance, and sample sizes. Based on this information, respective statistical test was performed (Table 2-6), followed by a post-hoc analysis for multiple comparisons. Values were presented with means ± SD.

Statistical test	Normality	Homogeneity of variance	Sample sizes
Ordinary one-way ANOVA	Pass	Pass	Equal
	Pass	Pass	Not equal
Welch's ANOVA	Pass	Fail	Equal
Kruskal-Wallis test	Pass	Fail	Not equal
	Fail	Pass	Equal
	Fail	Pass	Not equal
	Fail	Fail	Equal
	Fail	Fail	Not equal

Table 2-6. Statistical tests. Data were checked for normality, homogeneity of variance, and if the sample size is equal for each treatment. The information was used to select which statistical test to perform for each specific experimental setup.

Chapter 3: Studying the functional importance of the DLL4 C2 domain using cancer database variants

3.1 Introduction

The N-terminal module of canonical Notch ligands was recognised to be a lipid-binding C2 domain conserved in *Drosophila* and all mammalian species, and was shown to modulate Notch signalling *in vitro* (sections 1.3.2.1 and 1.5.4) (Chillakuri et al., 2013; Suckling et al., 2017). Previously studied examples showed that C2 domains with a type II topology predominantly interact with the membrane using the apical loops (sections 1.5.2 and 1.5.3), forming the putative lipid-binding site (Y. Hirano et al., 2019; Larsen & Sansom, 2021). A number of disease-associated mutations mapping to the C2 domain have been identified in Notch ligands (Section 1.2.2, Figure 1-5). Whilst ALGS missense mutations were found within the JAG1-C2 hydrophobic core, leading to protein misfolding and ER retention (Chillakuri et al., 2013), EHBA variants were found on the C2 loops, leading to reduced lipid-binding and Notch activation without affecting protein secretion or Notch receptor binding (Suckling et al., 2017). On the other hand, only two AOS missense mutations (G28R, A121P) mapping to DLL4-C2 have been identified (Meester et al., 2015; Rojnueangnit et al., 2022)—whilst G28R is involved in the receptor binding interface, A121P is located within the hydrophobic core and likely to cause misfolding. Due to the small number of DLL4 variants identified in genetic diseases, other potential disease-related C2 domain substitutions would be helpful to establish the functional importance of C2 domain in Notch signalling.

As an important regulator of embryonic development and tissue homeostasis, the Notch pathway is dysregulated in many cancers, playing either an oncogenic or tumour-suppressing role (see Section 1.2.3). In particular, DLL4, which plays a key role in vascular development (see Section 1.2.1.1), has major implications in tumour angiogenesis (Fasoulakis et al., 2022). DLL4 overexpression was observed in tumour cells and tumour vasculature (Patel et al., 2005; Yen et al., 2012; Y.-Z. Zhang et al., 2015), suggesting a prognostic role in cancer development. Therefore, cancer databases, such

as the Catalogue of Somatic Mutations in Cancer (COSMIC) (Forbes et al., 2016) and the National Cancer Institute Genomic Data Commons (GDC) data portal might provide an alternative source to identify DLL4 variants with mutations affecting the C2 apical loops. This approach has been used to study JAG1-C2 domain, allowing identification of functionally important N-glycan variants from cancer databases (Meng et al., 2022).

This chapter aims to investigate the functional impact of amino acid substitutions within the DLL4-C2 apical loops using tumour-associated missense mutations. A total of 14 DLL4 variants were generated using site-directed mutagenesis and expressed as DLL4 N-terminal fragments (from C2 to EGF3, i.e., NE3) from HEK293F cells. The Notch activation capacity of these variants was tested using split-luciferase reporter cells. Selective loop β1-2 variants were then expressed as FL-ligands by transiently transfecting HEK293T cells, and the activity was assessed using a coculture assay. To further confirm the functional importance of the C2 apical loops, β1-2 and β5-6 loop-shortening variants were generated and tested using similar approaches.

3.2 Cancer database search

COSMIC is the world' largest and most comprehensive database for somatic mutations in human cancer. It combines high precision data from large scale sequencing analysis of tumour genomes with manual curation of over 27,000 peer-reviewed publications (August 2024). The GDC data portal is another cancer database, which has recorded clinical and genomic data from 44,736 independent cases (August 2024). These databases provide genome-level profiling across all cancers, allowing annotations of both coding and non-coding genetic alterations, such as nonsense, missense, synonymous, insertion, deletion, and inversion mutations.

In the COSMIC database, DLL4 somatic mutations have been recorded in 46748 samples (August 2024), which identified 429 unique coding mutations (nucleotide-level) with the majority (~60%) being missense mutations (Table 3-1A). 10 of the missense mutations have obvious functional implications by substituting Cys residues involved in the disulphide bonds that stabilise the ligand ECD. The importance of Cys in the proper folding of the EGF-like domain has been described in many disorders, including ALGS, CADASIL, and Marfan syndrome (Bauer et al., 2010; Gilbert et al., 2019; Haritunians et al., 2005; Le Caignec et al., 2002; Schrijver et al., 1999; Whiteman & Handford, 2003), suggesting a high propensity of Cys-loss variants to be disease-causing. Therefore, the Cys-loss mutations identified in DLL4 are likely associated with loss-of-function effects due to protein misfolding.

Missense mutations were found throughout the entire *DLL4* gene, showing no mutational hotspot, except for EGF7 and the short linking region between EGF8 and the TMD, which seemed more prone to mutations (Figure 3-1A, Appendix 8.3.1). In complement with the GDC data portal, a total of 45 missense mutations were found within the C2 domain, including 16 mutations mapped to the apical loop region (Figure 3-1B). These mutations were identified from various types of tumours in different primary tissues (Table 3-1B). Most of the loop mutations were identified in one or two cases, except for R100G and S162R, which were found in 18 and 5 independent tumour samples, respectively. However, there is currently no evidence to show that these mutations are the driving cause of cancer or tumour development.

14 tumour-related C2 loop missense mutations (listed in Table 3-1B) were selected to probe their functional impact on DLL4 activity. The functional effect of P52S and S162R was not yet studied because they are novel variants identified more recently. The mutations are distributed on the C2 apical loops (Figure 3-1B), among which the β1-2, β3-4, and β5-6 loops form the putative lipid-binding site (see Section 1.5). On the other

hand, the β7-8 loop, albeit not a canonical lipid-binding loop, is located at the apex in close proximity to the other apical loops, therefore may potentially be involved in C2-membrane interactions. Mutations located on the β-strands consisting the hydrophobic core of C2 domain were not selected, because they are expected to lead to protein misfolding and ER retention, as suggested by observations made in JAG1 studies (Chillakuri et al., 2013; Meng et al., 2022). In addition, the DSL domain double mutant F195A/Y216A, which is a Notch-binding-deficient variant (Figure 3-1B), was used as a negative control in activity assays.

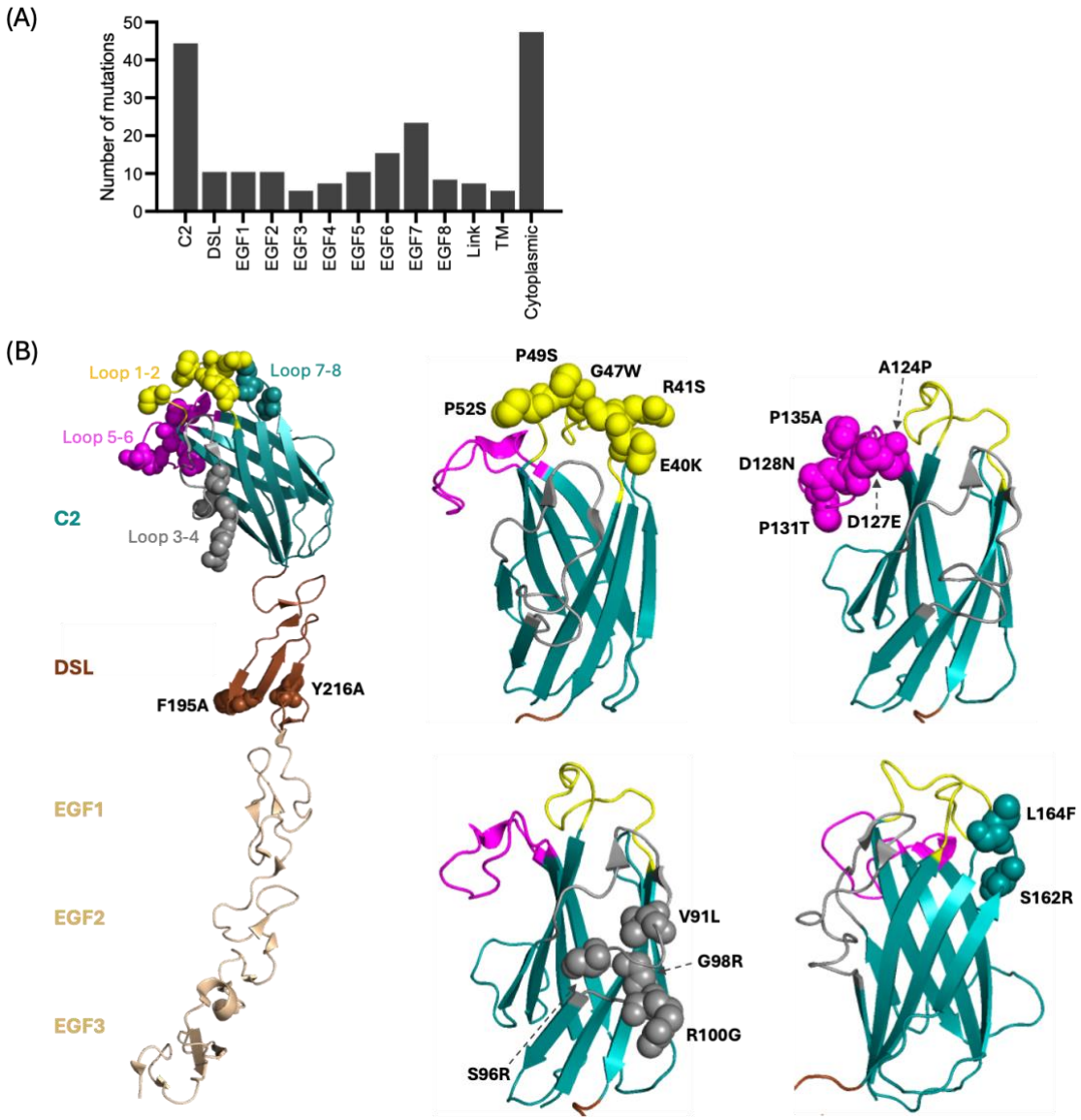


Figure 3-1. DLL4 missense mutations identified in cancer databases. (A) Distribution of missense mutations in DLL4, which shows the number of mutations identified in each domain, including the C2, DSL, EGF1-8, transmembrane (TM), and cytoplasmic domains, as well as

the short link between EGF8 and the TM domain. (B) Locations of the tumour-related missense mutations mapped to the DLL4-C2 apical loops. The crystal structure of DLL4 C2-EGF3 (PDB: 5MVX) is shown in ribbon representation (C2: teal, DSL: orange, EGF: wheat). Loop β1-2 is shown in yellow, loop β3-4 in grey, loop β5-6 in magenta, and loop β7-8 in teal. Note that loop β3-4 is located more sideways compared to the apical loops β1-2 and β5-6, and loop β7-8 is very short. Residues with missense mutations identified in cancer databases are shown in sphere representation. The locations of the F195A and Y216A substitutions in the DSL domain are also shown in sphere representation.

(A)

Sample type	DLL4
Total unique samples screened	46748
Total unique samples with coding mutations	429
Substitutions (nonsense, missense, and synonymous)	359
Missense mutations	256
Missense mutations affecting disulphide bonds in ECD	10
Missense mutations within the C2 domain	45

(B)

Missense mutation	Region within C2 domain	Primary tissue	Histology	Number of cases	Source
E40K	β1-β2 loop	Urinary tract	Carcinoma	1	COSMIC & GDC
R41S	β1-β2 loop	Liver	Neoplasm	1	COSMIC
G47W	β1-β2 loop	Liver	Neoplasm	1	COSMIC
P49S	β1-β2 loop	Endometrium	Endometrioid carcinoma	1	COSMIC & GDC
P52S	β1-β2 loop	n/a	n/a	1	GDC
V91L	β3-β4 loop	Ovary	Mixed adenosquamous carcinoma	1	COSMIC
S96R	β3-β4 loop	Large intestine	Adenocarcinoma	1	COSMIC
G98R	β3-β4 loop	Haematopoietic and lymphoid	Acute lymphoblastic T cell leukaemia	1	COSMIC
R100G	β3-β4 loop	Upper aerodigestive tract	Squamous cell carcinoma	18	COSMIC
A124P	β5-β6 loop	Skin	Malignant melanoma	1	COSMIC & GDC
D127E	β5-β6 loop	Bronchus and lung	Squamous cell carcinoma	1	COSMIC & GDC

D128N	β5-β6 loop	Haematopoietic and lymphoid	Lymphoid neoplasm	2	COSMIC & GDC
		Skin	Malignant melanoma		
P131T	β5-β6 loop	Central nervous system	Glioma	1	COSMIC & GDC
P135A	β5-β6 loop	Ovary	Serous Neoplasm	1	GDC
S162R	β7-β8 loop	Liver	Carcinoma	5	COSMIC
L164F	β7-β8 loop	Skin	Malignant melanoma	1	GDC

Table 3-1. Summary of mutations recorded in cancer database (updated as of August 2024). (A) Statistical information about DLL4 cancer-related coding mutations recorded in the COSMIC database. Information about non-coding mutations, such as intronic mis-splicing variants, was not available. The variants encompass frameshift (deletions and insertions), non-sense (substitutions), missense (substitutions), and synonymous (substitutions) mutations. The most common mutation type is missense mutations (60%). Approximately 15% of the total number of missense mutations mapped to the C2 domain. (B) Missense mutations recorded in the COSMIC and GDC databases that are found within DLL4 C2 apical loops. These mutations were identified from various types of tumours in different primary tissues. Website URLs: https://cancer.sanger.ac.uk/cosmic/gene/analysis?ln=DLL4; https://portal.gdc.cancer.gov/genes/ENSG00000128917.

3.3 Preparation of ligand protein constructs

3.3.1 Target site mutagenesis and secretion tests

3.3.1.1 NE3 constructs of cancer database variants

Site-directed mutagenesis was performed to introduce each of the selected missense mutations identified in cancer databases (see Section 3.2, Table 3-1) into *pcDNA3.1-DLL4*$_{NE3\text{-}Fc\text{-}His}$ plasmid construct. Figure 3-2 shows an example of the overlap extension PCR products (see Materials and Methods) of the D128N variant (see Appendix 8.2.1 for primer sequences and the expected size of the target bands). In addition to the 14 single substitution mutants, two double mutants (E40K/D128N, R41S/P131T) were also

made to study any additive effect of having missense mutations on both β1-2 and β5-6 loops. The correct DNA sequence was confirmed by Sanger sequencing in each case.

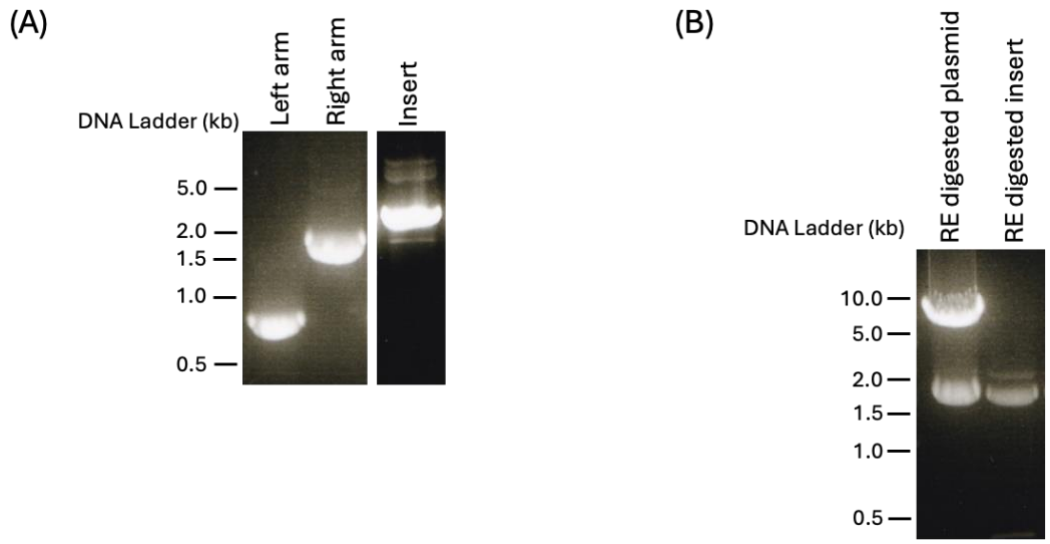


Figure 3-2. Agarose gels showing site-directed mutagenesis products. (A) The products from the first (left arm ~730 bp, right arm ~1640 bp) and second round (insert ~2360 bp) of PCR reactions. (B) Insert (~1700 bp) and vector (~5400 bp) DNA fragments after digestion by *EcoRI* and *XhoI* restriction enzymes (RE). A DNA ladder was run alongside samples for size estimation. See Materials and Methods section 2.1 for detailed cartoon explanations (Figure 2-1 and 2-2).

The plasmids that carry DNA encoding each of the 14 cancer database substitutions, alongside WT-DLL4$_{NE3\text{-}Fc\text{-}His}$ plasmid and the Notch-binding-deficient negative control F195A/Y216A, were transfected into HEK293F cells (see Materials and Methods). Conditioned medium and cell lysate samples were analysed by Western blot to check any effect of the introduced mutation on protein trafficking and secretion into medium (Figure 3-3). At least two independent transient transfection and secretion tests were performed. DLL4 variants, expressed as Fc-dimerised NE3 fragments, were analysed under both reducing and non-reducing (results not shown) SDS-PAGE conditions and detected with an anti-His-HRP antibody. The unmodified DLL4$_{NE3}$ construct has a theoretical MW ~64 kDa (monomer) or ~128 kDa (dimer), whereas experimentally, the protein generally migrates to a higher MW position on SDS-PAGE, most likely due to

PTMs such as glycosylation. In addition, some His-tagged proteins were observed to migrate to an unexpected position on SDS-PAGE due to a phenomenon termed 'gel shifting', resulting in a higher than expected MW on gel (Shelake et al., 2017).

Checking of post-transfection medium samples showed that ten of the C2-loop single substitution variants tested (E40K, P49S, V91L, S96R, R100G, D127E, D128N, P131T, P135A, L164F) had similar secretion levels to WT-DLL4 (Figure 3-3A). Furthermore, R41S, although present in the medium, had slightly lower secretion compared to WT-DLL4 as suggested by the less dense band in Western blot. For the three variants, G47W, G98R and A124P, which were shown to be non-secretory, analysis of their cell-lysate samples showed that these variants were expressed intracellularly at similar levels to WT-DLL4 (Figure 3-3B), suggesting successful transfection but ER retention likely due to protein misfolding. Another possibility is that these variants were secreted but more susceptible to extracellular degradation. However, no lower-MW protein fragments were observed in the medium sample, suggesting that this hypothesis was unlikely.

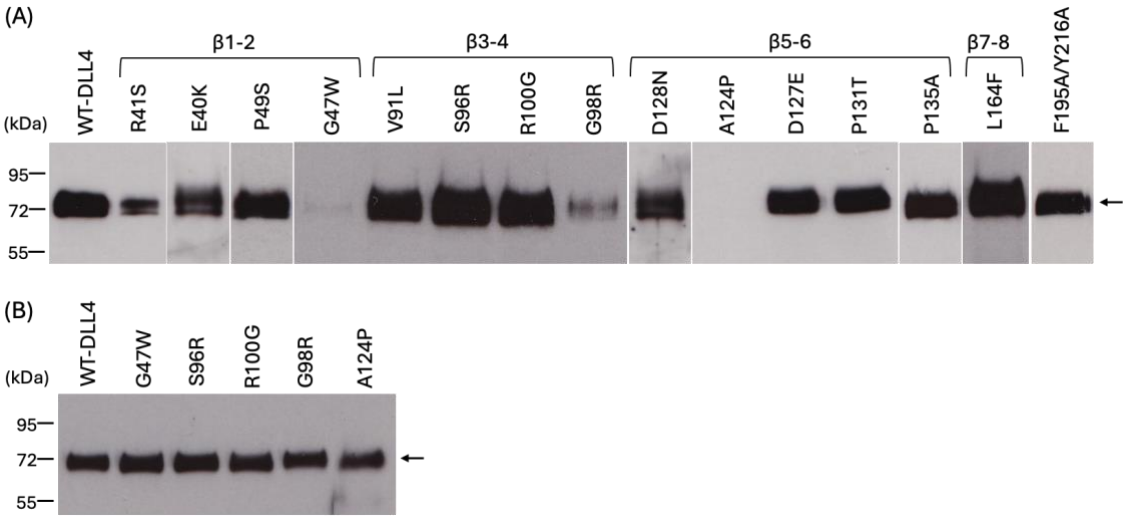


Figure 3-3. Western blot analysis of medium (A) and cell lysate (B) samples of DLL4 cancer database variants. Proteins were separated by reducing SDS-PAGE and detected by anti-His-HRP antibody. The theoretical monomeric MW of $DLL4_{NE3\text{-}Fc\text{-}His}$ is ~64 kDa, whilst experimentally, the monomer migrated to a higher MW position ~72 kDa. A pre-stained protein ladder was run alongside samples for size estimation. Target bands with desired MW were indicated by arrows. Note the thinner band of the R41S medium sample compared to

WT-DLL4, suggesting lower secretion. A lower concentration of G47W, G98R, and A124P was detected in the medium, suggesting ER retention.

In addition, two double mutants, E40K/D128N and R41S/P131T, which contain one single substitution on each of the β1-2 and β5-6 loops, were generated using overlap extension PCR and expressed using HEK293F similarly as described above. The post-transfection medium and cell lysate samples of the double mutants were analysed by Western blot, alongside WT-DLL4 and the respective single substitution mutants, to check any effect of the substitutions on protein trafficking and secretion (Figure 3-4). Two independent transient transfection and secretion tests were performed.

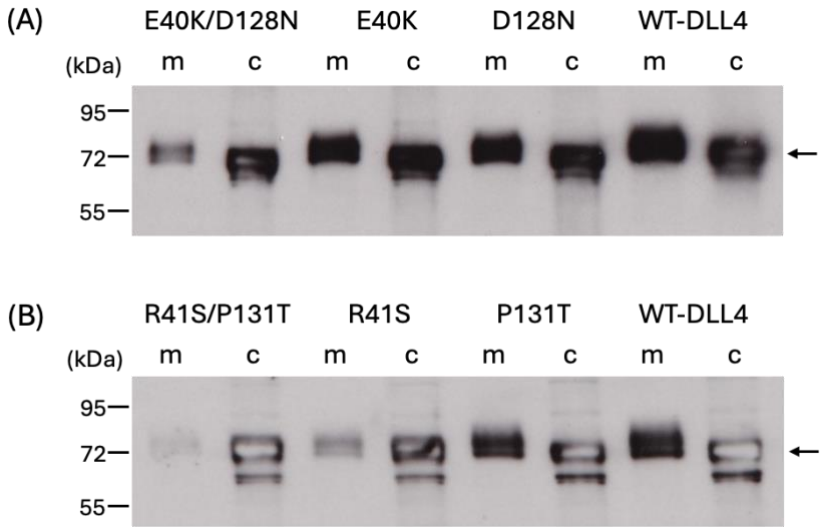


Figure 3-4. Western blot analysis of medium ('m') and cell lysate ('c') samples of DLL4 C2 loop double mutants. Proteins were separated by reducing SDS-PAGE, and then subjected to Western blotting and detected by anti-His-HRP antibody. A pre-stained protein ladder was run alongside samples for size estimation. Target bands with desired MW were indicated by arrows. Note the less dense band of the E40K/D128N medium sample compared to WT-DLL4 in (A), suggesting lower secretion. Little R41S/P131T was detected in the medium sample in (B), suggesting ER retention.

Whilst both E40K and D128N appeared to be secreted similarly to WT-DLL4, the E40K/D128N double mutant showed significantly lower secretion compared to WT-DLL4

(Figure 3-4A), suggesting partial protein misfolding and ER retention. P131T had a similar secretion level to WT-DLL4, whereas R41S already showed significantly lower secretion, thus as expected, the R41S/P131T double mutant was shown to have even lower secretion compared to R41S and was non-secretory (Figure 3-4B). These results collectively suggest that both the C2 β1-2 and β5-6 loops may be important for protein folding, such that having missense mutations on both loops resulted in detrimental effects on protein secretion.

3.3.1.2 NE3 constructs of C2 loop shortening variants

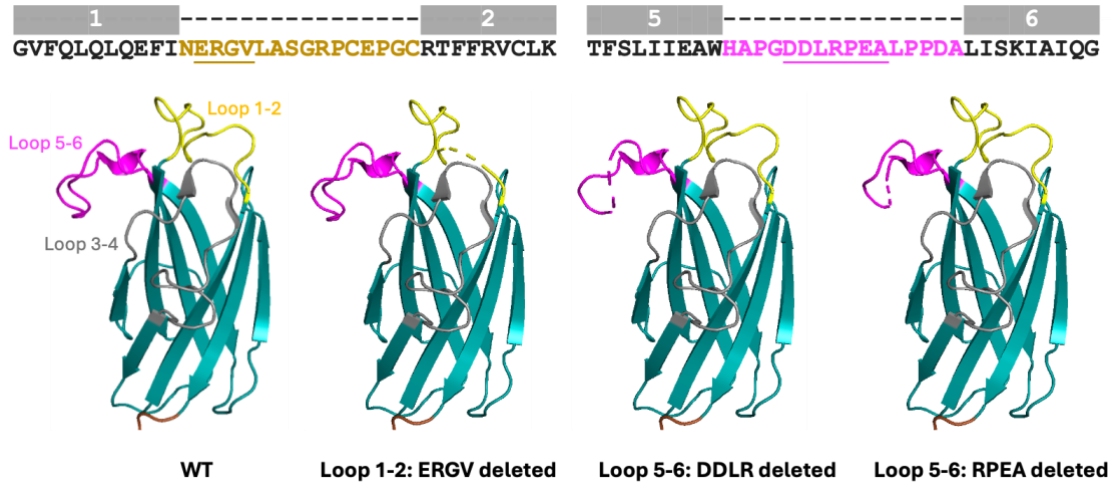


Figure 3-5. DLL4-C2 loop shortening variants. The structures of the loop shortening variants compared to the wildtype (PDB: 5MVX) C2 domain (C2: teal, loop β1-2: yellow, loop β3-4: grey, loop β5-6: magenta) are shown in ribbon representation. The sequences of the loops are shown above (β-strands: grey bar), where residues in loop β1-2 are coloured in yellow, and residues in loop β5-6 are coloured in magenta. The amino acids deleted in loop β1-2 or loop β5-6 are underlined.

Three loop-shortening variants (Figure 3-5), each containing a deletion of four amino acids in either the β1-2 or β5-6 loop, were generated using overlap extension PCR and expressed using HEK293F similarly as described in section 3.3.1.1 (see Appendix 8.2.1 for primer sequences and the expected size of the target bands). The post-transfection medium and cell lysate samples of these variants were analysed by Western blot as

described in Section 3.3.1.1, alongside WT-DLL4, to check any effect of the loop deletions on protein trafficking and secretion into medium (Figure 3-6). Three independent transient transfection and secretion tests were performed. Analysis of post-transfection medium samples showed that all three loop-shortening variants had less secretion into the medium, as suggested by the very faint bands in Western blot. Analysis of the cell lysate samples showed similar steady-state levels of proteins, suggesting successful translation but partial ER retention, likely due to protein misfolding. A C2-truncated DLL4 fragment (i.e., DSL-EGF3 or DE3) was also tested (Appendix 8.3.2), which was shown to be non-secretory in HEK293F.

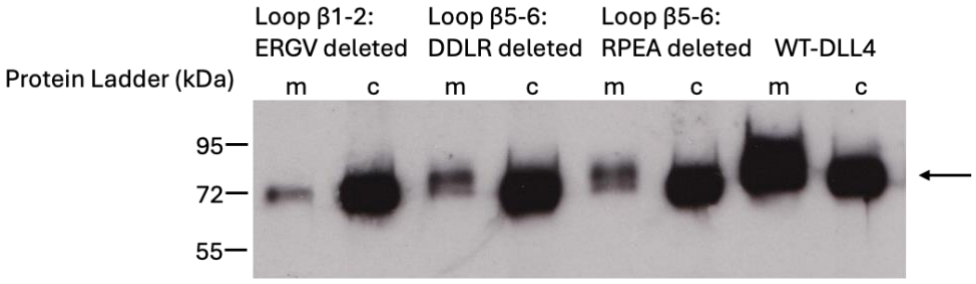


Figure 3-6. Western blot analysis of medium ('m') and cell lysate ('c') samples of DLL4 C2 loop-shortening variants. Proteins were separated by reducing SDS-PAGE and detected by anti-His-HRP antibody. A pre-stained protein ladder was run alongside samples for size estimation. Target bands with desired MW were indicated by arrows. Note the very faint bands of the variants compared to WT-DLL4, suggesting partial ER retention.

3.3.2 Protein purification

The 11 DLL4 variants (E40K, R41S, P49S, V91L, S96R, R100G, D127E, D128N, P131T, P135A, and L164F) with single amino acid substitutions on their C2 apical loops (shown to be secretory in Section 3.3.1.1), as well as the double mutant E40K/D128N, were expressed as NE3 fusion proteins in HEK293F cells and purified using IMAC and SEC (see Materials and Methods). Protein purification intermediate products from IMAC and SEC were analysed by Western blot using His-tag detection and SDS-PAGE.

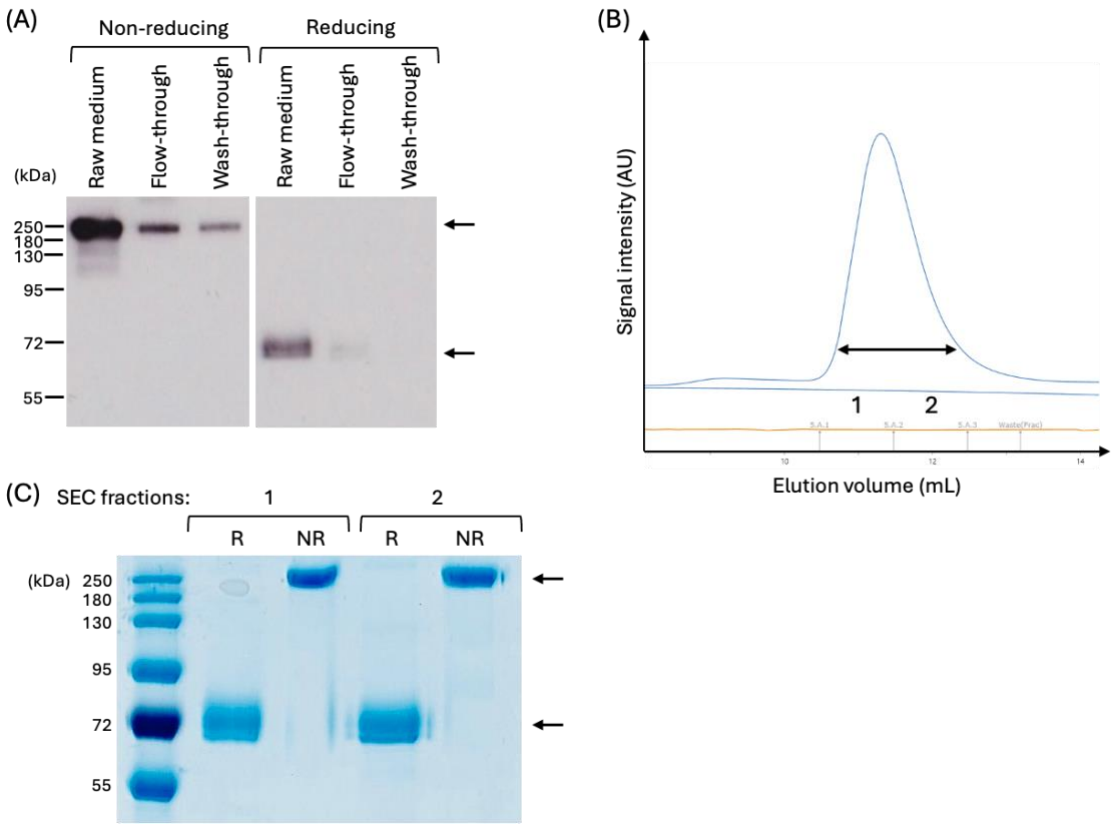


Figure 3-7. Purification of WT-DLL4$_{NE3\text{-}Fc\text{-}His}$ from HEK293F. (A) Western blot analysis of IMAC intermediate products of WT-DLL4. A pre-stained protein ladder was run alongside samples for size estimation. Target bands with desired MW were indicated by arrows. The theoretical MW of DLL4$_{NE3\text{-}Fc\text{-}His}$ is ~64 kDa (monomer) or ~128 kDa (dimer), whilst experimentally, the protein bands migrated to a higher MW position ~72 kDa (monomer) or ~250 kDa (dimer). (B) The size exclusion chromatogram of WT-DLL4, where the protein elution peak is indicated by a double-headed arrow. (C) Reducing/R and non-reducing/NR SDS-PAGE to check the identity and purity of the eluted WT-DLL4. Both fractions showed clear single bands, suggesting homogeneous product with >90% purity.

Figure 3-7 uses WT-DLL4 as an example to show the protein purification process. Low levels of WT-DLL4 constructs were detected in the flow-through and wash-through samples from IMAC (Figure 3-7A), suggesting effective immobilisation of His-tagged protein by the Ni^{2+} column. The size exclusion chromatogram shows a single clear elusion peak (Figure 3-7B), suggesting that fractions 1 and 2 contained the protein of interest (indicated by a double-headed arrow). SDS-PAGE was performed to check the identity and purity of the eluted protein, where both fractions showed a protein band at

the expected MW under both reducing (R) and non-reducing (NR) conditions (Figure 3-7C). The predominant protein band on SDS-PAGE suggested >90% protein purity, and thus these fractions were pooled together as purified WT-DLL4.

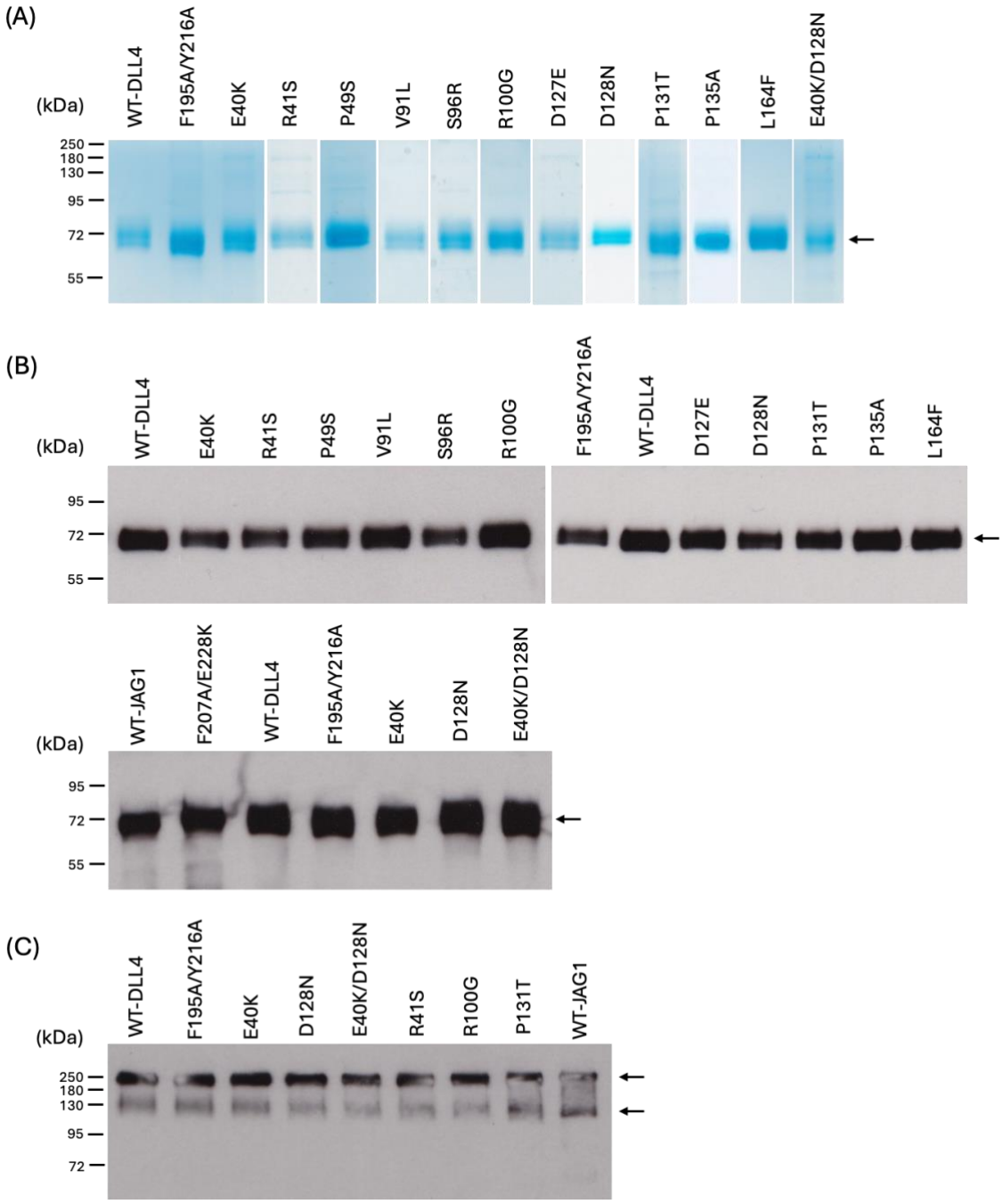


Figure 3-8. Western blot and SDS-PAGE analyses of purified DLL4 cancer database variants. (A) Reducing SDS-PAGE to check the identity and final purity of the DLL4 variants obtained from the SEC eluate. A pre-stained protein ladder was run alongside samples for size estimation. Target bands with desired MW were indicated by arrows. (B) Western blot analyses of purified DLL4 variants, alongside WT-DLL4, WT-JAG1, and their Notch-binding-deficient variants (DLL4: F195A/Y216A, JAG1: F207A/E228K). All protein bands migrated to

a similar position on reducing SDS-PAGE, and had similar intensity or thickness, suggesting that same amount of protein was added for each variant. (C) Western blot analysis of ligand constructs under non-reducing conditions.

The DLL4 cancer database variants, including the E40K/D128N double mutant, all had similar IMAC and SEC profiles compared to WT-DLL4 (results not shown). All purified proteins were checked for their identity and purity. The SDS-PAGE analyses of final protein fractions collected for each variant showed good purity (Figure 3-8A). The protein concentration of purified DLL4 constructs was estimated using Nanodrop (see Materials and Methods), and the final concentration was confirmed using Western blot (Figure 3-8B). Under non-reducing conditions, the variants all showed major protein bands corresponding to the MW of a dimerised construct (~250kDa) (Figure 3-8C). A second lower MW band ~130kDa was observed, which might correspond to a small proportion of unmodified ligand dimer (theoretical MW ~128kDa). These results suggested that dimer formation was not affected by the introduced amino acid substitutions.

3.4 Testing Notch activation capacity of the purified DLL4$_{NE3}$ cancer database variants

To investigate the effects of introducing cancer database missense mutations into the C2 apical loops on DLL4-induced Notch activation, activity assays were performed using HEK293 mN1/2-NLuc/CLuc-RBPJ reporter cells (see Materials and Methods, Figure 2-3). In the reporter system, the NICD released associates with RBPJ to reform the enzymatically active luciferase from NLuc and CLuc, whereby the luminescence signal produced is directly proportional to the level of activatory Notch signalling (Ilagan et al., 2011). TC plates were immobilised with a high concentration (150nM) of ligand proteins,

the level of which was determined by a plate-based ELISA assay using anti-His-HRP antibody (see Materials and Methods).

11 cancer database variants carrying a single amino acid substitution on their C2 apical loops (β1-2: E40K, R41S, P49S; β3-4: V91L, S96R, R100G; β5-6: D127E, D128N, P131T, P135A; β7-8: L164F) were tested initially using HEK293 mN1-NLuc/CLuc-RBPJ reporter cells, alongside WT-DLL4 and F195A/Y216A. A subset of variants (E40K, V91L, S96R, D128N) were observed to result in slightly reduced Notch activation, whilst another subset of variants (R41S, R100G) was observed to enhance Notch activation (Figure 3-9A). The range of functional effects observed was generally narrow, with an increase or decrease within ±20% of the WT-DLL4 activity. The F195A/Y216A negative control showed very low Notch activation ~20% of WT-DLL4 activity (as expected for a Notch-binding deficient variant) and was approximately the same as the 'cells only' background control.

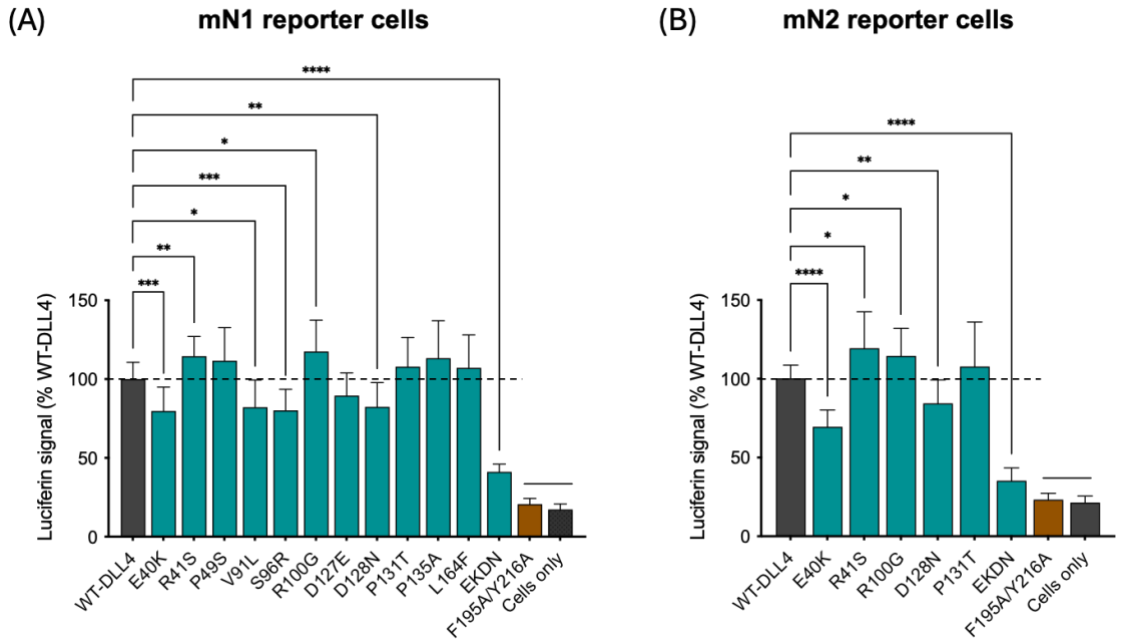


Figure 3-9. Notch activation by purified DLL4$_{NE3}$ cancer database variants at high ligand concentrations. (A) Notch activation by the 11 single substitution variants and the double mutant E40K/D128N was assessed by HEK293 mN1-NLuc/CLuc-RBPJ reporter cells, alongside WT-DLL4 and F195A/Y216A. (B) Notch activation by 5 selected single substitution variants and E40K/D128N was assessed by HEK293 mN2-NLuc/CLuc-RBPJ reported cells,

alongside WT-DLL4 and F195A/Y216A. The luminescence intensity readout was used to quantify the amount of NICD released upon Notch activation. The data was normalised as percentage of WT-DLL4 activity and presented as mean ± SD, representing combined results of n=3 independent experiments, in which 6 technical repeats were measured in each experiment. 'Cells only' was used as a background control. Statistical analysis was performed in each case using Welch ANOVA followed by Dunnett's T3 multiple comparison test. *$P \leq 0.05$, **$P \leq 0.01$, ***$P \leq 0.001$, ****$P \leq 0.0001$.

In addition to the single amino acid substitution variants, a double mutant E40K/D128N was purified and tested. Whilst the loop β1-2 variant E40K and the loop β5-6 variant D128N both led to slightly decreased Notch activation ~80% of the WT-DLL4 activity, the double mutant resulted in much more significantly reduced Notch activation that was ~40% of the WT-DLL4 activity (Figure 3-9A). This result showed an additive effect of the missense mutations, suggesting that the apical loops β1-2 and β5-6 may act synergistically to modulate Notch activation since they both contribute to the putative lipid-binding site (Figure 3-1). A selection of variants (β1-2: E40K, R41S; β3-4: R100G; β5-6: D128N, P131T; E40K/D128N) were further tested using HEK293 mN2-NLuc/CLuc-RBPJ reporter cells. Similar activity outcome was observed (Figure 3-9B), suggesting that the functional effect of the DLL4 cancer database variants applied to both Notch1 and Notch2. Not all variants tested in mN1 reporter cells were tested in mN2 reporter cells, but the selected variants already represented point mutations identified in each of the putative lipid-binding loops and had consistent activity results in both mN1 and mN2 reporter cells.

Furthermore, titration was performed to check if the narrow range of functional effects observed were consistent at lower ligand concentrations. A serial dilution was performed when immobilising ligand proteins on TC plates. The ELISA results (Figure 3-10A) showed that, when ligand constructs were added into wells at a range of concentrations

from 0nM to 150nM, WT-DLL4, its variants (R41S and D128N), and WT-JAG1 showed similar titration curves, suggesting that they immobilised to plate surface similarly.

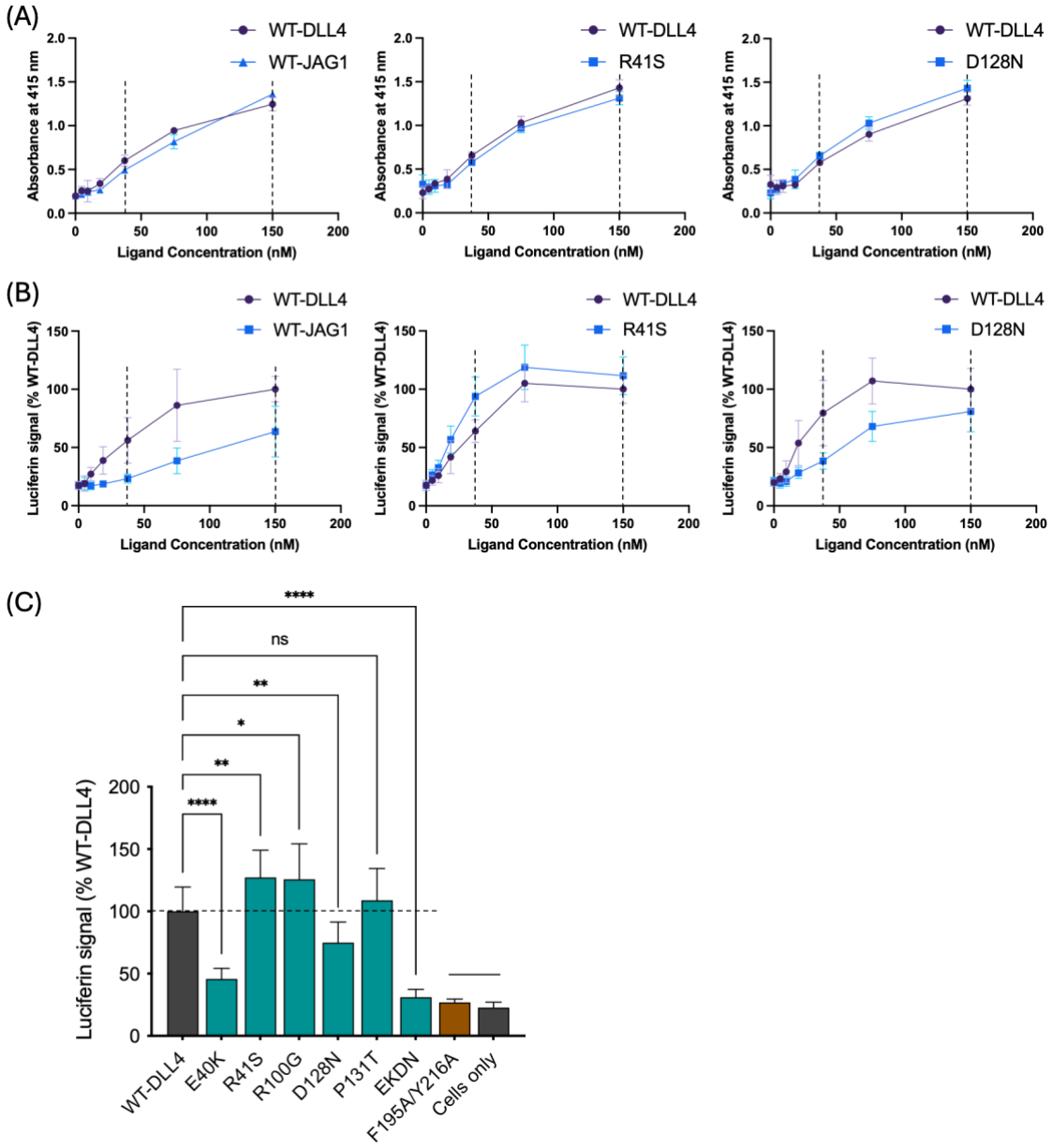


Figure 3-10. Notch activation by purified DLL4$_{NE3}$ cancer database variants at low ligand concentrations. (A) Serial dilution titration tests of ligand immobilisation on TC plates, analysed by ELISA using an anti-His-HRP antibody. The absorbance readout was used to quantify the amount of ligand protein immobilised. Both WT-DLL4 and its variants (R41S, D128N) showed similar titration curves. High (150nM) and low (37.5nM) ligand concentrations are indicated by vertical dotted lines. (B) Serial dilution titration tests of ligand activities, assessed by HEK293 mN1-NLuc/CLuc-RBPJ reported cells. Notch activation by WT-JAG1 was consistently lower than the activity of WT-DLL4. R41S showed increased Notch activation, whereas D128N showed decreased Notch activation compared to WT-DLL4 at both high (150nM) and low (37.5nM) ligand concentrations (indicated by vertical

dotted lines). (C) Notch activation by DLL4 cancer database variants was assessed by HEK293 mN1-NLuc/CLuc-RBPJ reported cells at low protein concentrations (37.5nM). In (B) and (C), the luminescence intensity readout was used to quantify activity levels. The data was normalised as percentage of WT-DLL4 activity and presented as mean ± SD, representing combined results of n=3 independent experiments, in which 6 technical repeats were measured in each experiment. Statistical analysis was performed using Welch ANOVA followed by Dunnett's T3 multiple comparison test. ns (not statistically significant) $P>0.05$, *$P \leq 0.05$, **$P \leq 0.01$, ***$P \leq 0.001$, ****$P \leq 0.0001$.

Titration of the activity was performed using HEK293 mN1-NLuc/CLuc-RBPJ reporter cells (Figure 3-10B). As expected, WT-JAG1 was shown to have significantly lower activity than WT-DLL4 at all concentrations (see Section 1.3.3.1 for details). For the two DLL4 variants tested, R41S showed higher Notch activation than WT-DLL4 at all concentrations, whereas D128N showed reduced activity compared to WT-DLL4 at all concentrations. Furthermore, the functional effects of DLL4 variants tested at a low, non-saturating protein concentration (37.5nM) (Figure 3-10C) were broadly consistent with the activity measurements obtained at a saturating protein concentration (150nM, Figure 3-9A).

3.5 Full-length DLL4 variants cell surface expression

3.5.1 Plasmids preparation and RNA expression tests

Whilst it is generally agreed that the shorter NE3 fragment can recapitulate the activity of the full-length (FL) Notch ligand, the actual biological environment may be a possible limitation of the protein-based signalling assay (Section 3.4.1). A coculture assay would be advantageous by presenting the ligand in its physiological form in the presence of a membrane and allowing engagement of mechanical forces during Notch *trans*-activation. Plasmids containing FL-ligand protein sequences were required for transiently

transfecting HEK293T cells to express FL transmembrane Notch ligands. *pcDNA3.1-DLL4*$_{NE3\text{-}Fc\text{-}His}$ plasmids carrying the desired amino acid substitutions or loop-shortening mutations were prepared in Section 3.3.1 and restriction digested alongside wildtype *pcDNA3.1-FL-DLL4* plasmid using the same pair of restriction enzymes (*BamHI* + *XcmI* for β1-2 variants; *BamHI* + *BlpI* for β5-6 variants and F195A/Y216A). The insert from DLL4$_{NE3}$ plasmid and the vector from FL-DLL4 plasmid were ligated to generate *pcDNA3.1-FL-DLL4* plasmids carrying the desired mutations, and the correct DNA sequence was confirmed by Sanger sequencing (see Materials and Methods).

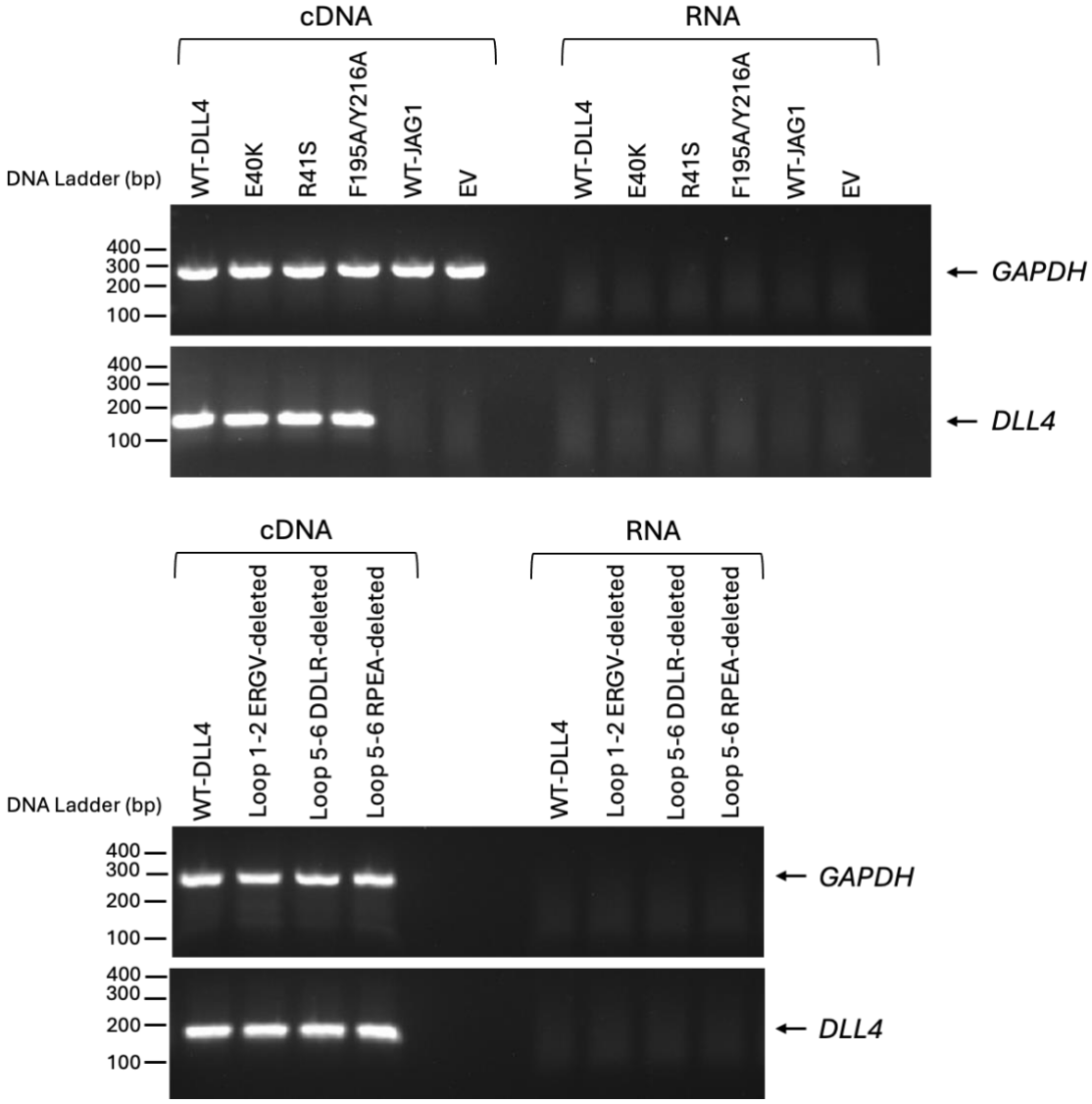


Figure 3-11. Agarose gels showing RNA expression levels of *GAPDH* and *DLL4* in transiently transfected HEK293T cells. HEK293T cells were transiently transfected to express FL-DLL4 containing missense or loop-shortening mutations. The RNA expression

levels of these variants were tested, alongside WT-DLL4, WT-JAG1, and EV, by RT-PCR (shown as cDNA templates). The RNA templates (without RT-PCR) were tested alongside to show no genomic DNA contamination in the samples. The internal control, *GAPDH*, had uniform expression in all samples, whereas *DLL4* expression in variants was similar to WT-DLL4. EV and WT-JAG1 were used as negative controls, which did not express *DLL4*. A DNA ladder was run alongside samples for size estimation.

The plasmid that carries DNA encoding the transmembrane FL-DLL4 with either a missense (E40K, R41S, F195A/Y216A) or loop-shortening (β1-2 ERGV-deleted, β5-6 DDLR-deleted, β5-6 RPEA deleted) mutation, alongside WT-DLL4, WT-JAG1, and the empty vector (*pcDNA3.1-EV*), were transfected into HEK293T cells (see Materials and Methods). 24 hours after transfection, the expression levels of *DLL4* were checked by reverse transcription PCR (RT-PCR) using *GAPDH* as an internal control (see Materials and Methods). The amplified *GAPDH* and *DLL4* target bands have an expected size of 237bp and 139bp, respectively (see Appendix 8.2.1 for RT-PCR primer sequences). Analyses of the RT-PCR products by agarose gel electrophoresis showed that, whilst *GAPDH* had a relatively uniform expression in all samples, *DLL4* was only expressed in samples transfected with DLL4-containing plasmids, and the RNA expression levels of all DLL4 variants were similar to WT-DLL4 (Figure 3-11).

3.5.2 Cell surface expression of FL-DLL4 variants

The cell surface expression level of DLL4 in transiently transfected HEK293T cells (as described in section 3.5.1) was analysed by flow-cytometry using an anti-DLL4 primary antibody (MAB1506) and a PE-conjugated secondary antibody (see Materials and Methods, Figure 3-12A). Titration tests were performed for the primary and secondary antibodies (results not shown) to confirm their specificity and make sure a saturating antibody concentration was used in the assay. To optimise the transfection protocol, HEK293T cells were transfected with different amount of WT-DLL4 plasmid and tested

for ligand surface expression. The empty vector (EV) sample acted as a background control, whilst cells transfected with either 2µg or 4µg WT-DLL4 plasmid showed similar DLL4 surface expression levels (Figure 3-12B), suggesting that 2µg plasmid was sufficient to saturate ligand expression on the cell surface. 4µg plasmid was added for transfection in later experiments to ensure saturated surface ligand expression. The histogram of cells expressing WT-DLL4 showed a bimodal distribution, suggesting significant variations of expression levels between cells even after optimising the transfection protocol. As a possible explanation, some HEK293T cells might fail to be transfected as efficiently as the rest of the cells, resulting in low-expression and high-expression subpopulations. The median fluorescence intensity (MFI, indicated by vertical dotted lines) of the two subpopulations (P1 and P2, indicated by horizontal double-headed arrows) was analysed separately to ease comparison (Figure 3-12B, see Appendix 8.3.3 for detailed data analysis).

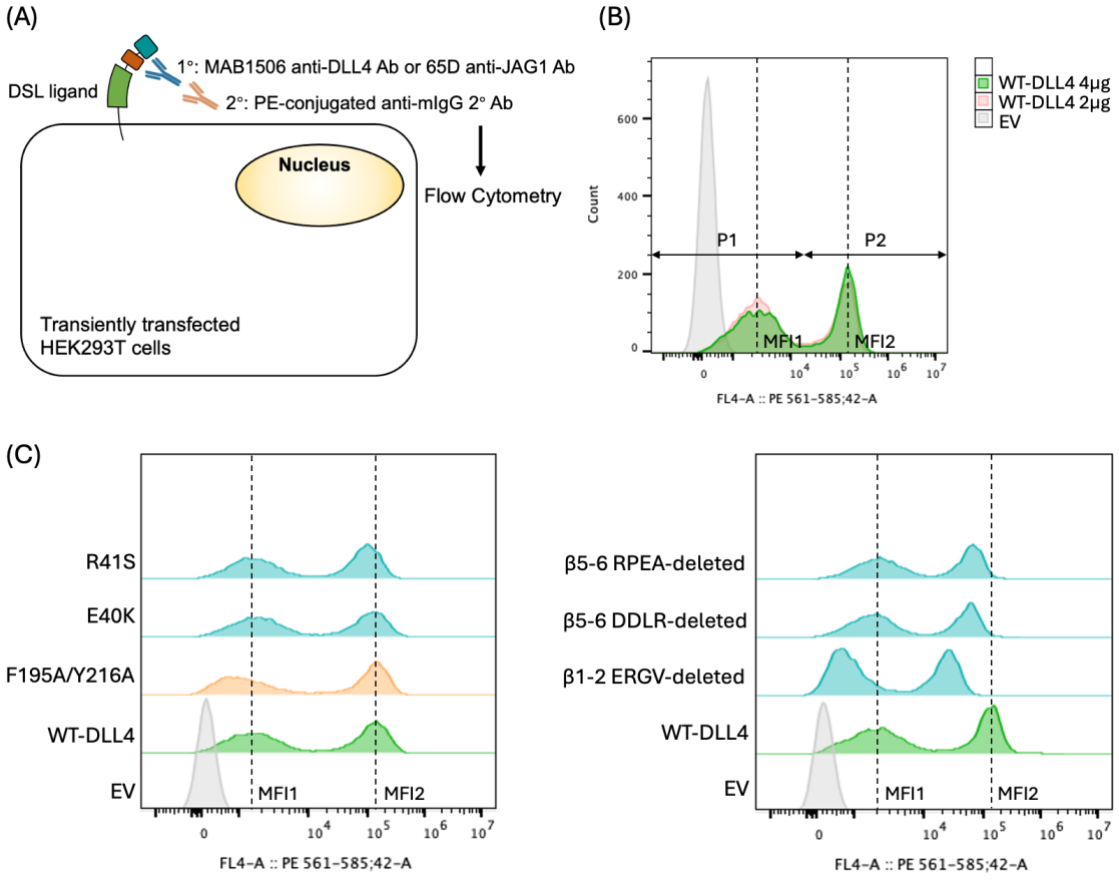


Figure 3-12. Cell surface expression of FL-DLL4 variants in HEK293T cells. HEK293T cells were transiently transfected to express FL-DLL4. Cell surface expression of DLL4

variants was tested, alongside WT-DLL4 and empty vector (EV), by flow cytometry. 30,000 cells were measured in each reading. (A) Cartoon illustrating the flow cytometry-based ligand surface expression assay (see Materials and Methods). DLL4 is probed by MAB1506 primary antibody, followed by PE-conjugated secondary antibody. Alternatively, this assay can be used to probe JAG1 surface expression using 65D primary antibody. (B) Surface expression of WT-DLL4 in cells transfected with 2μg (pink) or 4μg (green) plasmids. Similar WT-DLL4 surface expression levels were observed, as suggested by the overlapped peaks. *pcDNA3.1-EV* (grey) was used as a background control, showing a single peak at the zero point. (C) Representative histograms showing surface expression levels of DLL4 variants. The vertical dotted lines indicate the MFIs of the two cell subpopulations in the WT-DLL4 sample. The peaks (corresponding to MFI2) of the loop-shortening variants (teal) showed a leftward shift compared with WT-DLL4 (green), indicating reduced surface expression. Three independent transient transfection and surface expression tests were performed, showing consistent results.

Using the optimised transfection and antibody staining protocols, cell surface expression of FL-DLL4 missense mutation variants (E40K, R41S, F195A/Y216A) were measured and compared with WT-DLL4 (Figure 3-12C Left). Since cells expressing WT-DLL4 or its variants showed a bimodal distribution, the two subpopulations were analysed and compared separately, using the MFIs of the WT-DLL4 sample as a reference (indicated by vertical dotted lines). By overlaying both peaks in their flow cytometry histograms, the results showed that E40K, R41S, and F195A/Y216A all had a similar surface expression level to WT-DLL4. Three independent transient transfection and surface expression tests were performed, showing consistent results (Appendix 8.3.3). Notably, the shorter $R41S_{NE3}$ fragment showed significantly lower steady-state concentration in the medium (Figure 3-3), whereas FL-R41S variant showed similar surface expression to WT-DLL4, suggesting differences in secretion levels between the shorter and longer ligand constructs.

Likewise, although the NE3 fragments of loop-shortening variants showed significantly lower steady-state concentrations in the medium than $WT\text{-}DLL4_{NE3}$ (Figure 3-6) and were

not able to be purified, these variants might be normally expressed on the cell surface as a FL-ligand, acting as potential lipid-binding deficient negative controls. Therefore, the cell surface expression level of FL-DLL4 loop-shortening variants (β1-2 ERGV-deleted, β5-6 DDLR-deleted, β5-6 RPEA deleted) were analysed (Figure 3-12C Right). Compared to WT-DLL4, the histograms of loop-shortening variants showed a significant leftward shift, suggesting that these loop-shortening variants all had reduced surface expression, likely due to protein misfolding and partial ER retention. The β1-2 ERGV-deleted variant appeared to have even lower surface expression than the two β5-6 loop-shortening variants, as suggested by the more leftward shifted peaks. Likewise, statistical analysis of their MFIs showed that β1-2 ERGV-deleted variant had a surface expression level <50% of WT-DLL4, whereas the β5-6 loop-shortening variants had slightly higher surface expression levels that were ≥50% of WT-DLL4 expression level (Appendix 8.3.3).

3.6 Testing Notch activation capacity of the FL-DLL4 variants using a coculture assay

To confirm that the functional effects observed for the purified $DLL4_{NE3}$ cancer database variants (section 3.4) was recapitulated in a cellular context, Notch activation by cells expressing FL-DLL4 was tested in a coculture assay using transiently transfected HEK293T cells and HEK mN1-NLuc/CLuc-RBPJ reporter cells (Figure 3-13A, see Materials and Methods for details). Expression of WT-DLL4 and its variants after transient transfection was confirmed at both RNA (section 3.5.1) and protein (section 3.5.2) levels. The activity of WT-DLL4 and its C2 β1-2 loop missense mutation variants (E40K, R41S) and loop-shortening variants (β1-2 ERGV-deleted, β5-6 DDLR-deleted, β5-6 RPEA deleted) were measured by the coculture assay (Figure 3-13B). WT-JAG1 and F195A/Y216A were tested alongside as controls.

WT-JAG1 showed lower Notch activation than WT-DLL4 (Figure 3-13B) as previously described (see section 1.3.3.1 for details), although the expression level differences between these two ligands were not able to be directly compared in this experiment. As expected, the Notch-binding-deficient DLL4 variant F195A/Y216A showed significantly lower Notch activation that was less than 50% of WT-DLL4 activity. For the two loop β1-2 missense mutations, E40K showed slightly decreased activity whereas R41S showed slightly increased activity compared to WT-DLL4, which were consistent with the functional effects observed in section 3.4. In addition, the three loop-shortening variants all showed significantly decreased Notch activation that was ~70% of WT-DLL4 activity.

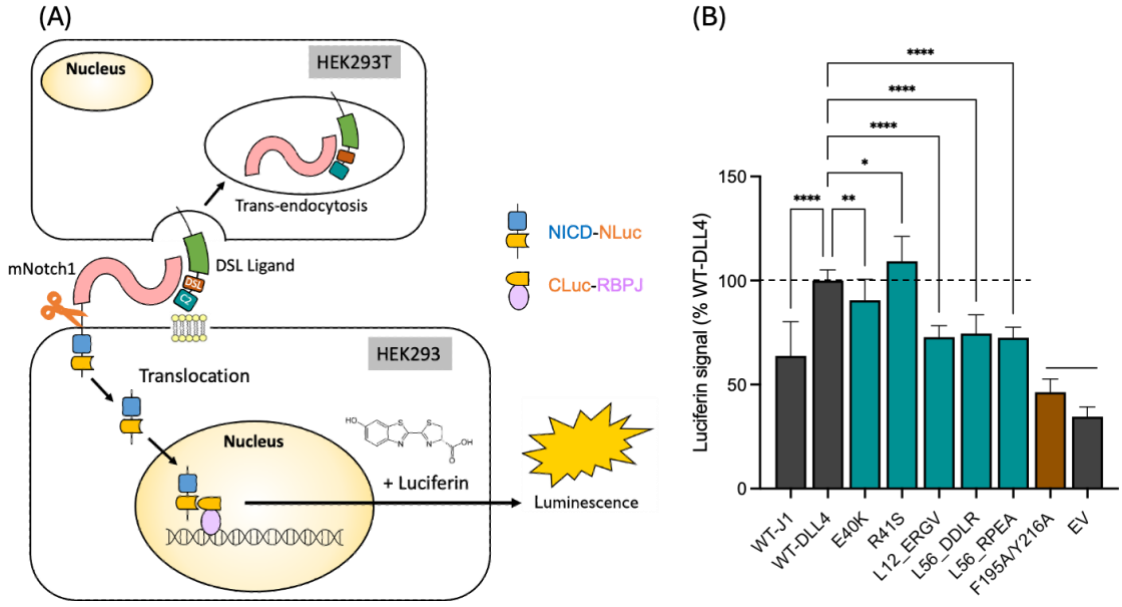


Figure 3-13. Notch activation by cell-surface-expressed FL-DLL4 cancer database and loop-shortening variants. (A) Cartoon illustrating the coculture assay using transiently transfected HEK293T cells which express Notch ligands on their cell surface and HEK293 mN1-NLuc/CLuc-RBPJ reported cells (see Materials and Methods for details). (B) Notch activation by DLL4 cancer database and loop-shortening variants was assessed by the coculture assay. The luminescence intensity readout was used to quantify activity levels. The data was normalised as percentage of WT-DLL4 activity and presented as mean ± SD, representing combined results of n=3 independent experiments, in which 6 technical repeats were measured in each experiment. Statistical analysis was performed using Welch ANOVA followed by Dunnett's T3 multiple comparison test. ns (not statistically significant) $P>0.05$, *$P \leq 0.05$, **$P \leq 0.01$, ***$P \leq 0.001$, ****$P \leq 0.0001$.

3.7 Conclusion

- **Cancer database missense mutations affected DLL4$_{NE3}$ secretion**

In this chapter, 14 missense mutations mapped to the DLL4-C2 apical loop region were selected from cancer databases (Table 3-2). The effects of these amino acid substitutions on protein secretion were analysed using conditioned medium from transiently transfected HEK293F cells that are able to secrete extracellular proteins (e.g., DLL4$_{NE3}$). Meanwhile, the detection of endogenous DLL4$_{NE3}$ produced by transfected cells provided an internal reference for the secretion test. Comparative Western blot analyses showed a band of expected mass in the conditioned medium of cells transfected with WT-DLL4, F195A/Y216A, E40K, R41S, P49S, V91L, S96R, R100G, D127E, D128N, P131T, P135A, and L164F constructs, suggesting that these substitutions do not significantly affect secretion (Figure 3-3). Although R41S, which was successfully purified, appeared to have a lower concentration in the extracellular medium, suggesting reduced secretion.

On the other hand, three variants, G47W, G98R, and A124P, were not present in the extracellular medium (Figure 3-3), consistent with intracellular retention. Since these mutant constructs were detected in the cell lysate samples, these observations rule out defective translation as the cause of the observed lack of secretion. In addition, no degraded fragments of these mutant constructs were detected in the conditioned medium samples, suggesting that susceptibility to extracellular proteolysis is unlikely the cause. Therefore, the affected secretion was most likely due to protein misfolding and intracellular retention, which may lead to loss-of-function effects. Furthermore, the double mutants, E40K/D128N and R41S/P131T, containing one missense mutation on each of the β1-2 and β5-6 loops, showed significantly decreased secretion compared to

the respective single substitution variants (Figure 3-4), suggesting possible interactions between the β1-2 and β5-6 loops during protein folding.

Mutation	Position in C2 domain	Secretion	Cell surface expression	Protein-based activity assay	Coculture-based activity assay
E40K	β1-2	√	√	↓	↓
R41S	β1-2	↓	√	↑	↑
G47W	β1-2	×	n/a		n/a
P49S	β1-2	√	n/a	no effect	n/a
V91L	β3-4	√	n/a	↓	n/a
S96R	β3-4	√	n/a	↓	n/a
G98R	β3-4	×	n/a		n/a
R100G	β3-4	√	n/a	↑	n/a
A124P	β5-6	×	n/a		n/a
D127E	β5-6	√	n/a	no effect	n/a
D128N	β5-6	√	n/a	↓	n/a
P131T	β5-6	√	n/a	no effect	n/a
P135A	β5-6	√	n/a	no effect	n/a
L164F	β7-8	√	n/a	no effect	n/a
E40K/D128N	β1-2, β5-6	↓	n/a	↓↓↓	n/a
R41S/P131T	β1-2, β5-6	×	n/a		n/a
F195A/Y216A		√	√	↓↓↓↓	↓↓↓
ERGV deleted	β1-2	×	↓↓↓↓		↓↓
DDLR deleted	β5-6	×	↓↓		↓↓
RPEA deleted	β5-6	×	↓↓		↓↓

Table 3-2. Summary of effects of DLL4 cancer database and loop-shortening variants on secretion/expression and activation. The single substitution variants showed a narrow range of functional effects, generally having an increase or decrease within ±20% of the WT-DLL4 activity, therefore are annotated as '↑ or ↓'. The activity of WT-DLL4 is normalised to 100%. '↓↓': 20%~40% decrease in activity; '↓↓↓': 40%~60% decrease in activity; '↓↓↓↓': 60%~80% decrease in activity. Likewise, the β1-2 ERGV deletion led to ~80% decrease in surface expression, whilst the other two β5-6 loop-shortening variants showed ~40% decrease in surface expression, therefore were annotated as '↓↓↓↓' and '↓↓' respectively. 'No effect': no statistically significant difference compared to WT-DLL4. Some variants were not tested in these assays, thus are marked as 'n/a' (data not available).

- **Surface expression of FL-DLL4 E40K and R41S variants was unaffected**

The effect of the cancer database missense mutations, E40K and R41S, on FL-DLL4 cell surface expression was analysed in transiently transfected HEK293T cells. Equivalent gene expression was observed by RT-PCR, providing an internal reference for the expression test (Figure 3-11). The overlaid flow cytometry histograms showed similar surface expression levels of E40K, R41S, and F195A/Y216A compared to WT-DLL4 (Figure 3-12C), suggesting that these substitutions do not significantly affect expression on the cell membrane. Notably, the $R41S_{NE3}$ fragment had much lower secretion than WT-$DLL4_{NE3}$, but the FL-R41S had a similar surface expression level to FL-WT-DLL4.

- **DLL4 cancer database variants had functional effects on Notch activation**

After successful purification of the cancer database variants as $DLL4_{NE3\text{-}Fc\text{-}His}$ constructs, activity of the purified proteins was assessed by the split-luciferase Notch activation assay using HEK mN1-NLuc/CLuc-RBPJ reporter cells (Table 3-2). Six out of the 11 single substitution variants showed functional effects, ranging from slightly decreased Notch activation (~80%) by E40K, V91L, S96R, and D128N, to slightly enhanced Notch activation (~120%) by R41S and R100G (Figure 3-9A). In addition, the purified double mutant E40K/D128N resulted in more significantly reduced Notch activation (~40%) compared to E40K and D128N, suggesting additive functional effects of these two mutations. Consistent activity results were obtained when using HEK mN2-NLuc/CLuc-RBPJ reporter cells (Figure 3-9B) or lower ligand concentrations (Figure 3-10). In both cases, E40K, D128N, and the double mutant E40K/D128N showed reduced Notch activation, whereas R41S and R100G showed increased Notch activation.

Furthermore, FL transmembrane ligands containing the cancer database missense mutations, E40K and R41S (both located on β1-2 loop), were expressed in HEK293T

cells and tested for Notch activation using HEK mN1-NLuc/CLuc-RBPJ reporter cells (Table 3-2). E40K showed slightly decreased Notch activation (~90%) whereas R41S showed slightly enhanced Notch activation (~110%) (Figure 3-13B), which were consistent with the results from protein-based activity assays. Whilst protein engineering is a useful approach to probe structure-function relationships for DLL4 variants, the coculture assay allows the ligand to be presented in its physiological form and engage the mechanical components when *trans*-activating Notch.

- **Shortening of C2 loops significantly reduced DLL4$_{NE3}$ secretion and FL-DLL4 surface expression and activity**

Comparative Western blot analyses using HEK293F cells demonstrated that the DLL4$_{NE3}$ loop-shortening variants, β1-2 ERGV-deleted, β5-6 DDLR-deleted, and β5-6 RPEA deleted (Figure 3-6), as well as a C2-truncated DLL4$_{DE3}$ construct (Appendix 8.3.2) were presented at significantly lower concentrations in the extracellular medium (Table 3-2), consistent with intracellular retention likely due to protein misfolding. The secretion test results suggested that, not only the hydrophobic core of the C2 domain, but also the C2 apical loops appeared to play an important role in DLL4 protein folding and secretion.

Flow cytometry analyses using HEK293T cells transiently transfected with wildtype or mutant FL-DLL4 demonstrated that the three FL loop-shortening variants all had reduced cell surface expression compared with FL-WT-DLL4 (Figure 3-12C). Equivalent gene expression was observed by RT-PCR, ruling out unsuccessful transfection or defective transcription as the cause of the observed reduction in surface expression (Figure 3-11). Interestingly, the β1-2 ERGV-deleted variant had even lower surface expression than the β5-6 DDLR- or RPEA- deleted variants, suggesting that the C2 β1-2 loop may play a more important role in protein folding than the β5-6 loop. Moreover, activity analysis by coculture assay showed that all three loop-shortening variants resulted in significantly reduced Notch activation (~70%) compared to WT-DLL4, probably due to a combined

effect of their lower surface expression levels (Figure 3-12) and impaired C2 apical loop structures (Figure 3-1).

Overall, results from secretion tests and Notch activation assays showed that the DLL4-C2 apical loops are important for proper protein folding/trafficking and ligand activity, in which the β1-2 and β5-6 loops may act synergistically to modulate DLL4 structure and function. A range of functional effects were observed for the DLL4 cancer database missense mutations, which were consistent in both protein-based and coculture assays, suggesting that these tumour-related mutations may play a functional role to modulate DLL4-induced Notch activation. Shortening of the β1-2 or β5-6 loop showed loss-of-function effects, confirming the importance of C2 apical loops for optimal DLL4 activity.

Chapter 4: Studying the functional importance of the DLL4 C2 domain in physiologically relevant HUVECs

4.1 Introduction

This chapter aims to develop a reverse transcription quantitative PCR (RT-qPCR) assay using HUVECs to investigate any functional effects of DLL4-C2 cancer database

missense mutations (analysed in Chapter 3) on Notch signalling in a physiologically relevant context. Although the reporter lines used previously are extremely useful to identify general effects on Notch signalling, these data are strengthened if shown to be recapitulated in a non-protein-engineered cell, more reflective of the native environment in which Notch signalling operates.

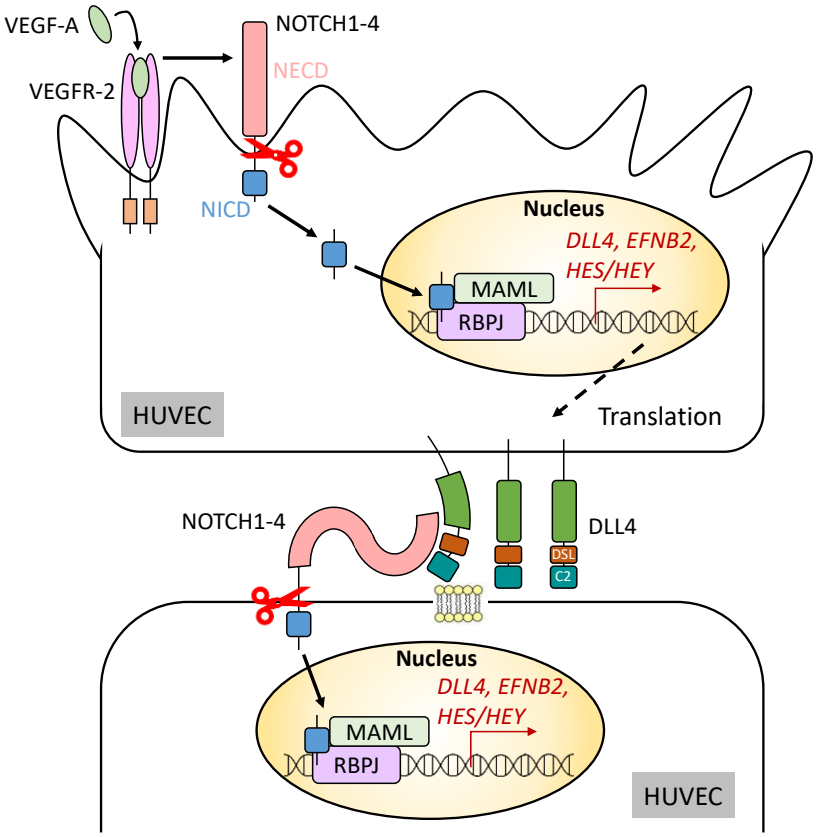


Figure 4-1. Gene expression in HUVECs regulated by a crosstalk between VEGF/ VEGFR and DLL4/NOTCH signalling pathways. HUVECs express all four Notch receptors (NOTCH1-4). VEGF-A/VEGFR-2 signalling induces DLL4 expression through NOTCH1/4 activation, which in turn activates Notch signalling in the neighbouring cells. DLL4-induced Notch activation stimulates expression of downstream target genes, including the *HES/HEY* families, the DLL4-selective marker *EFNB2*, and *DLL4* itself via a feed-forward mechanism.

As discussed in Chapter 1 Section 1.2.1.1, Notch signalling plays a key role in vascular development, including sprouting angiogenesis, where DLL4 and JAG1 have opposite effects on endothelial cell (EC) differentiation into tip/stalk phenotypes (Figure 1-4). Consistently, dysregulated DLL4 activity in ECs plays a key role in tumour angiogenesis

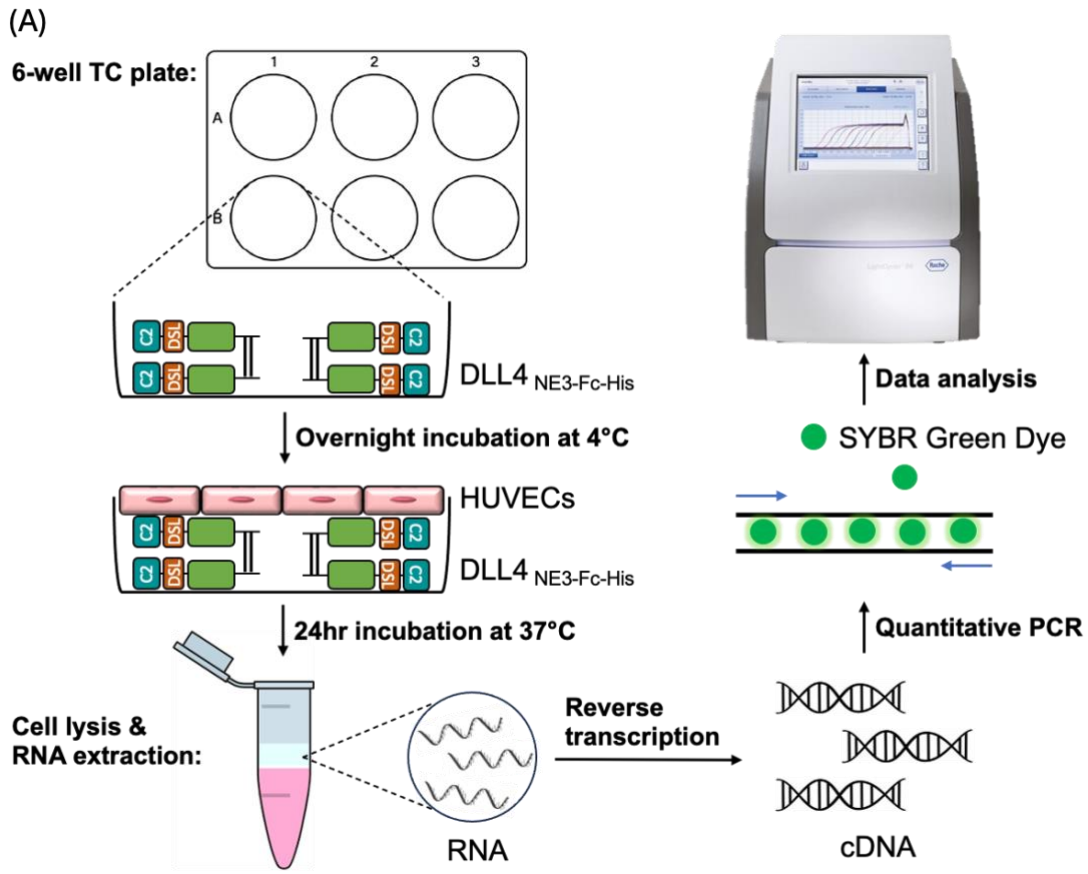
and cancer development (Hu et al., 2011; Indraccolo et al., 2010; Mendonça et al., 2019; Minuzzo et al., 2015; Patel et al., 2005). As illustrated in Figure 4-1, the Notch pathway regulates angiogenesis via crosstalk with VEGF-A/VEGFR-2 signalling, which induces DLL4 expression in ECs via a Notch-dependent mechanism and promotes a tip cell phenotype (Hellström et al., 2007; Phng & Gerhardt, 2009). A positive feed-forward mechanism was observed in the propagation of Notch signalling, in which the DLL4-induced NOTCH1 *trans*-activation upregulated *DLL4* expression in the neighbouring ECs (Caolo et al., 2010).

The human umbilical vein endothelial cells (HUVECs), which express all four Notch receptors (NOTCH1-4) and four canonical Notch ligands (JAG1, JAG2, DLL1, and DLL4) (Patel et al., 2005), provide a physiologically relevant cell model for studying Notch signalling (Figure 4-1). RNA analysis in early studies showed the expression of numerous Notch pathway downstream targets in HUVECs, including *HES1*, *HEY1*, as well as *EFNB2*, which codes for the arterial marker ephrin B2 (Hainaud et al., 2006; Patel et al., 2005). Knockdown of *DLL4* expression by RNA interference was observed to significantly downregulate *HEY1* and *EFNB2* expression, therefore these genes may act as an indicator of DLL4-induced signalling level. In particular, *EFNB2*, whose expression was only induced by DLL4 but not JAG1, has been recognised as a DLL4-selective marker in ECs (Iso et al., 2006).

qPCR is a common method used to analyse gene expression levels, which uses fluorescent probes (e.g., SYBR Green Dye) that bind double-stranded DNA (dsDNA) to collect real-time fluorescence data during the amplification of a target cDNA template (Figure 4-2A, see Materials and Methods). qPCR data is usually analysed by absolute quantification (ΔC_T) or relative quantification ($\Delta\Delta C_T$) method—the former quantifies the amount of input template based on a standard curve, whilst the latter compares fold

changes in gene expression relative to a reference sample (Livak & Schmittgen, 2001; Van Guilder et al., 2008). An amplification plot (Figure 4-2B) is generated for each reaction, which records the reporter dye fluorescence (R_n) in each PCR cycle. The value is usually normalised to a passive dye to increase the precision of measurements. Alternatively, the amplification curve can be plotted as fluorescence change (ΔR_n) against PCR cycles, where:

$$\Delta R_n = R_n \text{ (experimental sample)} - R_n \text{ (baseline)}$$



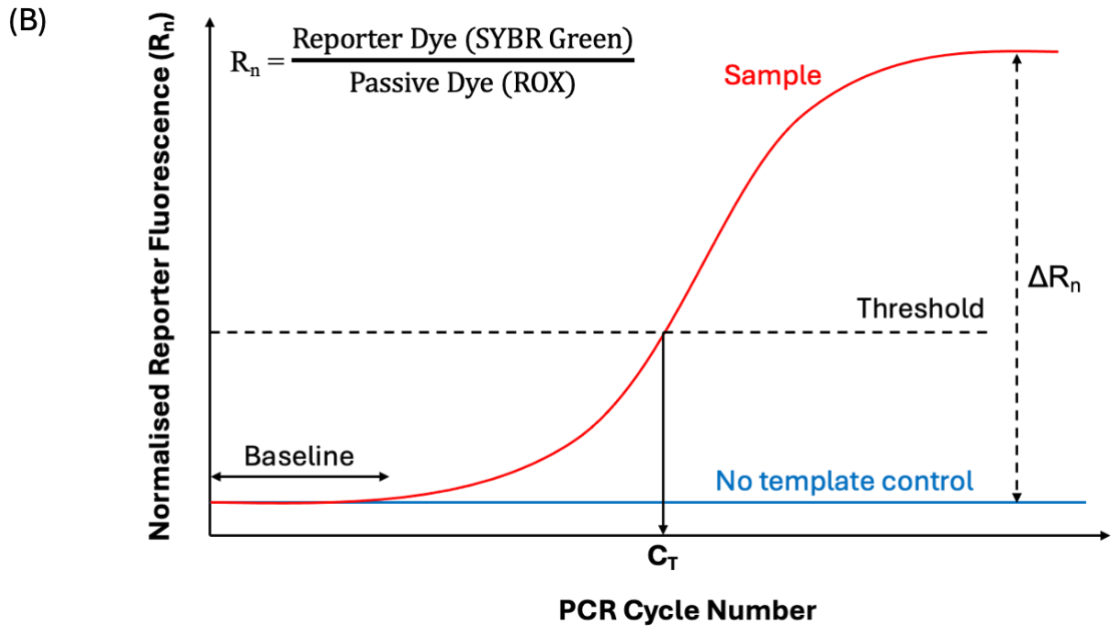


Figure 4-2. RT-qPCR experimental setup and data analysis. (A) RT-qPCR experimental procedures as described in Chapter 2: Materials and Methods. (B) qPCR amplification plot adapted from (Van Guilder et al., 2008). Amplification of the sample cDNA template (red) consists of three main phases: (i) an initial baseline (indicated by a solid double-headed arrow) when a small amount of product is hard to detect, which then gradually transitions into (ii) an exponential growth phase when the reaction is close to 100% efficiency, followed by (iii) a plateau when reagents are exhausted. A no template negative control (blue) is shown alongside, which theoretically has no amplification. C_T: the intersection between the sample amplification curve (red) and a threshold line (black dotted). R_n: the fluorescence of the reporter dye (e.g., Applied Biosystems™ SYBR™ Green dye) is normalised to the fluorescence of a passive reference dye (e.g., ROX dye) to increase the precision of technical replicates by accounting for potential variations, such as evaporation, condensation, bubbles in wells, and instrument issues. Fluorescence change (ΔR_n) is indicated by a dotted double-headed arrow, which represents the fluorescence increase of experimental samples compared to the baseline.

A crossing threshold is set to determine the number of cycles (C_T) taken for each reaction to reach the threshold fluorescence value. The threshold should be set within the exponential phase where all amplification curves of different samples are parallel (Nolan et al., 2006). In addition, when independent reactions were performed to reproduce the data, the variability of C_T values increased when the threshold was set lower in the exponential phase (Ruiz-Villalba et al., 2021). Generally, a C_T of more than 30 cycles is

considered unreliable because this suggests that the copy number of the input template is too small to be precisely estimated.

The assay was optimised for cell incubation conditions, input ligand protein concentration, RT-qPCR reaction conditions, and selections of appropriate qPCR target genes and primers. Using the optimised conditions, the relative expression levels of Notch target genes in HUVECs, seeded on WT-DLL4 or its variants (in the form of purified NE3 proteins as in Chapter 3), were quantified using the $\Delta\Delta C_T$ method. Table 4-1 shows a typical experimental design for this RT-qPCR assay, in which the expression levels of a gene of interest (i.e., the target gene, e.g., *EFNB2*) and an endogenous control gene (i.e., the reference gene *GAPDH*) were measured in two samples—the reference sample was seeded on BSA, and the target sample was seeded on Notch ligand constructs such as WT-DLL4$_{NE3\text{-}Fc\text{-}His}$ (in each case proteins were immobilised to plate surfaces, as shown in Figure 4-2A.). The expression level of the target gene is calculated as a relative quantity value (RQ), such that all BSA sample gene expression levels are calibrated as 1-fold, using the equations below:

$$\Delta C_T = C_{T(EFNB2)} - C_{T(GAPDH)}$$

$$\Delta\Delta C_T = \Delta C_{T(WT\text{-}DLL4)} - \Delta C_{T(BSA)} = (C_{T(D)} - C_{T(B)}) - (C_{T(C)} - C_{T(A)})$$

$$\text{RQ (i.e., fold change)} = 2^{-\Delta\Delta C_T}$$

	Reference sample (e.g., BSA)	Target sample (e.g., WT-DLL4)
Reference gene (e.g., *GAPDH*)	A	B
Target gene (e.g., *EFNB2*)	C	D

Table 4-1. RT-qPCR assay experimental design.

4.2 Development of an RT-qPCR assay to measure DLL4-induced signalling

4.2.1 Expression of Notch target genes in HUVECs

HUVECs were incubated in the presence of VEGF (see Materials and Methods) with purified WT-DLL4$_{NE3\text{-}Fc\text{-}His}$ proteins for 24 hours, followed by RNA extraction and reverse transcription to produce a cDNA library (see Materials and Methods, Figure 4-2A). To confirm the expression of Notch target genes in HUVECs, PCR was performed using the cDNA template to amplify transcripts of known target genes (Hainaud et al., 2006; Patel et al., 2005), including the *HES/HEY* families, *DLL4*, and *EFNB2*, alongside *JAG1* and the housekeeping gene *GAPDH* (see Appendix 8.2.1 for detailed information of qPCR primers and amplicon sizes).

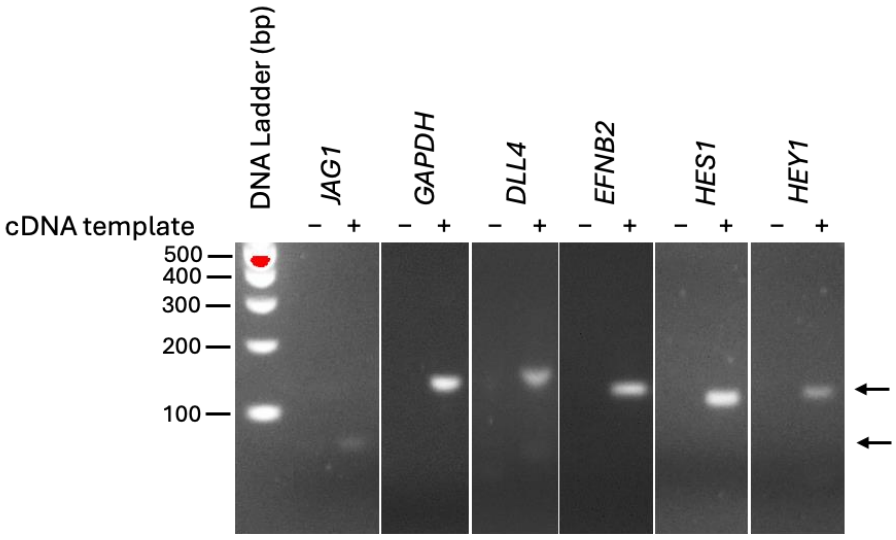


Figure 4-3. Expression of Notch downstream target genes in HUVECs. The expression of a variety of Notch target genes in WT-DLL4-treated (+) HUVECs was analysed by RT-PCR. A "no template" control (−) was tested alongside each target to check that the primer pairs did not self-anneal. The genes were amplified by qPCR primers (see Appendix 8.2.1 for primer details) and visualised by agarose gel electrophoresis. A DNA ladder was run alongside samples for size estimation. Target bands with expected lengths were indicated by arrows (*GAPDH*: 131bp, *DLL4*: 139bp, *EFNB2*: 135bp, *HES1*: 111bp, *HEY1*: 125bp, *JAG1*: 71bp). Note that *JAG1* has not been reported as a downstream target of DLL4/Notch signalling in ECs, and its expression was detected at a very low level in HUVECs, as suggested by the faint band (arrowed).

The amplicons were visualised by agarose gel electrophoresis, which showed expression of *HES1, HEY1, DLL4, JAG1, EFNB2,* and *GAPDH* in WT-DLL4 treated HUVECs (Figure 4-3). A single band with expected size was observed for each gene, suggesting that a single, pure amplicon was produced using the specific primer pair. Some of the other *HES/HEY* family genes such as *HES2* and *HEY2* were also tested (see Appendix 8.4.1), which generally showed weaker expression compared to *HES1* and *HEY1*. Moreover, "no template" controls (NTC) were tested alongside, showing that no primer dimers were formed or amplified by the primer pairs (Figure 4-3). Two independent expression tests were performed to ensure reliable results.

4.2.2 Optimisation of assay conditions

HUVECs were seeded on WT-DLL4, the Notch-binding-deficient variant F195A/Y216A, and the reference sample BSA (all as purified proteins immobilised to a plate, see Materials and Methods), and RNA expression levels of the five target genes (see Section 4.2.1) and *GAPDH* were measured. Various experimental conditions were tested to determine: i) the appropriate target gene(s) in HUVECs which respond to DLL4-Notch signalling sensitively; ii) the appropriate ligand concentration and incubation time for HUVECs to produce an optimal transcriptional outcome; and iii) the optimal reaction conditions to produce reliable and reproducible qPCR data.

Firstly, HUVECs were seeded on 5ng/μL ligand proteins with varying incubation times from 8 to 48 hours (Figure 4-4A). For *EFNB2, DLL4, HES1*, and *HEY1*, treatment of cells with WT-DLL4 resulted in significantly increased gene expression compared to cells treated with BSA, whilst Notch binding deficient variant F195A/Y216A had no effect on gene expression compared to the BSA sample, suggesting that these genes were specifically upregulated by DLL4-induced Notch activation. Time-dependent increases in expression levels were observed over 48 hours, likely due to the sustained DLL4-

Notch activatory signalling. Longer incubation times (≥24 hours) generally resulted in larger differences between the positive (i.e., WT-DLL4) and negative (i.e., F195A/Y216A) controls, maximising sensitivity. However, since HUVECs have a doubling time of 28-36 hours (N. Lai et al., 2009; Lau et al., 2022), 24-hour incubation was preferred over 48-hour incubation because cell duplication may complicate data interpretation. Moreover, although a weak band for *JAG1* gene expression was observed in Figure 4-3, no increase in expression over and above the F195A/Y216A negative control was observed in Figure 4-4A, suggesting that WT-DLL4 did not induced *JAG1* expression regardless of the incubation time.

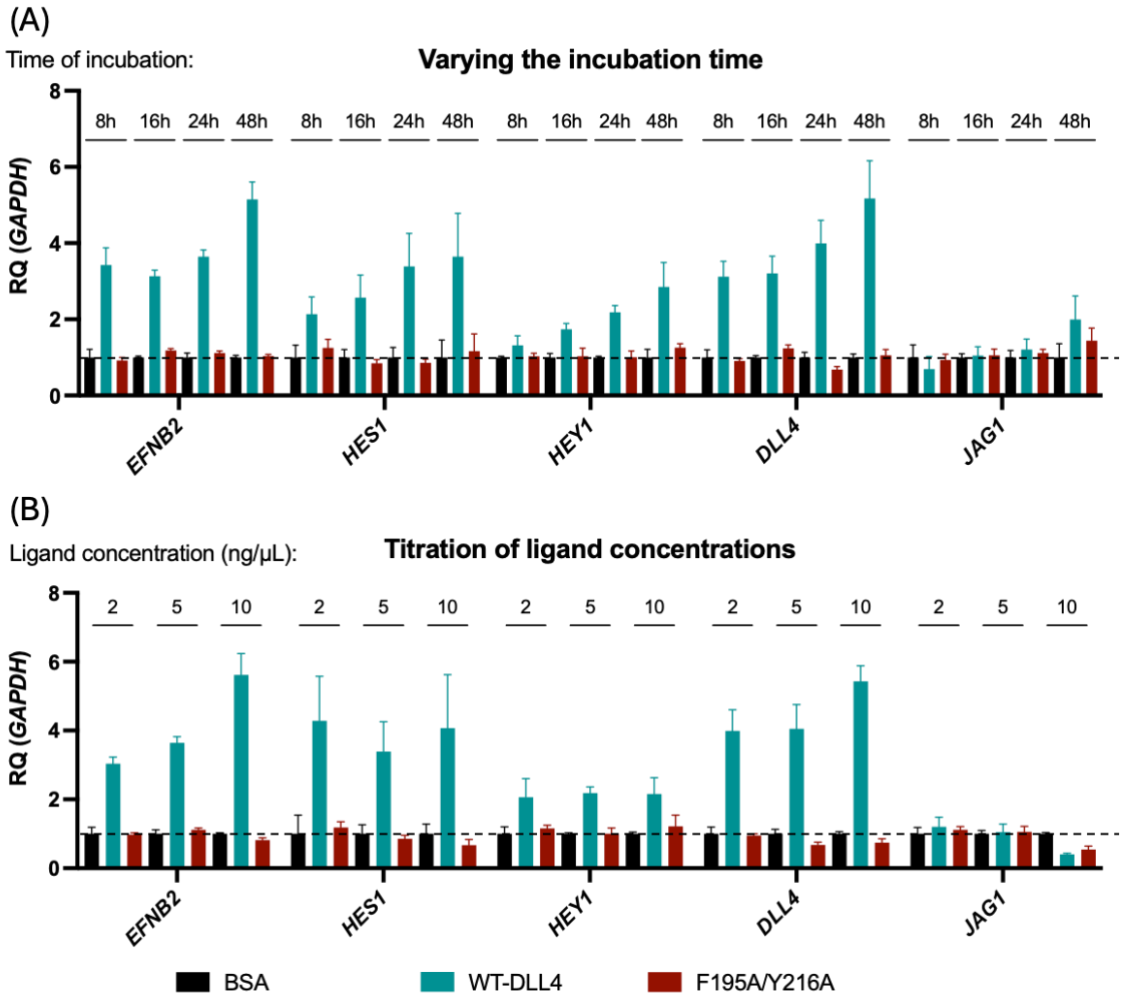


Figure 4-4. Optimisation of RT-qPCR assay conditions. RT-qPCR was performed for HUVECs samples incubated under different conditions: (A) HUVECs were seeded on 5ng/μL WT-DLL4 (teal), F195A/Y216A (brown), or BSA (black) for varying durations; (B) HUVECs were incubated with different concentrations of ligand proteins for 24 hours. The expression

levels of five target genes, normalised by the endogenous control *GAPDH*, were quantified using the $\Delta\Delta C_T$ method as an RQ value, indicating a fold change relative to the BSA sample. The RQ values of all BSA samples were calibrated to 1-fold (indicated by the black dotted line). Data was presented as mean ± SD of triplicate measurements.

Secondly, HUVECs were seeded on ligand proteins at varying concentrations for 24 hours (Figure 4-4B). Whilst expression of *EFNB2, DLL4, HES1*, and *HEY1* was all clearly upregulated by WT-DLL4, only *EFNB2* and *DLL4* showed a dose-dependent increase in expression levels, with a more than 5-fold increase compared to the BSA and F195A/Y216A controls when 10ng/μL WT-DLL4 was used. On the other hand, *HES1* and *HEY1* showed relatively similar expression levels regardless of the protein concentrations. It should be noted, however that the error bars of *HES1* expression were large, whilst WT-DLL4-induced expression of *HEY1* resulted in only a 2-fold increase compared to the BSA control, making these results difficult to interpret. Similar to results in Figure 4-4A, WT-DLL4 had no effect on *JAG1* expression regardless of the ligand concentration (Figure 4-4B), further suggesting that *JAG1* is not a DLL4-Notch signalling target gene in HUVECs.

Overall, given their expression levels were significantly upregulated by WT-DLL4 and were relatively stable in cells over the incubation time, these results suggested that *EFNB2* and *DLL4* were the most appropriate target genes to probe DLL4-Notch signalling in HUVECs. *HES1* expression was also tested alongside, since although it did not exhibit convincing concentration-dependence on DLL4, it showed a clear difference in expression in response to WT or Notch-binding-negative DLL4. It is also a well-known Notch target gene (De Decker et al., 2021; Dhanesh et al., 2016; Monahan et al., 2009; Takeshita et al., 2007; K. Zhang et al., 2015). To optimise the transcriptional outcome, HUVECs were incubated with 10ng/μL ligand proteins for 24 hours for later experiments. In addition, reaction conditions, such as annealing temperature (55°C, 58°C or 60°C)

and cDNA input amount (250ng, 500ng, or 1µg per reaction), were optimised for qPCR (see Appendix 8.4.2). Annealing was performed at 60°C, which was more stringent to prevent non-specific annealing. In addition, around 500ng template cDNA was used per reaction to keep the C_T value within 30 cycles for reliable results (as explained in Section 4.1).

4.3 Testing Notch activation capacity of the purified DLL4 cancer database variants

To investigate if the Notch activation effects of the DLL4 cancer database variants observed in the split-luciferase reporter cells (Section 3.4) can be recapitulated in physiologically relevant HUVECs, RT-qPCR assays using the optimised protocol (as describe in Section 4.2.2) were performed for WT-DLL4, DLL4-F195A/Y216A and the eleven purified DLL4 variants (β1-2: E40K, R41S, P49S; β3-4: V91L, S96R, R100G; β5-6: D127E, D128N, P131T, P135A; β7-8: L164F). WT-JAG1 and JAG1-F207A/E228K were tested alongside to provide a ligand-ligand comparison. The ligand constructs were purified as Fc-dimerised NE3 fragments and have been qualitatively and quantitatively analysed in Section 3.3.2, showing good protein purity and similar working concentrations, as well as the ability to activate Notch in a reporter cell setting (see Section 3.4 for details).

4.3.1 Quality check of RNA and cDNA templates

Prior to qPCR, the total RNA was extracted from HUVECs and reverse transcribed to a cDNA library (see Materials and Methods). The target gene-specific cDNA produced was checked by PCR and agarose gel electrophoresis using *GAPDH* primers (see Materials and Methods). For the RNA samples, no amplicon band was observed, suggesting that the RNA was free of DNA contamination, otherwise the contaminant DNA would be

amplified (Figure 4-5). RNA concentrations were measured by a NanoDrop spectrophotometer, and the same amount of input RNA template was used for reverse transcription to produce similar amount of cDNA (see Materials and Methods). The cDNA samples were also subjected to PCR, followed by gel electrophoresis. As expected, all cDNA samples showed uniform expression of *GAPDH* (Figure 4-5), suggesting that the same amount of cDNA template was used per reaction in the RT-qPCR assay. This quality check test was performed for each RT-qPCR experiment.

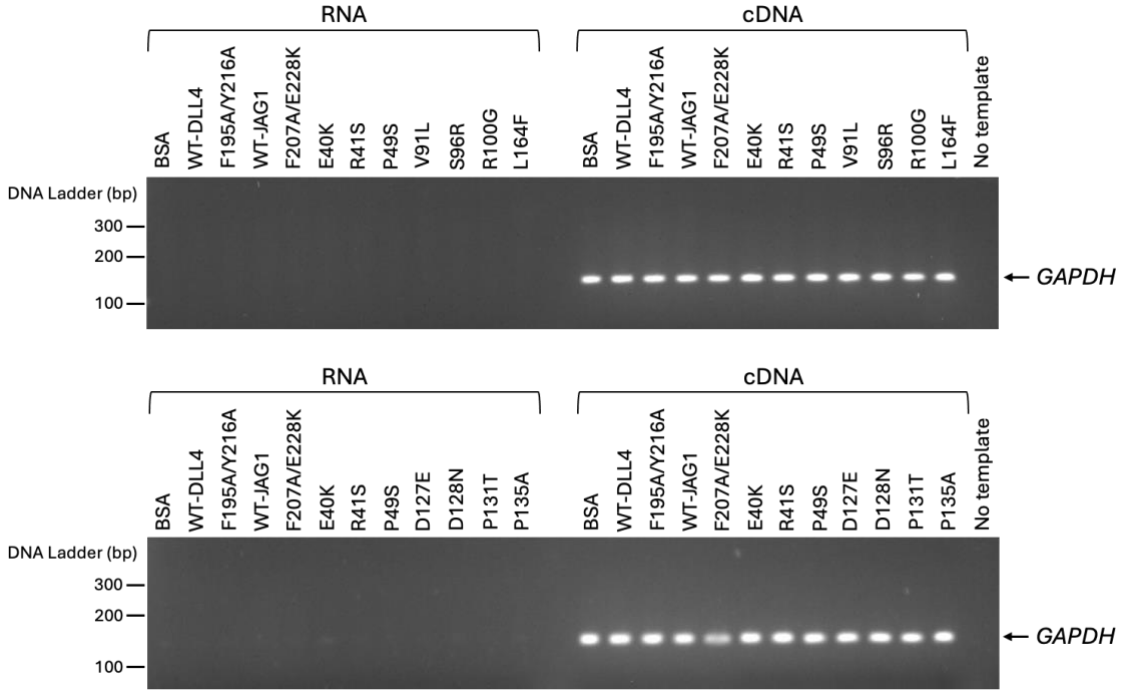


Figure 4-5. RT-PCR amplification of *GAPDH* gene using RNA and cDNA templates from ligand-treated HUVECs. HUVECs were incubated with WT-DLL4, DLL4 cancer database variants, DLL4-F195A/Y216A, WT-JAG1, JAG1-F207A/E228K, alongside BSA as a reference sample. After incubation, RNA was extracted from HUVECs and reverse transcribed to cDNA. *GAPDH* target sequence was amplified using the RNA or cDNA as template and visualised by agarose gel electrophoresis (the target band is arrowed). *GAPDH*, as an endogenous control, showed uniform expression in all cDNA samples.

4.3.2 Analysis of qPCR raw data

The raw qPCR data collected was outputted as an amplification plot to show fluorescence change (ΔR_n) over time (Figure 4-6A). As explained in Section 4.1, a C_T

value can be derived from each amplification curve, indicating the number of PCR cycles required for the starting material to reach a threshold fluorescence value (Figure 4-2). The amplification plot of *GAPDH* showed that the curves of independent samples generally intersected the threshold line at the same position, suggesting that similar C_T values were obtained, and this housekeeping gene was stably and constantly expressed in all samples regardless of the state of the cells (Figure 4-6A).

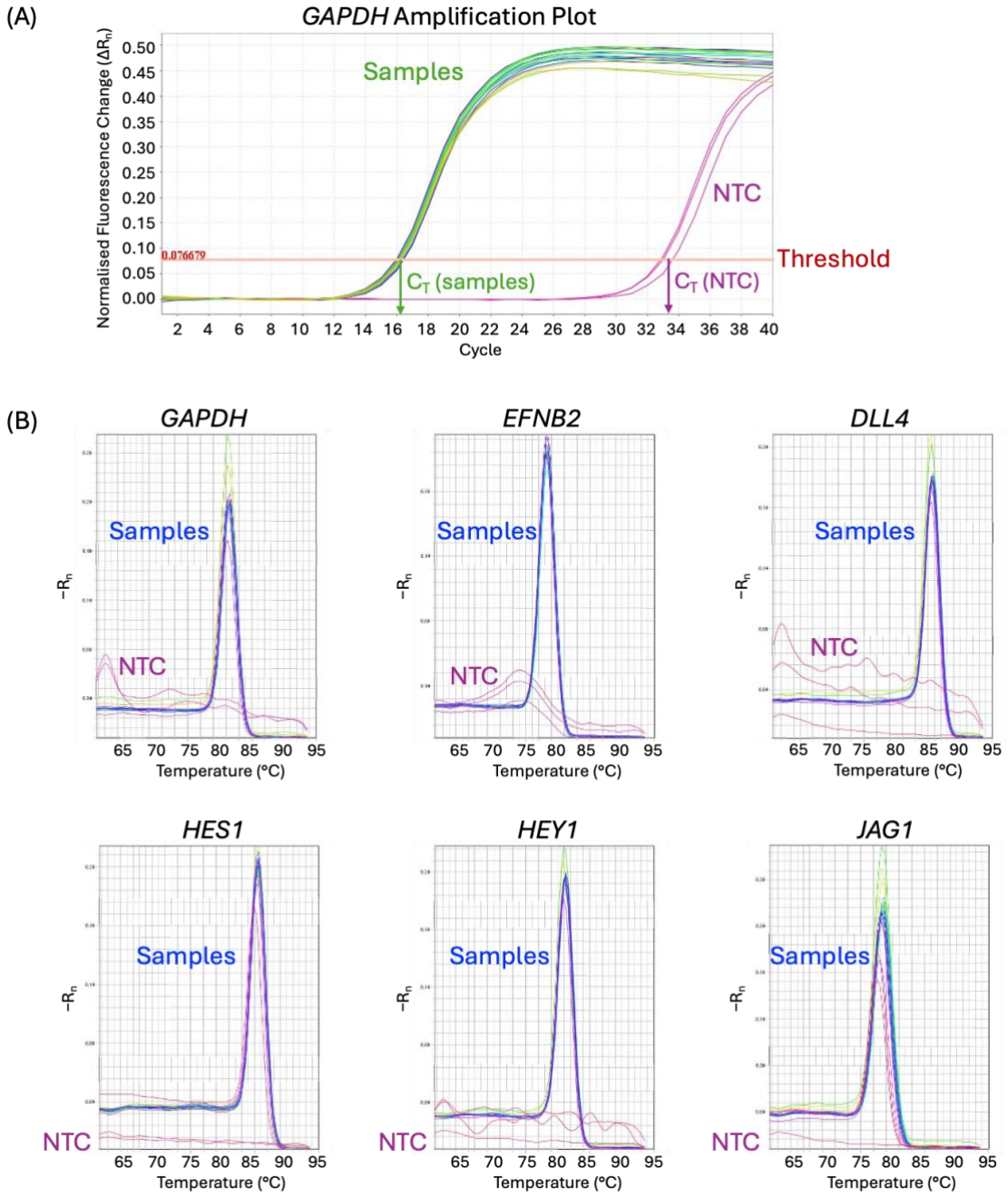


Figure 4-6. qPCR data analysis. (A) A representative amplification plot showing triplicate measurements of *GAPDH* expression in cDNA samples (green) and NTC (magenta). The C_T

of each sample was determined by the intersection between the threshold line (red) and the amplification curve. The C_T values of all cDNA samples (arrowed) are similar because *GAPDH* is a constitutively expressed endogenous control gene. Note that the amplification curves of NTC samples generated a C_T >30 cycles (arrowed), which could be due to primer dimer formation, a phenomenon commonly observed when SYBR™ Green dye is used. (B) Melt curve analyses of HUVEC target genes selected, which plotted fluorescence decrease ($-R_n$) against temperature increase to assess the purity of qPCR amplicons. Experimental samples (blue) and NTC samples (magenta) were indicated.

NTC samples were tested alongside, which showed baseline expression until 30 cycles of PCR, suggesting that primer dimers were not formed in the first 30 cycles of reactions. An exponential phase was observed after 30 cycles, likely due to primer dimer formation. This phenomenon is common when using SYBR™ Green as the intercalating dye, because any primer dimers will cause higher background and may lead to a generation of C_T < 40 for NTC samples (D'haene et al., 2010; J. Yang et al., 2016). However, since the sample C_T was determined within the first 30 cycles, the primer dimers formed afterwards did not alter the C_T of the experimental samples or change the interpretation of expression levels.

Furthermore, a dissociation profile was generated after each qPCR reaction and plotted as a melt curve (Figure 4-6B). Since the intercalating dye (e.g., SYBR™ Green) used in qPCR produces fluorescence only when bound to dsDNA, denaturation of dsDNA into single-stranded DNA (ssDNA) at high temperature will cause the dye to dissociate from ssDNA and lose fluorescence. This fluorescence decrease ($-R_n$) was plotted against temperature increase in a melt curve to assess the amplicon size and purity of the qPCR product. The amplicons of target genes, which had a size of ~100bp, typically dissociated at a temperature above 75°C, although the exact melting temperature would vary depending on the band size and GC content (Figure 4-6B, see Appendix 8.2.1 for the expected size of each qPCR amplicon). The peak observed for each gene suggested a

single amplicon without any primer dimer or other nonspecific amplification artefacts. These melting profiles were consistent with agarose gel electrophoresis results (Figure 4-3). Theoretically, no peak should be observed in the melt curves of NTC samples, suggesting the absence of a target amplicon since no template was added. Occasionally, melt peaks below 75°C were observed due to primer dimer formation, which generally happened after the first 30 PCR cycles (as explained above).

4.3.3 Expression of Notch target genes induced by DLL4 variants

The quality check of input materials (Section 4.3.1) and appropriate analyses of reaction output (Section 4.3.2) suggested that the qPCR data collected was reproducible. The RQ data of variants obtained using the $\Delta\Delta C_T$ method was normalised as percentage of WT-DLL4 RQ to account for potential variability associated with different batches of HUVECs. Figure 4-7A presents the combined results of three independent experiments. Both *EFNB2* and *DLL4* expression levels varied significantly in response to transcriptional induction by different DLL4 variants as compared to WT-DLL4, suggesting a range of functional effects of these variants in HUVECs. The expression patterns of these two genes in response to ligand variants were similar, both showed a decrease in expression for E40K, D127E and D128N, and an increase in expression for R41S, R100G and P131T. On the other hand, all DLL4 variants resulted in upregulated *HES1* expression that was not statistically significantly different from WT-DLL4, suggesting insensitivity of this gene to subtle changes in activity. WT-JAG1 was tested alongside, which showed a much lower capacity to induce expression of *EFNB2, DLL4,* or *HES1*, resulting in less than 50% of WT-DLL4-induced expression levels (Figure 4-7A). As expected, the Notch-binding-deficient variants DLL4-F195A/Y216A and JAG1-F207A/E228K both showed loss-of-function effects, resulting in basal levels of gene expression similar to the BSA reference control.

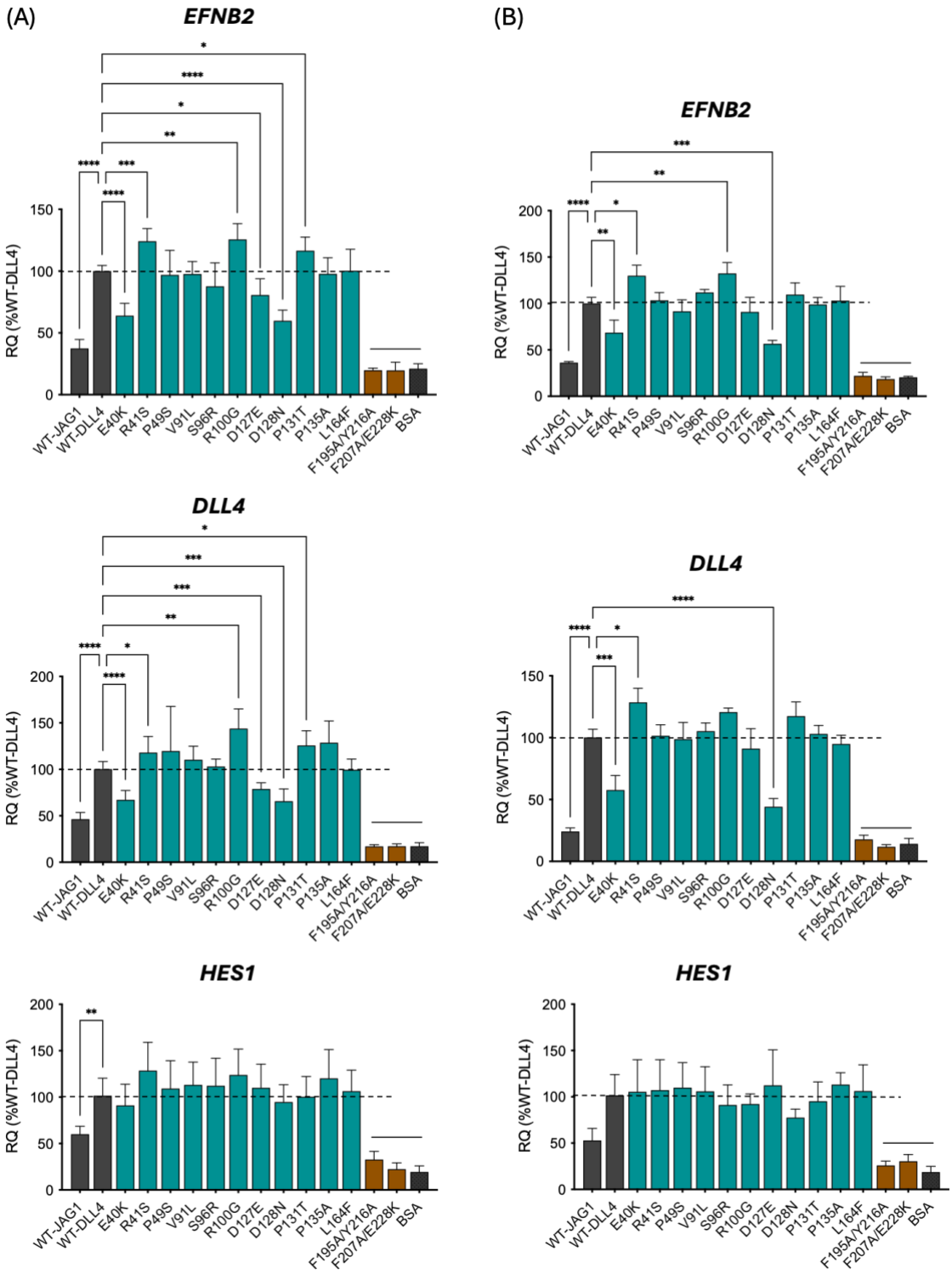


Figure 4-7. Expression of Notch target genes in HUVECs induced by purified DLL4$_{NE3}$ cancer database variants. RT-qPCR was performed for HUVECs samples seeded on WT-DLL4 (black), its cancer database variants (teal), and DLL4-F195A/Y216A (brown), alongside WT-JAG1 (black) and JAG1-F207A/E228K (brown). Cells seeded on BSA (black) were used as a reference sample. The expression levels of three target genes, *EFNB2, DLL4* and *HES1*, normalised by the endogenous control *GAPDH*, were quantified using the $\Delta\Delta C_T$ method as an RQ value. (A) Collective results of n=3 independent experiments, each with 3 technical

repeats. (B) Blind test results, which took triplicate measurements of each sample. The data was normalised as percentage of WT-DLL4 activity and presented as mean ± SD. Statistical analysis was performed using Welch ANOVA followed by Dunnett's T3 multiple comparison test (*EFNB2* and *DLL4* in (A)) or ordinary one-way ANOVA followed by Dunnett's post hoc test (*HES1* in (A); *EFNB2, DLL4, HES1* in (B)). **P* ≤ 0.05, ***P* ≤ 0.01, ****P* ≤ 0.001, *****P* ≤ 0.0001. The rest of the variants showed no statistically significant difference compared to WT-DLL4.

Additionally, a blind experiment was performed, in order to reduce any possibility of research bias. The blind test results (Figure 4-7B) largely agreed with the unblind test results described above (Figure 4-7A), suggesting the functional effects observed were consistent. Variants E40K, R41S, R100G (for *EFNB2* only), and D128N consistently resulted in statistically significant increase or decrease of *EFNB2* and *DLL4* expression. Variants R100G (for *DLL4* only), D127E, and P131T showed a consistent trend to enhance or reduce *EFNB2* and *DLL4* expression, although the differences were not statistically significant compared to WT-DLL4. Likewise, the activity of WT-JAG1 was consistently lower than the activity of WT-DLL4 in the blind test, although the difference was not statistically significant in *HES1* expression. Overall, there was good agreement between the blind and unblind experiments.

4.4 Conclusion

In this chapter, a novel RT-qPCR assay was developed and optimised to probe DLL4-induced target gene expressions in physiologically relevant HUVECs. ECs were chosen as a model system for screening DLL4 functionality due to the known involvement of this ligand in endothelial sprouting (Caolo et al., 2010; Hellström et al., 2007; Phng & Gerhardt, 2009). Transcriptional analyses of potential target genes under varying experimental conditions identified *EFNB2* and *DLL4* as two of the most sensitive genes that responded to DLL4-Notch signalling levels (Figure 4-4). In addition, various

optimisation steps, such as primer design (Figure 4-3), sample preparation, quality check of input and output materials (Figure 4-5), threshold setting, and raw data analysis (Figure 4-6), were standardised to generate reliable and reproducible RT-qPCR data.

Mutation	Position in C2 domain	RT-qPCR activity assay in HUVECs		
		EFNB2 **expression**	***DLL4*** **expression**	***HES1*** **expression**
E40K	β1-2	↓↓	↓↓	no effect
R41S	β1-2	↑	↑	no effect
P49S	β1-2	no effect	no effect	no effect
V91L	β3-4	no effect	no effect	no effect
S96R	β3-4	no effect	no effect	no effect
R100G	β3-4	↑↑	↑↑	no effect
D127E	β5-6	↓	↓	no effect
D128N	β5-6	↓↓	↓↓	no effect
P131T	β5-6	↑	↑	no effect
P135A	β5-6	no effect	no effect	no effect
L164F	β7-8	no effect	no effect	no effect
F195A/Y216A		↓↓↓↓	↓↓↓↓	↓↓↓↓
WT-JAG1		↓↓↓	↓↓↓	↓↓↓
F207A/E228K		↓↓↓↓	↓↓↓↓	↓↓↓↓
BSA		↓↓↓↓	↓↓↓↓	↓↓↓↓

Table 4-2. Summary of effects of DLL4 cancer database variants on expression of Notch target genes in HUVECs. Some variants resulted in a slight increase or decrease of about ±20% of WT-DLL4 activity and are annotated as '↑ or ↓'. Some variants resulted in a more significant increase or decrease of about ±40% of WT-DLL4 activity and are annotated as '↑↑ or ↓↓'. WT-JAG1 had an activity that was lower than 50% of WT-DLL4 activity, therefore is annotated as '↓↓↓'. Negative controls generally resulted in a basal level of gene expression that was ~20% of the WT-DLL4 activity, therefore are annotated as '↓↓↓↓'. 'No effect': no statistically significant difference compared to WT-DLL4.

DLL4 and JAG1 have distinct expression patterns in ECs and play opposite roles in promoting or inhibiting angiogenic sprouting (Benedito et al., 2009) (see Section 1.2.1.1 and refer to Figure 1-4 for details), making HUVECs a good model system to study ligand-specific differences. In this study, WT-JAG1 mildly induced the expression of *EFNB2, DLL4* and *HES1*, although the expression levels were dramatically lower than

those induced by WT-DLL4 (Table 4-2), consistent with observations made in earlier studies (Iso et al., 2006; Oon et al., 2017). Early RT-PCR experiments combined with Northern blot analyses showed that DLL4, but not JAG1, markedly upregulated *EFNB2* expression in HUVECs, but not in other cell types such as C2C12 or vascular smooth muscle cells (VSMCs) (Iso et al., 2006). Moreover, all negative controls, including DLL4-F195A/Y216A, JAG1-F207A/E228K, and BSA, resulted in basal expression of target genes.

Using the optimised protocol, the activity of eleven DLL4 cancer database variants, purified as $DLL4_{NE3\text{-}Fc\text{-}His}$ constructs from HEK293F and tested in split-luciferase reporter cells (Chapter 3), was assessed using this RT-qPCR assay (Table 4-2). Six out of the eleven variants showed functional effects, ranging from reduced *EFNB2* expression induced by E40K, D127E and D128N, to enhanced *EFNB2* expression induced by R41S, R100G and P131T (Figure 4-7A). The variants altered *DLL4* expression levels in a similar manner, suggesting consistency in different DLL4-Notch signalling target genes.

On the other hand, *HES1* failed to show the subtle differences between cancer database variants and WT-DLL4. This may be due to the short half-life of *HES1* mRNA (~20 min in murine cell lines) and an oscillatory nature of expression (Bonev et al., 2012; Hirata et al., 2002; Kageyama et al., 2007; Monk, 2003). *HES1* was previously observed to act as a cellular oscillator and shown to display highly variable expression levels within and between cells (Kobayashi & Kageyama, 2010; Maeda et al., 2023; Sabherwal et al., 2021), consistent with the large error bars seen in its RT-qPCR results (Figure 4-7A).

Overall, the DLL4 cancer database variants resulted in a range of functional effects on the expression of Notch target genes, which were observed for both *EFNB2* and *DLL4*. The RT-qPCR results were largely consistent with the activity assay results measured using the split-luciferase Notch activation assay (see Chapter 3, Table 3-2).

Chapter 5: Investigating the Notch-binding and membrane-interacting properties of DLL4 variants

5.1 Introduction

As discussed in Chapter 1, the N-terminal C2 domain of canonical Notch ligands was known to confer both receptor- and lipid-binding properties (Chillakuri et al., 2013; Luca et al., 2015, 2017; Suckling et al., 2017). Structural studies of Notch/ligand complexes showed that C2 bound Notch receptor via a disulfide-bonded loop (β2-3) at the base of the domain (Luca et al., 2015, 2017), a site distinct from that located in the DSL domain. This Notch binding region was located distal to the apical loop region implicated in lipid binding (Chillakuri et al., 2013; Martins et al., 2021; Suckling et al., 2017) (see section 1.3.3 and section 1.5.4 for details). The separate, nonoverlapping receptor- and membrane-interacting sites on the C2 domain seemed independent of each other, as suggested by the JAG1 EHBA variants, which reduced lipid binding without affecting Notch binding (Suckling et al., 2017). However, recent data on JAG1 N-glycan variants observed some detrimental effect on Notch binding (Meng et al., 2022), suggesting that C2 apical loops may indirectly affect receptor binding.

The DLL4 cancer database variants described in Chapter 3 and Chapter 4 showed a range of functional effects, from a reduction in Notch activation to slightly enhanced activity. Whether these DLL4-C2 missense mutations affected ligand activity due to changes in receptor-binding affinity or membrane-interacting property remained to be investigated. Therefore, molecular assays were performed to probe the receptor- and lipid-binding ability of these DLL4 variants. A well-established plate-based binding assay using purified receptor and ligand fragments, as well as two cell-based binding assays using either complete full-length (FL) Notch receptors or ligands expressed on the cell surface were carried out to measure ligand-receptor binding. For ligand-membrane binding assessment, a recently developed flow cytometry-based liposome aggregation assay was utilised (Meng et al., 2022). Moreover, in previous studies, molecular dynamics (MD) simulations were shown to be useful in visualising possible molecular

mechanisms underlying C2-membrane interactions (Larsen & Sansom, 2021; Meng et al., 2022). Thus, MD analyses were performed to predict possible binding orientations of DLL4-C2 interacting with membranes of different lipid compositions.

5.2 Preparation of receptor protein constructs

5.2.1 Expression of recombinant Notch receptors in S2 insect cells

Limited fragments of recombinant Notch receptors (see Appendix 8.2.8 for protein sequences), $NOTCH1_{EGF11\text{-}13}$, $NOTCH2_{EGF11\text{-}13}$, and $NOTCH1_{EGF7\text{-}13}$, were expressed in S2 insect cells for secretion as C-terminally BirA- and His- tagged fusion proteins (see Materials and Methods). The S2 system allows high level of protein expression and efficient O-glycosylation, as shown by previous structural data (Martins et al., 2021; Suckling et al., 2017). To confirm that the correct DNA sequence was cloned and expressed, total DNA and RNA were extracted from the cells, amplified with pEXS2-2 primers (see Appendix 8.2.1 for primer details) by PCR (Figure 5-1A) or RT-PCR (Figure 5-1B), and the sequences of the amplicons were checked by Sanger sequencing (see Materials and Methods).

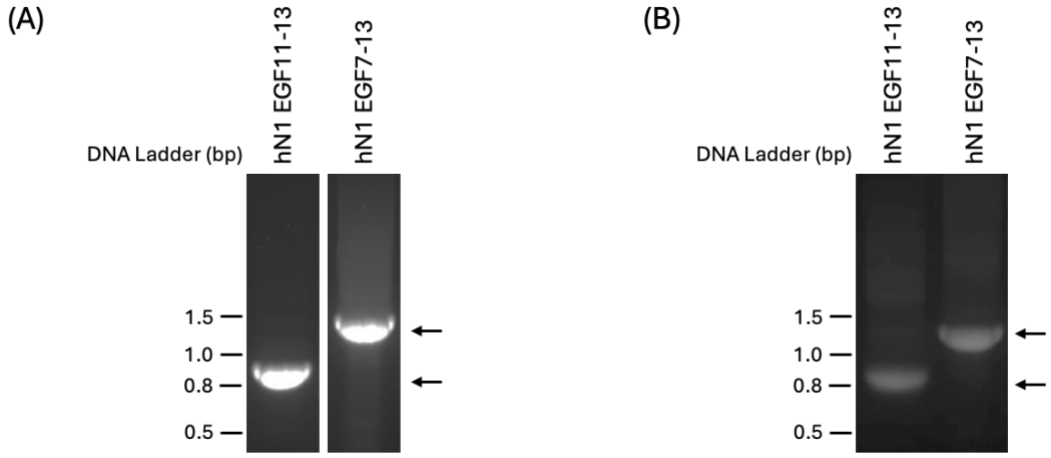


Figure 5-1. Agarose gels showing (A) DNA and (B) RNA levels of *$NOTCH1_{E11\text{-}13}$* and *$NOTCH1_{E7\text{-}13}$* in S2 stable cell lines. S2 insect cells were transfected to stably express $NOTCH1_{E11\text{-}13}$ or $NOTCH1_{E7\text{-}13}$. Total DNA and RNA were extracted, and the target sequences (*$NOTCH1_{E11\text{-}13}$*: 877 bp or *$NOTCH1_{E7\text{-}13}$*: 1342 bp) were expanded by (A) PCR or

(B) RT-PCR using pEXS2-2 primers (see Appendix 8.2.1 for primer details and Appendix 8.2.8 for amino acid sequence of the protein constructs) to confirm successful transfection and expression of NOTCH1 constructs in the cell lines. A DNA ladder was run alongside samples for size estimation.

5.2.2 Purification of recombinant Notch receptors

Conditioned medium of S2 cells containing recombinantly expressed Notch receptors was filtered and purified by IMAC via His-tag, followed by SEC (see Materials and Methods). The protein purification intermediates and products were analysed by SDS-PAGE and Western blot with an anti-His antibody (Figure 5-2). The unmodified receptor constructs have a theoretical MW ~18kDa ($NOTCH1_{E11\text{-}13\text{-}BirA\text{-}His}$) or ~35 kDa ($NOTCH1_{E7\text{-}13\text{-}BirA\text{-}His}$) but showed a higher apparent MW on gels (similar to the $DLL4_{NE3}$ variants analysed in Chapter 3), likely because the peptides were posttranslationally modified by O-glycosylation (Martins et al., 2021; Suckling et al., 2017). Another possible explanation is the phenomenon termed 'metal gel-shift', which may result in His-tagged proteins migrating to unexpected position on gel (Shelake et al., 2017).

Both NOTCH1 constructs were detected in the conditioned medium samples as His-tagged fusion proteins, suggesting normal protein trafficking and secretion (Figure 5-2A&D). The Ni^{2+} column effectively immobilised the His-tagged proteins, although low levels of NOTCH1 proteins were detected in the IMAC flow-through and wash-through samples. The size exclusion chromatograms of $NOTCH1_{E11\text{-}13}$ (Figure 5-2B) and $NOTCH1_{E7\text{-}13}$ (Figure 5-2E) both showed a sharp protein elution peak (indicated by a double-headed arrow). The corresponding protein elution fractions were analysed by SDS-PAGE (Figure 5-2C&F), which showed a clear target band at the expected MW for both NOTCH1 constructs, suggesting >90% protein purity. Purified $NOTCH2_{E11\text{-}13}$ proteins had a similar chromatography profile and comparable protein purity ($NOTCH2_{E11\text{-}13}$ purification was performed by Dr Yao Meng, see Appendix 8.5.1).

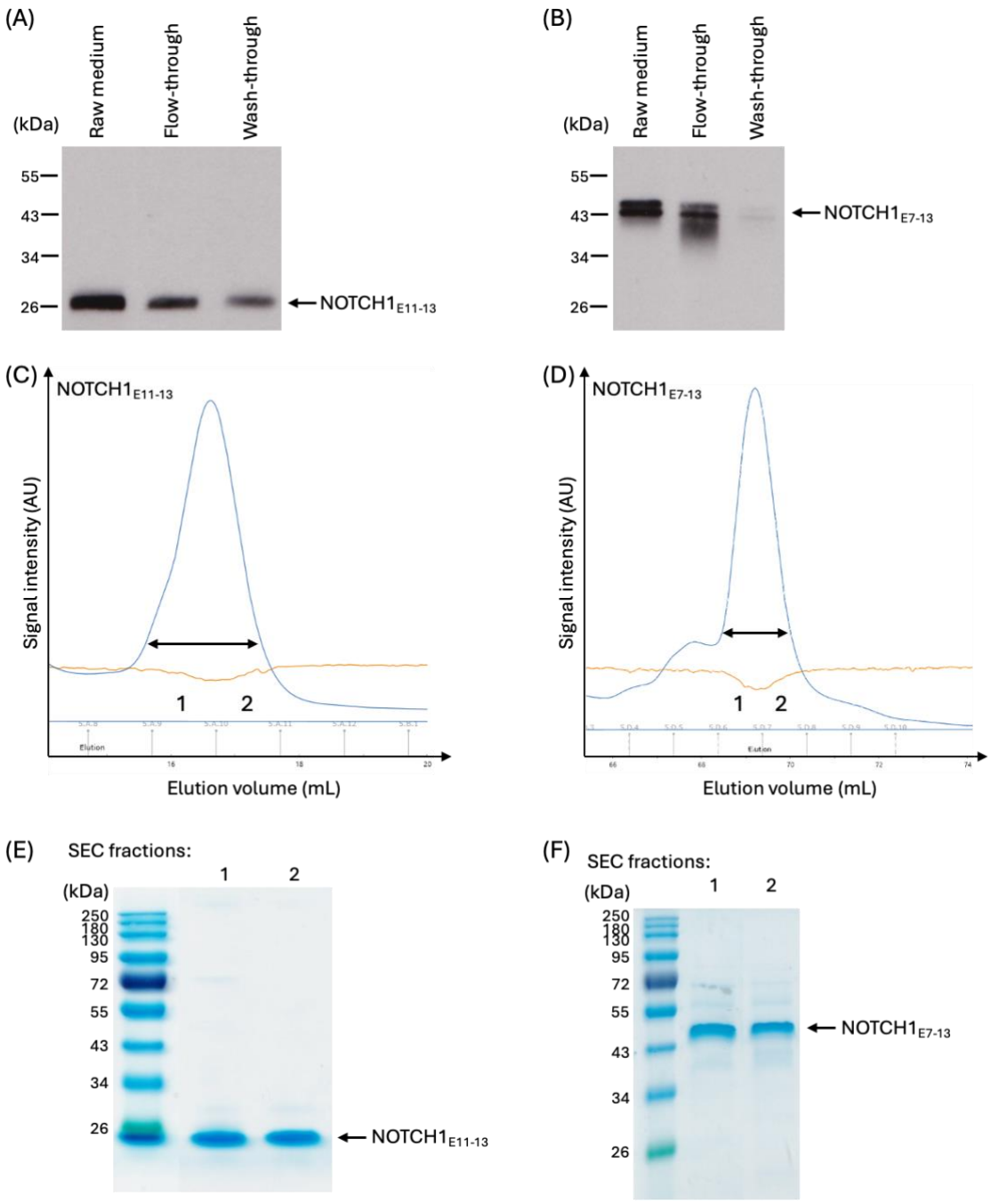


Figure 5-2. Purification of NOTCH1$_{E11-13}$ and NOTCH1$_{E7-13}$ from S2 cell lines. (A, B) Western blot analyses of IMAC intermediate products of (A) NOTCH1$_{E11-13}$ and (B) NOTCH1$_{E7-13}$. A pre-stained protein ladder was run alongside samples for size estimation. Target bands with desired MW were indicated by arrows. The theoretical MW of NOTCH1$_{E11-13-BirA-His}$ is ~18 kDa and of NOTCH1$_{E7-13-BirA-His}$ is ~35 kDa, whilst experimentally, the protein bands migrated to a higher MW position ~26 kDa (NOTCH1$_{E11-13-BirA-His}$) or ~50 kDa (NOTCH1$_{E7-13-BirA-His}$). (C, D) The size exclusion chromatograms of (C) NOTCH1$_{E11-13}$ and (D) NOTCH1$_{E7-13}$. The protein elution peak is indicated by a double-headed arrow. (E, F) Non-reducing SDS-PAGE to check the identity and purity of the eluted proteins. Both (E)

$NOTCH1_{E11-13}$ and (F) $NOTCH1_{E7-13}$ showed clear target bands, suggesting homogenous product with >90% purity.

5.3 Binding of purified $DLL4_{NE3}$ variants to purified Notch receptors

5.3.1 Optimisation of plate-based Notch binding assay

5.3.1.1 Saturation tests on Maxisorp plate

Plate-based Notch-binding assay was carried out as described previously (Chillakuri et al., 2013) using purified $DLL4_{NE3}$ variants and recombinant Notch receptors (see Materials and Methods). The purity of the protein preparations was checked by SDS-PAGE (see Section 3.3.2 Figure 3-8 for ligands purity, Section 5.2.2 Figure 5-2 for receptors purity). Titration tests were performed to check immobilisation of NOTCH1/2 constructs on MaxiSorp plates (Figure 5-3). For all three constructs ($NOTCH1_{E11-13}$, $NOTCH1_{E7-13}$, and $NOTCH2_{E11-13}$), an excess concentration of 400nM receptor protein was able to saturate each well and used for later assays.

Titration curves were also plotted for WT-$DLL4_{NE3}$ and WT-$JAG1_{NE3}$ to determine the saturating amount of ligand bound to each receptor construct immobilised on the MaxiSorp plates (Figure 5-4). WT-$DLL4_{NE3}$ appeared to saturate $NOTCH1_{E11-13}$, $NOTCH1_{E7-13}$, or $NOTCH2_{E11-13}$ coated plates at 50nM, 50nM, and 150nM protein concentrations, respectively. WT-$JAG1_{NE3}$ appeared to saturate $NOTCH1_{E7-13}$ and $NOTCH2_{E11-13}$ binding at 150nM but showed poor binding to $NOTCH1_{E11-13}$. For consistency and to ensure saturation, an excess of ligand (150nM) was used for later assays. Although the binding affinities of the two Notch ligands were not able to be directly measured in this experiment, these assays at the very least compared binding behaviours under similar conditions. The titration curves suggested that both $NOTCH1_{E7-13}$ and $NOTCH2_{E11-13}$ had higher maximum binding capacity for WT-$DLL4_{NE3}$ than WT-

$JAG1_{NE3}$ under identical conditions, since when both ligands were saturated (plateau), WT-$DLL4_{NE3}$ showed higher Abs_{415} reading than WT-$JAG1_{NE3}$ (Figure 5-4B&C). Moreover, compared to the $NOTCH1_{E11-13}$ binding curve of WT-$DLL4_{NE3}$ (Figure 5-4A), which showed a sharp increase and reached saturation at a lower ligand concentration (150nM), the $NOTCH2_{E11-13}$ binding curve of WT-$DLL4_{NE3}$ (Figure 5-4C) showed a gentle slope and reached saturation at a higher ligand concentration (350nM), suggesting a lower apparent affinity (the ligand concentration which produced 50% of the maximum binding capacity) for $NOTCH2_{E11-13}$ than for $NOTCH1_{E11-13}$. Similarly, the $NOTCH1_{E7-13}$ binding curves (Figure 5-4B) suggested that WT-$JAG1_{NE3}$ had a lower apparent affinity for $NOTCH1_{E7-13}$ than WT-$DLL4_{NE3}$. In all cases, the DLL4 negative control F195A/Y216A$_{NE3}$ showed defective Notch binding, as expected for a Notch-binding deficient variant. Two independent titration tests were performed.

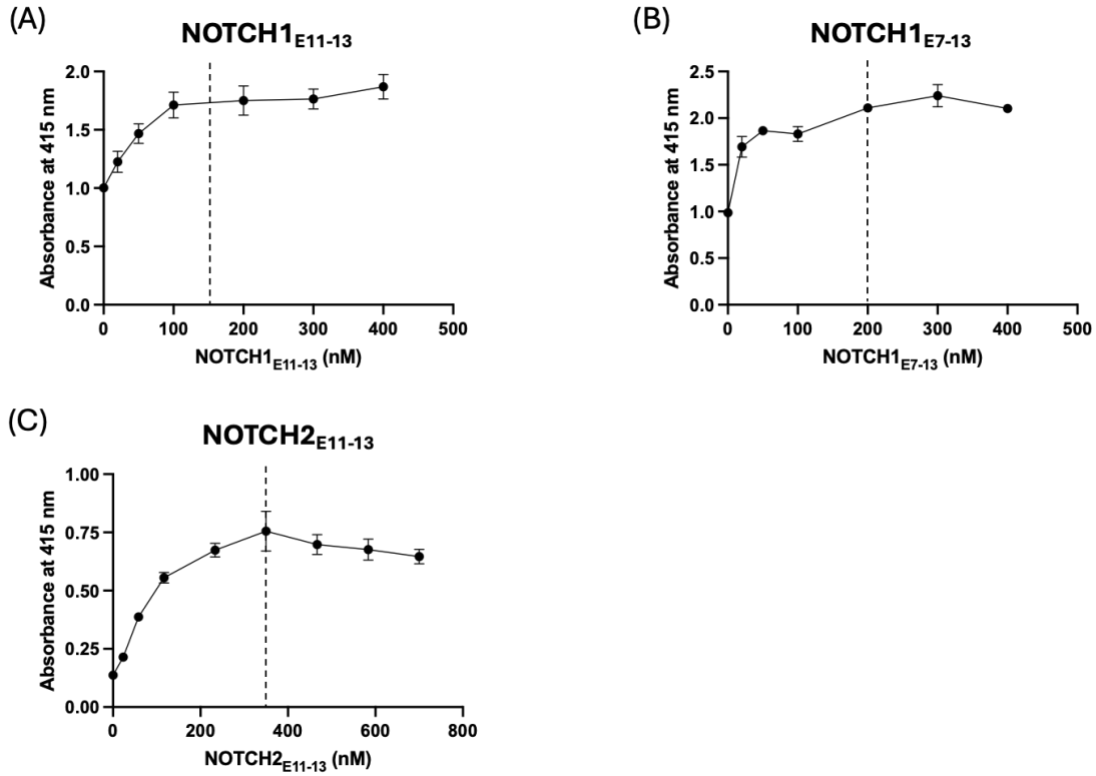


Figure 5-3. Saturation tests of purified NOTCH receptors on MaxiSorp plates. Immobilisation of purified (A) $NOTCH1_{E11-13}$, (B) $NOTCH1_{E7-13}$, and (C) $NOTCH2_{E11-13}$ on MaxiSorp plates were analysed by ELISA-based serial dilution titration tests using an anti-

His-HRP antibody. The absorbance readout was used to quantify the amount of receptor proteins immobilised. The immobilisation curves reached a plateau at high receptor concentrations, suggesting saturation of the wells. As indicated by the vertical dotted lines, $NOTCH1_{E11\text{-}13}$ saturated the plate at 150nM, $NOTCH1_{E7\text{-}13}$ saturated the plate at 200nM, and $NOTCH2_{E11\text{-}13}$ saturated the plate at 350nM. A concentration above the saturation point (i.e., 400nM) was used for later assays. The zero point reading (i.e., 0nM), in which no receptor protein was added, can be seen as a negative control.

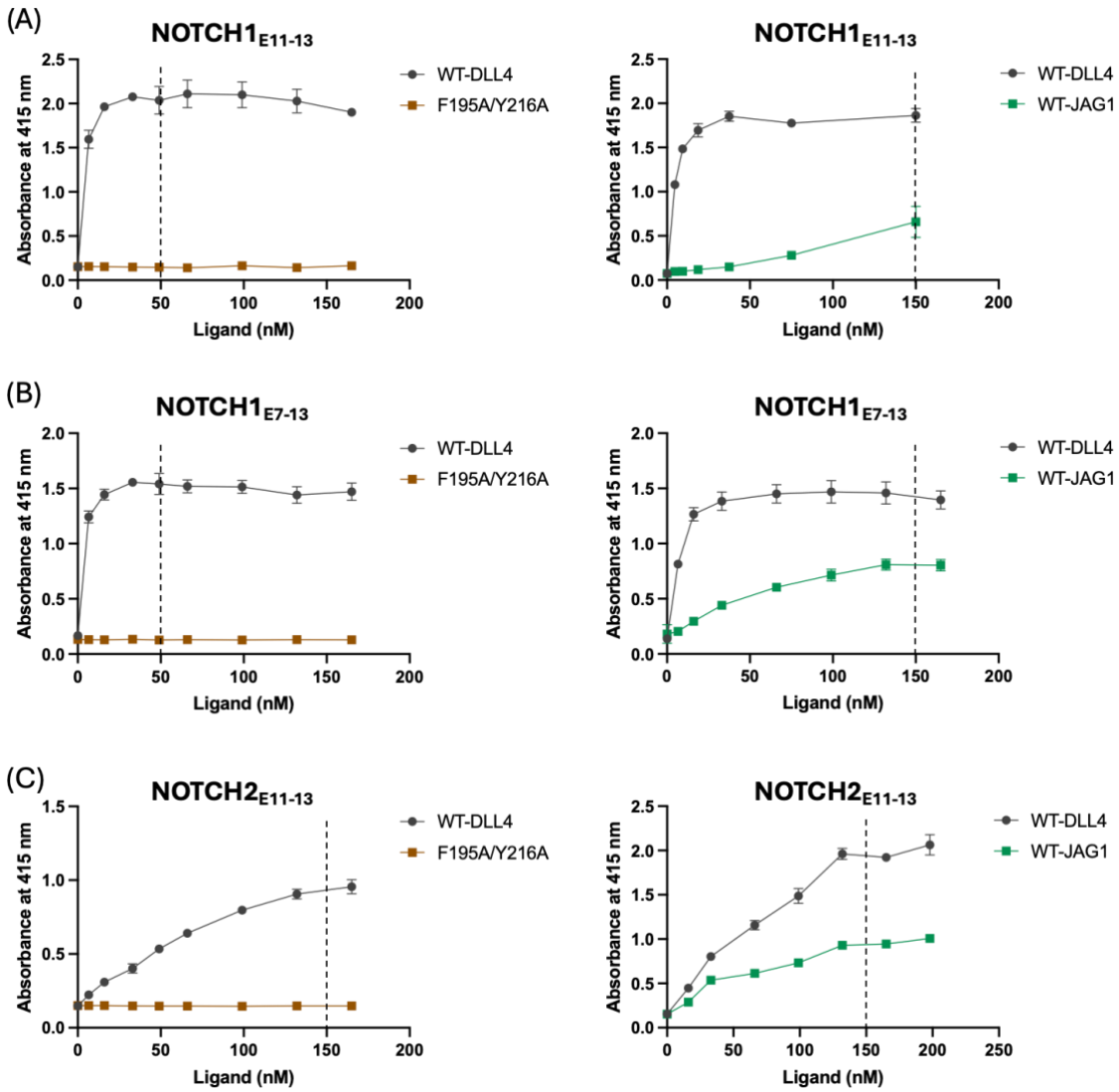


Figure 5-4. Saturation tests of purified WT-DLL4$_{NE3}$ and WT-JAG1$_{NE3}$ on receptor-precoated MaxiSorp plates. Binding of purified WT-DLL4$_{NE3}$ (black), F195A/Y216A$_{NE3}$ (brown), and WT-JAG1$_{NE3}$ (green) to 400nM (A) $NOTCH1_{E11\text{-}13}$, (B) $NOTCH1_{E7\text{-}13}$, or (C) $NOTCH2_{E11\text{-}13}$ precoated on MaxiSorp plates were analysed by ELISA-based serial dilution titration tests using an anti-Fc-HRP antibody. The absorbance readout was used to quantify the amount of ligand proteins immobilised. The immobilisation curves reached a plateau at

high ligand concentrations, suggesting saturation of the wells. As indicated by the vertical dotted lines, WT-DLL4$_{NE3}$ was able to saturate NOTCH1$_{E11-13}$, NOTCH1$_{E7-13}$, and NOTCH2$_{E11-13}$ precoated plates at 50nM, 50nM, and 150nM, respectively. DLL4$_{NE3}$-F195A/Y216A was not able to bind any of the three NOTCH receptor constructs, as expected for a Notch-binding deficient variant. WT-JAG1$_{NE3}$ was able to saturate receptor binding at 150nM, except for NOTCH1$_{E11-13}$, which showed poor binding at all ligand concentrations.

5.3.2 Notch binding assay of DLL4$_{NE3}$ cancer database variants

5.3.2.1 DLL4$_{NE3}$ cancer database variants

To assess the effects of cancer database missense mutations mapping to the C2 apical loops on DLL4-Notch binding, plate-based binding assays were performed using the optimised conditions (Section 5.3.1). Purified WT-DLL4$_{NE3}$, twelve DLL4$_{NE3}$ variants, and WT-JAG1$_{NE3}$ were tested alongside the negative controls, DLL4$_{NE3}$-F195A/Y216 and 'block only'. All eleven single substitution variants (E40K, R41S, P49S, V91L, S96R, R100G, D127E, D128N, P131T, P135A, and L164F), as well as the double mutant E40K/D128N, showed similar binding to NOTCH1$_{E11-13}$, NOTCH1$_{E7-13}$, and NOTCH2$_{E11-13}$ compared with WT-DLL4$_{NE3}$ (Figure 5-5), suggesting that these missense mutations were unlikely to significantly affect to the C2 receptor-binding site. For all three receptor constructs, binding of WT-JAG1$_{NE3}$ was significantly lower than WT-DLL4$_{NE3}$, as expected for DLL4 as a higher binding affinity ligand (see Section 1.3.3.1 for details). The DLL4$_{NE3}$-F195A/Y216A Notch-binding deficient variant showed very low (<10% of WT-DLL4$_{NE3}$ binding) Notch binding similar to the 'block only' background control, suggesting that the two amino acid substitutions effectively impaired the receptor-binding site in the DSL domain.

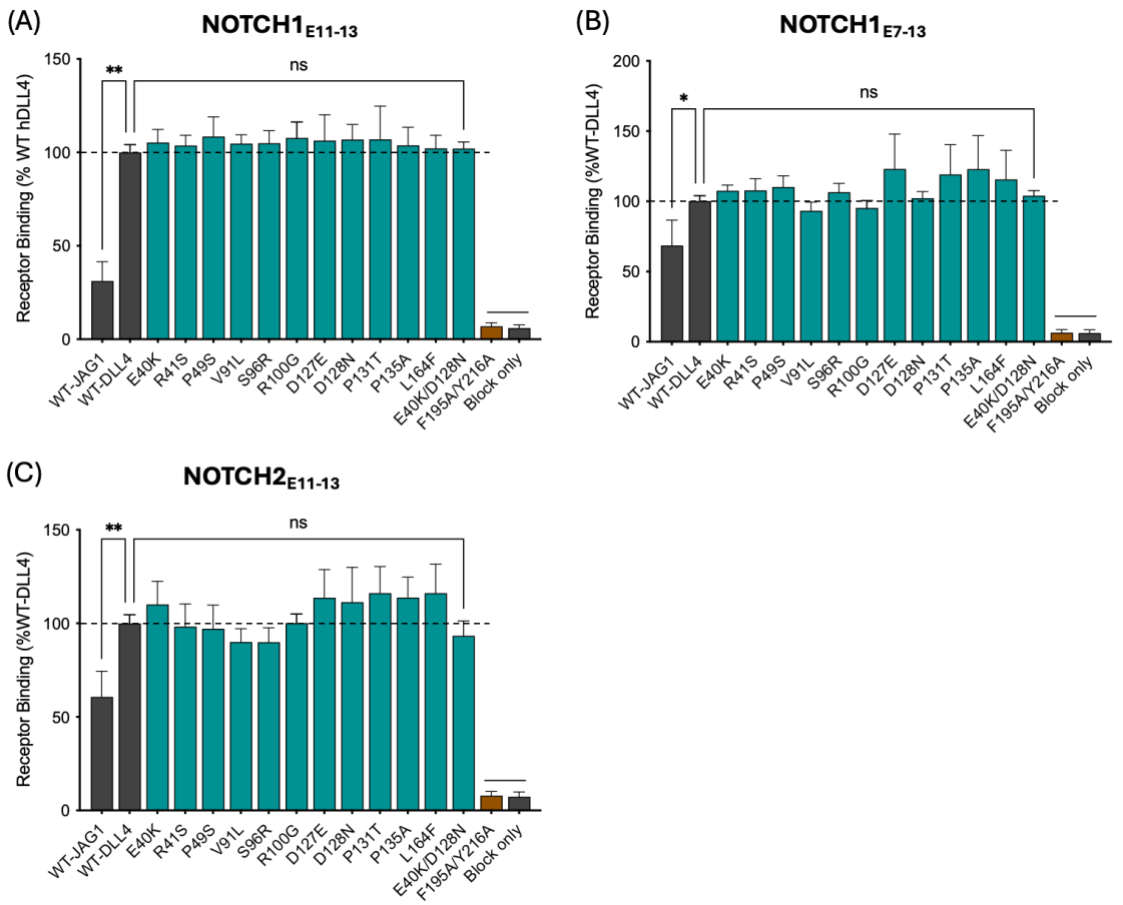


Figure 5-5. NOTCH binding by purified DLL4$_{NE3}$ cancer database variants in plate-based assays. MaxiSorp plates were precoated with 400nM (A) NOTCH1$_{E11-13}$, (B) NOTCH1$_{E7-13}$, or (C) NOTCH2$_{E11-13}$, after which 150nM WT-DLL4$_{NE3}$, DLL4$_{NE3}$ cancer database variants, or WT-JAG1$_{NE3}$ was added to analyse receptor-ligand binding using an anti-Fc-HRP antibody. The data was normalised as percentage of WT-DLL4$_{NE3}$ binding and presented as mean ± SD, representing combined results of n≥3 independent experiments. F195A/Y216A$_{NE3}$ and 'block only' were used as negative controls. Statistical analysis was performed in each case using Kruskal-Wallis test followed by Dunn's multiple comparison test. ns (not statistically significant) P>0.05, *P ≤ 0.05, **P ≤ 0.01, ***P ≤ 0.001, ****P ≤ 0.0001.

5.3.2.2 Titration tests of DLL4$_{NE3}$ variants

Whilst binding assays in Section 5.3.2.1 were performed at high ligand concentrations and identified large changes in binding, they might not reveal smaller differences. Hence, serial dilution titration tests were performed to assess receptor-binding by DLL4$_{NE3}$ C2-loop variants across a range of ligand concentrations (0-150nM). As analysed in Chapter 3 and Chapter 4, the loop β1-2 variants E40K, R41S, the loop β5-6 variant D128N, and

the double mutant E40K/D128N showed consistently decreased (E40K, D128N, E40K/D128N) or increased (R41S) ability to activate Notch, therefore these four representative variants were selected for testing. Using the longer Notch fragment $NOTCH1_{E7\text{-}13}$, all four variants showed a similar saturation curve compared to that of WT-$DLL4_{NE3}$ (Figure 5-6), suggesting that they had similar Notch-binding affinity at both saturating and non-saturating ligand concentrations.

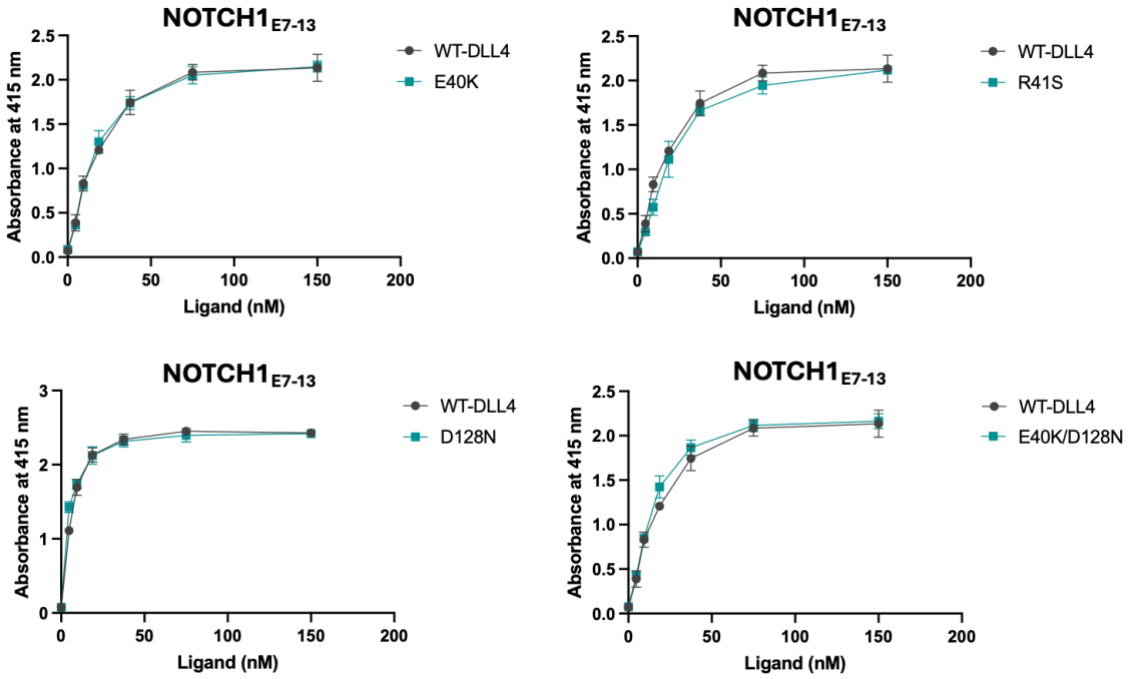


Figure 5-6. Titration tests of purified $DLL4_{NE3}$ cancer database variants binding to $NOTCH1_{E7\text{-}13}$ precoated on MaxiSorp plates. Binding of purified WT-$DLL4_{NE3}$ (black) and $DLL4_{NE3}$ cancer database variants (teal), $E40K_{NE3}$, $R41S_{NE3}$, $D128N_{NE3}$, and $E40K/D128N_{NE3}$, to 400nM $NOTCH1_{E7\text{-}13}$ precoated on MaxiSorp plates were analysed by ELISA-based serial dilution titration tests using an anti-Fc-HRP antibody. Both WT-$DLL4_{NE3}$ and its variants showed similar titration curves, suggesting that they all had similar binding affinity for $NOTCH1_{E7\text{-}13}$ at a range of ligand concentrations (0-150nM).

5.4 Ligand binding of purified DLL4$_{NE3}$ variants by cells expressing FL-Notch receptors

Whilst the plate-based binding assay using purified Notch proteins (Section 5.3) probed binding of DLL4$_{NE3}$ to the LBR of Notch receptors, the limited fragments did not reflect the actual binding environment involving the cell membrane, and lacked other potential receptor-ligand interaction sites apart from the LBR (Zeronian et al., 2021). Hence, a cell-based ligand binding assay was advantageous by presenting FL-Notch receptors on the cell surface, that allowed DLL4$_{NE3}$ to bind receptors in a more biologically relevant environment.

5.4.1 Ligand binding by HEK293-mN1 cells

Flow cytometry-based ligand binding assay using HEK293 cells expressing complete FL-mNotch1 and purified DLL4$_{NE3}$ proteins was performed as previously described (Meng et al., 2022) (see Materials and Methods). The ligand proteins purified previously in Section 3.3.2 (same as the proteins used in Section 5.3) were qualitatively (i.e., purity) and quantitatively (i.e., amount) checked by SDS-PAGE and Western blot analyses (see Section 3.3.2). A representative selection of DLL4$_{NE3}$ variants (β1-2: E40K, R41S; β3-4: R100G; β5-6: D127E, D128N, P131T; E40K/D128N), which showed functional effects in activity assays (Chapter 3&4), were tested. These variants all showed a similar binding affinity for FL-mNotch1 compared with WT-DLL4$_{NE3}$ (Figure 5-7A), consistent with the results obtained using shorter NOTCH1 fragments (Section 5.3.2). The negative control DLL4$_{NE3}$-F195A/Y216A showed defective Notch binding (~10% of WT-DLL4$_{NE3}$) as expected for a Notch-binding deficient variant.

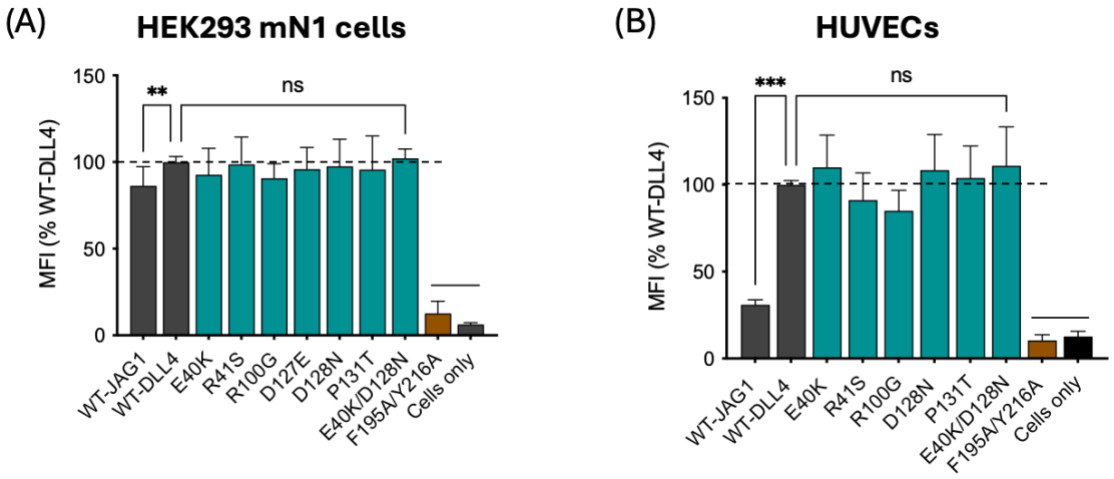


Figure 5-7. Binding of purified DLL4$_{NE3}$ cancer database variants to complete FL-Notch receptors expressed on cell surface. 50nM WT-DLL4$_{NE3}$, DLL4$_{NE3}$ cancer database variants, and WT-JAG1$_{NE3}$ conjugated with 75nM anti-human IgG/AF488 antibody (for 1:1 clustering) were bound to (A) HEK293 cells expressing FL-mNotch1, or (B) HUVECs expressing FL-NOTCH1/2/3/4 receptors. Receptor-ligand binding was analysed by flow cytometry and quantified as median fluorescence intensity (MFI). The data was normalised as percentage of WT-DLL4$_{NE3}$ binding and presented as mean ± SD, representing combined results of n≥3 independent experiments, in which 30,000 cells were measured in each reading. F195A/Y216A$_{NE3}$ and 'cells only' were used as negative controls. Statistical analysis was performed in each case using Kruskal-Wallis test followed by Dunn's multiple comparison test. ns (not statistically significant) P>0.05, **$P \leq 0.01$, ***$P \leq 0.001$.

5.4.2 Ligand binding by HUVECs

Similar to Section 5.4.1, a flow cytometry-based ligand binding assay was carried out using purified DLL4$_{NE3}$ proteins and HUVECs (see Materials and Methods), which express a range of FL-Notch receptors (NOTCH1-4) (Patel et al., 2005). Detection was by anti-human IgG/AF488 antibody, which had been conjugated with Fc-tagged ligand proteins. A representative selection of DLL4$_{NE3}$ variants (β1-2: E40K, R41S; β3-4: R100G; β5-6: D128N, P131T) showing functional effects in the HUVECs-based RT-qPCR Notch activation assay (Chapter 4), as well as the E40K/D128N double mutant were tested. All these variants showed similar binding to HUVECs compared with WT-DLL4$_{NE3}$ (Figure 5-7B), consistent with earlier results obtained in plate-based assays with purified ligand

and receptor fragments (Figure 5-5 & Figure 5-7A). Notably, WT-JAG1$_{NE3}$ showed dramatically lower binding to HUVECs that was ~30% of WT-DLL4$_{NE3}$, but only showed slightly lower binding to HEK293-mN1 cells (~85% of WT-DLL4$_{NE3}$), suggesting cell type-dependent differences. The Notch-binding deficient DLL4$_{NE3}$-F195A/Y216A showed very low binding (~10% of WT-DLL4$_{NE3}$) similar to the 'cells only' background control.

5.5 Receptor binding of recombinant NOTCH1 receptors by HEK293T cells expressing FL-DLL4 variants

5.5.1 Titration test

An alternative flow cytometry-based receptor binding assay was designed to probe receptor-ligand binding, which used B16 or HEK293T cells expressing complete FL-DLL4 and purified NOTCH1 EGF11-13 or EGF7-13 fragments (same as the receptor proteins used in Section 5.3, see Figure 5-2 for protein purity) conjugated with anti-His/APC antibody (Figure 5-8A, see Materials and Methods). Whilst the ligand binding assay described in Section 5.4 used Fc-dimerised N-terminal fragments of DLL4, this receptor binding assay allowed FL-DLL4 to be presented in its physiological form on the cell surface. Cells expressing FL-JAG1 were tested alongside for comparison.

During assay development, titration tests were performed using B16 cells stably expressing FL-WT- mDll4 or mJag1. WT-B16 cells not expressing any Notch ligands were used as a negative control. Addition of NOTCH1-antibody conjugates did not shift the WT-B16 histogram, ruling out the possibility of non-specific binding (Figure 5-8B). For B16-mJag1 cells, NOTCH1$_{E7-13}$ appeared to bind weakly, whilst NOTCH1$_{E11-13}$ seemed not bound at all to the mJag1 cells regardless of the receptor concentration used (Figure 5-8C), suggesting a poor binding affinity. On the other hand, B16-mDll4 cells showed concentration-dependent increase in binding to NOTCH1$_{E11-13}$ and NOTCH1$_{E7-}$

$_{13}$, as suggested by the more rightward shifted peaks of the histograms when increased concentrations of receptors were added (Figure 5-8D). Moreover, B16-mDll4 cells showed enhanced binding to NOTCH1$_{E7-13}$ compared with NOTCH1$_{E11-13}$ at a range of receptor concentrations (50-200nM), as suggested by the more rightward shifted histogram of NOTCH1$_{E7-13}$ compared to that of NOTCH1$_{E11-13}$. 'Cells only' sample, in which no receptor protein was added, was used as a background control. Based on the titration results, 200nM NOTCH1$_{E7-13}$, which showed a more prominent binding, was used for later experiments.

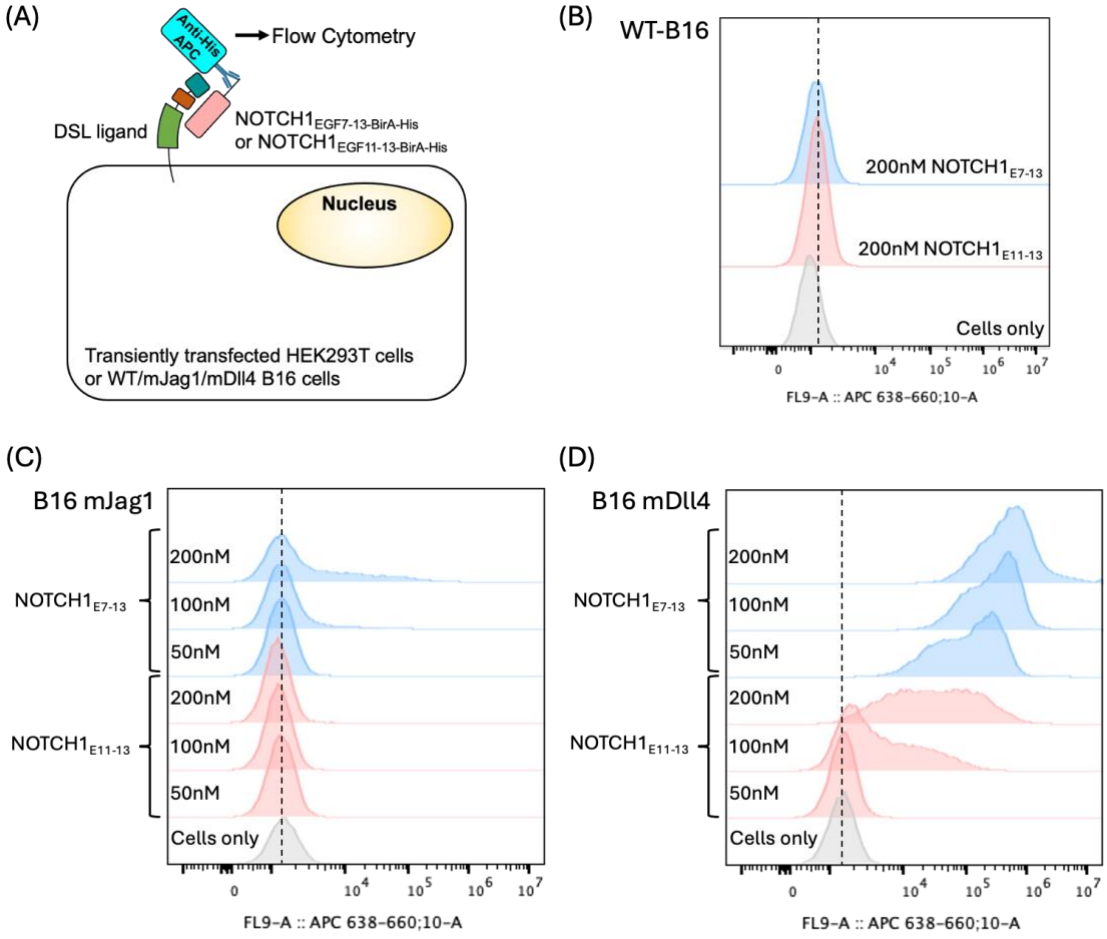


Figure 5-8. Titration tests of purified recombinant NOTCH1 receptors binding to complete full-length ligands expressed on cell surface. (A) Cartoon illustrating the flow-cytometry-based receptor binding assay (see Materials and Methods). Purified NOTCH1$_{E11-13}$ or NOTCH1$_{E7-13}$ conjugated with anti-His/APC antibody were bound to (i) HEK293T cells transiently transfected to express FL-DLL4 or FL-JAG1, or (ii) engineered B16 cell lines stably expressing FL-mJag1 or FL-mDll4. Receptor-ligand binding was analysed by flow cytometry. (B) Neither NOTCH1$_{E11-13}$ (red) nor NOTCH1$_{E7-13}$ (blue) bound to WT-B16 cells.

(C) B16 cells expressing complete FL-mJag1 showed poor binding to $NOTCH1_{E11-13}$ (red) and $NOTCH1_{E7-13}$ (blue) at a range of receptor concentrations (50-200nM), as suggested by the positions of the histograms (indicated by a vertical dotted line) compared to the 'cells only' (grey) negative control. (D) B16 cells expressing complete FL-mDll4 bound $NOTCH1_{E7-13}$ (blue) better than $NOTCH1_{E11-13}$ (red), as suggested by the more rightward shifted peak of the histograms. Titration tests also showed concentration-dependent increase in binding.

5.5.2 Receptor binding by HEK293T cells expressing FL-DLL4

5.5.2.1 Cancer database variants

HEK293T cells were transiently transfected to express FL-DLL4, and the surface expression levels of the FL-DLL4 variants were assessed by flow cytometry as described in Section 3.5 (Figure 5-9A). HEK293T cells expressing FL-DLL4 variants were then assessed for $NOTCH1_{E7-13}$ binding, using the optimised protocol described in Section 5.5.1. Consistent with the surface expression profile of ligand (Figure 5-9A), $NOTCH1_{E7-13}$ binding results also had a bimodal distribution (Figure 5-9B), suggesting a higher receptor-binding (P2) and a lower receptor-binding subpopulation (P1). The MFI (indicated by vertical dotted lines) of the two subpopulations (indicated by horizontal double-headed arrows) was analysed separately to ease comparison (see Appendix 8.5.2 for data analysis). Cells transfected with *pcDNA3.1-empty vector* (EV) were used as a background control, and a rightward shift of histogram suggested increased Notch binding to DLL4. The two FL-DLL4 variants, E40K and R41S, both showed similar binding to $NOTCH1_{E7-13}$ compared with FL-WT-DLL4, as suggested by overlaying both peaks in their flow cytometry histograms (Figure 5-9C). The FL-F195A/Y216A negative control, showing significantly lower Notch binding, had a more leftward-shifted histogram. The observations were consistent with the results obtained in the other two binding assays, including the plate-based assay using purified ligand and receptor fragments and the flow-cytometry-based assay using FL-Notch-expressing cells to bind purified ligand fragments (Section 5.3 & 5.4).

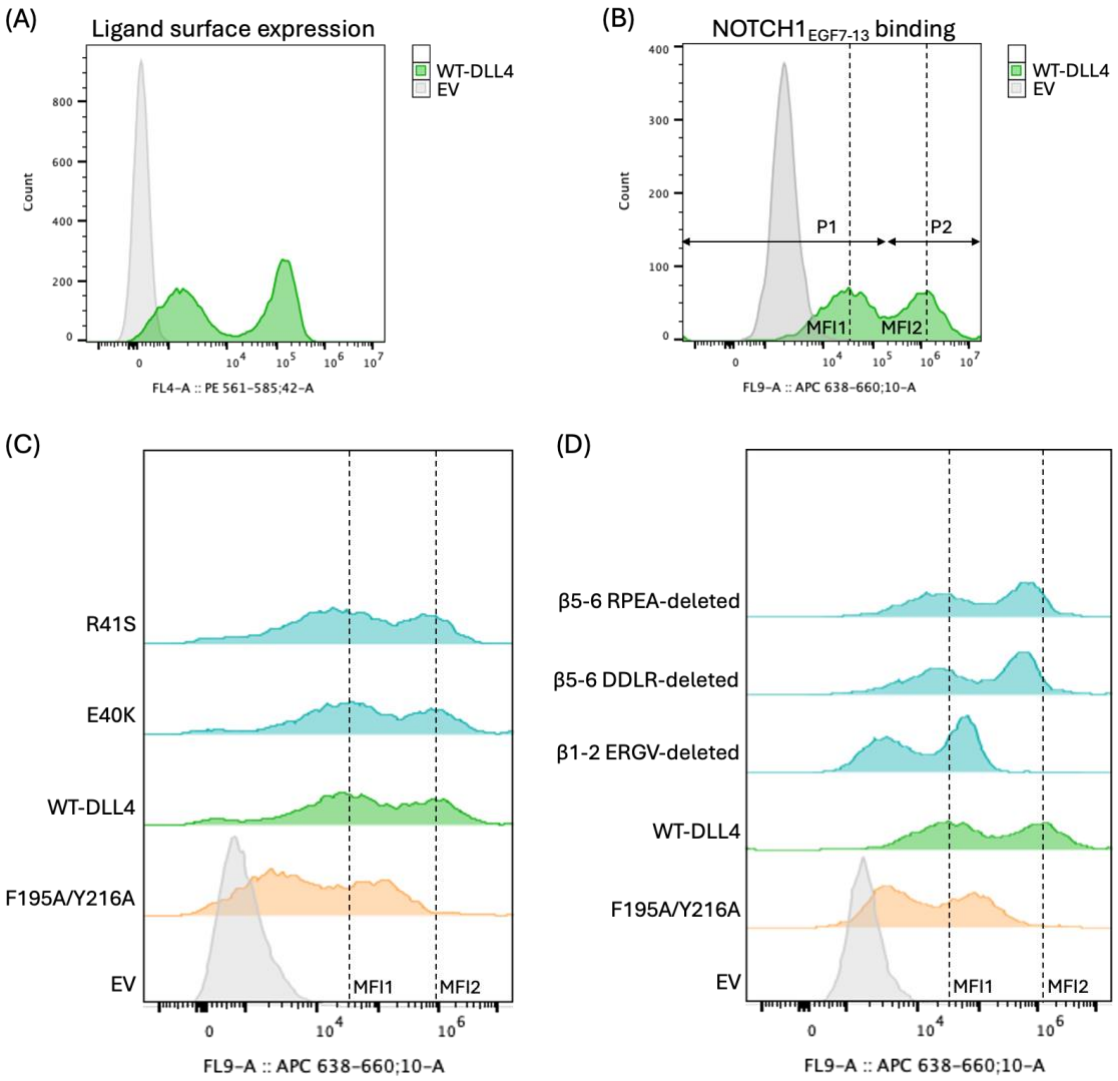


Figure 5-9. Binding of purified NOTCH1$_{E7-13}$ to complete FL-DLL4 variants expressed on cell surface. (A) Surface expression of FL-WT-DLL4 (green) in transiently transfected HEK293T cells, which showed a bimodal distribution as explained in Section 3.5.2. (B) 200nM purified NOTCH1$_{E7-13}$ conjugated with anti-His/APC antibody (ab72579) were bound to HEK293T cells expressing FL-WT-DLL4. A bimodal distribution was shown, consistent with FL-WT-DLL4 (green) surface expression pattern seen in (A). The histogram suggests two subpopulations with significantly different Notch binding levels. *pcDNA3.1-EV* (grey) was used as a background control. (C, D) Representative histograms showing Notch binding by FL-DLL4 (C) cancer database variants (teal) and (D) C2-loop-shortening variants (teal). FL-F195A/Y216A (orange) and EV (grey) were used as negative controls. The vertical dotted lines indicate the MFIs of the two cell subpopulations in the FL-WT-DLL4 sample. Note the leftward shifts of the three loop-shortening variants and FL-F195A/Y216A compared with FL-WT-DLL4, indicating reduced Notch binding. Three independent transient transfection and receptor-binding experiments were performed to ensure reliable results.

5.5.2.2 C2-loop-shortening variants

$NOTCH1_{E7\text{-}13}$ receptor binding was also tested for the three FL-DLL4 C2-loop-shortening variants (β1-2 ERGV-deleted, β5-6 DDLR-deleted, β5-6 RPEA deleted). As analysed in Chapter 3, these variants showed significantly reduced cell surface expression levels compared with FL-WT-DLL4 (see representative histograms in Section 3.5.2, Figure 3-12, and detailed data analysis in Appendix 8.3.3). As expected, these variants all showed reduced receptor binding compared with FL-WT-DLL4, as suggested by their leftward-shifted histograms (Figure 5-9D). Moreover, the FL-DLL4 β1-2 ERGV-deleted variant showed a different flow cytometry profile compared to the other two β5-6 loop-shortening variants, suggesting a much lower $NOTCH1_{E7\text{-}13}$ binding ability, most likely due to its significantly lower surface expression level than the other two β5-6 loop-shortening variants (Figure 3-12C, Appendix 8.3.3). In support of this, statistical analysis of their MFI (see Appendix 8.5.2) showed that cells expressing β1-2 ERGV-deleted variant had even lower receptor binding ability than the F195A/Y216A receptor-binding-deficient negative control, suggesting a combined outcome of low cell surface expression and protein misfolding at the C2-receptor binding site.

5.6 Liposome binding

To investigate if the cancer database missense mutations affect the ability of DLL4 to bind lipid membranes, a flow cytometry-based liposome aggregation assay (see Materials and Methods) was performed. Due to the relatively weak lipid binding shown by Notch ligands (Suckling et al., 2017), purified $DLL4_{NE3}$ proteins were immobilised to protein G fluorescent beads at a saturating concentration (Figure 5-10A) and incubated with fluorescent liposomes to form ligand-bead-liposome aggregates, which were then analysed by flow cytometry and quantified as a percentage of aggregation (see Appendix 8.5.1.1 for a set of representative raw data). Four types of liposomes with different lipid

compositions were prepared, including PC-rich liposomes (POPC:DOPS:PE-CF = 70:25:5), SM-rich liposomes (POPC:SM:DOPS:PE-CF = 30:40:25:5), PIP_2-containing liposomes (POPC:DOPS:$PI(4,5)P_2$:PE-CF = 70:20:5:5), and ganglioside-rich liposomes (POPC:DOPS:Ganglioside:PE-CF = 30:25:40:5). Whilst PC-rich liposomes are commonly used as a simplified membrane model, SM- or ganglioside- rich liposomes represent a simplified model of the outer leaflet of plasma membrane, whereas PIP_2 is enriched in the inner leaflet of plasma membrane. The size and homogeneity of these liposome preparations were analysed by DLS prior to use (see Appendix 8.5.1.2).

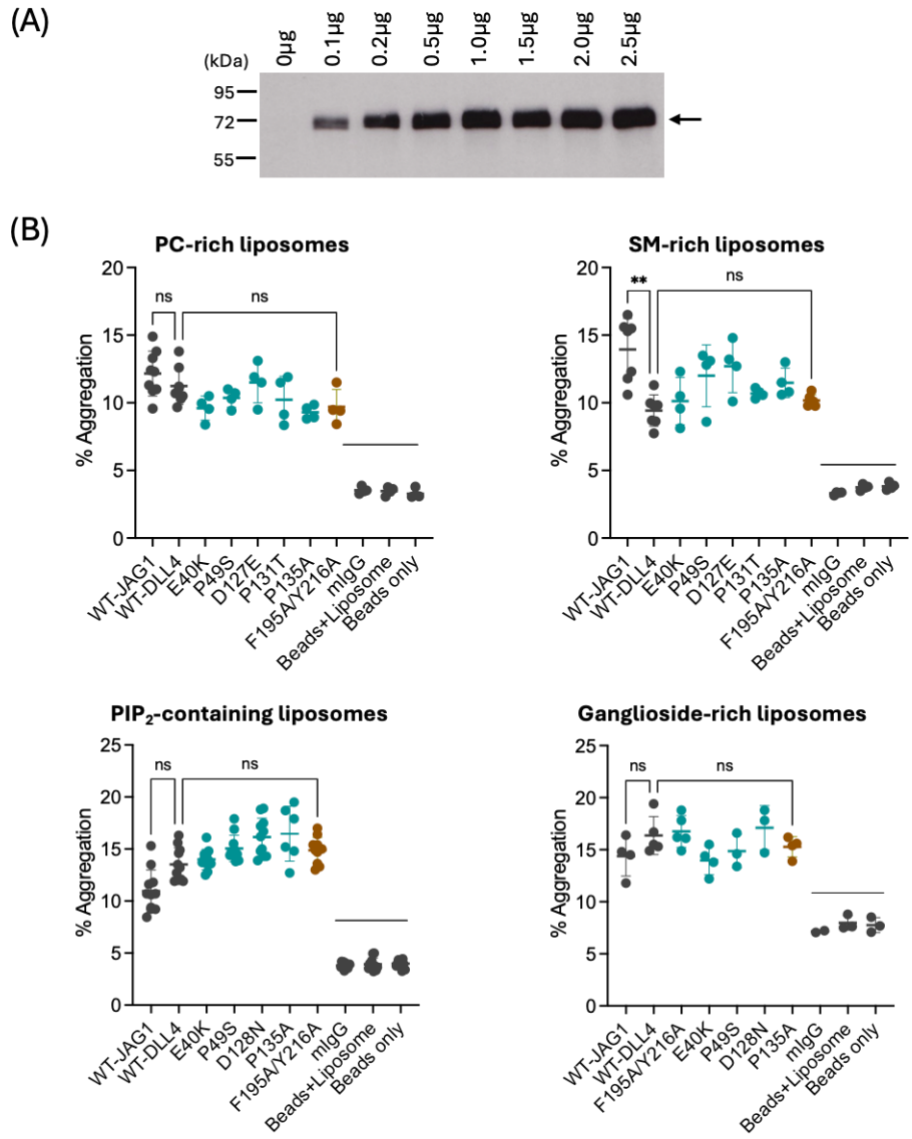


Figure 5-10. Liposome binding by purified $DLL4_{NE3}$ cancer database variants. (A) Western blot analysis showing saturation of protein G beads by WT-$DLL4_{NE3\text{-}Fc\text{-}His}$, viewed on a reducing gel using anti-His-HRP antibody. A serial dilution of WT-$DLL4_{NE3}$, ranging from 0-

2.5 µg/sample, was used for bead coating. Bead saturation was observed when ~1µg ligand protein was added, and 2 µg ligand protein was added for later experiments. (B) Binding of PC-rich, SM-rich, PIP_2-containing, or ganglioside-rich liposomes to ligand-coated beads was assessed by flow cytometry and quantified as percentage aggregation. Data were presented as mean ± SD, which represented combined results of n≥3 independent experiments, in which 10,000 events were recorded in each reading. 'Beads only', 'beads + liposome' and mIgG were used as background controls. In all cases, statistical analysis was performed using Kruskal-Wallis test followed by post hoc Dunn's multiple comparison test. ns (not statistically significant) $P>0.05$, $*P \leq 0.05$. See Appendix 8.5.1.1 for a set of representative FACS raw data.

In preliminary studies, a selection of $DLL4_{NE3}$ cancer database variants mapping to the C2 apical loops, as well as the $DLL4_{NE3}$-F195A/Y216A Notch-binding-defective variant were tested. WT-$DLL4_{NE3}$ and WT-$JAG1_{NE3}$ were tested alongside as positive controls, which showed similar binding to PC-rich, PIP_2-containing, or ganglioside-rich liposomes. A binding preference for SM-rich liposomes by WT-$JAG1_{NE3}$ was observed (Figure 5-10B), as reported previously in plate-based liposome binding assays (Suckling et al., 2017). However, unlike previous plate assay results, the binding preference of WT-$DLL4_{NE3}$ for ganglioside-rich liposomes was not shown in this experiment. mIgG, 'beads + liposomes', and 'beads only' samples were used as background controls, which generally showed <5% aggregation. For the selection of $DLL4_{NE3}$ variants tested, no statistically significant difference was detected between the variants and WT-$DLL4_{NE3}$ for all four types of liposomes.

5.7 Mechanistic insight from Molecular Dynamics Simulations

To explore possible binding modes of DLL4-C2 domain to lipid membranes, coarse-grained MD simulations were performed using three different anionic lipid compositions. These experiments and MD data analysis were performed by Dr Andreas Larsen (Department of Neuroscience, University of Copenhagen) using a previously described

protocol (Larsen & Sansom, 2021; Meng et al., 2022). During the simulation, a coarse-grained truncated DLL4 structure (PDB 5MVX) containing only the N-terminal C2 domain was solvated and positioned above a lipid bilayer. The C2 domain was restrained to only encounter the membrane upper leaflet when equilibration was run for the system.

To investigate how the lipid composition may affect the membrane-binding orientations, three different membranes, either PS-containing (PC:PS = 75:25), or ganglioside-containing (PC:GM1:GM3 = 90:5:5), or PIP_2-containing (PC:PC:PIP_2 = 80:15:5), were generated for interactions with the WT-DLL4 C2 domain. These membrane compositions were commonly used as simplified models of mammalian cell membranes. To further explore whether or not membrane binding may be affected by amino acid substitutions in the β1-2 loop, DLL4-C2 variants (E40K or R41S) were subsequently simulated using the three different membranes and compared with the WT-DLL4. 25 independent repeats were run for each protein/membrane combination, and a distance (distance between the centre-of-mass of the protein and the centre-of-mass of the membrane) versus R_{zz} (the 'zz' component of the rotation matrix with respect to a reference frame) plot was generated to represent the binding modes observed for each protein/membrane combination.

5.7.1 Binding modes of WT-DLL4-C2 interacting with different membranes

Simulation results of WT-DLL4 C2 domain interacting with three different membranes suggest that alternative binding modes are possible depending on the lipid compositions. The PS-containing membrane provided a simple anionic lipid bilayer model, where WT-DLL4-C2 predominantly settled in a nonphysical mode (i.e., the mode was physically incompatible because the covalently attached domains C-terminal to the C2 domain in the FL-ligand would overlap with the membrane) (Figure 5-11A). Upon binding, the PS lipids were evenly distributed in the membrane without any clustering effect, the C2

domain interacted with the upper leaflet using its bottom C-terminal side, where the basal loops β2-3, β4-5 and β6-7 all seemed to have lipid contacts. However, alignment of a FL-ligand (DLL1: PDB 4XBM) with the C2 domain shows steric clashes of the DSL domain and EGF repeats with the membrane, suggesting that this mode of binding is nonphysical for FL-DLL4.

The ganglioside-containing membrane, which provided a simplified mimic of the outer leaflet of the plasma membrane, had several possible binding modes with WT-DLL4-C2, including a different binding mode shown in Figure 5-11B, which was not observed for the PS-containing membrane. The C2 domain bound the upper leaflet in an upright orientation with the apical loops β1-2, β5-6, and β7-8 partly inserted into the membrane. Interestingly, ganglioside molecules were observed to cluster around the C2 domain upon binding, suggesting potential binding preference. Whilst the binding for a single ganglioside molecule is relatively weak, the formation of lipid clusters suggested that a single C2 domain may bind multiple ganglioside molecules, resulting in a stronger avidity-driven binding. Alignment of the C2 domain with a longer Dll4 fragment bound in a complex to the Notch1 LBR (PDB 4XL1) comprising EGF11-13 shows that the C-terminal region of the C2 domain was pointing away from the membrane without any steric clashes, and therefore may be physiologically relevant when unbound to receptor. The Notch1 fragment, however, showed potential clashes of EGF13 with the membrane, suggesting that the FL-receptor may also encounter steric clashes when bound to membrane-bound DLL4-C2.

The PIP_2-containing membrane provided a model for the inner leaflet of the plasma membrane, which is less relevant for extracellular Notch-ligand interactions but is useful for probing the effect of a very different lipid on ligand-membrane interactions. Simulations also showed several possible binding modes including an orientation parallel to the membrane (Figure 5-11C). In this binding mode, the C2 domain bound the

membrane using its side face, where the side loop β3-4, in addition to the apical loops β1-2, β5-6, were involved in membrane binding. Similar to ganglioside, the PIP_2 molecules were also observed to cluster around the bound C2 in all binding modes. Overall, these MD results establish that DLL4-C2 membrane interactions can be identified, despite their relatively weak nature, and, in simulations, can be modulated by lipid composition.

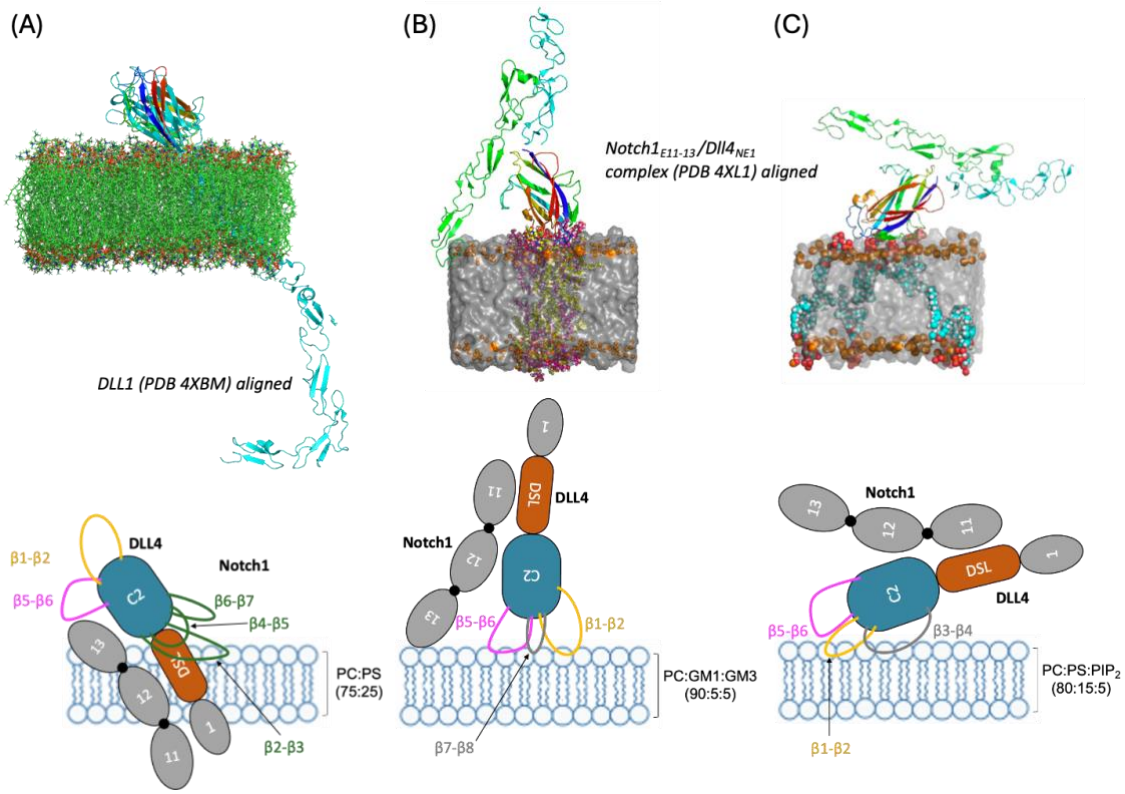


Figure 5-11. Molecular dynamics simulations showing different binding orientations of WT-DLL4-C2 bound to membranes of varying composition. Simulations were performed using truncated DLL4-C2 domain (PDB 5MVX, rainbow coloured). Cartoons highlighting the C2 loops involved in membrane-binding are shown below. (A) Predominant nonphysical binding mode with PS-containing membrane (molar ratio of PC:PS = 75:25). Full-ectodomain DLL1 structure (PDB 4XBM, cyan) is aligned to show steric clashes. (B) One possible binding mode with ganglioside-containing membrane (molar ratio of PC:GM1:GM3 = 90:5:5). Binding is mainly contributed by C2 apical loops β1-2, β5-6, and β7-8. (C) One possible binding mode with PIP_2-containing membrane (molar ratio of PC:PS:PIP_2 = 80:15:5). Binding is mainly contributed by C2 apical loops β1-2, β5-6, and side loop β3-4. (B,C) The co-crystallised structure (PDB 4XL1) of $Dll4_{NE1}$ (cyan) bound with $Notch1_{E11-13}$ (green) is aligned to show possible ternary complex formation.

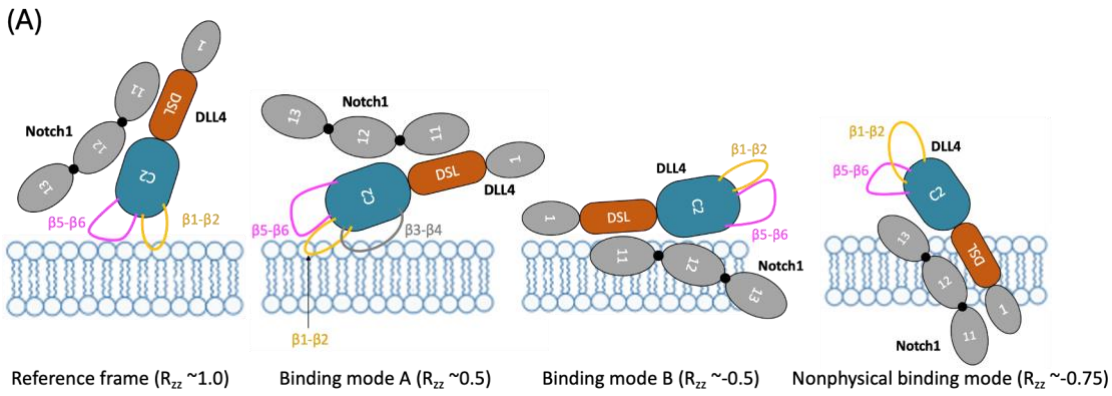
GM1: monosialotetrahexosylganglioside, GM3: monosialodihexosylganglioside.

5.7.2 Binding modes of E40K and R41S variants

Comparison of the membrane binding modes of WT, E40K, and R41S DLL4-C2 domains interacting with the three different anionic lipid bilayers shows changes in the landscape of binding (i.e., the orientation vs distance plot). Four typical binding modes were obtained from simulations, including an “upright” apical-binding orientation which was set as the reference frame, two ‘horizontal’ orientations (binding modes A and B) which were bound to the membrane with different side faces, and a nonphysical binding mode with steric clashes (Figure 5-12A). Alignment of a receptor-ligand complex suggested that both the reference frame and binding mode A potentially allowed receptor binding to a FL-ligand, whereas the C2-DSL Notch binding sites faced the membrane in binding mode B.

Whilst simulations of binding of WT DLL4-C2 with PS-containing membrane showed a clearly preferred nonphysical mode of binding, both E40K and R41S showed some effects on the membrane interaction. E40K substantially shifted the landscape towards the binding modes A and B, which were both compatible with a FL-ligand ectodomain but only mode A has the Notch receptor binding sites exposed (Figure 5-12B, Table 5-1). R41S had a similar but subtler effect. When simulations were performed using a ganglioside-containing membrane, WT DLL4-C2 displayed an altered landscape of binding orientations, which showed more physically possible binding modes, including an upright apical-binding orientation that was not observed for binding to the PS-containing membrane (Table 5-1). Both E40K and R41S shifted the distance vs orientation landscape, resulting in more simulations ending in the reference frame and binding mode A (Figure 5-12B, Table 5-1).

Likewise, when simulations were performed using a PIP_2-containing membrane, an altered binding profile was shown, which is different from the results of the other two membrane compositions (Figure 5-12B). In the WT simulations, there was also a clear shift towards physically possible binding modes compared to the PS-containing membrane (Table 5-1). The E40K substitution led to a similar effect observed in the other two membrane compositions, resulting in significantly more simulations ending in the reference frame and binding mode A (Figure 5-12B, Table 5-1). However, the R41S substitution showed an opposite effect, which shifted the binding orientation landscape towards the unphysical binding mode.



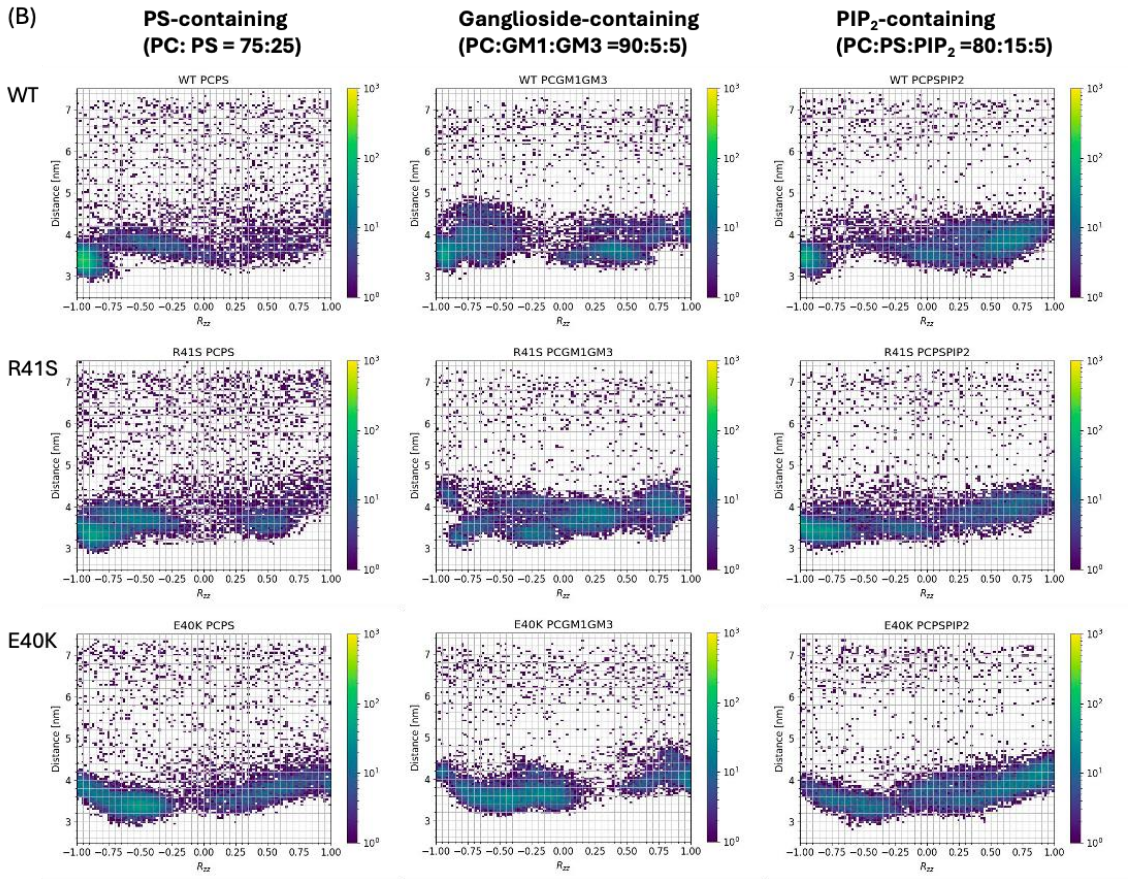


Figure 5-12. Representative binding modes and distance vs orientation plots. (A) Cartoons show the four possible DLL4-C2 membrane-binding modes generated by MD simulations. A DLL4-Notch1 complex is aligned with the C2 domain, suggesting possible steric clashes with the membrane and physically possible ternary complex formation. Simulations of WT-, E40K-, or R41S-C2 interacting with PS-, ganglioside-, or PIP_2-containing membrane generally ended up in one of the four binding modes. The reference frame was used to generate the distance vs orientation plots. (B) Orientation (R_{zz}) vs distance plots for WT, E40K, and R41S DLL4-C2 binding to PS-, ganglioside-, or PIP_2- containing membranes. The R_{zz} values range from ~-0.75 for the nonphysical binding mode to ~1.0 for the reference frame, as shown in (A). Differences between the plots represent shifts in the landscape of binding orientations.

Combination	Reference frame	Binding mode A	Binding mode B	Nonphysical binding mode
WT + PS	0	0	4	21
R41S + PS	0	3	7	15
E40K + PS	0	5	12	8
WT + GM	1	8	8	8
R41S + GM	3	11	9	2

E40K + GM	4	8	10	3
WT + PIP_2	3	8	2	12
R41S + PIP_2	1	4	9	11
E40K + PIP_2	8	9	2	6

Table 5-1. Summary of the results of DLL4-C2 binding to PS-, ganglioside-, or PIP_2-containing membranes. A total of 25 repeats were performed for each combination. Binding modes A and B are compatible with a FL-ligand ectodomain but only A has the Notch receptor binding region exposed. The reference frame is also compatible with a FL-ligand ectodomain, and a ligand-bound Notch EGF11-13 fragment. However, due to the missing piece of information of the FL-Notch receptor structure, the remaining EGF repeats C-terminal to EGF13 may or may not have steric clashes with the membrane, depending on the shape, rigidity and flexibility of their domain interfaces, and whether a *trans*- or *cis*-complex is formed.

The different outcomes of E40K and R41S mutations could be explained by electrostatic interactions, since the PIP_2 molecules in the membrane are highly anionic with a net charge of -4. Whilst the exchange of a negatively charged residue with a positively charged residue (E40K) promoted interactions of the C2 apex with the membrane, the exchange of a positively charged residue with a neutral residue (R41S) reduced the binding between the C2 apex and membrane. Although PIP_2 lipids are rarely found in the outer leaflet of the plasma membrane (Casares et al., 2019), therefore are less physiologically relevant in the extracellular environment, these results collectively suggest that the β1-2 loop acts as an anchor for C2-membrane binding, and the weak C2-lipid interactions can be influenced by charge changes on both the membrane and C2 domain.

5.8 Conclusion

- **C2 cancer database missense mutations had no effect on receptor binding**

In this chapter, eleven cancer database missense mutations mapping to the DLL4-C2 apical loops were tested for their receptor- and lipid-binding properties. Three different

ligand-receptor binding assays were used, each had its own advantages and disadvantages (Table 5-2). Whilst the plate-based binding assay allowed accurate quantification of the amount of protein used, the cell-based binding assays allowed either the Notch receptor or the ligand to be expressed in its full-length physiological form. Using all three techniques, the DLL4 cancer database variants tested showed non-statistically significant difference in receptor binding compared with WT-DLL4 (Table 5-3), suggesting that these C2-apical-loop missense mutations did not affect the receptor binding site on C2 domain.

Assay type	Advantages	Disadvantages
Plate-based	• low experimental cost • the amount of receptor and ligand proteins tested can be easily and accurately controlled • easy to analyse and compare the results quantitatively (as absorbance reading)	• recombinant ligand proteins were purified as Fc-dimerised NE3 fragments, not physiological • recombinant receptor proteins were purified as C-terminally BirA-tagged EGF11-13 or EGF7-13 fragments, not physiological
Cell-based ligand binding	• high-throughput screening • the amount of ligand protein added can be easily and accurately controlled • easy to analyse and compare the results quantitatively (as MFI) • complete FL-Notch receptors were expressed in their physiological form on the cell surface • allow comparison of cell type-dependent differences (HEK293-mN1 vs HUVECs)	• high experimental cost • recombinant ligand proteins were purified as Fc-dimerised NE3 fragments, not physiological • different batches of cells may increase variability between independent experiments
Cell-based receptor binding	• high-throughput screening • the amount of receptor protein added can be easily and accurately controlled • complete, monomeric FL-DLL4 variants were expressed in their physiological form on the cell surface	• high experimental cost • more difficult to control the surface expression level of FL-DLL4 variants • difficult to combine and analyse results quantitatively due to the bimodal distribution of the histograms

		• recombinant receptor proteins were purified as C-terminally BirA-tagged EGF11-13 or EGF7-13 fragments, not physiological • each independent transient transfection may increase variability across experimental repeats

Table 5-2. Comparison of plate-based Notch-binding assay with cell-based ligand binding or receptor binding assays. The advantages and disadvantages of the three different techniques are listed.

Three different purified Notch constructs, NOTCH1$_{E11-13}$, NOTCH1$_{E7-13}$, NOTCH2$_{E11-13}$, were tested in the plate-based assay, allowing receptor-dependent differences to be compared. For instance, WT-JAG1$_{NE3}$ showed poor binding to NOTCH1$_{E11-13}$ but improved binding to NOTCH1$_{E7-13}$ (Figure 5-4), consistent with earlier structural data of the additional binding site between Jag1-EGF3 and Notch1-EGF8 (Luca et al., 2017) (see section 1.3.3 for details). On the other hand, the titration profiles of WT-DLL4$_{NE3}$ (Figure 5-4) suggest that it binds NOTCH1$_{E11-13}$ and NOTCH1$_{E7-13}$ with similar affinities, but with a higher affinity than does WT-JAG1$_{NE3}$. These results are also consistent with previous SPR measurements, which showed that WT-Dll4$_{NE3}$ binding to Notch1$_{E8-12}$ only led to a 0.3-fold increase in Kd compared with binding to Notch1$_{E11-12}$, whereas WT-Jag1$_{NE3}$ binding to these Notch1 fragments was too weak to allow reliable determination of Kd values (Luca et al., 2017). Similarly, a previous flow-cytometry-based binding assay using cells expressing FL- WT-Dll4 or WT-Jag1 to bind NOTCH1$_{E11-13}$ fragments immobilised on beads suggested that FL-Dll4 had a higher affinity than FL-Jag1 for NOTCH1$_{E11-13}$, regardless if the O-fucose^{T466} on NOTCH1$_{E11-13}$ was modified (Taylor et al., 2014; Weisshuhn et al., 2016). Overall, it is generally agreed that WT-DLL4 has a higher binding affinity than WT-JAG1 for NOTCH1, but these results were insufficient to determine if EGF8 contains an additional binding site for DLL4, as identified for JAG1. DLL4$_{NE3}$ cancer database variants, including the double mutant E40K/D128N that showed dramatically reduced ability to activate Notch (Chapter 3), all appeared to have

a Notch-binding affinity similar to WT-DLL4$_{NE3}$ for all three receptor constructs (Figure 5-5).

Mutation	Position in C2 domain	Plate-based binding	Cell-based ligand binding	Cell-based receptor binding	Liposome binding
E40K	β1-2	no effect	no effect	no effect	no effect
R41S	β1-2	no effect	no effect	no effect	n/a
P49S	β1-2	no effect	n/a	n/a	no effect
V91L	β3-4	no effect	n/a	n/a	n/a
S96R	β3-4	no effect	n/a	n/a	n/a
R100G	β3-4	no effect	no effect	n/a	n/a
D127E	β5-6	no effect	no effect	n/a	no effect
D128N	β5-6	no effect	no effect	n/a	no effect
P131T	β5-6	no effect	no effect	n/a	no effect
P135A	β5-6	no effect	n/a	n/a	no effect
L164F	β7-8	no effect	n/a	n/a	n/a
E40K/D128N	β1-2, β5-6	no effect	no effect	n/a	n/a
F195A/Y216A		↓↓↓↓↓	↓↓↓↓↓	↓↓↓↓↓	no effect
ERGV deleted	β1-2			↓↓↓↓↓	
DDLR deleted	β5-6			↓↓↓	
RPEA deleted	β5-6			↓↓↓	

Table 5-3. Summary of effects of DLL4 cancer database and loop-shortening variants on receptor binding and lipid interactions. The cancer database variants, including the E40K/D128N double mutant, showed no statistically significant effect on receptor binding in both the plate-based binding assays and the cell-based ligand or receptor binding assays. Binding by WT-DLL4 is normalised to 100%, F195A/Y216A resulted in >80% decrease in binding, thus was annotated as '↓↓↓↓↓' (each '↓' represents a 20% decrease). The β1-2 ERGV-deleted variant resulted in >80% decrease in receptor binding, thus was annotated as '↓↓↓↓↓', whereas both β5-6 loop-shortening variants resulted in ~50% decrease in receptor binding, thus were annotated as '↓↓↓'. The reduction in receptor binding observed for these loop-shortening variants can be correlated to their reduced surface expression levels. No detectable difference was observed between the cancer database variants and WT-DLL4. Some variants were not tested in these assays, thus are marked as 'n/a' (data not available).

Two different cell types, HEK293-mN1 and HUVECs, were used in the ligand binding assay, in which the latter have previously been shown to express all four Notch paralogues (NOTCH1-4) with physiologically-relevant Fringe modifications (Benedito et al., 2009; Patel et al., 2005). Therefore, the binding results allowed the assessment of cell-type dependent differences, which are quite complex, including but not limited to different receptor types and expression levels, various types and amount of PTMs, diverse membrane lipid compositions, varied signalling dynamics, and specific expression of non-canonical ligand-binding partners such as CD46 on the cell surface. For instance, WT-JAG1$_{NE3}$ showed slightly lower binding to HEK293-mN1 cells that was ~85% of WT-DLL4$_{NE3}$ binding, but dramatically lower binding to HUVECs that was only ~30% of WT-DLL4$_{NE3}$ binding (Figure 5-7). This could be accounted for by cell type-dependent differences, such as the type(s) of Notch prologues present, the context-dependent glycosylation patterns, and the cell type-specific membrane components. However, in both cell types, binding did not appear to be affected by any of the DLL4$_{NE3}$ cancer database missense mutations tested, despite their functional effects in Notch activation (see Chapter 3&4), suggesting that the binding results are likely to be consistent in different biological contexts.

A new receptor binding assay was designed, which was advantageous by presenting complete FL-DLL4 variants in their physiological form but was limited by the surface expression levels of these variants (see Section 3.5.2 for details). In this assay, FL-WT-mDll4 not only showed higher binding to NOTCH1 fragments than FL-WT-mJag1 as expected (see Section 1.3.3.1 for details), but also showed significantly enhanced binding to NOTCH1$_{E7-13}$ compared to NOTCH1$_{E11-13}$ (Figure 5-8), which was not reported in previous studies where Dll4$_{NE3}$ showed similar binding affinity for Notch1$_{E8-12}$ and Notch1$_{E11-12}$ in SPR measurements (Luca et al., 2017). This observation could suggest additional interactions between Notch1 EGF7-10 and FL-Dll4. However, contradictory results were reported in a flow-cytometry-based binding assay using B16-mDll4 or B16-

mJag1 cells to bind NOTCH1 fragments immobilised on beads (Weisshuhn et al., 2016). In this early study, binding of FL-WT-mDll4 to NOTCH1$_{E9-13}$ or NOTCH1$_{E10-13}$ appeared to be significantly reduced compared with binding to NOTCH1$_{E11-13}$, whereas FL-WT-mJag1 showed similar binding to all three NOTCH1 fragments. Since these NOTCH1 fragments did not contain EGF8 where the additional ligand-binding site (observed for Jag1/Notch1) resides on, the contradictory results observed could suggest that EGF10 alone has an inhibitory effect on Dll4-NOTCH1 binding, but further addition of EGF7 and EGF8 promotes binding and outcompetes this inhibitory effect. Moreover, the assay conditions were different by presenting NOTCH1 fragments as soluble proteins in the receptor binding assay but immobilising multiple NOTCH1 fragments on bead surface in the previous binding assay, which may promote aggregation and shield the LBR.

Another interesting observation was that NOTCH1$_{11-13}$ appeared not to bind to mJag1-B16 cells at all in the receptor binding assay (Figure 5-8C). Nevertheless, previous binding assays, using biotinylated NOTCH1$_{E11-13}$ immobilised on avidin-coated beads to bind mJag1-B16 cells, showed clear receptor-ligand interactions (Taylor et al., 2014). The differences observed could be explained by the avidity effect, since NOTCH1$_{E11-13}$ was mixed with ligand-expressing cells as soluble proteins in the receptor binding assay (Section 5.5), whereas beads-coupling increased the local concentration of NOTCH1$_{E11-13}$, leading to enhanced binding strength. Likewise, in both the plate-based binding assay (Section 5.3) and ligand binding assay (Section 5.4), ligands were expressed as dimerised proteins, resulting in an avidity-driven effect. On the other hand, ligands may be presented as monomers on the cell surface, such that the receptor binding assay reflected the more biological interactions between the monomeric Notch receptor and the monomeric ligand.

Furthermore, FL-DLL4 loop β1-2 variants, E40K and R41S, both showed similar surface expression and NOTCH1$_{E7-13}$ binding compared with FL-WT-DLL4 (Figure 5-9),

strengthening the observations made in other binding assays. On the other hand, FL-DLL4 loop-shortening variants all showed lower $NOTCH1_{E7-13}$ binding, likely correlated to their lower surface expression levels (Figure 3-12). Moreover, whilst the Notch-binding deficient variant $F195A/Y216A_{NE3}$ generally showed minimal binding (~10%) to Notch receptors similar to the background control (Section 5.3 & 5.4), FL-F195A/Y216A showed significantly higher Notch binding compared to the 'cells only' background control (Figure 5-9).

Overall, the receptor-binding ability of DLL4 cancer database variants appeared to be unaffected under various conditions tested. Therefore, the C2 apical loops are likely to modulate ligand-induced Notch activation without directly affecting the receptor-ligand binding affinity. However, earlier data showed that addition of $NOTCH1_{E11-13}$ at low ligand concentrations appeared to boost DLL4- and JAG1- liposome binding, suggesting that receptor binding was indirectly coupled to lipid binding, probably by rigidifying the ligand structure to reduce the loss of entropy upon membrane binding (Suckling et al., 2017).

- **Cancer database missense mutations showed no detectable effects on liposome binding**

The lipid-binding ability of $DLL4_{NE3}$ cancer database variants was assessed by a recently developed liposome aggregation assay (Meng et al., 2022). Whilst the PC-rich liposomes provided a common and simple membrane model, the SM-rich liposomes acted as a simplified mimic of the outer leaflet of the plasma membrane (Casares et al., 2019). Similar to SM, gangliosides are also primarily located in the outer leaflet of the plasma membrane and typically enriched in microdomains known as lipid rafts (P. H. H. Lopez & Schnaar, 2009; Simons & Ikonen, 1997; Simons & Toomre, 2000). On the other hand, PIP_2 is mainly found in the inner leaflet of plasma membrane or on the cytosolic face of organelle membranes (Bochud & Conzelmann, 2015; Viaud et al., 2016), but early studies showed that PI could be flopped to the luminal face of ER by ER flippase

(Vishwakarma et al., 2005), suggesting relevance to the extracellular C2 of Notch ligands in the protein secretory pathway. WT-JAG1$_{NE3}$ showed a binding preference for SM-rich liposomes, consistent with earlier data obtained from a plate-based liposome binding assay (Suckling et al., 2017). However, unlike the plate assay results, WT-DLL4$_{NE3}$ did not show a statistically significant preference to bind ganglioside-rich liposomes in the bead-based assay, probably because the ligand-lipid interactions were weak such that more experimental repeats were needed to show a statistically significant difference.

For all four types of liposomes, the DLL4$_{NE3}$ C2 variants, as well as the F195A/Y216A$_{NE3}$ receptor-binding negative control showed no detectable difference in lipid-binding compared with WT-DLL4$_{NE3}$ (Table 5-3). Since the formation of ligand-bead-liposome aggregates was highly avidity-driven, this assay may not be sensitive to small differences in lipid binding. Given the functional effects of the DLL4$_{NE3}$ cancer database variants were also relatively narrow (as described in Chapters 3 & 4), these C2 missense mutations were not expected to cause significant changes in lipid binding. Despite the experimental approach attempted to quantify C2-membrane interactions, it remained challenging for current techniques to probe ligand C2-lipid binding, especially because they are not expected to have deep membrane penetration, based on their sequence and behaviour in previous assays (see Section 1.5 for details). Moreover, the bead-based liposome aggregation assay is highly avidity-driven by immobilising Fc-dimerised ligand NE3 fragments on bead surface to increase the combined strength of multiple weak C2-lipid interactions. The high local concentration and bead-based immobilisation of ligands may also restrain the orientation of C2, which, as suggested by MD analyses (Section 5.7), may interact with the membrane in an ‘upright’ apical-binding orientation or in a ‘horizontal’ side-binding orientation (the latter might not be feasible under the assay conditions). Therefore, the liposome aggregation assay may not be able to recapitulate all possible C2-membrane binding orientations or reveal the small differences in lipid binding for DLL4$_{NE3}$ C2 variants. However, this assay did show the

differences between JAG1 and DLL4 based on membrane compositions, suggesting its capacity to compare lipid-binding strengths to some extent. On the other hand, the F195A/Y216A DSL domain missense mutations are located distally from the C2 domain and thus are unlikely to affect C2-membrane interactions.

- **Membrane lipid compositions and β1-2 loop sequence both contributed to DLL4-C2 membrane binding orientation in MD analyses**

The lipid-binding properties of DLL4-C2 were further analysed by MD simulations, which simulated the binding of WT-DLL4-C2 and its loop β1-2 variants, E40K and R41S, to three different anionic lipid membranes. The binding orientation of WT-DLL4-C2 varied with changes in the anionic lipid composition of the bilayer (PS, ganglioside, or PIP_2), suggesting nonspecific electrostatic interactions (Figure 5-12). Clustering of ganglioside or PIP_2 molecules around the bound C2 domain suggested stronger binding affinity than the PS-containing membrane, which might be contributed by short-range protein-lipid interactions (Figure 5-11). In addition, missense mutations in the β1-2 loop, E40K and R41S, both shifted the binding orientation landscape compared with WT-DLL4-C2 (Table 5-1). Although DLL4-C2 does not have obvious cluster of positively charged residues, the electrostatic property of the C2 apical loops could still modulate C2-membrane binding orientation via nonspecific electrostatic interactions, as observed for other peripheral membrane proteins (Khan et al., 2016; Larsen et al., 2022). Lipid binding could also be modulated by cation-π interactions between aromatic residues and choline head groups of PC molecules, providing additional molecular insights.

Overall, the MD results suggest that amino acid substitutions in loop β1-2 can alter the binding modes of DLL4-C2 with the membrane, and the exact changes in the binding orientation landscape depend on both the specific amino acid substitution and the specific membrane lipid compositions. This provides molecular insights into the functional effects observed for the DLL4 cancer database variants, and the differences

in activity observed between different cell types (Chapter 3&4). However, since structural data of the Notch receptor full-ectodomain is still missing, and the crystal structure aligned with the C2 domain in MD analysis was resolved from force-independent receptor-ligand complex, it remains uncertain whether the ligand-bound receptor indeed has steric clashes with the membrane. Moreover, the pulling force generated by transendocytosis could induce subtle conformational changes, which may slightly rearrange the domain interfaces to engage a 'catch-bond'-like effect (Luca et al., 2017), or push the equilibrium of the Ca^{2+}-bound EGF domains towards their Ca^{2+}-free state which gives more flexibility. Hence, the C2-membrane interaction mode may be altered upon application of a mechanical force. Whilst MD simulations are valuable and allow us to monitor the binding of ligand C2 domains to bilayers of different lipid composition, the results should be used with caution because the experiment cannot simulate the exact biological context during Notch activation.

Chapter 6: Studying the functional importance of a conserved N-glycan in JAG1 C2 domain

6.1 Introduction

As discussed in Chapter 1, both Notch receptors and ligands are extensively glycosylated. O-glycosylation, which plays multifaceted regulatory roles in the Notch pathway, is relatively well studied (Section 1.4.1). On the other hand, less is known about N-glycosylation in the context of Notch signalling. Whilst O-glycans are attached to specific S/T residues in EGF domain consensus sequences, N-linked oligosaccharides are added to acceptor asparagine in the N-X-(S/T) consensus sequence (X is any amino acid except for proline) (Breitling & Aebi, 2013). A number of N-glycosylation consensus sites were identified in Notch receptors and ligands, although their functional roles remain to be investigated (Johansen et al., 1989; Moloney, Shair, et al., 2000; Suckling et al., 2017). As a common PTM found on the ECD of membrane proteins, N-glycans are known to modulate protein folding, stability and signal transduction (Azimzadeh Irani et al., 2017; Esmail & Manolson, 2021; H. S. Lee et al., 2015). From quality control in the ER, to glycan-mediated receptor oligomerisation and ligand binding, to glycan-modulated trafficking and cell surface expression, N-glycosylation could potentiate cellular signalling via various mechanisms (Azimzadeh Irani et al., 2017; Boscher et al., 2011; Tannous et al., 2015; C. Xu & Ng, 2015).

N-glycosylation in eukaryotic cells involves a number of processing reactions in the ER and Golgi. These include some conserved biosynthetic steps, such as the covalent attachment of the dolichol-oligosaccharide precursors to the acceptor Asn, which take place in the ER. The early-stage biosynthetic pathways resulted in the core N-glycan structure as indicated in Figure 6-1, where the initial linkage involves two core GlcNAc monosaccharides and the first three mannose residues. Further processing of the core structure in the Golgi results in structurally diverse N-glycan subtypes that can be classified into oligomannose (or high-mannose), hybrid and complex N-glycans (Figure 6-1). In mammals, the first enzyme required for building complex N-glycan structures is

GlcNAc-transferase I (GnT-I, encoded by *Mgat1*). In addition, GnT-III (encoded by *Mgat3*), which catalyses the addition of a β-1,4-bisecting-GlcNAc on N-glycans, was found to regulate Notch expression and activation, suggesting a potential mechanism modulating Notch trafficking (Allam et al., 2017). Another common structural feature among N-glycans is the core fucosylation, in which an α-1,6-fucose was added to the innermost GlcNAc residue linked to the Asn. The GlcNAc-bearing branches identified in the hybrid or complex N-glycan subtypes are referred to as antennae. Multi-antennary N-glycan structures up to five branches have been observed on vertebrate glycoproteins.

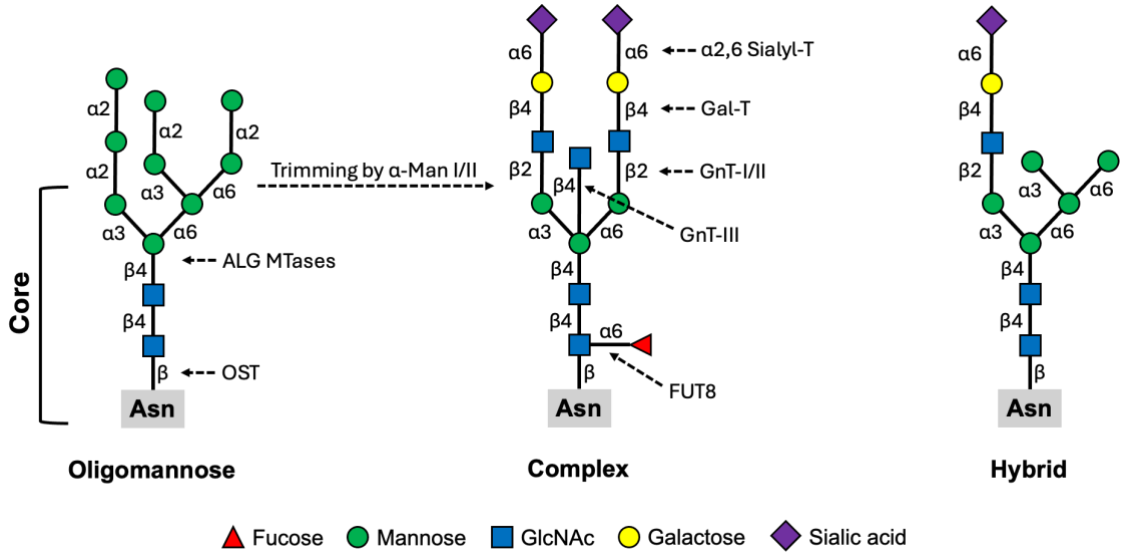


Figure 6-1. Types of N-glycans and enzymes involved in the biosynthesis. Three major N-glycan structure subtypes are shown. A lipid-glycan precursor is synthesised by ER-based asparagine-linked glycosylation (ALG) mannosyltransferases (MTases), which catalyse the sequential addition of mannoses to the two core GlcNAc residues (S.-T. Li et al., 2019). The precursor glycan is transferred to Asn by oligosaccharyltransferase (OST), producing a high-mannose N-glycan that is released from the ER (Reily et al., 2019). The N-glycan is subsequently modified in the ER and Golgi for structural diversification, such as the removal of mannoses by α-mannosidase I and II (α-Man I/II), core fucosylation by the fucosyltransferase (FUT) FUT8 **(García-García et al., 2021)**, and further processing by GlcNAc transferases (GnT-I/II/III), β-1,4-galactosyltransferase (Gal-T), and α-2,6-sialyltransferase (α2,6 Sialyl-T). All N-glycan subtypes share the same core structure (indicated by bracket). The oligomannose subtype terminates in mannose residues. The complex subtype has both the α3- and α6-linked mannose substituted with GlcNAc moieties. The hybrid subtype refers to those with both substituted GlcNAc moiety and unsubstituted mannose residues.

The analysis of COSMIC variants, mapping to the JAG1 C2 domain and found in various tumour lines, identified a substitution T145N that impairs an N-glycosylation consensus located on the C2 β5-6 loop (Meng et al., 2022). This variant and N143A, which impairs the same N-glycan motif, were expressed as NE3 fragments and found to display significantly lower Notch activation *in vitro* and have reduced liposome binding due to loss of the N-glycan on N143. Similar functional effects were not observed for a protein-engineered variant $N217A_{NE3}$, which also impairs an N-glycosylation site in the DSL domain, suggesting the functional importance of the N-glycan on the C2 lipid-binding loop. This chapter aims to further investigate the importance of N-glycosylation using full-ectodomain JAG1 protein (FL-J1) with PNGase F treatment, as well as another $JAG1_{NE3}$-N143Q variant ($N143Q_{NE3}$). In addition, using purified JAG1 NE3 fragment produced from HEK293S cells ($JAG1_{NE3}$/S), which lack GnT-I activity and therefore are unable to synthesise complex N-glycans (Reeves et al., 2002), the importance of the N-glycan structure for JAG1 function was investigated.

6.2 Conservation of the N-glycosylation site on C2 β5-6 loop in the Jagged/Serrate family

Sequence analysis showed that the Jagged family but not Delta-like family ligands, except for *Drosophila* Delta, all contain a conserved NX(S/T) motif on their C2 β5-6 loop (Figure 6-2). This N-glycan site is conserved in Jagged/Serrate ligands in all higher metazoans, from *Drosophila* to human. Crystal structures confirmed the presence of a complex N-glycan on N137 in an NE3 fragment of *Drosophila* Delta, and an α(1,6)-linked fucose on N153 in JAG2 (Figure 6-3B) (Martins et al., 2021; Suckling et al., 2017). The N-glycan on N153 of JAG2 was shown to pack against the side chain of W151 in JAG2 β5-6 loop, which may stabilise the apical loop structure (Suckling et al., 2017). Structure-based modelling suggested that the conserved NX(S/T) motif on loop β5-6 of JAG1

(N143) and *Drosophila* Serrate (N192) could also accommodate an N-glycan (Figure 6-3). Apart from the conserved C2 N-glycan, additional N-glycans on *Drosophila* Delta C2 domain (N98, N167), Serrate DSL domain (N243), and JAG1 DSL domain (N217) were identified by crystal structures (Chillakuri et al., 2013; Martins et al., 2021). Additional NX(S/T) consensus sequences are also present in DLL4 C2 (N108) and DSL domains (N183, N205), and in *Drosophila* Serrate C2 domain (N148), but unlike the Jagged C2 β5-6 N-glycosylation site, these sequences are poorly conserved (Table 6-1).

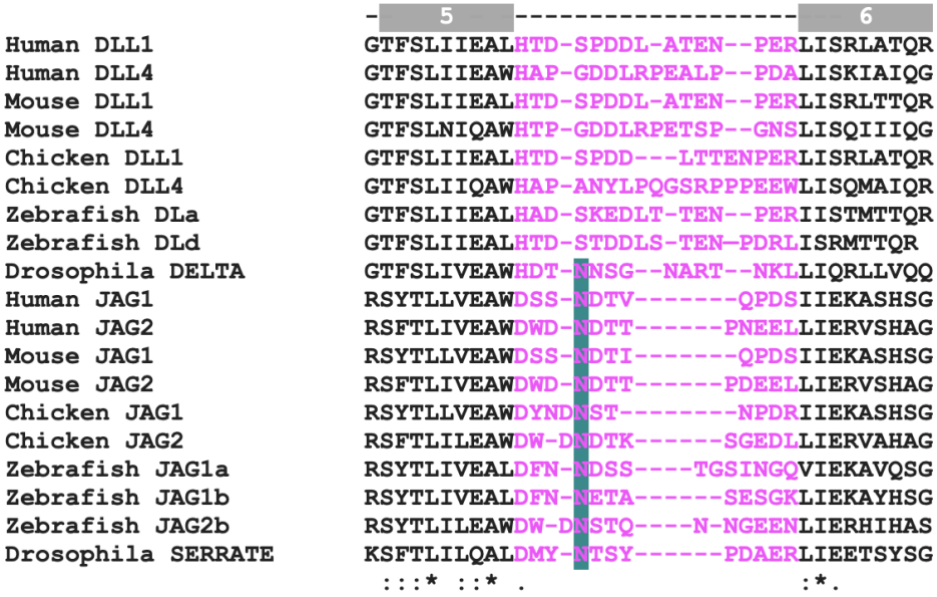


Figure 6-2. Sequence alignment showing conservation of the N-glycosylation consensus in C2 β5-6 loop of Jagged/Serrate family ligands. Amino acid sequence alignment of the C2 β5-6 loop of canonical Notch ligands. The grey bars indicate the β5 and β6 strands of the C2 domain. Residues in loop β5-6 are coloured in magenta. The asparagine residues of the NX(S/T) consensus are highlighted in teal, indicating conservation of the loop β5-6 N-glycosylation site in Jagged/Serrate but not Delta ligands, except for *Drosophila* Delta. Symbols: an asterisk (*) indicates a fully conserved residue, a colon (:) indicates conservation between groups of strongly similar properties, a period (.) indicates conservation between groups of weakly similar properties.

Notch ligand	N-glycosylation consensus
Serrate	N148, N192, N243, N327, N408, N448, N554, N735, N961, N973, N1000, N1026, N1146
JAG1	N143, N217, N382, N559, N745, N960, N991, N1045, N1064
JAG2	N153, N570, N619, N752, N1058
Delta	N98, N137, N167
DLL1	N477
DLL4	N108, N183, N205, N393

Table 6-1. N-glycosylation consensus in Notch ligands. A number of NX(S/T) motifs are identified in the ECD of *Drosophila* and human Notch ligands. Whilst the C2 β5-6 N-glycan site is well conserved in the Jagged/Serrate family, the other sites are all poorly conserved.

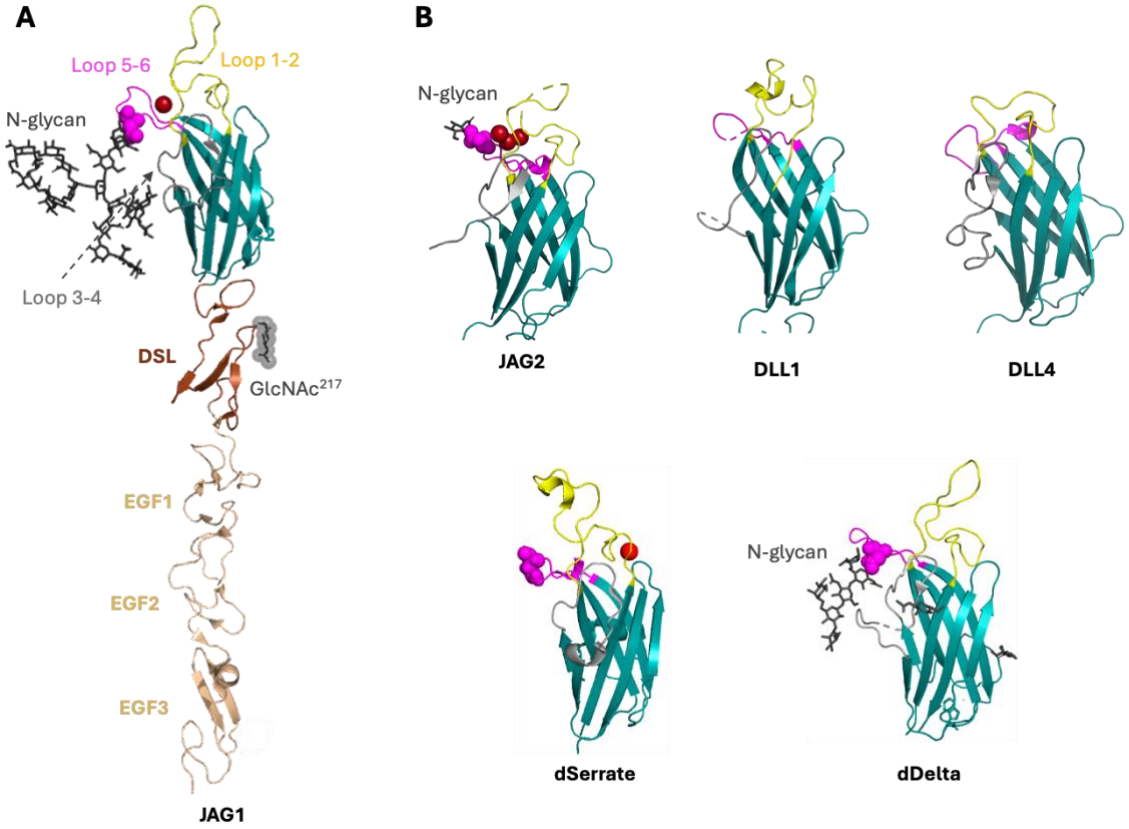


Figure 6-3. Structure of the conserved C2 N-glycosylation site in Jagged/Serrate family ligands. (A) The structure of $JAG1_{NE3}$ (PDB: 4CBZ) is shown in ribbon representation (C2: teal, DSL: orange, EGF: wheat, Ca^{2+}: red sphere). Putative lipid-binding loops in the C2 domain are highlighted with colours (loop β1-2: yellow, loop β3-4: grey, loop β5-6: magenta). The conserved Asn in the NX(S/T) motif in loop β5-6 is shown in sphere representation. A complex N-glycan (dark grey) on the C2 N143 residue is modelled based on JAG2 (PDB: 5MWF) and *Drosophila* Delta structures (PDB: 7ALK). Another N-glycan on DSL N217 residue is indicated. (B) Structures of C2 domains of other human and *Drosophila* Notch ligands are shown using the same colour scheme as (A). The conserved N-glycan on JAG2 C2 N153 residue (PDB: 5MW5) and dDelta C2 N137 residue (PDB: 7ALK) are indicated. This N-glycosylation motif is not conserved in the Delta family except for dDelta.

6.3 Preparation of protein constructs

6.3.1 Target site mutagenesis and secretion tests

The N143Q single amino acid substitution allowed abrogation of site-specific N-glycan but maintained chemical similarity of the C2 loop. Site-directed mutation was introduced into *pHL-sec-JAG1*$_{NE3\text{-}Fc\text{-}His}$ plasmid construct using overlap extension PCR (Figure 6-4, see Appendix 8.2.1 for primer sequences), and the correct DNA sequence was confirmed by Sanger sequencing (see Materials and Methods).

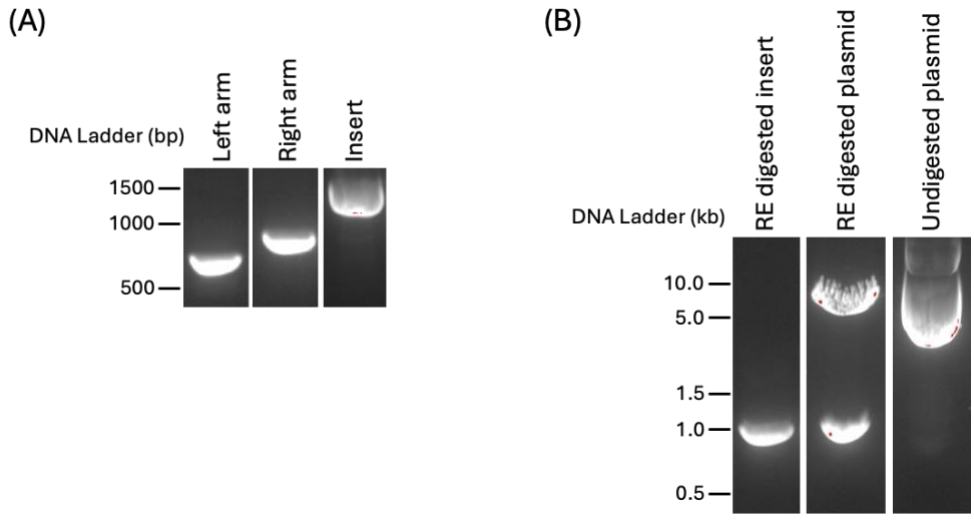


Figure 6-4. Agarose gels showing site-directed mutagenesis products. (A) The products from the first and second round of PCR reactions. (B) Insert and vector DNA fragments after digestion by *EcoRI* and *KpnI* restriction enzymes (RE). See Materials and Methods Section 2.1 for detailed cartoon explanations (Figure 2-1 and 2-2).

The plasmid that carries DNA encoding the N143Q substitution, alongside WT-JAG1$_{NE3\text{-}Fc\text{-}His}$ plasmid, were transfected into HEK293T cells (see Materials and Methods). Post-transfection medium samples were analysed by Western blot to check any effect of the introduced mutation on protein trafficking and secretion (Figure 6-5). Two independent transient transfection and secretion tests were performed. JAG1$_{NE3\text{-}Fc\text{-}His}$ constructs were detected using an anti-His-HRP antibody and visualised under both reducing and non-reducing SDS-PAGE conditions (similar to the DLL4$_{NE3}$ variants analysed in Chapter 3). The unmodified NE3 constructs have a theoretical MW ~65 kDa (monomer) or ~130 kDa

(dimer). However, the experimental band migration on SDS-PAGE generally shows a higher MW than the theoretical value (similar to the $DLL4_{NE3}$ variants analysed in Chapter 3), likely due to PTMs such as glycosylation and the 'gel shifting' phenomenon associated with the His-tag (Shelake et al., 2017). Checking of post-transfection medium samples showed that $N143Q_{NE3}$ had slightly lower secretion compared to WT-$JAG1_{NE3}$, as suggested by the less dense band in Western blot (Figure 6-5). A MW drop was also observed for $N143Q_{NE3}$ compared to WT-$JAG1_{NE3}$, as shown by the band shift (arrowed), suggesting that the N143 N-glycosylation site was occupied in WT-$JAG1_{NE3}$ but lacked the N-glycan in the $N143Q_{NE3}$ variant. A similar MW drop was previously observed for the $N143A_{NE3}$ and $T145N_{NE3}$ variants (Meng et al., 2022).

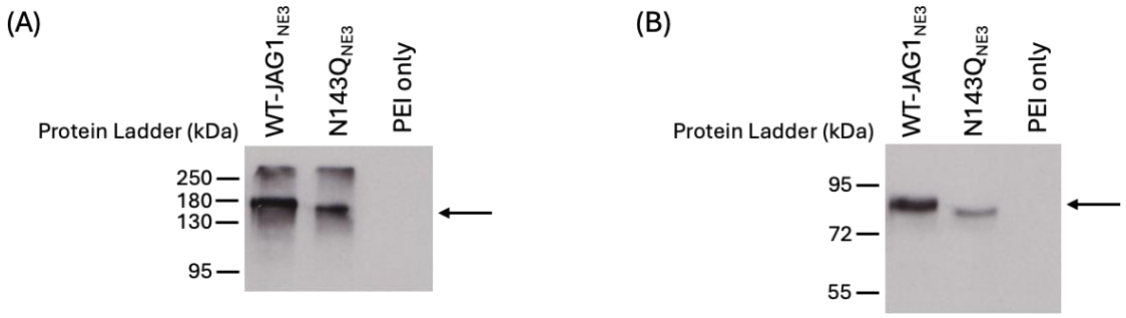


Figure 6-5. Western blot analysis of medium samples of $N143Q_{NE3\text{-}Fc\text{-}His}$ and WT-$JAG1_{NE3\text{-}Fc\text{-}His}$. Proteins were separated by non-reducing (A) and reducing (B) SDS-PAGE and detected by anti-His-HRP antibody. The theoretical monomeric MW of $JAG1_{NE3\text{-}Fc\text{-}His}$ is ~65kDa and the Fc-dimer had a theoretical MW ~130kDa, whereas experimentally, the bands migrated to a higher MW position ~90kDa (monomer) or ~180kDa (dimer). Target bands with desired MW were indicated by arrows, showing the MW drop of $N143Q_{NE3}$ compared to WT-$JAG1_{NE3}$, as seen previously in $N143A_{NE3}$ and $T145N_{NE3}$ variants (Meng et al., 2022).

6.3.2 Protein purification

6.3.2.1 $JAG1_{NE3\text{-}Fc\text{-}His}$ N143Q from HEK293T

The JAG1 N-glycan variant $N143Q_{NE3}$ was expressed as an NE3 fusion protein using HEK293T cells and purified using IMAC and SEC (see Materials and Methods). Protein purification intermediate products from IMAC and SEC were analysed using Western

blot with His-tag detection and SDS-PAGE. Low levels of $JAG1_{NE3}$ were detected in the flow-through and wash-through samples from IMAC (Figure 6-6A), suggesting that the Ni^{2+} column effectively immobilised His-tagged $JAG1_{NE3}$. The size exclusion chromatogram of $N143Q_{NE3}$ was analysed alongside that of WT-$JAG1_{NE3}$ (Figure 6-6B), suggesting that fractions 3 and 4 corresponded to the protein elution peak (indicated by a solid double-headed arrow).

SDS-PAGE was performed to check the identity of the protein eluted in each fraction, in which fractions 3 and 4 showed a protein band at the expected MW under both non-reducing (Figure 6-6C) and reducing (Figure 6-6D) conditions. The clearer target band in fraction 4 suggested higher protein purity, and thus only fraction 4 was collected as purified $N143Q_{NE3}$, which was further assessed by Western blot using anti-His antibody (Figure 6-6E). Band shifts (arrowed) were observed, suggesting the MW drop as explained earlier in Section 6.3.1.

Furthermore, unlike the elusion profile of WT-$JAG1_{NE3}$ which only has a single elution peak, a second peak (i.e., fractions 1 and 2), indicated by a dashed double-headed arrow in Figure 6-6B, was observed in the size exclusion chromatogram of $N143Q_{NE3}$. This peak corresponds to higher MW materials because it was eluted before fractions 3 and 4. SDS-PAGE (Figure 6-6C&D) and Western blot (Appendix Figure 8-2A) analyses of these protein fractions showed that they had a higher MW under non-reducing conditions but a normal MW when reduced and were immunoreactive to anti-His antibody. These results suggested that fractions 1 and 2 also contained His-tagged $N143Q_{NE3}$ protein, which might exist as aggregates. The different elusion profile of $N143Q_{NE3}$ compared to WT-$JAG1_{NE3}$ suggested that $N143Q_{NE3}$ might have partial misfolding or decreased solubility due to loss of the N143-glycan.

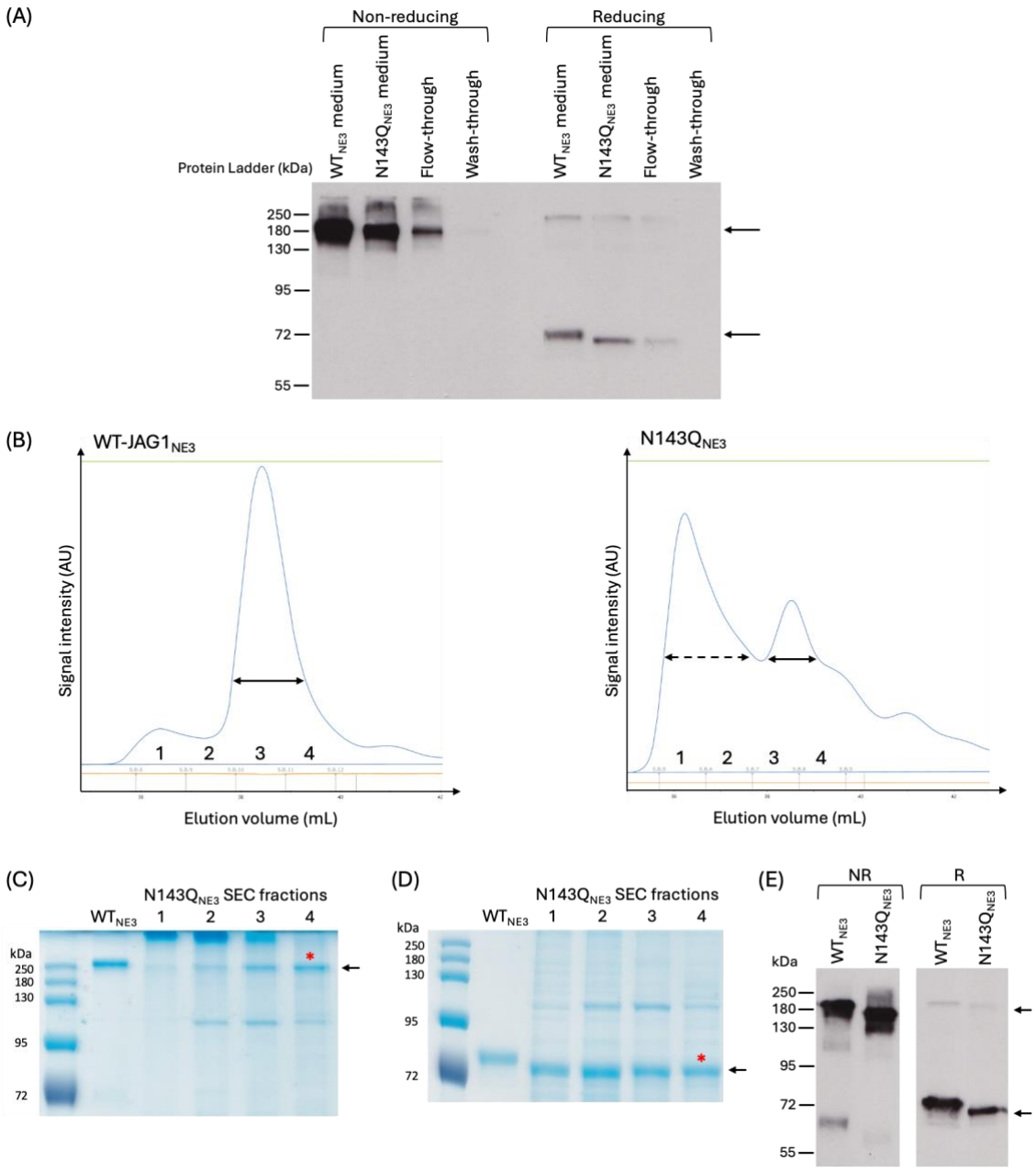


Figure 6-6. Purification of JAG1$_{NE3\text{-}Fc\text{-}His}$ N143Q variant from HEK293T. (A) Western blot analysis of IMAC intermediate products of JAG1$_{NE3\text{-}Fc\text{-}His}$ N143Q variant. Target bands with desired MW were indicated, showing the MW drop of N143Q$_{NE3}$ compared to WT-JAG1$_{NE3}$ in reducing and non-reducing conditions (arrowed). (B) Size exclusion chromatograms of WT-JAG1$_{NE3}$ (left) and N143Q$_{NE3}$ (right). The protein elution peak is indicated with a solid double-headed arrow. The second peak in N143Q$_{NE3}$ is indicated with a dashed double-headed arrow. (C) Non-reducing and (D) reducing SDS-PAGE to check the identity and purity of the N143Q$_{NE3}$ protein. Red asterisks indicate the fraction containing homogeneous product that was collected for further experiments. (E) Purified N143Q$_{NE3}$ collected from fraction 4 in (B) was assessed alongside WT-JAG1$_{NE3}$ by Western blot using anti-His-HRP antibody. Band shifts suggesting a MW drop are shown (arrowed).

6.3.2.2 $JAG1_{NE\text{-}Fc\text{-}His}$ from HEK293S

WT-$JAG1_{NE\text{-}Fc\text{-}His}$ was expressed and purified using GnT-I$^-$ HEK293S cells to prepare a sample (denoted as '$JAG1_{NE3}$/S') with N-linked oligomannose modifications instead of complex N-glycan modifications (Figure 6-1). $JAG1_{NE3}$/S was purified from post-transfection medium via IMAC and SEC, and the protein purification intermediates and products were analysed using Western blot and SDS-PAGE (see Materials and Methods).

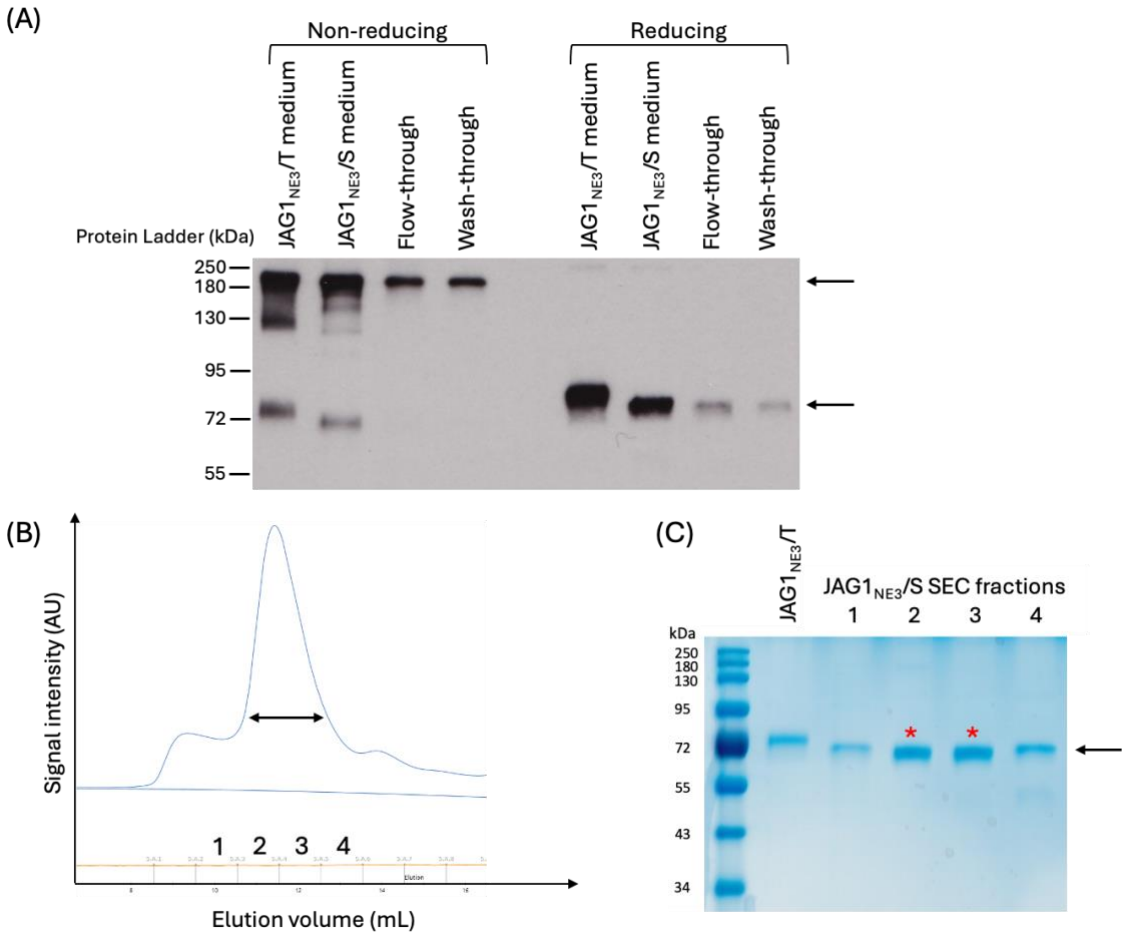


Figure 6-7. Purification of $JAG1_{NE3\text{-}Fc\text{-}His}$ from HEK293S. (A) Western blot analysis of IMAC intermediate products of WT-$JAG1_{NE3}$ produced from HEK293S ($JAG1_{NE3}$/S). WT-$JAG1_{NE3}$ produced from HEK293T ($JAG1_{NE3}$/T) was loaded alongside, showing the band shifts compared to $JAG1_{NE3}$/S (arrowed). (B) Size exclusion chromatogram of $JAG1_{NE3}$/S. The protein elution peak is indicated with a double-headed arrow. (C) Reducing SDS-PAGE analysis of SEC products of $JAG1_{NE3}$/S. Red asterisks indicate the fractions that was collected for further experiments.

Little JAG1$_{NE3}$/S protein was detected in the flow-through and wash-through from IMAC (Figure 6-7A). Under non-reducing conditions, apart from the target band ~180kDa which corresponds to the ligand dimer, a faint lower band ~75kDa was observed, which could be a small amount of ligand monomer that was not dimerised. The size exclusion chromatogram of JAG1$_{NE3}$/S (Figure 6-7B) showed a clear single peak similar to WT-JAG1$_{NE3}$ produced from HEK293T cells (denoted as 'JAG1$_{NE3}$/T', Figure 6-6B), and the main peak fractions (indicated by asterisks in Figure 6-7C) were pooled together after analysis by SDS-PAGE. JAG1$_{NE3}$/S was modified by high-mannose rather than complex N-glycan, thus having a lower MW than JAG1$_{NE3}$/T as expected.

6.3.3 PNGase F digestion of ligand constructs

6.3.3.1 PNGase F digestion of JAG1$_{NE3}$ and DLL4$_{NE3}$

PNGase F digestion was performed for Notch ligand constructs (see Materials and Methods), which allowed removal of all N-glycans on the protein without changing their amino acid sequences (Figure 6-8A). Apart from the potential N-glycosylation sites in Notch ligands as listed in Table 6-1, there is an additional N-glycan site on the Fc tag. To optimise the amount of PNGase F required for digestion, a titration was performed using a range of enzyme concentrations (Figure 6-8B). Although the protocol from the manufacturer suggests using 2μL enzyme (500,000 units/ml) per 20μL reaction, when 1/10 of the enzyme (0.2μL) was used, a clear MW drop could still be observed between the digested and undigested JAG1$_{NE3}$ samples. Moreover, when JAG1$_{NE3}$ digested at this low concentration of PNGase F was subjected to a second round of digestion using the standard protocol (i.e., 2μL/20μL PNGase F added), no further MW drop was observed (Figure 6-8C). These results suggested that complete digestion had been achieved in the first round using the lower concentration of enzyme. In addition, ligands were incubated without PNGase F ('+ve' control) for up to 48hr, and the band remained at the same position as the untreated WT-JAG1$_{NE3}$, suggesting that JAG1$_{NE3}$ was stable under

the incubation conditions without any autonomous deglycosylation. A second band ~36kDa was observed in digested samples, which corresponds to the MW of PNGase F. $JAG1_{NE3\text{-}Fc\text{-}His}$ and $DLL4_{NE3\text{-}Fc\text{-}His}$ were digested using PNGase F, and both showed a MW reduction after digestion (Figure 6-8D). The clear band ~130kDa observed by SDS-PAGE suggested that the digestion was complete, resulting in homogenous products.

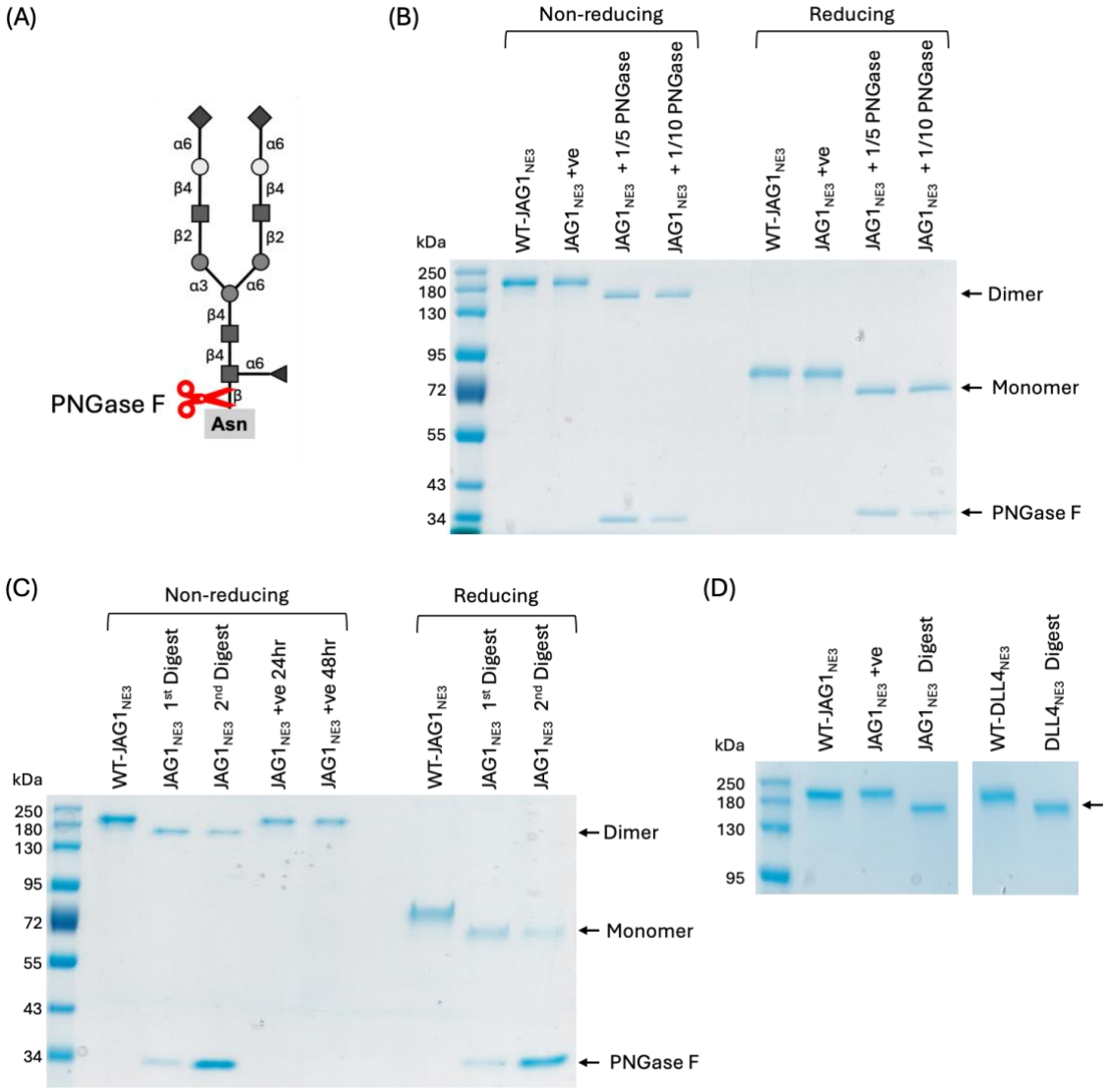


Figure 6-8. PNGase F digestion of $JAG1_{NE3}$ and $DLL4_{NE3}$. (A) PNGase F (scissors) catalyses the cleavage of N-linked complex, hybrid or high-mannose oligosaccharides by breaking the glycosidic bond between the innermost GlcNAc and Asn residue. (B) Titration of PNGase F showed that 1/10 of enzyme was sufficient for efficient digestion. (C) Double digestion of $JAG1_{NE3}$ showed that complete digestion was achieved in the first round of digestion. $JAG1_{NE3}$ positive control incubated without PNGase F ('+ve') remained at the same MW after 48hr of incubation. (D) Non-reducing SDS-PAGE showed MW drop of $JAG1_{NE3}$ and

$DLL4_{NE3}$ after PNGase F digestion. Target bands at expected MW ($JAG1_{NE3}$ dimer: ~180kDa, $JAG1_{NE3}$ monomer: ~90kDa, PNGase F: ~36kDa) are indicated by arrows.

6.3.3.2 PNGase F digestion of FL-J1

Full-ectodomain JAG1 Fc chimera (FL-J1) was similarly digested with PNGase F and analysed by Western blot (Figure 6-9). Bands corresponding to FL-J1 were detected using anti-Fc-HRP antibody. Under both reducing and non-reducing conditions, a MW reduction could be observed between digested and undigested samples. Complete digestion of FL-J1 was confirmed by double digestion with fresh enzyme (Figure 6-9B).

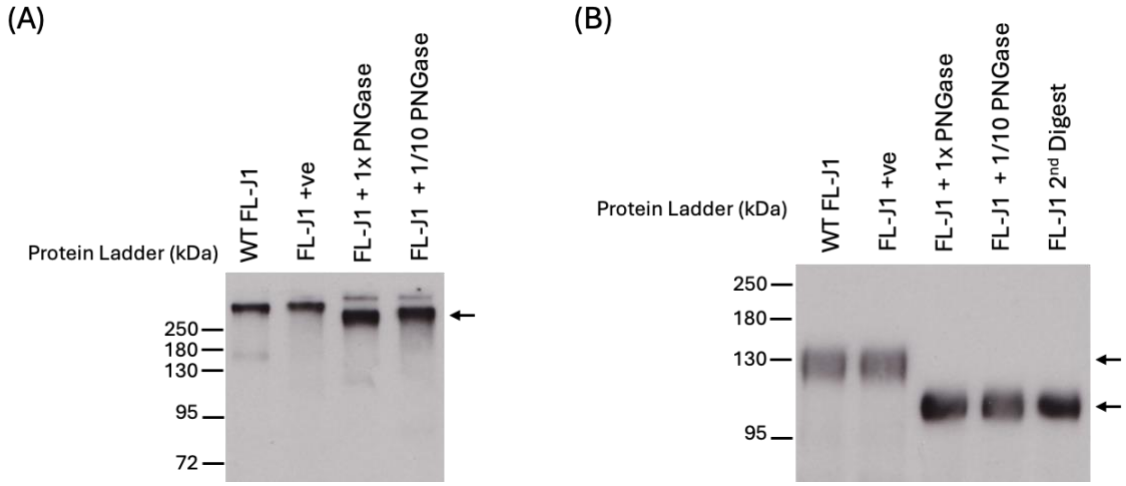


Figure 6-9. PNGase F digestion of FL-J1. Western blot analysis of PNGase F digested FL-J1 under (A) non-reducing or (B) reducing conditions using anti-Fc-HRP antibody. Titration of PNGase F showed that 1/10 of enzyme was sufficient for efficient digestion. Double digestion of FL-J1 showed that complete digestion was achieved after the first round of digestion with 1/10 PNGase F. Undigested FL-J1 has an expected MW ~274 kDa (dimer) or ~137 kDa (monomer). Digestion by PNGase F resulted in a MW drop (arrowed), and the digested FL-J1 has a reduced MW ~250 kDa (dimer) or ~110 kDa (monomer).

6.3.4 Glycoproteomic analysis of JAG1 N-glycan structure

Prior to activity analyses, WT-$JAG1_{NE3}$ samples expressed by HEK293T and HEK293S were subjected to mass spectrometry-based glycoproteomic analysis to confirm the nature of the N-glycan on the C2 and DSL domains. These experiments were performed

by Dr Sean Burnap from Professor Weston Struwe's lab (University of Oxford) using proteins prepared in Section 6.3.2.2. HEK293T/S-derived $JAG1_{NE3}$ proteins were subjected to SDS-PAGE, gel extraction, and tryptic digestion, after which the protein fragments were analysed using liquid chromatography-mass spectrometry (LC-MS). Data analysis was performed by Professor Weston Struwe's lab, and a results summary is shown in Figure 6-10.

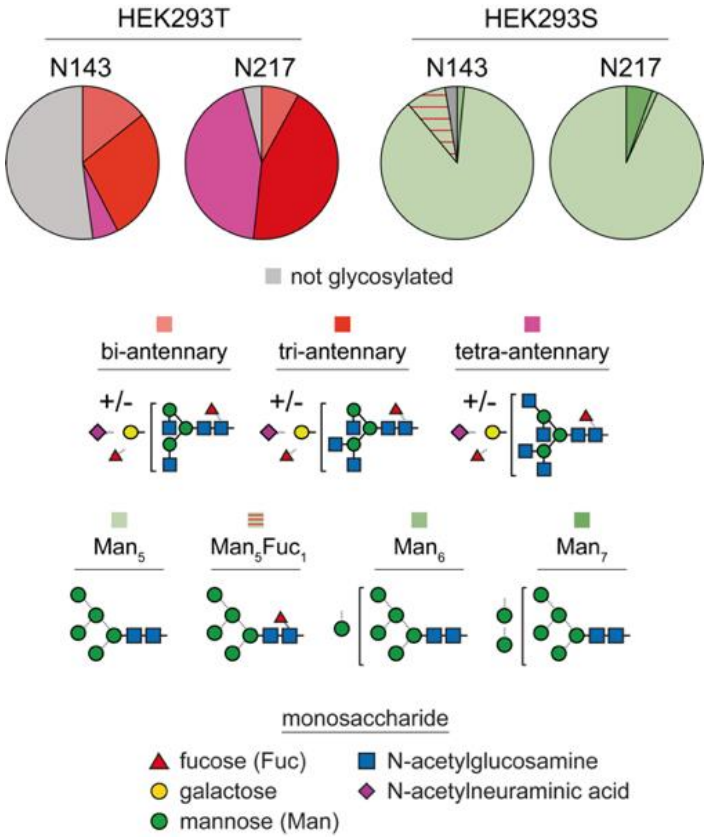


Figure 6-10. Glycoproteomic analysis results summary. Glycoproteomic analysis of WT-$JAG1_{NE3}$ expressed from HEK293T and HEK293S cells (cited from (Meng et al., 2022)). The structures and relative amount of N-glycans found on the N143 (C2 domain) and N217 (DSL domain) sites were shown as pie charts.

Both the N143 (C2) and N217 (DSL) sites were modified by N-glycosylation, showing a range of N-glycan structures with different branches. In $JAG1_{NE3}$/T, both sites were occupied by complex N-glycans existing in bi-, tri- or tetra- antennary forms with varying degrees of sialyation and fucosylation, among which the tri- and tetra- antennary sugars

were identified as the major species. Core fucosylation was observed on N-glycans at both sites. Unlike the N217 site, which was almost fully glycosylated, only 40% of the N143 site was shown to be glycosylated. However, considering the SDS-PAGE results in Figure 6-6, where purified $N143Q_{NE3}$ showed a clear single band with a lower MW compared to WT-$JAG1_{NE3}$, the glycoproteomic analysis results were likely caused by oversampling of the non-glycosylated material. As expected, in $JAG1_{NE3}$/S, the N-glycans on both N143 and N217 sites were identified to be oligomannose. Both sites were nearly fully glycosylated, with the high-mannose $Man_6GlcNAc_2$-Asn N-glycan being the major species.

6.4 Testing native fold with 65D monoclonal antibody

6.4.1 Optimising ligand immobilisation

A human/rat-specific JAG1 monoclonal antibody (65D MAb) was used, which recognises a specific epitope within the receptor binding site on the DSL domain comprising residues F199, R203, F207 and E228 (Figure 6-11A) (Masiero et al., 2019). Single substitutions within the receptor binding site, such as F207A and E228D, have previously been shown to impair effective 65D binding. In addition, the MAb itself was shown to effectively block Notch binding and therefore activation. Hence, this antibody was chosen to test the native fold of JAG1 N-glycan variants and PNGase F-digested peptides using a plate-based assay (see Materials and Methods, and Appendix 8.6.2).

In preliminary studies, titration curves were plotted for JAG1 to determine the saturating amount of ligand immobilised on the TC plate. For both shorter ($JAG1_{NE3}$, Figure 6-11B) and longer (FL-J1, Figure 6-11C) fragments, a concentration of 5ng/μL ligand was sufficient to saturate each well. To ensure saturation, an excess of ligand (10ng/μL) was used in the assay. The saturation curve of the PNGase F digestion positive control is

very similar to that of the untreated JAG1$_{NE3}$, suggesting that ligand immobilisation and epitope recognition by 65D MAb were not affected by the incubation conditions (Figure 6-11B).

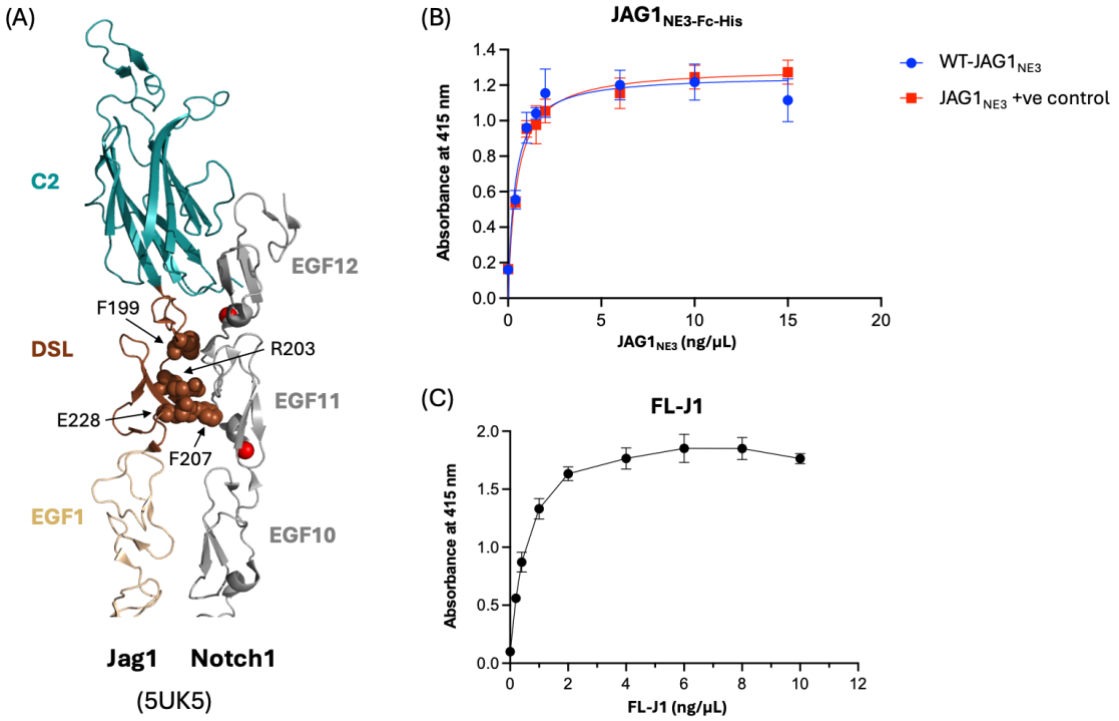


Figure 6-11. 65D epitope mapping and saturation curves of JAG1 immobilised on TC plates. (A) The X-ray structure of Notch1/Jag1 complex (PDB: 5UK5). Jag1 C2, DSL and EGF1 domains are shown in teal, orange and wheat respectively. Notch1 fragment is shown in grey (Ca^{2+} ions: red spheres). Key residues involved in 65D MAb binding are shown in sphere representations. (B) Saturation curve generated for JAG1$_{NE3}$ and its PNGase F digestion positive control ('+ve control') using 65D MAb and anti-mIgG-HRP secondary antibody. (C) Saturation curve generated for FL-J1 using the same antibodies in (B).

6.4.2 Epitope recognition of N143Q$_{NE3}$ variant and PNGase digested JAG1$_{NE3}$ and FL-J1

To assess epitope recognition by 65D MAb as a measure of native fold, assays were performed for N143Q$_{NE3}$ variant, HEK293S-derived WT-JAG1$_{NE3}$ (JAG1$_{NE3}$/S), and PNGase F digested WT-JAG1$_{NE3}$ (JAG1$_{NE3}$/T) and FL-J1 using optimised conditions (Section 6.4.1). WT-DLL4$_{NE3}$ was tested alongside other negative controls ('no ligand'

and 'block only'), which all showed a basal level of absorbance reading, confirming the specificity of 65D MAb and the effectiveness of blocking (Figure 6-12A). The N143Q$_{NE3}$ variant and WT-JAG1$_{NE3}$/S both bound 65D MAb similarly as WT-JAG1$_{NE3}$/T, suggesting that their epitope site was not affected (Figure 6-12A). The other N143Q$_{NE3}$ SEC fractions obtained in Section 6.3.2.1 were also tested (Appendix Figure 8-1), which showed a lower 65D binding affinity compared to WT-JAG1$_{NE3}$/T, likely due to aggregation and partial misfolding. The PNGase F digested WT-JAG1$_{NE3}$/T and its positive control, as well as an immediate mix of ligand protein with PNGase F without incubation ('PNGase Mix') all had similar binding affinity for 65D as the untreated WT-JAG1$_{NE3}$/T, suggesting that epitope recognition was unaffected by the incubation conditions or digestion (Figure 6-12A).

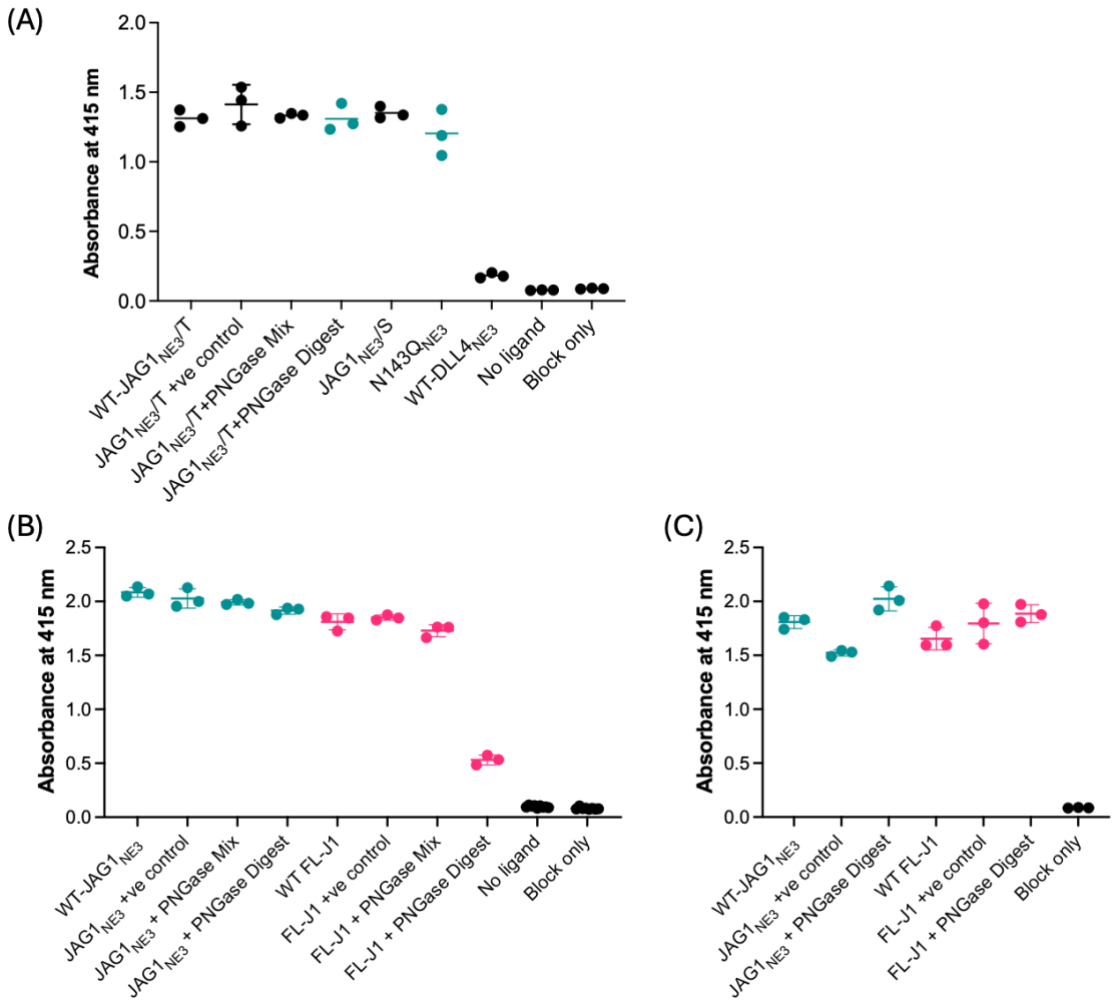


Figure 6-12. Epitope recognition of JAG1 constructs analysed by 65D MAb. (A) Epitope recognition of N143Q$_{NE3}$ (teal), WT-JAG1$_{NE3}$/S (black), WT-DLL4$_{NE3}$ (black), and PNGase F

digested WT-JAG1$_{NE3}$/T (teal). (B) Binding of 65D MAb to PNGase F digested FL-J1 (magenta) without precoating. PNGase F digested JAG1$_{NE3}$/T (teal) samples were analysed alongside. (C) Binding of 65D MAb to FL-J1 (magenta) with protein G precoating to orientate Fc-tagged ligands. PNGase F digested JAG1$_{NE3}$/T (teal) samples were analysed alongside.

FL-J1 digested by PNGase F was also tested for epitope recognition by 65D. Surprisingly, the PNGase F digested sample had dramatically reduced 65D binding compared to the untreated FL-J1 and the positive control (Figure 6-12B), suggesting that either adsorption occluded the epitope, or the epitope site was misfolded. However, when plates were precoated initially with protein G to orientate FL-J1 via its Fc tag (see Materials and Methods), the PNGase F digested sample showed similar 65D binding affinity as the untreated FL-J1 (Figure 6-12C). These results suggest that PNGase F digestion does not affect the native fold of FL-J1, but removal of N-glycans affects ligand adsorption to the plate surface.

6.5 Testing Notch activation capacity of the JAG1 constructs

To investigate the effects of the N143Q substitution and PNGase F deglycosylation on JAG1-induced Notch activation, activity assays were performed using CHO-K1 hN1G4^{esn} reporter cells (see Materials and Methods, Figure 2-4). TC plates were immobilised with JAG1 proteins using conditions established in Section 6.4.

6.5.1 NOTCH1 activation by N143Q$_{NE3}$ variant

Similar to the other N-glycan variants (N143A$_{NE3}$, T145N$_{NE3}$), the N143Q$_{NE3}$ variant also had a lower MW compared to WT-JAG1$_{NE3}$, consistent with the loss of a site-specific N-glycan (Figure 6-13A) and showed reduced ability to activate Notch (Figure 6-13B). Notch activation by N143Q$_{NE3}$ was ~20% of the WT positive control and only slightly higher than the receptor-binding deficient negative control (F207A/E228K$_{NE3}$ or FAEK$_{NE3}$),

suggesting a loss-of-function effect. The other SEC fractions of $N143Q_{NE3}$ obtained in Section 6.3.2.1 were also tested (Appendix Figure 8-2), which showed even lower activity than the purified $N143Q_{NE3}$ (fraction 4 in Figure 6-6B), suggesting likely aggregation and partial misfolding.

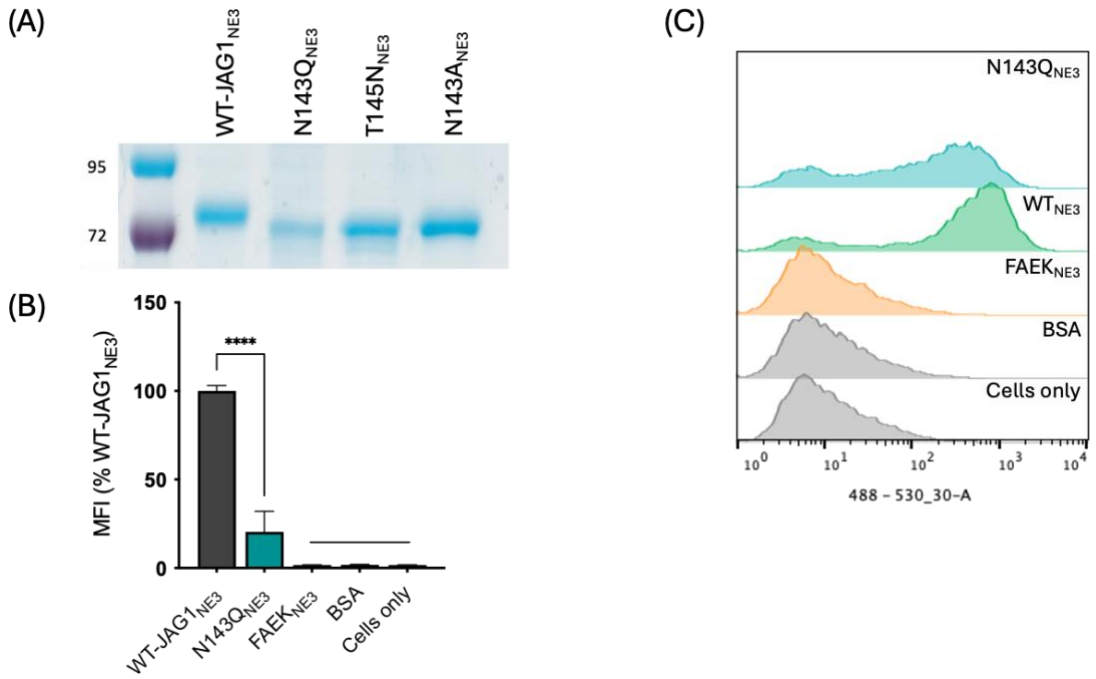


Figure 6-13. Notch activation by $N143Q_{NE3}$ variant. (A) Purified WT-$JAG1_{NE3}$ and its N-glycan variants ($N143Q_{NE3}$, $N143A_{NE3}$, $T145N_{NE3}$) were viewed using a reducing SDS-PAGE. (B) Notch activation by WT-$JAG1_{NE3}$, $N143Q_{NE3}$ and $FAEK_{NE3}$ was assessed by CHO-K1 $hN1G4^{esn}$ reporter cells. YFP expression levels were quantified as median fluorescence intensity (MFI). Data, presented as mean ± SD, represent combined results of n≥3 independent experiments, in which 10,000 cells were measured in each reading. BSA and 'cells only' were used as the background control. Statistical analysis was performed using Welch's t-test. ****$P \leq 0.0001$. (C) A representative histogram showing YFP expression levels measured by flow cytometry. Note the leftward shift of $N143Q_{NE3}$ and the $FAEK_{NE3}$ negative control compared with WT-$JAG1_{NE3}$ as an indication of decreased Notch activation.

6.5.2 NOTCH1 activation by deglycosylated $JAG1_{NE3}$ and $DLL4_{NE3}$

To confirm that the decrease in Notch activation by $N143Q_{NE3}$ and other N-glycan variants was a result of loss of the N-glycan on C2 β5-6 loop, rather than localised protein misfolding due to the amino acid substitution, WT-$JAG1_{NE3}$ was subjected to PNGase F

digestion and assessed for activity. WT-DLL4$_{NE3}$, which does not contain the C2 β5-6 loop N-glycan, was digested and tested for activity alongside, acting as a control which should retain its activity after digestion.

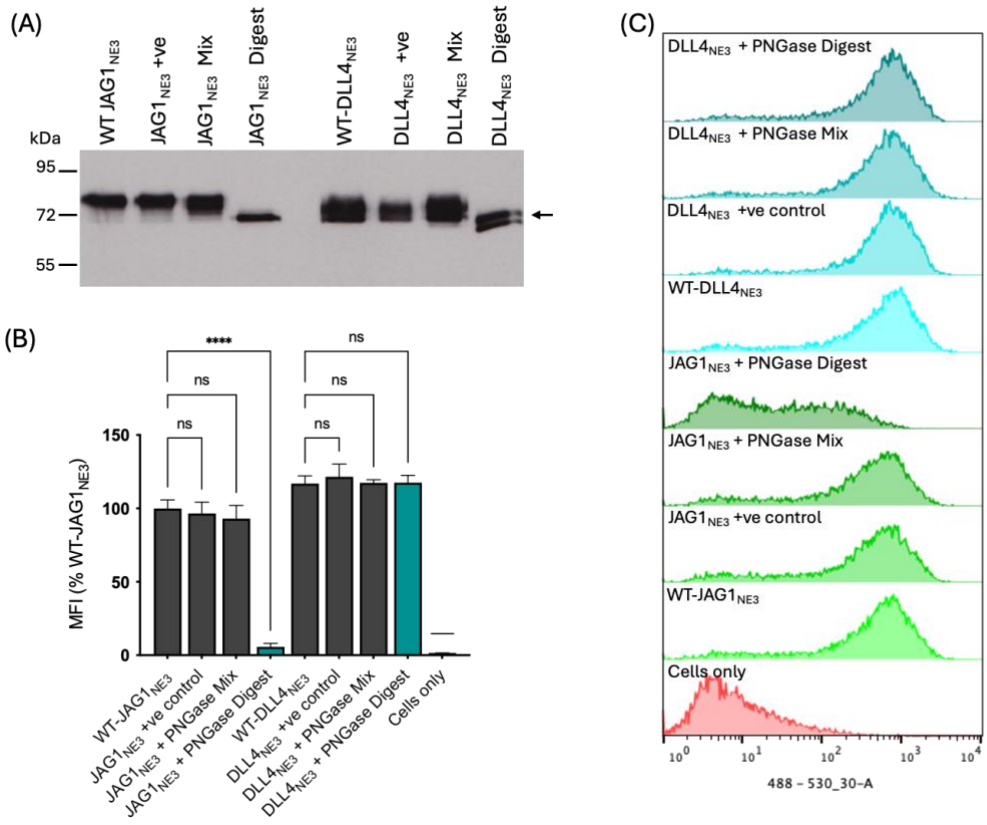


Figure 6-14. Notch activation by PNGase F digested JAG1$_{NE3\text{-}Fc\text{-}His}$ and DLL4$_{NE3\text{-}Fc\text{-}His}$. (A) WT-JAG1$_{NE3}$ and WT-DLL4$_{NE3}$, and their PNGase F digested samples were analysed by Western blot of a reducing SDS-PAGE. The PNGase F digestion positive controls ('+ve': proteins incubated under similar conditions without PNGase F) and an immediate mix of ligand proteins with PNGase F without incubation ('PNGase Mix') were analysed alongside. (B) Notch activation by the ligand samples in (A) was assessed by CHO-K1 hN1G4^{esn} reporter cells. YFP expression levels were quantified as MFI. Data, presented as mean ± SD, represent combined results of n≥3 independent experiments, in which 10,000 cells were measured in each reading. 'Cells only' was used as the background control. Statistical analysis was performed using ordinary one-way ANOVA followed by Šídák's multiple comparisons test. ns (not statistically significant), ****$P \leq 0.0001$. (C) A representative histogram showing the leftward shift of the PNGase F digested JAG1$_{NE3}$ sample compared with untreated WT-JAG1$_{NE3}$, suggesting decreased Notch activation. Note that the digested and undigested DLL4$_{NE3}$ samples have similar peaks, suggesting activity was unaffected.

Western blot analyses of PNGase F-digested $JAG1_{NE3}$ and $DLL4_{NE3}$ both showed a MW drop compared to the untreated WT samples, confirming efficient digestion (Figure 6-14A). Activity of the deglycosylated ligands was assessed using CHO-K1 $hN1G4^{esn}$ reporter cells. Whilst PNGase F digested $JAG1_{NE3}$ showed substantially reduced Notch activation that was ~10% of the untreated WT-$JAG1_{NE3}$, Notch activation by $DLL4_{NE3}$ was unaffected after PNGase F digestion (Figure 6-14B/C). The positive controls, either ligands directly mixed with PNGase F without incubation ('PNGase Mix'), or ligands incubated under similar conditions without the enzyme ('+ve control'), activated Notch similarly to the WT sample. These data collectively suggest that the reduced Notch activation associated with $N143Q_{NE3}$ is due to loss of the site-specific N-glycan on JAG1-C2 β5-6 loop, rather than any indirect effect caused by digestion conditions or localised protein misfolding in the secretory pathway during protein expression.

6.5.3 N-glycan structure requirements for activity

To investigate the importance of the N-glycan structure for activity, $JAG1_{NE3}$ purified from GnT-I^- HEK293S cells ($JAG1_{NE3}$/S), which had oligomannose N-glycans, was digested with PNGase F and assessed for activity alongside $JAG1_{NE3}$ purified from HEK293T ($JAG1_{NE3}$/T), which had complex N-glycans (see Section 6.3.4, Figure 6-10). PNGase F digested $JAG1_{NE3}$/S and $JAG1_{NE3}$/T samples were viewed on a reducing SDS-PAGE, which showed a MW drop compared to the untreated WT proteins, suggesting efficient digestion (Figure 6-15A). The untreated $JAG1_{NE3}$/S and $JAG1_{NE3}$/T activated Notch similarly, whereas their deglycosylated forms both led to significantly reduced Notch activation (Figure 6-15B/C). These data suggest that oligomannose N-glycans are sufficient to activate Notch.

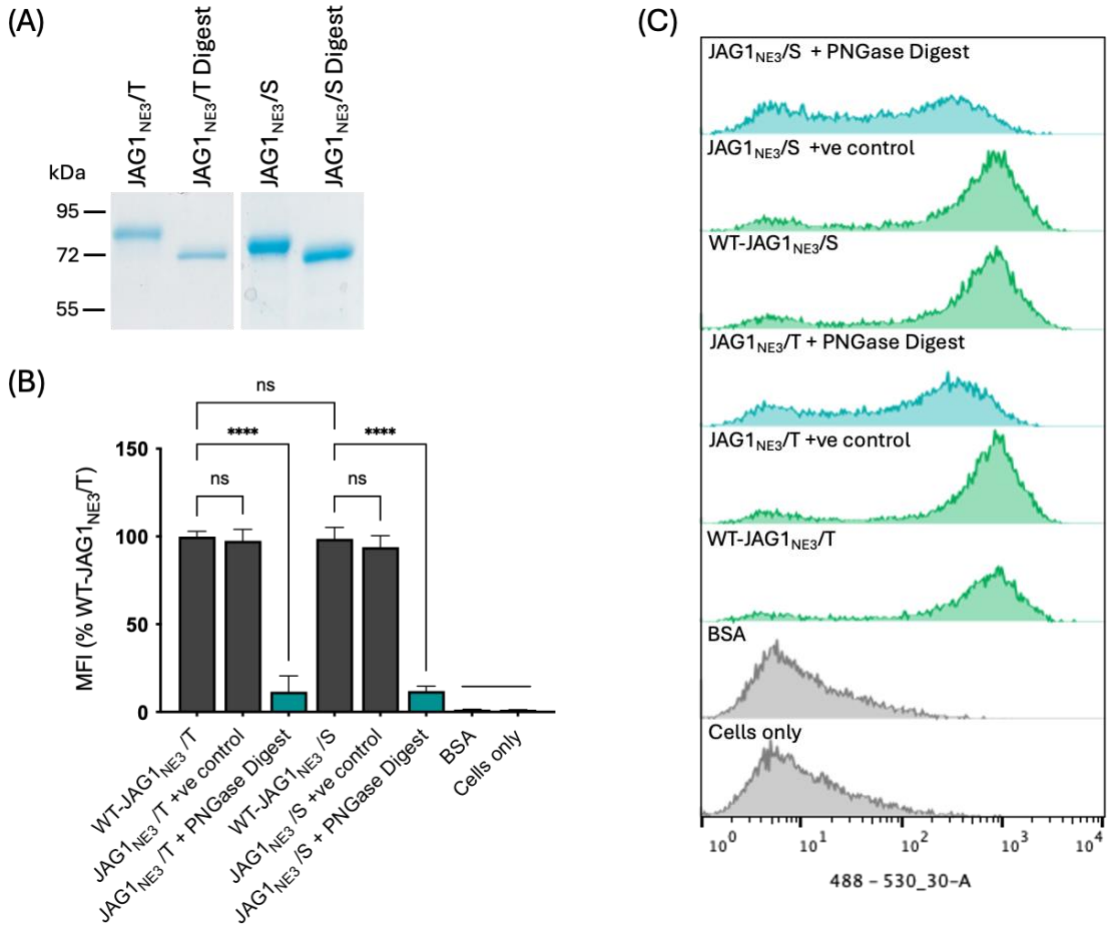


Figure 6-15. Notch activation by PNGase F digested JAG1$_{NE3}$ purified from HEK293T/S. (A) JAG1$_{NE3}$/S and JAG1$_{NE3}$/T and their PNGase F digested samples were viewed by reducing SDS-PAGE. (B) Notch activation by the samples in (A) was assessed by CHO-K1 hN1G4^{esn} reporter cells, with the PNGase F digestion positive controls (proteins incubated under similar conditions without PNGase F) analysed alongside. YFP expression levels were quantified as MFI. Data were presented as mean ± SD, which represented combined results of n≥3 independent experiments, in which 10,000 cells were measured in each reading. 'Cells only' was used as the background control. Statistical analysis was performed using ordinary one-way ANOVA followed by Šídák's multiple comparisons test. ns (not statistically significant), ****$P \leq 0.0001$. (C) A representative histogram showing the leftward shift of the PNGase F digested JAG1$_{NE3}$/S or JAG1$_{NE3}$/T samples compared with undigested samples, suggesting decreased Notch activation. Note that WT-JAG1$_{NE3}$/S has a similar peak as WT-JAG1$_{NE3}$/T, suggesting similar ability to activate Notch.

6.5.4 NOTCH1 activation by deglycosylated FL-J1

To confirm that the reduced activity observed for the deglycosylated JAG1$_{NE3}$ was recapitulated by a complete ectodomain of JAG1, FL-J1 was subjected to PNGase F

digestion and tested for Notch activation. Due to the results observed in Section 6.4.2 for epitope recognition, protein G-precoating was used to directionally immobilise the PNGase F digested FL-J1 via its Fc tag to expose the receptor-binding site (for control experiments see Appendix 8.6.3). Efficient N-glycan removal by PNGase F digestion was confirmed using SDS-PAGE, where the digested FL-J1 showed MW drop compared to the untreated FL-J1 (Figure 6-16A). Similar to the NE3 fragments tested in Section 6.5.2, deglycosylated FL-J1 showed significantly reduced ability to activate Notch with signal ~7% of the untreated FL-J1 or the positive control (Figure 6-16B/C). Despite being different lengths, both ligand constructs showed good Notch activation ability and similar outcomes after PNGase F digestion, suggesting importance of N-glycans for activity.

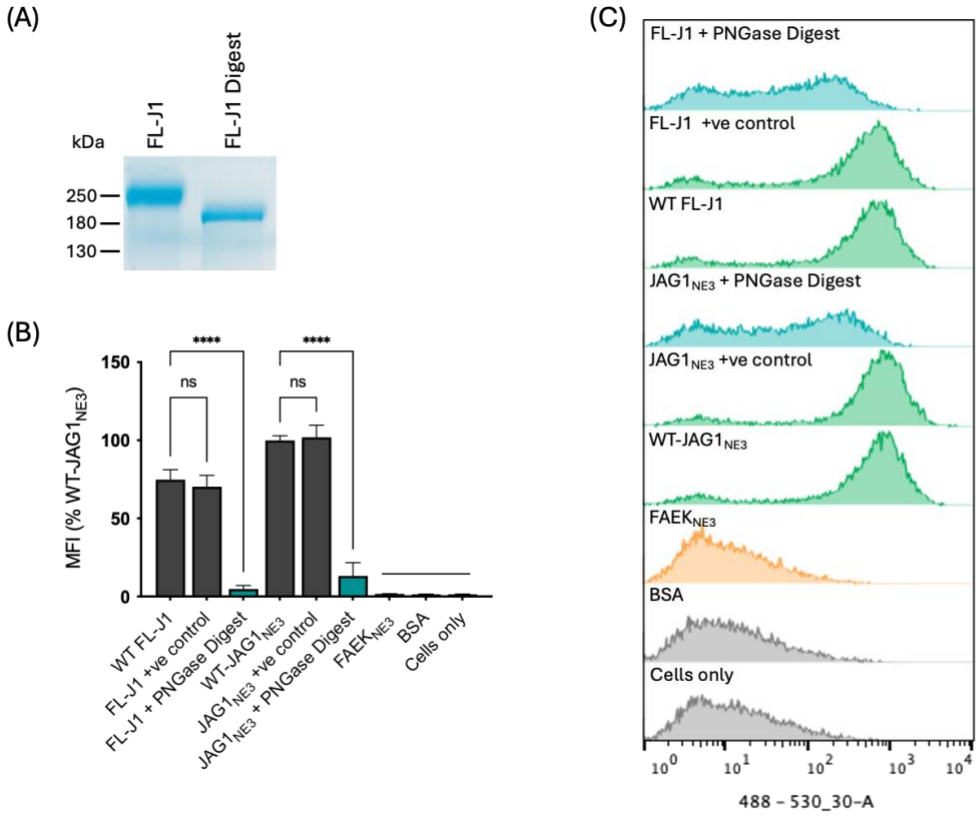


Figure 6-16. Notch activation by PNGase F digested $JAG1_{NE3}$ and FL-J1. (A) FL-J1 and its PNGase F digested sample were viewed by reducing SDS-PAGE. (B) Notch activation by $JAG1_{NE3}$ and FL-J1, their PNGase F digested samples, and the positive controls (proteins incubated under similar conditions without PNGase F) was assessed by CHO-K1 $hN1G4^{esn}$ reporter cells. YFP expression levels were quantified as MFI. Data were presented as mean ± SD, which represented combined results of n≥3 independent experiments, in which 10,000

cells were measured in each reading. 'Cells only' was used as the background control. Statistical analysis was performed using ordinary one-way ANOVA followed by Šídák's multiple comparisons test. ns (not statistically significant), ****$P \leq 0.0001$. (C) A representative histogram showing the leftward shift of the PNGase F digested $JAG1_{NE3}$ or FL-J1 samples compared with the untreated WT, suggesting decreased Notch activation.

6.6 Investigating lipid-binding properties of deglycosylated $JAG1_{NE3}$

To investigate the effect of N-glycan removal on the lipid-binding properties of JAG1, a FACS-based liposome aggregation assay (see Materials and Methods) was performed. $JAG1_{NE3}$ was immobilised to protein G fluorescent beads and then digested with PNGase F (Figure 6-17A). Samples incubated under similar conditions without adding PNGase F were used as positive controls. Fluorescent PC-rich liposomes (POPC:DOPS:PE-CF = 70:25:5) and SM-rich liposomes (POPC:SM:DOPS:PE-CF = 30:40:25:5), which acted as a simplified model of the plasma membrane outer leaflet, were freshly prepared by extrusion and analysed by DLS to check liposome size and homogeneity (see Appendix 8.6.4.1).

Ligand-coated beads were incubated with liposomes, followed by flow cytometry analysis to identify ligand-bead-liposome aggregates. The extent of liposome binding was quantified as a percentage of aggregation. For either PC-rich (Figure 6-17B) or SM-rich (Figure 6-17C) liposomes, both $JAG1_{NE3}$/T and $JAG1_{NE3}$/S showed significantly reduced liposome binding after PNGase F digestion, suggesting impaired lipid binding due to removal of N-glycans. The undigested positive control bound liposomes similarly to the untreated WT-$JAG1_{NE3}$ (Figure 6-17B), suggesting that lipid binding was unaffected by the incubation conditions.

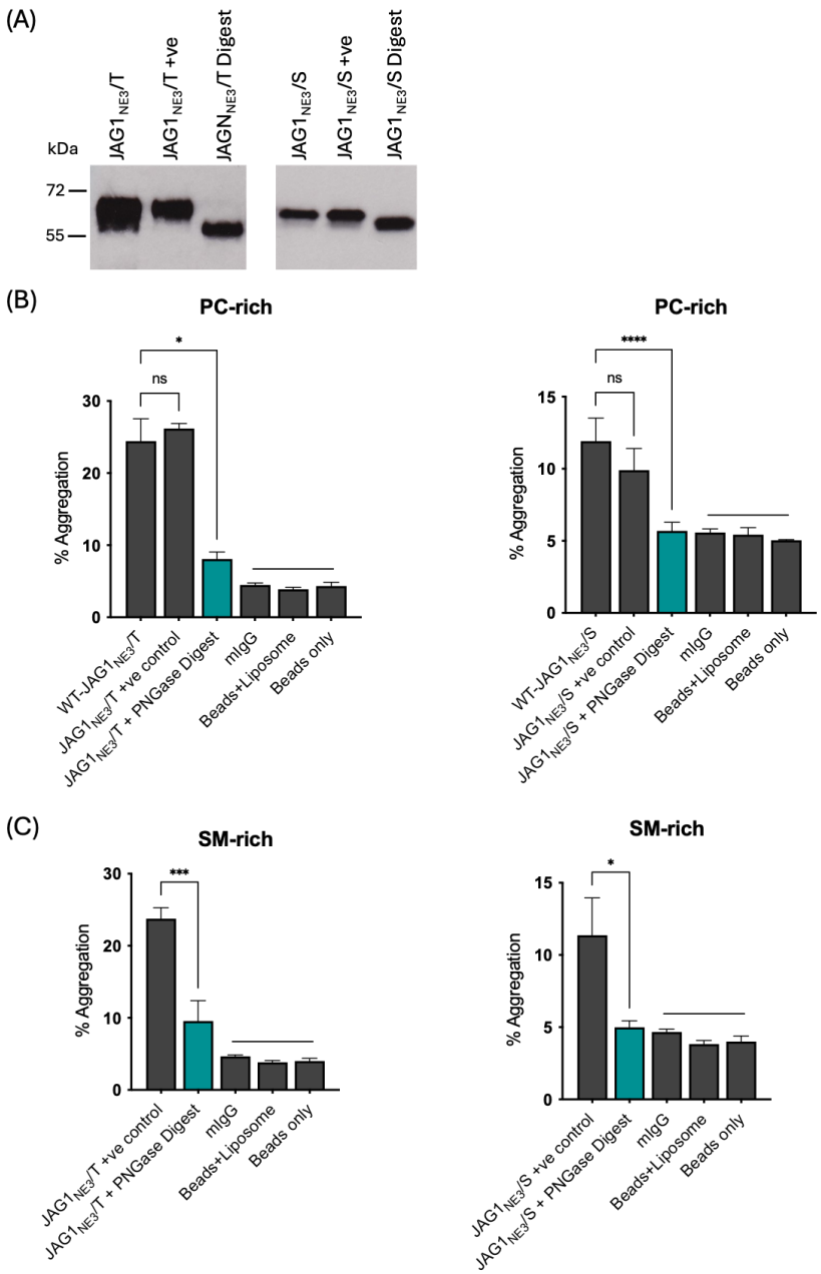


Figure 6-17. Liposome binding by PNGase F digested JAG1$_{NE3}$. (A) Western blot analysis of JAG1$_{NE3}$/T and JAG1$_{NE3}$/S digested on beads by PNGase F, viewed on a reducing gel using anti-His-HRP antibody. Binding of (B) PC-rich or (C) SM-rich liposomes to ligand-coated beads was assessed by flow cytometry and quantified as percentage aggregation. Data were presented as mean ± SD, which represented combined results of n≥3 independent experiments, in which 10,000 events were recorded in each reading. 'Beads only', 'beads + liposome' and mIgG were used as background controls. Statistical analysis was performed using (B) Kruskal-Wallis test followed by post hoc Dunn's multiple comparison test or (C) Welch's t-test. ns (not statistically significant) P>0.05, *P ≤ 0.05, **P ≤ 0.01, ***P ≤ 0.001, ****P ≤ 0.0001. See Appendix 8.6.4.2 for sets of representative FACS raw data.

6.7 Conclusion

In this chapter, the functional importance of a Jagged-family-specific N-glycan on the β5-6 loop of C2 domain was studied (Table 6-2). An N-glycan site was identified in a study of JAG1 COSMIC variants, in which the variant T145N showed dramatically lower Notch activation ability in both HEK293 mN1/2 split-luciferase and CHO-K1 hN1G4^{esn} reporter cells (Meng et al., 2022). Another N-glycan variant N143A, which impaired the same 'NXT' N-glycosylation consensus, resulted in a similar loss-of-function effect. On the other hand, N217A, which impaired a DSL domain N-glycosylation site, showed similar Notch activation and lipid-binding property to WT-JAG1$_{NE3}$. These data suggested that the site-specific N-glycan on C2 β5-6 loop was important for JAG1-mediated Notch activation and ligand-lipid interactions.

In this project, another N-glycan variant N143Q$_{NE3}$ was made, which impaired the C2 N-glycosylation site by substituting N143 with a chemically similar amino acid, and a similar reduction in Notch activation was observed, suggesting that the loss-of-function effect observed in all three C2 N-glycan variants was a result of loss of the C2 β5-6 loop N-glycan (Table 6-2). Moreover, N143Q$_{NE3}$ was secreted at slightly lower levels than WT-JAG1$_{NE3}$ (Figure 6-5), suggesting a minor effect on folding, although majority of the protein was secreted. In particular, an additional SEC peak was observed compared with WT-JAG1$_{NE3}$ (Figure 6-6B), which corresponds to higher MW materials that were also recognised by anti-His antibody (Appendix Figure 8-2A), suggesting that in the absence of N143-glycan, the ligand may be more prone to aggregation. The N143Q$_{NE3}$ fraction which was eluted similarly to WT-JAG1$_{NE3}$ was tested in the activity assay. These observations suggested a protective role of N-glycosylation against protein aggregation, which is a commonly known mechanism in eukaryotic systems (Duran-Romaña et al., 2024).

To further confirm that the reduced activity was due to loss of N-glycan, PNGase F digestion was performed to remove N-linked sugars from the folded active WT-JAG1$_{NE3}$. After digestion, a similar decrease in Notch activation was observed for both the shorter (JAG1$_{NE3}$) and longer (FL-J1) fragments (Table 6-2), suggesting that direct removal of N-glycans also impaired ligand activity. Furthermore, FL-J1 recapitulated the results observed for JAG1$_{NE3}$, suggesting that the shorter NE3 fragment was able to represent the activity of the complete ligand ectodomain. However, considering the JAG1 constructs tested in this study were all purified Fc-dimers, the results could be further validated using a coculture assay, which allowed the ligand to be presented in its physiological form and engage the mechanical components when *trans*-activating Notch.

Ligand	Presence of C2 β5-6 loop N-glycan	Epitope recognition	Notch activation	Liposome binding
WT-JAG1$_{NE3}$/T	✔	✔	100%	100%
T145N$_{NE3}$*	✕	n/a	low	low
N143A$_{NE3}$*	✕	n/a	low	low
N143Q$_{NE3}$	✕	✔	low	n/a
N217A$_{NE3}$*	✔	n/a	no effect	no effect
PNGase F digested JAG1$_{NE3}$/T	✕	✔	low	low
WT-JAG1$_{NE3}$/S	✔	✔	no effect	no effect
PNGase F digested JAG1$_{NE3}$/S	✕	✔	low	low
FL-J1	✔	✔	no effect	n/a
PNGase F digested FL-J1	✕	✔	low	n/a
WT-DLL4$_{NE3}$	✕		100%	100%
PNGase F digested DLL4$_{NE3}$	✕		no effect	n/a

Table 6-2. Summary of effects of the C2 N-glycan. The C2 N-glycan variants (T145N$_{NE3}$, N143A$_{NE3}$, N143Q$_{NE3}$) and PNGase F digested JAG1$_{NE3}$ and FL-J1 lose the N-glycan on the C2 β5-6 loop. Ligands without the C2 N-glycan showed unaffected epitope recognition as a measure of native fold, but loss-of-function effects on Notch activation and lipid binding. N217A, which loses the DSL N-glycan, and WT-JAG1$_{NE3}$/S, which has oligomannose in place of complex N-glycan structure, both showed unaffected Notch activation and lipid-binding property. Notch activation by DLL4$_{NE3}$, which does not have the conserved β5-6 loop N-glycan, was unaffected after PNGase F digestion. Some constructs were not tested in

particular assays, thus are marked as 'n/a' (data not available). Note that the variants marked with an asterisk were made and tested by Dr Yao Meng, and the data was published in (Meng et al., 2022).

The functional importance of the N-glycan structure was investigated by using GnT-I⁻ HEK293S cells (Reeves et al., 2002) to express $JAG1_{NE3}$ that was modified with N-linked oligomannose ($JAG1_{NE3}$/S) instead of the complex N-glycan presented in HEK293T-derived JAG1 ($JAG1_{NE3}$/T). $JAG1_{NE3}$/S showed efficient protein secretion just like $JAG1_{NE3}$/T. The N-glycan on N143 and N217 were assessed by glycoproteomic analysis, which confirmed that $JAG1_{NE3}$/S was modified by high-mannose N-glycan only, whereas $JAG1_{NE3}$/T had more complex multi-antennary N-glycan structures. Despite the differences in the N-glycan structures, both $JAG1_{NE3}$/S and $JAG1_{NE3}$/T showed similar Notch activation ability (Table 6-2), suggesting that subtle changes in the N-glycan structure had no significant functional effect. Furthermore, WT-$DLL4_{NE3}$, which lacks the N-glycosylation consensus in its C2 β5-6 loop, showed normal Notch activation ability after PNGase F digestion (Table 6-2). The differences between JAG1 and DLL4 highlighted a potential ligand-specific regulatory mechanism mediated by the site-specific β5-6 loop N-glycan.

Considering the importance of the Jagged1-mediated Notch signalling in regulating the differentiation, proliferation, and cell survival of vascular smooth muscle cells (VSMCs) (High et al., 2007, 2008), the C2 N-glycan variants N143A and T145N were tested in a smooth muscle differentiation assay using primary VSMCs (experiments performed by Sami Sanlidag from Professor Cecilia Sahlgren's lab, data published in (Meng et al., 2022)). The production level of α-smooth muscle actin (α-SMA), a Jagged1/Notch signalling downstream target (Noseda et al., 2006), was found to be downregulated in VSMCs plated on $N143A_{NE3}$ or $T145N_{NE3}$ compared to cells plated on WT-$JAG1_{NE3}$, recapitulating the loss-of-function effect in a physiologically relevant context.

Given the knowledge of the importance of C2 apical loops in lipid binding (Y. Hirano et al., 2019), and previous studies which revealed the C2-lipid interactions of canonical Notch ligands (Chillakuri et al., 2013; Suckling et al., 2017), the N-glycan variants were studied for their lipid-binding properties. N143A and T145N both showed impaired binding to PC- or SM- rich liposomes, whereas N217A bound indistinguishably to liposomes as the WT (Table 6-2). Likewise, WT-$JAG1_{NE3}$ digested by PNGase F also showed significantly reduced binding to PC- or SM- rich liposomes, suggesting an important role of the N143-glycan in Notch activation that is mediated through lipid-binding.

Further molecular insights into the regulatory mechanism were provided by MD simulations of the JAG1-C2 domain interacting with a model lipid bilayer (performed by Dr Andreas Larsen from the University of Copenhagen, data published in (Meng et al., 2022)). A large variety of binding modes were predicted from MD simulations, suggesting that the JAG1-C2 domain alone does not dictate the ligand-membrane binding orientation, but the presence of an N-glycan on loop β5-6 may facilitate its membrane binding. Whilst a conserved N153-glycan at a similar position in JAG2-C2 was found to stabilise its β5-6 loop by packing against its Trp-151 side chain via an α-(1,6)-linked fucose (Suckling et al., 2017), the C2 apical loops in $JAG1_{NE3}$ crystal structures lacking the N143-glycan were shown to be mobile, as suggested by the different coordination shells within independent crystallography molecules (Chillakuri et al., 2013). Based on these data, it was proposed that the β5-6 loop N-glycan in Jagged family ligands may aid Ca^{2+} coordination of the C2 domain by interacting with the base of the β5-6 loop to reduce its flexibility, thereby promoting Ca^{2+}-mediated lipid binding (Y. Hirano et al., 2019; Meng et al., 2022).

Another possible molecular mechanism, based on the C2 N-glycan structure modelled from the *Drosophila* Delta crystal structure (PDB 7ALK, (Martins et al., 2021)), proposed that the large complex N-glycan may sterically restrain the ligand-membrane interactions (Meng et al., 2022). However, the $JAG1_{NE3}$/S activity results suggested that a simpler oligomannose N-glycan structure was sufficient for activity, as it can activate Notch similarly to $JAG1_{NE3}$/T. Hence, the oligomannose N-glycan may also provide steric restrains for ligand-membrane interactions just like the complex N-glycans, or this proposed molecular mechanism may not be held.

In summary, results from analyses of $N143Q_{NE3}$, $JAG1_{NE3}$/S, and PNGase F digested $JAG1_{NE3}$/T and FL-J1 suggest a novel functional role of the conserved C2 β5-6 loop N-glycan in facilitating JAG1-mediated Notch activation. These data, in combination with previous analyses of $N143A_{NE3}$ and $T145N_{NE3}$ variants, are consistent with a requirement of N-glycan for ligand-lipid binding in molecular assays and optimal Notch activation in reporter cell lines, suggesting a Jagged-specific regulatory mechanism mediated through ligand-membrane interactions.

Chapter 7: Discussion and future work

7.1 Objective of the thesis

The C2 domain of canonical Notch ligands was thought to contain a putative lipid-binding site, modulating ligand-induced Notch activation via interactions with the lipid membrane (Chillakuri et al., 2013; Suckling et al., 2017). The C2 apical loops show notable sequence variability among Notch ligands (see Section 1.5.4), suggesting ligand-specific membrane binding properties. The aim of this project was to investigate the functional importance of the C2 putative lipid-binding loops in DLL4, using missense mutations identified from cancer databases and engineered C2 loop deletions. The effects of DLL4 variants on Notch activation and receptor- or lipid-binding were tested by various biochemical and cell-based assays, and the physiological relevance of the functional effects observed was assessed in primary HUVECs. Molecular dynamics simulations were applied to further analyse the C2-membrane interactions.

In addition, the functional importance of a Jagged-family-specific N-glycan on loop β5-6 was investigated, using mutagenesis or enzymatic digestion to generate JAG1 N-glycan variants. The Notch activation, receptor- and lipid-binding properties of JAG1 variants were assessed using similar approaches. The comparative results from DLL4 and JAG1 studies raise the possibility of ligand-specific C2-mediated regulatory mechanisms in Notch signalling.

7.2 Expression and secretion of DLL4 variants

- **$DLL4_{NE3}$ protein folding and trafficking could be affected by the structure and length of the C2-loops**

Out of 14 missense mutations identified from cancer databases, 3 mutations (G47W, G98R, and A124P) led to intracellular retention and were non-secretory (Figure 3-3). Instead of affecting the hydrophobic core of C2 domain, these missense mutations all

mapped to the apical loop region of DLL4-C2 (G47W: loop β1-2; G98R: loop β3-4, A124P: loop β5-6), yet still resulted in defective extracellular secretion, suggesting that the apical loops may play a role in protein folding. Since all three variants substituted a small non-polar amino acid (Gly or Ala) with a bulkier residue, they are likely to have altered C2-loop structure, leading to protein misfolding and ER retention. In addition, the double mutants, E40K/D128N and R41S/P131T, containing one missense mutation on each of the β1-2 and β5-6 loops, showed significantly lower secretion than the respective single substitution variants (Figure 3-4). These results suggest that mutations on both loops may have a synergistic effect on protein folding, probably due to interactions between these proximally located loops (Figure 1-19). Moreover, the three protein-engineered C2-loop-shortening variants all showed significantly lower presence in the extracellular medium than WT-DLL4$_{NE3}$ (Figure 3-6), further suggesting the importance of C2 apical loops in protein folding and trafficking.

Whilst secretion test is a common approach to probe protein folding and trafficking in many studies (R. Schneider et al., 2010; Whiteman & Handford, 2003), it would be helpful to analyse the glycosylation pattern of these DLL4 variants, for which a lack of complex glycosylation but presence of core glycosylation will suggest retention in the ER. The trafficking profile can be further confirmed using coimmunoprecipitation to show if the retained fragments are associated with ER chaperones.

- **FL-DLL4 C2-loop-shortening variants showed reduced surface expression**

While expressed as complete FL-ligands, E40K and R41S both showed similar surface expression levels to FL-WT-DLL4, whereas the three C2-loop-shortening variants all showed reduced surface expression (Figure 3-12), consistent with secretion test results obtained using DLL4$_{NE3}$ fragments. Interestingly, unlike the DLL4 β1-2 loop-shortening variant, a C2-loop-shortening mutant of *Drosophila* Delta, generated by deleting 5 amino acids in its β1-2 loop, showed a similar surface expression level to WT-Delta and normal

trafficking (Martins et al., 2021). Since the β1-2 loop of DLL4 is significantly shorter than that of *Drosophila* Delta (Figure 1-20), further shortening of the DLL4 β1-2 loop is more likely to cause protein misfolding and intracellular retention.

- **The majority of tumour-associated missense mutations in C2 apical loops did not affect ligand secretion or surface expression**

Results from secretion and surface expression tests collectively showed that the NE3 fragments recapitulated the expression pattern of FL-ligands. However, some FL-DLL4 variants (R41S and C2-loop-shortening variants) exhibited better surface expression than their secretion test results, probably because FL-DLL4 is anchored to the lipid membrane by its transmembrane region and may be more stabilised in its native form, whereas the dimerised NE3 fragments may be more susceptible to local misfolding and therefore prone to aggregation. Most of the tumour-associated DLL4 missense mutations mapping to the C2 apical loops did not affect protein trafficking or secretion. Similar results were observed for $JAG1_{NE3}$-C2 variants, in which the majority of the loop variants, except for G47R in β1-2 loop, exhibited normal extracellular secretion (Meng et al., 2022).

7.3 The effects of DLL4 cancer database variants on Notch activation

- **Tumour-associated missense mutations in C2 apical loops affected the signalling strength of $DLL4_{NE3}$ to *trans*-activate mN1 and mN2 reporter cells**

HEK293 mN1- and mN2-NLuc/CLuc-RBPJ reporter cells allow measurement of Notch activation in live cells and in real time, by directly detecting the amount of active NICD associated with RBPJ transcription factor (Ilagan et al., 2011). Thus, these reporter cells are well suited for quantitatively analysing the activity changes caused by ligand mutations. A narrow range of functional effects was observed for $DLL4_{NE3}$ cancer database variants, from a small decrease in activity to slightly enhanced Notch activation (Table 7-1). The activity effects observed were consistent in mN1 and mN2 reporter cells,

both showed that E40K and D128N downregulated Notch activation, whereas R41S and R100G upregulated Notch activation (Figure 3-9), suggesting that these missense mutations had similar functional impact on both Notch paralogues.

Interestingly, compared to the activities of the single substitution variants (~20% decrease), the $DLL4_{NE3}$-E40K/D128N double mutant resulted in more significantly reduced Notch activation (~60% decrease) in both mN1 and mN2 reporter cells (Figure 3-9), albeit having similar Notch receptor binding affinity to WT-$DLL4_{NE3}$ (Figure 5-5). Structural data showed that β1-2 and β5-6 loops are proximal to each other in ligand C2-domain (Figure 1-19) and comparison of independently crystalised WT-$JAG1_{NE3}$ structures showed that these two apical loops are highly mobile (Chillakuri et al., 2013). Collectively, these results suggest that point mutations on β1-2 and β5-6 loops may interact with each other to additively affect ligand activity, probably by altering the C2-loop structure and/or electrostatic profile. Similar synergistic effect was observed in perforin-C2, where its CBL1 and CBL3 underwent Ca^{2+}-dependent conformational rearrangement to together form a lipid-binding groove (Traore et al., 2013; Yagi et al., 2015) (see Section 1.5.2 for more details).

- **Notch-binding-deficient variant F195A/Y216A impaired Notch activation**

The Notch-binding-deficient variant, F195A/Y216A, completely abolished $DLL4_{NE3}$-induced Notch1/2 activation, resulting in ~20% WT-$DLL4_{NE3}$ activity similar to the 'cells only' background control (Figure 3-9, Table 7-1). Similar DSL domain missense mutations impairing ligand-receptor interactions were identified in earlier studies using sequence alignment, structural data, and *Drosophila*-based functional analyses (Cordle et al., 2008; Luca et al., 2015). Consistent with activation assay results, defective binding of F195A/Y216A$_{NE3}$ to purified $NOTCH1_{E11-13}$, $NOTCH1_{E7-13}$, $NOTCH2_{E11-13}$, and cell-surface-expressing FL-mNotch1 was observed (Figure 5-5, Figure 5-7), establishing a correlation between defective Notch binding and deficit of Notch activation.

- **WT-DLL4$_{NE3}$ *trans*-activated Notch1 more strongly than WT-JAG1$_{NE3}$**

WT-JAG1$_{NE3}$, which is generally agreed to have a lower Notch1 binding affinity than WT-DLL4$_{NE3}$ (see Section 1.3.3.1), was shown to result in lower Notch1 activation than WT-DLL4$_{NE3}$ in activity assays (Table 7-1, Appendix 8.7.1). Although it is difficult to measure the absolute amount of ligand proteins immobilised on the TC-plate, ELISA-based control experiments suggested comparable WT-DLL4$_{NE3}$ and WT-JAG1$_{NE3}$ immobilisation (Figure 3-10A), allowing comparison of the relative activities of these ligands tested under similar conditions (Figure 3-10B). Our observations are consistent with other published work, which also showed that Dll4 activated Notch1 more strongly than Jag1 whilst activated Notch2 at levels comparable to that of Jag1 (Kakuda et al., 2020; Kuintzle et al., 2023).

- **Plated DLL4$_{NE3}$ variants activated Notch1 similarly to cell-expressed FL-DLL4 variants**

The coculture assay results generally have smaller error bars compared to the protein-based activation assay, likely because the reporter cells in the coculture were less disturbed in the final mixing step (see Materials and Methods), making the coculture assay more advantageous to discriminate small differences in activity. The β1-2 loop variants E40K and R41S, both showing WT-level cell surface expression when expressed as FL-ligands (Table 7-1), resulted in either statistically significant decrease (E40K) or increase (R41S) in Notch activation compared to FL-WT-DLL4. FL-F195A/Y216A, which also had a similar surface expression to FL-WT-DLL4, resulted in significantly lower Notch activation as expected for a Notch-binding-deficient variant. The consistency between the protein-based and coculture assays suggests that the NE3 fragments of DLL4 well represented the activity of the complete FL-ligand, despite their different presentation formats, either in plate-bound or cellular form.

Mutation	Position in C2 domain	Split-luciferase reporter assay		HUVECs RT-qPCR assay		NOTCH1 binding	Liposome binding	C2-membrane binding orientations predicted by MD simulations
		HEK293-mN1	HEK293-mN2	*EFNB2*	*DLL4*			
E40K	β1-2	↓	↓↓	↓↓	↓↓	no effect	no effect	binding modes were altered
R41S	β1-2	↑	↑	↑	↑	no effect	n/a	binding modes were altered
P49S	β1-2	no effect	n/a	no effect	no effect	no effect	no effect	n/a
V91L	β3-4	↓	n/a	no effect	no effect	no effect	n/a	n/a
S96R	β3-4	↓	n/a	no effect	no effect	no effect	n/a	n/a
R100G	β3-4	↑	↑	↑↑	↑↑	no effect	n/a	n/a
D127E	β5-6	no effect	n/a	↓	↓	no effect	no effect	n/a
D128N	β5-6	↓	↓	↓↓	↓↓	no effect	no effect	n/a
P131T	β5-6	no effect	no effect	↑	↑	no effect	no effect	n/a
P135A	β5-6	no effect	n/a	no effect	no effect	no effect	no effect	n/a
L164F	β7-8	no effect	n/a	no effect	no effect	no effect	n/a	n/a
E40K/D128N	β1-2&β5-6	↓↓↓	↓↓↓↓	n/a	n/a	no effect	n/a	n/a
F195A/Y216A		↓↓↓↓	↓↓↓↓	↓↓↓↓	↓↓↓↓	↓↓↓↓↓	no effect	n/a
WT-JAG1		↓↓	↓	↓↓↓	↓↓↓	↓↓	↑ for SM-rich liposomes	a distinct density map of orientation vs distance of C2 away from the membrane compared with that of WT-DLL4

Table 7-1. Summary of the effects for DLL4 cancer database missense mutations. Table summarises results of activity (Chapter 3 & 4) and binding assays (Chapter 5) performed using purified ligand NE3 proteins, as well as MD analyses simulated using the ligand C2 domain. The activity or binding of WT-DLL4 is normalised to 100%. '↑/↓': increase or decrease within ±20% of WT-DLL4 activity or binding; '↑↑/↓↓': 20%~40% increase or decrease; '↓↓↓': 40%~60% decrease; '↓↓↓↓': 60%~80% decrease; '↓↓↓↓↓': >80% decrease; 'no effect': no statistically significant difference compared to WT-DLL4. Some variants were not tested in these experiments, thus are marked as 'n/a' (data not available).

- **Cell-expressed FL-F195A/Y216A bound to and activated Notch1 more strongly than plated F195A/Y216A$_{NE3}$**

Compared to F195A/Y216A$_{NE3}$, which resulted in 20% of WT-DLL4$_{NE3}$ activity (1.2-fold of the background control), FL-F195A/Y216A resulted in 46% of FL-WT-DLL4 activity (1.4-fold of the background control) (Figure 3-9, Figure 3-13). Recent studies generally agreed that the plate-coated recombinant protein form of Notch ligands (Jag1, Delta^{MAX}, etc.) activated Notch1 more efficiently than their cellular formats, likely due to the potential differences in their tertiary structures and greater accessibility of the receptor-binding sites in the recombinant proteins (Gonzalez-Perez et al., 2023; Kuintzle et al., 2023). Therefore, the higher activity observed for FL-F195A/Y216A was less likely a result of its presentation format but may suggest potential sites of interactions between FL-DLL4 and FL-Notch1 apart from the C2-DSL domains.

In support of the activity results, cell-expressed FL-F195A/Y216A also appeared to bind NOTCH1$_{E7-13}$ more strongly than plate-coated F195A/Y216A$_{NE3}$ (Figure 5-7, Figure 5-9, Figure 8-6). Whilst F195A/Y216A$_{NE3}$ showed completely defective Notch-binding (1-fold of background control) in the plate-based ligand-coated binding assay, FL-F195A/Y216A showed clearly increased NOTCH1$_{E7-13}$ binding compared with the background control in the cell-based receptor binding assay. These binding differences observed could be a result of the different density or presentation formats of the ligand, the natural endocytic mechanism during receptor binding, the potential clustering behaviours of the cell-expressed ligand, or may suggest additional receptor binding sites on FL-DLL4 apart from the C2-DSL domains, as observed in the Jag1-Notch1 full-ectodomain complex (Zeronian et al., 2021) (see Section 1.3.3.3).

- **HUVECs-based RT-qPCR assay largely recapitulated functional results obtained from split-luciferase reporter cell lines**

A HUVECs-based RT-qPCR assay using *EFNB2* and *DLL4* as Notch target genes largely recapitulated the results obtained from the split-luciferase reporter systems (Table 7-1). *EFNB2*, the DLL4-selective marker in ECs (Iso et al., 2006), as well as *DLL4*, the target of DLL4 feed-forward signalling (Caolo et al., 2010), were both significantly upregulated in HUVECs plated on WT-DLL4$_{NE3}$ but not the Notch-binding-deficient F195A/Y216A$_{NE3}$ or the BSA negative control (Figure 4-4, Figure 4-7). Although WT-JAG1$_{NE3}$ also induced *EFNB2* and *DLL4* expression above the baseline, it appeared to be a less potent inducer than WT-DLL4$_{NE3}$ in this assay (Table 7-1).

In agreement with results obtained from the split-luciferase system, the RT-qPCR assay demonstrated a reduction in Notch activation by E40K and D128N, and enhanced Notch activation by R41S and R100G (Table 7-1). On the other hand, V91L and S96R, which showed slightly decreased activity in HEK293-mN1 cells, showed no effect in HUVECs, whilst D127E showed no effect in HEK293-mN1 cells but slightly decreased activity in HUVECs (Table 7-1). Although D127E showed no statistically significant difference compared with WT-DLL4 in HEK293-mN1 reporter cells, its mean activity was ~90% of WT-DLL4 activity (Figure 3-9A), suggesting a decreasing trend similar to that observed in HUVECs. Likewise, *EFNB2* expression levels in HUVECs showed that V91L and S96R resulted in 98% and 88% of WT-DLL4 activity respectively (Figure 4-7A), which was not statistically significant but did not contradict the decreasing trends observed in HEK293-mN1 cells. Therefore, despite these differences observed in the two systems, the activity results obtained from HEK293 reporter cells and HUEVCs largely agree with each other.

- **Cell-type dependent differences could modulate the functional effects of DLL4 variants in different systems**

We cannot exclude the possibility that the activity differences observed in the two systems reflected cell-type-dependent differences. Whilst HEK293 reporter cells were

engineered to express either mN1 or mN2, HUVECs were known to express all four human Notch paralogues (NOTCH1-4) (Patel et al., 2005). The PTMs types and levels also vary between cell types, which could affect DLL4-Notch interactions. For instance, RNA-sequencing data from NCBI Gene Expression Omnibus (GEO) show that the three human Fringe paralogues (LFNG, RFNG, MFNG) are differently expressed in HEK293 and HUVECs, with *LFNG* and *MFNG* having little expression in untreated HEK293 cells but much higher expression in untreated HUVECs (Table 7-2). Modifications by MFng or LFng typically promote *trans*-activation by the Delta-like family ligands but have an opposite effect on the Serrate/Jagged family ligands, thereby potentiating Delta/Delta-like induced Notch signalling (Benedito et al., 2009; Kuintzle et al., 2023; Panin et al., 1997). This may explain why WT-JAG1$_{NE3}$ resulted in ~60% lower activation level than WT-DLL4$_{NE3}$ in the HUVECs-based RT-qPCR assay, but only ~25% lower activation level than WT-DLL4$_{NE3}$ in HEK293-mN1 reporter assays (Figure 3-9, Figure 4-7). Considering the diverse modulatory effects of Fringe modifications on different Notch receptor-ligand pairs (see Section 1.4.1.1 for details), the specific Notch receptor(s) with different PTMs presented in each cell type may interact differently with the DLL4 variants, leading to variations in activation levels in different assays.

GEO Series ID	Cell type & treatment	Expression level (in FPKM or RPKM)		
		LFNG	***MFNG***	***RFNG***
GSE260954	HUVEC & PBS	2.27623	189.282	17.1733
	HUVEC & PBS	1.75903	202.035	16.9305
	HUVEC & PBS	9.34049	137.089	18.9181
GSE146991	HEK293 & Neurobasal medium	0.69367	0.19482	11.4629
	HEK293 & Neurobasal medium	0.49908	0.05514	12.2944

Table 7-2. Different expression levels of Fringe enzymes in HEK293 cells and HUVECs. High-throughput functional genomic data are available on the GEO public repository. Table summarises fringe enzymes' expression data obtained from two recent RNA sequencing analyses: GSE260954 (Kosaka et al., 2024), and GSE146991 (Genestine et al., 2021). The relative expression of each transcript is normalised as Reads/Fragments Per Kilobase of transcript per Million mapped reads (RPKM or FPKM).

The plasma membrane compositions may also vary vastly between different cell types, thereby affecting the ligand-receptor-membrane ternary complex formation and signalling outcome. For instance, as a CD46-positive cell type, HUVECs expressed the complement regulator protein CD46 which acts as a non-canonical JAG1 receptor (Collard et al., 1997, 1999; Le Friec et al., 2012). Cell-type-dependent expression of such non-canonical ligand binding proteins on the plasma membrane may affect ligand-Notch interactions, such as by competing with Notch for ligand binding (e.g., CD46) or facilitating ligand recruitment to Notch receptors.

Additionally, although our current knowledge lacks detailed information of the plasma membrane lipid compositions in different cell types, Notch ligands were shown to have binding preferences for different lipid types (Figure 5-10) (Suckling et al., 2017), suggesting that cell-type dependent differences in membrane lipids could modulate the signalling outcome induced by the same receptor-ligand pair. HEK293 cells, initially derived from a fetal kidney, were generally found to exhibit epithelial morphology, though the exact cell type from which HEK293 originated remained uncertain (Graham et al., 1977; Inada et al., 2016; Shaw et al., 2002). However, unlike epithelial cells which exhibit apical-basolateral polarity with asymmetric distribution of lipids and SM clustering in the microvilli (Abe et al., 2012; Ikenouchi, 2018; Ikenouchi et al., 2013; Koichi et al., 1974), HEK293 cells are unable to polarise (Van Beest et al., 2006). A recent lipidomic analysis showed that, compared with mouse myeloma SP2/0 and CHO cell lines, HEK293 cells contained significantly higher levels of lysophosphatidylethanolamine (LPE) and lysophosphatidylcholine (LPC), both are minor constituents of cell membranes (Y. Zhang et al., 2017). Apart from PC and phosphatidylethanolamine (PE) as the major lipid components, the presence of PI, PS, PG, PA, and SM as the lower-level contents were also shown in HEK293 cells, though the exact proportion on the plasma membrane outer leaflet were unknown.

Detailed analyses of the lipid composition of human endothelial cells have also been reported, showing that most phospholipids were within the normal biological ranges expected, except relatively high choline plasmalogen and LPE contents (Murphy et al., 1992). In HUVECs, PC and PE also appeared to be the two major components of the cell membrane, but serum deprivation resulted in higher SM contents and lower proportion of PC (Cansell et al., 1997; Héliès-Toussaint et al., 2006). Interestingly, PS, which is mainly distributed in the inner leaflet of the plasma membrane (Connor et al., 1992), appeared to be externalised to the outer leaflet of the endothelial cell membrane in choroidal neovascularisation or solid tumours (T. Li et al., 2015; Ran & Thorpe, 2002), suggesting that the lipid composition of the same cell type may vary depending on other physiological or disease-related factors.

Overall, in both systems, amino acid substitutions in the C2 apical loops (β1-2, β3-4, and β5-6), except loop β7-8, showed some functional effects, indicating that these loops are all important for Notch signal generation. The agreement between different systems gives more reliability in results, showing that E40K, R41S, R100G, and D128N are most likely to cause increased (R41S, R100G) or decreased (E40K, D128N) Notch activation in different cellular contexts.

7.4 The effects of DLL4 C2-loop-shortening variants on Notch activation

Due to the challenge of generating purified DLL4 C2-loop-shortening variant proteins (see Section 7.2), a coculture assay was used to study their functional effects. A significant reduction in Notch activation was observed for all three C2-loop-shortening variants (β1-2 ERGV-deleted, β5-6 DDLR-deleted, β5-6 RPEA deleted), as expected based on their significantly reduced surface expression levels (Figure 3-12, Figure 3-13).

Surprisingly, whilst β1-2 ERGV-deleted variant showed significantly lower cell surface expression compared with the two β5-6 loop-shortening variants, all three variants resulted in similar levels of Notch activation that were ~70% of FL-WT-DLL4 activity. These results suggest that β1-2 ERGV-deleted variant had reduced activity mainly due to a decrease in surface expression, whereas the other two β5-6 loop-shortening variants had reduced ability to activate Notch due to other molecular mechanism(s) other than significantly downregulated surface expression.

Mutation	**Position in C2 domain**	**Secretion**	**Cell surface expression**	**HEK293-mN1 split-luciferase reporter assay**	**NOTCH1$_{E7-13}$ receptor binding**
ERGV deleted	β1-2	×	↓↓↓↓	↓↓	↓↓↓↓↓
DDLR deleted	β5-6	×	↓↓	↓↓	↓↓↓
RPEA deleted	β5-6	×	↓↓	↓↓	↓↓↓
F195A/Y216A		no effect	no effect	↓↓↓	↓↓↓↓↓

Table 7-3. Summary of the effects for DLL4 C2-loop-shortening mutations. The table summarises the effects of C2-loop shortening on protein secretion, surface expression, Notch activation, and receptor binding (Chapter 3 & 5). The activity or binding of WT-DLL4 is normalised to 100%. Each '↓' represents a 20% decrease in activity or binding; '↓↓': 20%~40% decrease; '↓↓↓': 40%~60% decrease; '↓↓↓↓': 60%~80% decrease; '↓↓↓↓↓': >80% decrease.

7.5 The effects of DLL4 variants on Notch receptor binding and lipid binding

Various types of binding assays, each has its own pros and cons (Table 5-2), were used to assess the Notch binding capacity of our DLL4 variants. Under all assay conditions tested, DLL4-C2 cancer database variants showed no detectable effect on Notch binding (Table 5-3), suggesting that the C2 apical loops are not directly involved in Notch binding, as similarly observed for the JAG1-C2 variants in previous studies (Chillakuri et al., 2013;

Meng et al., 2022; Suckling et al., 2017). The DLL4 C2-loop-shortening variants showed decreased Notch receptor binding, mainly due to a reduction in their surface expression (Figure 3-12, Figure 5-9).

Different from the JAG1-C2 N-glycan variants, which showed a decrease in liposome binding as the key factor contributing to their reduced ability to activate Notch (Table 6-2) (Meng et al., 2022), the DLL4-C2 cancer database variants showed no detectable effect on liposome binding (Figure 5-10), likely because this avidity-driven liposome binding assay was not sensitive to small differences. On the other hand, as a high-throughput approach, MD simulations have been used to predict protein-membrane interactions in many contexts (Larsen et al., 2022; Larsen & Sansom, 2021; Meng et al., 2022; E. Yamamoto et al., 2016). In our case, this method provides significant mechanistic insights into C2-lipid binding that is challenging to study using experimental or structural techniques. The range of binding modes obtained demonstrates that, while C2-lipid binding occurs primarily via the apical loop region, these loops could be differently involved in positioning the C2 domain in different orientations (Figure 5-11). In addition, MD analysis showed that both the membrane lipid compositions and the amino acid sequence of the β1-2 loop could modulate the binding orientation of DLL4-C2 with respect to the lipid bilayer (Table 7-1), suggesting potential molecular mechanism underlying the functional effects observed (Figure 7-1).

7.6 Possible implications of the C2-membrane mediated regulatory mechanism of Notch signalling

Current hypothesis suggested that, during *trans*-activation (and maybe *cis*-inhibition), DLL4 binds to NOTCH1 in an antiparallel orientation and this interaction is augmented by contacts of the C2 apical loops with the ‘receiver’ cell membrane (or ‘sender’ cell

membrane in *cis*-inhibition) to induce optimal Notch signalling (Luca et al., 2015; Martins et al., 2021) (Figure 7-1). Considering the flexibility of Notch ligand ectodomain, the C2 domain could interact with lipid bilayer in different binding orientations (exemplified in Figure 7-1 as modes 1-3), which may or may not expose the receptor-binding region. As discussed in Section 5.7, a horizontal membrane-binding orientation with sideway loop β3-4 facing the membrane (mode 3) exposes the receptor binding sites, which may favour ternary complex formation and Notch activation. On the contrary, a horizontal membrane-binding orientation with the receptor binding region facing the membrane (mode 1) hinders ternary complex formation due to steric clashes, which may reduce Notch activation. An upright apical-binding orientation (mode 2) may or may not be compatible with receptor binding, depending on the unresolved FL-Notch/FL-ligand structure.

Whether the C2 domain will end up in a particular membrane-binding mode depends both on the membrane lipid properties and the sequence of the C2-loops (Table 5-1). Comparison with other well-studied C2 examples shows poor conservation of lipid-interacting residues in Notch ligands (Figure 1-15). However, as these residues are mainly charged or polar amino acids that engage phospholipid molecules through salt bridges or hydrogen bonds, we cannot eliminate the possibility that residues resembling these chemical natures in Notch ligand C2-apical-loops may interact with the membrane in a similar manner. Interestingly, four of the cancer database variants with functional effects all involve mutation of a charged residue (E40K, R41S, R100G, D128N). As illustrated in Figure 7-1, these mutations are distributed on loops β1-2, β3-4, or β5-6, which could alter the electrostatic properties of the C2 domain. Assuming the cell membrane outer layer is electrostatically negative due to the negatively charged phosphate head groups of phospholipids, mutation of a positively charged residue (e.g., R41S, R100G) may weaken C2-membrane binding whereas mutation of a negatively charged residue (e.g., E40K, D128N) may strengthen lipid binding. This may in turn alter

the membrane-binding mode of DLL4-C2, shifting towards either a more receptor-binding-favourable orientation or the reverse, thereby changing the activation levels. The importance of ionic strength in C2-lipid binding has been observed for other C2-containing proteins (e.g., PTEN, Syt1-C2B; see Section 1.5.3 for details).

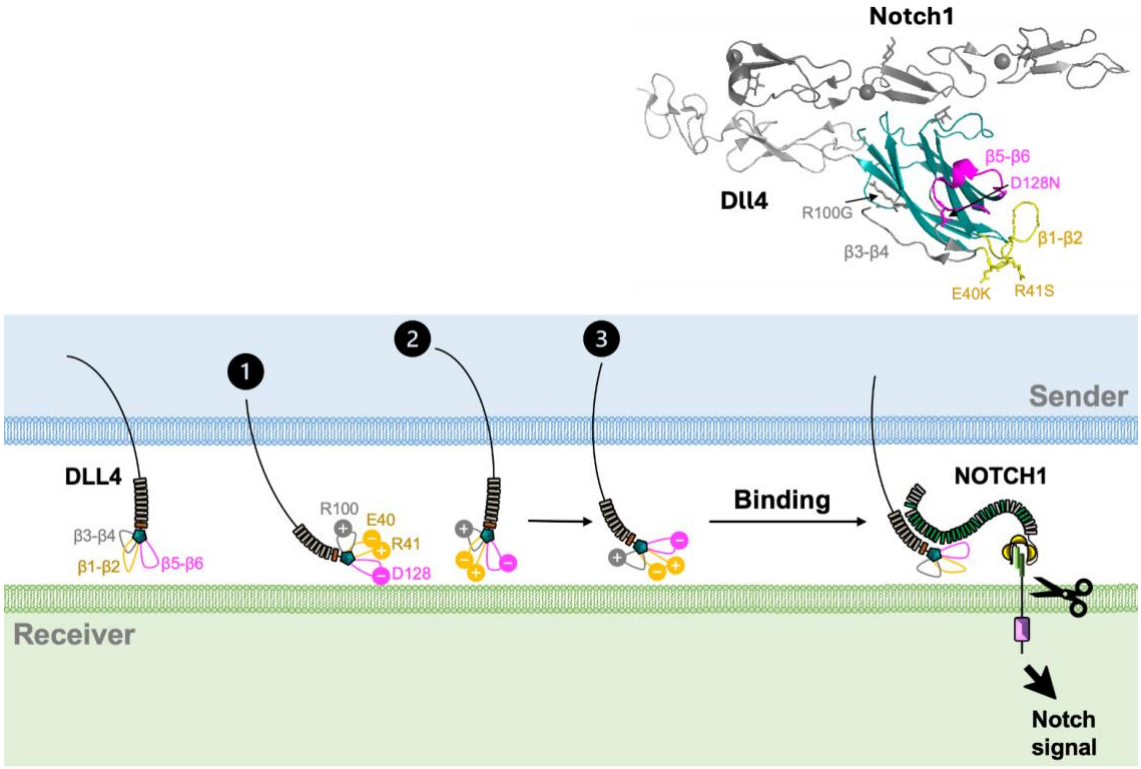


Figure 7-1. Proposed molecular mechanism mediated by DLL4-C2-membrane interactions. The cartoon illustrates ternary complex formation by DLL4, NOTCH1, and 'receiver' cell membrane based on Dll4/Notch1 crystal structure (PDB: 4XLW). DLL4 expressed on the 'sender' cell surface adopts alternative membrane binding modes (three examples are labelled 1-3) depending on which apical loops (β1-2: yellow, β3-4: grey, β5-6: magenta) are in contact with the lipid bilayer. The four DLL4-C2 cancer database missense mutations are shown in stick representations in the crystal structure, and the respective residues are labelled with their charges ('+': R41, R100; '−': E40, D128) in the cartoon. Before receptor-ligand engagement, DLL4 may reorientate itself by altering its membrane-binding mode to expose its receptor-binding region, thereby allowing Notch binding and activation.

In general, since solvent-exposed aromatic residues that have implications in membrane binding (e.g., perforin, cPLA2α) occur at a significantly lower frequency on Notch ligand C2-apical-loops, ligand C2 domains are unlikely to have a deep membrane penetration

or strong membrane binding. Furthermore, unlike other Ca^{2+}-independent C2 domains (e.g., PTEN, see Section 1.5.3 for details) which contain apical loops with enriched basic residues to mimic the positively charged property of Ca^{2+}-bound C2 domains and bind membrane constitutively, the Ca^{2+}-independent C2 domains of the Delta-family Notch ligands do not have a polybasic sequence in their C2-apical-loops. Therefore, the DLL4-C2 domain may only allow weak and conditional membrane interactions. Nevertheless, the surface electrostatic potential of Notch ligand C2 domains reveals a basic patch at a conserved concave surface region, although the cationic property is significantly weaker compared to other C2 (e.g., PKCα and PTEN) (see Appendix 8.7.2), suggesting that the C2 in Notch ligands may also engage the membrane via a commonly conserved cationic β-groove (D. Zhang & Aravind, 2010). Compared with JAG1-C2, DLL4-C2 loop mutations appeared to have a smaller functional impact, possibly owing to differences in their Notch-binding affinities. As a higher-affinity Notch ligand (see Section 1.3.3.1), DLL4 by itself binds Notch strongly, therefore changes in its lipid-binding property led to smaller effects on Notch activation.

7.7 Future directions

Cancer databases act as a useful source to identify tumour-associated somatic mutations that are potentially pathogenic or have a functional impact. Similar approaches have been applied in JAG1 and NOTCH1 studies, which picked out a functionally important N-glycan variant (T145N) in the JAG1 COSMIC database (Chapter 6) (Meng et al., 2022), and a subset of NOTCH1 COSMIC variants that impaired O-fucosylation and led to dysregulated Notch signalling (Pennarubia et al., 2022). Likewise, the DLL4 cancer database variants tested in our study also showed functional effects in *in vitro* experiments, facilitating our understanding of the impact of individual mutations

accumulating in cells. A key future challenge is to understand the consequences of such functional effects in physiological and disease contexts.

Considering the importance of DLL4-Notch signalling in inducing the differentiation of pluripotent stem cells (iPSCs) into T-lineage cells (Michaels et al., 2022; Trotman-Grant et al., 2021) and the differentiation of mesenchymal stem cells (MSC) into osteogenic cells (Zhao et al., 2022), stem cells, MSC spheroids, artificial thymic organoids from the MS5-DLL4 murine bone marrow stromal cell line (Seet et al., 2017), or complex bone marrow organoids from iPSCs (Frenz-Wiessner et al., 2024) can all potentially be utilised as models to study the functional importance of DLL4. Moreover, since DLL4 plays a key role in angiogenesis and vasculature (see Section 1.2.1.1), vascular or tumour organoids can also be used as 3D-models to assess DLL4's roles in vascular development and tumour angiogenesis (J.-L. Li et al., 2007; X.-Y. Sun et al., 2022; Wimmer et al., 2019). Specific mutations can be introduced by CRISPR-Cas gene editing to generate DLL4-C2-loop variants *ex vivo* or *in vivo*, as used in *Drosophila* to study the effects of dDelta-C2 loop deletion (Martins et al., 2021). Additionally, vascular development modulated by DLL4-Notch can be studied in mouse models, where mutations may lead to functional and morphological alterations (Corada et al., 2010).

Due to the complexity and difficulty of determining the outer layer lipid compositions of specific cell membranes, which could vary depending on the cell morphology, developmental stage, and environmental factors (Cansell et al., 1997; Gerl et al., 2012; Sampaio et al., 2011; S. Yan et al., 2024), it is hard to conclude how different cell systems would affect the activity of our DLL4 variants. Nevertheless, advanced techniques, such as cyclodextrin-induced lipid exchange (Suresh & London, 2022, 2024), could be employed to investigate the effect of changing outer leaflet lipid properties on Notch ligand functions. In addition, whilst the HUVECs RT-qPCR assay provides a more physiologically relevant system to study DLL4 variants, this system could be further

employed using a more complex sprouting angiogenesis assay (Pauty et al., 2018; Tiemeijer et al., 2018, 2022) to investigate whether these DLL4 variants could elicit different spatial control on endothelial sprouting. Recent technical advances that combine cryogenic electron microscopy (cryo-EM) with lipid nanodiscs could allow visualisation of the C2 orientation and receptor-ligand organisation at the membrane. With the use of cryo-electron tomography (cryo-ET), C2-membrane interactions could even be visualised under more physiological conditions. Furthermore, the transiently transfected HEK293T cells showed a bimodal distribution of ligand surface expression, posing difficulties to data analysis in binding assays. To better analyse the results, it would be useful to sort the different cell populations by FACS before the coculture and binding experiments.

Last but not least, comparative studies of JAG1- and DLL4-C2 variants showed that, whilst JAG1-C2 COSMIC variants generally led to loss-of-function effects, DLL4-C2 cancer database variants showed a narrow range of increased or decreased activity, suggesting ligand-specific differences. Further analysis of their lipid-binding properties also suggests different regulatory mechanisms underlying their functional effects, with JAG1-C2 variants showing significantly reduced liposome binding, whereas DLL4-C2 variants showing unaffected liposome binding but altered membrane binding orientations. To further investigate the ligand-specific regulatory roles of C2 lipid-binding loops, it would be useful to study other Notch ligands, such as JAG2 and DLL1, using similar approaches.

Bibliography

Abby, E., Dentro, S. C., Hall, M. W. J., Fowler, J. C., Ong, S. H., Sood, R., Herms, A., Piedrafita, G., Abnizova, I., Siebel, C. W., Gerstung, M., Hall, B. A., & Jones, P. H. (2023). Notch1 mutations drive clonal expansion in normal esophageal epithelium but impair tumor growth. *Nature Genetics 2023 55:2*, *55*(2), 232–245. https://doi.org/10.1038/s41588-022-01280-z

Abe, M., Makino, A., Françoise, F. H., Kamijo, K., Yoshiko, Y. O., Hanada, K., Mizuno, H., Miyawaki, A., & Kobayashi, T. (2012). A role for sphingomyelin-rich lipid domains in the accumulation of phosphatidylinositol-4,5-bisphosphate to the cleavage furrow during cytokinesis. *Molecular and Cellular Biology*, *32*(8), 1396–1407. Scopus. https://doi.org/10.1128/MCB.06113-11

Acar, M., Jafar-Nejad, H., Takeuchi, H., Rajan, A., Ibrani, D., Rana, N. A., Pan, H., Haltiwanger, R. S., & Bellen, H. J. (2008). Rumi is a CAP10 domain glycosyltransferase that modifies Notch and is required for Notch signaling. *Cell*, *132*(2), 247–258. https://doi.org/10.1016/j.cell.2007.12.016

Adams, F. H., & Oliver, C. P. (1945). Hereditary deformities in man. *Journal of Heredity*, *36*(1), 3–7. https://doi.org/10.1093/oxfordjournals.jhered.a105415

Agrawal, N., Frederick, M. J., Pickering, C. R., Bettegowda, C., Chang, K., Li, R. J., Fakhry, C., Xie, T. X., Zhang, J., Wang, J., Zhang, N., El-Naggar, A. K., Jasser, S. A., Weinstein, J. N., Treviño, L., Drummond, J. A., Muzny, D. M., Wu, Y., Wood, L. D., … Myers, J. N. (2011). Exome sequencing of head and neck squamous cell carcinoma reveals inactivating mutations in NOTCH1. *Science (New York, N.Y.)*, *333*(6046), 1154–1157. https://doi.org/10.1126/SCIENCE.1206923

Alabi, R. O., Farber, G., & Blobel, C. P. (2018). Intriguing Roles for Endothelial ADAM10/Notch Signaling in the Development of Organ-Specific Vascular Beds. *Physiological Reviews*, *98*(4), 2025–2061. https://doi.org/10.1152/physrev.00029.2017

Alcolea, M. P., Greulich, P., Wabik, A., Frede, J., Simons, B. D., & Jones, P. H. (2014). Differentiation imbalance in single Oesophageal progenitor cells causes clonal immortalization and field change. *Nature Cell Biology*, *16*(6), 615. https://doi.org/10.1038/NCB2963

Algaze, C., Esplin, E. D., Lowenthal, A., Hudgins, L., Tacy, T. A., & Selamet Tierney, E. S. (2013). Expanding the phenotype of cardiovascular malformations in Adams-Oliver syndrome. *American Journal of Medical Genetics. Part A*, *161A*(6), 1386–1389. https://doi.org/10.1002/ajmg.a.35864

Allam, H., Johnson, B. P., Zhang, M., Lu, Z., Cannon, M. J., & Abbott, K. L. (2017). The glycosyltransferase GnT-III activates Notch signaling and drives stem cell expansion to promote the growth and invasion of ovarian cancer. *The Journal of Biological Chemistry*, *292*(39), 16351–16359. https://doi.org/10.1074/jbc.M117.783936

Andrawes, M. B., Xu, X., Liu, H., Ficarro, S. B., Marto, J. A., Aster, J. C., & Blacklow, S. C. (2013). Intrinsic selectivity of Notch 1 for Delta-like 4 over Delta-like 1. *The Journal of Biological Chemistry*, *288*(35), 25477–25489. https://doi.org/10.1074/jbc.M113.454850

Antfolk, D., Sjöqvist, M., Cheng, F., Isoniemi, K., Duran, C. L., Rivero-Muller, A., Antila, C., Niemi, R., Landor, S., Bouten, C. V. C., Bayless, K. J., Eriksson, J. E., & Sahlgren, C. M. (2017). Selective regulation of Notch ligands during angiogenesis is mediated by vimentin. *Proceedings of the National Academy of Sciences*, *114*(23), E4574–E4581. https://doi.org/10.1073/pnas.1703057114

Aricescu, A. R., Lu, W., & Jones, E. Y. (2006). A time- and cost-efficient system for high-level protein production in mammalian cells. *Acta Crystallogr D Biol Crystallogr*, *62*(Pt 10), 1243–1250. https://doi.org/10.1107/s0907444906029799

Artavanis-Tsakonas, S., Muskavitch, M. A., & Yedvobnick, B. (1983). Molecular cloning of Notch, a locus affecting neurogenesis in Drosophila melanogaster. *Proceedings of the National Academy of Sciences of the United States of America*, *80*(7), 1977–1981. https://doi.org/10.1073/pnas.80.7.1977

Ascano, J. M., Beverly, L. J., & Capobianco, A. J. (2003). The C-terminal PDZ-Ligand of JAGGED1 Is Essential for Cellular Transformation*. *Journal of Biological Chemistry*, *278*(10), 8771–8779. https://doi.org/10.1074/jbc.M211427200

Aster, J. C., Pear, W. S., & Blacklow, S. C. (2017). The Varied Roles of Notch in Cancer. *Annual Review of Pathology: Mechanisms of Disease*, *12*(1), 245–275. https://doi.org/10.1146/annurev-pathol-052016-100127

Austin, J., & Kimble, J. (1989). Transcript analysis of glp-1 and lin-12, homologous genes required for cell interactions during development of C. elegans. *Cell*, *58*(3), 565–571. https://doi.org/10.1016/0092-8674(89)90437-6

Azimzadeh Irani, M., Kannan, S., & Verma, C. (2017). Role of N-glycosylation in EGFR ectodomain ligand binding. *Proteins: Structure, Function and Bioinformatics*, *85*(8), 1529–1549. Scopus. https://doi.org/10.1002/prot.25314

Baloul, S., Roussos, C., Gomez-Lamarca, M., Muresan, L., & Bray, S. (2024). Changes in searching behaviour of CSL transcription complexes in Notch active conditions. *Life Science Alliance*, *7*(3). https://doi.org/10.26508/lsa.202302336

Basmanav, F. B., Oprisoreanu, A.-M., Pasternack, S. M., Thiele, H., Fritz, G., Wenzel, J., Größer, L., Wehner, M., Wolf, S., Fagerberg, C., Bygum, A., Altmüller, J., Rütten, A., Parmentier, L., El Shabrawi-Caelen, L., Hafner, C., Nürnberg, P., Kruse, R., Schoch,

S., … Betz, R. C. (2014). Mutations in POGLUT1, encoding protein O-glucosyltransferase 1, cause autosomal-dominant Dowling-Degos disease. *American Journal of Human Genetics*, *94*(1), 135–143. https://doi.org/10.1016/j.ajhg.2013.12.003

Bauer, R. C., Laney, A. O., Smith, R., Gerfen, J., Morrissette, J. J. D., Woyciechowski, S., Garbarini, J., Loomes, K. M., Krantz, I. D., Urban, Z., Gelb, B. D., Goldmuntz, E., & Spinner, N. B. (2010). Jagged1 (JAG1) mutations in patients with tetralogy of fallot or pulmonic stenosis. *Human Mutation*, *31*(5), 594–601. https://doi.org/10.1002/HUMU.21231

Becam, I., Fiuza, U.-M., Arias, A. M., & Milán, M. (2010). A role of receptor Notch in ligand cis-inhibition in Drosophila. *Current Biology : CB*, *20*(6), 554–560. https://doi.org/10.1016/j.cub.2010.01.058

Bellavia, D., Checquolo, S., Campese, A. F., Felli, M. P., Gulino, A., & Screpanti, I. (2008). Notch3: From subtle structural differences to functional diversity. *Oncogene*, *27*(38), 5092–5098. https://doi.org/10.1038/onc.2008.230

Benedito, R., & Hellström, M. (2013). Notch as a hub for signaling in angiogenesis. *Experimental Cell Research*, *319*(9), 1281–1288. https://doi.org/10.1016/j.yexcr.2013.01.010

Benedito, R., Roca, C., Sörensen, I., Adams, S., Gossler, A., Fruttiger, M., & Adams, R. H. (2009). The Notch Ligands Dll4 and Jagged1 Have Opposing Effects on Angiogenesis. *Cell*, *137*(6), 1124–1135. https://doi.org/10.1016/j.cell.2009.03.025

Bernasconi-Elias, P., Hu, T., Jenkins, D., Firestone, B., Gans, S., Kurth, E., Capodieci, P., Deplazes-Lauber, J., Petropoulos, K., Thiel, P., Ponsel, D., Hee Choi, S., Lemotte, P., London, A., Goetcshkes, M., Nolin, E., Jones, M. D., Slocum, K., Kluk, M. J., … Fryer, C. J. (2016). Characterization of activating mutations of NOTCH3 in T cell acute lymphoblastic leukemia and anti-leukemic activity of NOTCH3 inhibitory antibodies. *Oncogene*, *35*(47), 6077. https://doi.org/10.1038/ONC.2016.133

Bierkamp, C., & Campos-Ortega, J. A. (1993). A zebrafish homologue of the Drosophila neurogenic gene Notch and its pattern of transcription during early embryogenesis. *Mech Dev*, *43*(2–3), 87–100. https://doi.org/10.1016/0925-4773(93)90027-u

Birtel, J., Eisenberger, T., Gliem, M., Müller, P. L., Herrmann, P., Betz, C., Zahnleiter, D., Neuhaus, C., Lenzner, S., Holz, F. G., Mangold, E., Bolz, H. J., & Charbel Issa, P. (2018). Clinical and genetic characteristics of 251 consecutive patients with macular and cone/cone-rod dystrophy. *Scientific Reports*, *8*(1), 4824. https://doi.org/10.1038/s41598-018-22096-0

Bittova, L., Sumandea, M., & Cho, W. (1999). A Structure-Function Study of the C2 Domain of Cytosolic Phospholipase A2: IDENTIFICATION OF ESSENTIAL CALCIUM

LIGANDS AND HYDROPHOBIC MEMBRANE BINDING RESIDUES*. *Journal of Biological Chemistry*, *274*(14), 9665–9672. https://doi.org/10.1074/jbc.274.14.9665

Bjornson, C. R. R., Cheung, T. H., Liu, L., Tripathi, P. V., Steeper, K. M., & Rando, T. A. (2012). Notch signaling is necessary to maintain quiescence in adult muscle stem cells. *Stem Cells (Dayton, Ohio)*, *30*(2), 232–242. https://doi.org/10.1002/stem.773

Blaumueller, C. M., Qi, H., Zagouras, P., & Artavanis-Tsakonas, S. (1997). Intracellular cleavage of Notch leads to a heterodimeric receptor on the plasma membrane. *Cell*, *90*(2), 281–291. https://doi.org/10.1016/S0092-8674(00)80336-0

Bo, Z., Rowntree, T., Johnson, S., Nurmahdi, H., Suckling, R. J., Hill, J., Korona, B., Weisshuhn, P. C., Sheppard, D., Meng, Y., Liang, S., Lowe, E. D., Lea, S. M., Redfield, C., & Handford, P. A. (2024). Structural and functional studies of the EGF20-27 region reveal new features of the human Notch receptor important for optimal activation. *Structure (London, England : 1993)*, *32*(12), 2325-2336.e5. https://doi.org/10.1016/j.str.2024.10.012

Boareto, M., Jolly, M. K., Lu, M., Onuchic, J. N., Clementi, C., & Ben-Jacob, E. (2015). Jagged-Delta asymmetry in Notch signaling can give rise to a Sender/Receiver hybrid phenotype. *Proceedings of the National Academy of Sciences of the United States of America*, *112*(5), E402-409. https://doi.org/10.1073/pnas.1416287112

Bocci, F., Onuchic, J. N., & Jolly, M. K. (2020). Understanding the Principles of Pattern Formation Driven by Notch Signaling by Integrating Experiments and Theoretical Models. *Frontiers in Physiology*, *11*, 929. https://doi.org/10.3389/fphys.2020.00929

Bochud, A., & Conzelmann, A. (2015). The active site of yeast phosphatidylinositol synthase Pis1 is facing the cytosol. *Biochimica et Biophysica Acta*, *1851*(5), 629–640. https://doi.org/10.1016/j.bbalip.2015.02.006

Bonev, B., Stanley, P., & Papalopulu, N. (2012). MicroRNA-9 Modulates Hes1 Ultradian Oscillations by Forming a Double-Negative Feedback Loop. *Cell Reports*, *2*(1), 10–18. https://doi.org/10.1016/j.celrep.2012.05.017

Bonfiglio, F., Bruscaggin, A., Guidetti, F., Terzi di Bergamo, L., Faderl, M., Spina, V., Condoluci, A., Bonomini, L., Forestieri, G., Koch, R., Piffaretti, D., Pini, K., Pirosa, M. C., Cittone, M. G., Arribas, A., Lucioni, M., Ghilardi, G., Wu, W., Arcaini, L., … Rossi, D. (2022). Genetic and phenotypic attributes of splenic marginal zone lymphoma. *Blood*, *139*(5), 732–747. https://doi.org/10.1182/BLOOD.2021012386

Borggrefe, T., & Oswald, F. (2009). The Notch signaling pathway: Transcriptional regulation at Notch target genes. *Cellular and Molecular Life Sciences : CMLS*, *66*(10), 1631–1646. https://doi.org/10.1007/s00018-009-8668-7

Boscher, C., Dennis, J. W., & Nabi, I. R. (2011). Glycosylation, galectins and cellular signaling. *Current Opinion in Cell Biology*, *23*(4), 383–392. Scopus. https://doi.org/10.1016/j.ceb.2011.05.001

Boukhatmi, H., Martins, T., Pillidge, Z., Kamenova, T., & Bray, S. (2020). Notch Mediates Inter-tissue Communication to Promote Tumorigenesis. *Current Biology*, *30*(10), 1809-1820.e4. https://doi.org/10.1016/J.CUB.2020.02.088

Bray, S. J., & Gomez-Lamarca, M. (2018). Notch after cleavage. *Current Opinion in Cell Biology*, *51*, 103–109. https://doi.org/10.1016/J.CEB.2017.12.008

Breitling, J., & Aebi, M. (2013). N-linked protein glycosylation in the endoplasmic reticulum. *Cold Spring Harbor Perspectives in Biology*, *5*(8), a013359. https://doi.org/10.1101/cshperspect.a013359

Brennan, A. J., Law, R. H. P., Conroy, P. J., Noori, T., Lukoyanova, N., Saibil, H., Yagita, H., Ciccone, A., Verschoor, S., Whisstock, J. C., Trapani, J. A., & Voskoboinik, I. (2018). Perforin proteostasis is regulated through its C2 domain: Supra-physiological cell death mediated by T431D-perforin. *Cell Death & Differentiation*, *25*(8), 1517–1529. https://doi.org/10.1038/s41418-018-0057-z

Bridges, C.B., M., T. H. (1916). *Sex-linked Inheritance in Drosophila*.

Bridges, C.B., M., T. H. (1919). Contributions to the genetics of Drosophila melanogaster. The origin of gynandromorphs. *Publs Carnegie Instn*, *278*, 1–122.

Bridges, E., Sheldon, H., Kleibeuker, E., Ramberger, E., Zois, C., Barnard, A., Harjes, U., Li, J.-L., Masiero, M., MacLaren, R., & Harris, A. (2020). RHOQ is induced by DLL4 and regulates angiogenesis by determining the intracellular route of the Notch intracellular domain. *Angiogenesis*, *23*. https://doi.org/10.1007/s10456-020-09726-w

Brückner, K., Perez, L., Clausen, H., & Cohen, S. (2000). Glycosyltransferase activity of Fringe modulates Notch–Delta interactions. *Nature*, *406*(6794), 411–415. https://doi.org/10.1038/35019075

Cai, B., Caplan, S., & Naslavsky, N. (2012). cPLA2α and EHD1 interact and regulate the vesiculation of cholesterol-rich, GPI-anchored, protein-containing endosomes. *Molecular Biology of the Cell*, *23*(10), 1874–1888. https://doi.org/10.1091/mbc.E11-10-0881

Cansell, M., Gouygou, J. P., Jozefonvicz, J., & Letourneur, D. (1997). Lipid composition of cultured endothelial cells in relation to their growth. *Lipids*, *32*(1), 39–44. https://doi.org/10.1007/s11745-997-0006-3

Caolo, V., van den Akker, N. M., Verbruggen, S., Donners, M. M., Swennen, G., Schulten, H., Waltenberger, J., Post, M. J., & Molin, D. G. (2010). Feed-forward signaling by membrane-bound ligand receptor circuit: The case of NOTCH DELTA-like 4 ligand in endothelial cells. *J Biol Chem*, *285*(52), 40681–40689. https://doi.org/10.1074/jbc.M110.176065

Carrieri, F. A., Murray, P. J., Ditsova, D., Ferris, M. A., Davies, P., & Dale, J. K. (2019). CDK1 and CDK2 regulate NICD1 turnover and the periodicity of the segmentation clock. *EMBO Reports*, *20*(7), e46436. https://doi.org/10.15252/embr.201846436

Casares, D., Escribá, P. V., & Rosselló, C. A. (2019). Membrane Lipid Composition: Effect on Membrane and Organelle Structure, Function and Compartmentalization and Therapeutic Avenues. *International Journal of Molecular Sciences*, *20*(9), 2167. https://doi.org/10.3390/ijms20092167

Chapman, E. R., & Davis, A. F. (1998). Direct Interaction of a Ca2+-binding Loop of Synaptotagmin with Lipid Bilayers*. *Journal of Biological Chemistry*, *273*(22), 13995–14001. https://doi.org/10.1074/jbc.273.22.13995

Chapman, G., Major, J. A., Iyer, K., James, A. C., Pursglove, S. E., Moreau, J. L. M., & Dunwoodie, S. L. (2016). Notch1 endocytosis is induced by ligand and is required for signal transduction. *Biochimica et Biophysica Acta*, *1863*(1), 166–177. https://doi.org/10.1016/J.BBAMCR.2015.10.021

Chapman, G., Sparrow, D. B., Kremmer, E., & Dunwoodie, S. L. (2011). Notch inhibition by the ligand DELTA-LIKE 3 defines the mechanism of abnormal vertebral segmentation in spondylocostal dysostosis. *Human Molecular Genetics*, *20*(5), 905–916. https://doi.org/10.1093/hmg/ddq529

Chastagner, P., Israël, A., & Brou, C. (2008). AIP4/Itch Regulates Notch Receptor Degradation in the Absence of Ligand. *PLoS ONE*, *3*(7), e2735. https://doi.org/10.1371/journal.pone.0002735

Chastagner, P., Rubinstein, E., & Brou, C. (2017). Ligand-activated Notch undergoes DTX4-mediated ubiquitylation and bilateral endocytosis before ADAM10 processing. *Science Signaling*, *10*(483). https://doi.org/10.1126/scisignal.aag2989

Chillakuri, C. R., Sheppard, D., Ilagan, M. X., Holt, L. R., Abbott, F., Liang, S., Kopan, R., Handford, P. A., & Lea, S. M. (2013). Structural analysis uncovers lipid-binding properties of Notch ligands. *Cell Rep*, *5*(4), 861–867. https://doi.org/10.1016/j.celrep.2013.10.029

Chillakuri, C. R., Sheppard, D., Lea, S. M., & Handford, P. A. (2012). Notch receptor-ligand binding and activation: Insights from molecular studies. *Semin Cell Dev Biol*, *23*(4), 421–428. https://doi.org/10.1016/j.semcdb.2012.01.009

Chitnis, A., Henrique, D., Lewis, J., Ish-Horowicz, D., & Kintner, C. (1995). Primary neurogenesis in Xenopus embryos regulated by a homologue of the Drosophila neurogenic gene Delta. *Nature*, *375*(6534), 761–766. Scopus. https://doi.org/10.1038/375761a0

Cho, W., & Stahelin, R. V. (2006). Membrane binding and subcellular targeting of C2 domains. *Biochimica et Biophysica Acta (BBA) - Molecular and Cell Biology of Lipids*, *1761*(8), 838–849. https://doi.org/10.1016/J.BBALIP.2006.06.014

Choi, D., Park, E., Jung, E., Seong, Y. J., Yoo, J., Lee, E., Hong, M., Lee, S., Ishida, H., Burford, J., Peti-Peterdi, J., Adams, R. H., Srikanth, S., Gwack, Y., Chen, C. S., Vogel, H. J., Koh, C. J., Wong, A. K., & Hong, Y.-K. (2017). Laminar flow downregulates

Notch activity to promote lymphatic sprouting. *The Journal of Clinical Investigation*, *127*(4), 1225–1240. https://doi.org/10.1172/JCI87442

Choi, J. H., Park, J. T., Davidson, B., Morin, P. J., Shih, I. M., & Wang, T. L. (2008). Jagged-1 and Notch3 Juxtacrine Loop Regulates Ovarian Tumor Growth and Adhesion. *Cancer Research*, *68*(14), 5716–5723. https://doi.org/10.1158/0008-5472.CAN-08-0001

Choi, S. H., Wales, T. E., Nam, Y., O'Donovan, D. J., Sliz, P., Engen, J. R., & Blacklow, S. C. (2012). Conformational locking upon cooperative assembly of notch transcription complexes. *Structure (London, England : 1993)*, *20*(2), 340–349. https://doi.org/10.1016/j.str.2011.12.011

Chu, Q., Liu, L., & Wang, W. (2013). Overexpression of hCLP46 enhances Notch activation and regulates cell proliferation in a cell type-dependent manner. *Cell Proliferation*, *46*(3), 254–262. https://doi.org/10.1111/cpr.12037

Chyung, J. H., Raper, D. M., & Selkoe, D. J. (2005). γ-secretase exists on the plasma membrane as an intact complex that accepts substrates and effects intramembrane cleavage. *Journal of Biological Chemistry*, *280*(6), 4383–4392. https://doi.org/10.1074/jbc.M409272200

Coffman, C., Harris, W., & Kintner, C. (1990). Xotch, the Xenopus homolog of Drosophila notch. *Science*, *249*(4975), 1438–1441. https://doi.org/10.1126/science.2402639

Cohen, B., Bashirullah, A., Dagnino, L., Campbell, C., Fisher, W. W., Leow, C. C., Whiting, E., Ryan, D., Zinyk, D., Boulianne, G., Hui, C. C., Gallie, B., Phillips, R. A., Lipshitz, H. D., & Egan, S. E. (1997). Fringe boundaries coincide with Notch-dependent patterning centres in mammals and alter Notch-dependent development in Drosophila. *Nature Genetics*, *16*(3), 283–288. https://doi.org/10.1038/ng0797-283

Collard, C. D., Bukusoglu, C., Agah, A., Colgan, S. P., Reenstra, W. R., Morgan, B. P., & Stahl, G. L. (1999). Hypoxia-induced expression of complement receptor type 1 (CR1, CD35) in human vascular endothelial cells. *The American Journal of Physiology*, *276*(2), C450-458. https://doi.org/10.1152/ajpcell.1999.276.2.C450

Collard, C. D., Väkevä, A., Büküsoglu, C., Zünd, G., Sperati, C. J., Colgan, S. P., & Stahl, G. L. (1997). Reoxygenation of hypoxic human umbilical vein endothelial cells activates the classic complement pathway. *Circulation*, *96*(1), 326–333. https://doi.org/10.1161/01.cir.96.1.326

Collier, J. R., Monk, N. A., Maini, P. K., & Lewis, J. H. (1996). Pattern formation by lateral inhibition with feedback: A mathematical model of delta-notch intercellular signalling. *Journal of Theoretical Biology*, *183*(4), 429–446. https://doi.org/10.1006/jtbi.1996.0233

Connor, J., Pak, C. H., Zwaal, R. F., & Schroit, A. J. (1992). Bidirectional transbilayer movement of phospholipid analogs in human red blood cells. Evidence for an ATP-

dependent and protein-mediated process. *Journal of Biological Chemistry*, *267*(27), 19412–19417. https://doi.org/10.1016/S0021-9258(18)41791-7

Cooke, R. M., Wilkinson, A. J., Baron, M., Pastore, A., Tappin, M. J., Campbell, I. D., Gregory, H., & Sheard, B. (1987). The solution structure of human epidermal growth factor. *Nature*, *327*(6120), 339–341. https://doi.org/10.1038/327339a0

Cooper, M. T. D., & Bray, S. J. (2000). R7 photoreceptor specification requires Notch activity. *Current Biology*, *10*(23), 1507–1510. Scopus. https://doi.org/10.1016/S0960-9822(00)00826-5

Corada, M., Nyqvist, D., Orsenigo, F., Caprini, A., Giampietro, C., Taketo, M. M., Iruela-Arispe, M. L., Adams, R. H., & Dejana, E. (2010). The Wnt/beta-catenin pathway modulates vascular remodeling and specification by upregulating Dll4/Notch signaling. *Developmental Cell*, *18*(6), 938–949. https://doi.org/10.1016/j.devcel.2010.05.006

Corbalán-García, S., & Gómez-Fernández, J. C. (2006). Protein kinase C regulatory domains: The art of decoding many different signals in membranes. *Biochimica et Biophysica Acta (BBA) - Molecular and Cell Biology of Lipids*, *1761*(7), 633–654. https://doi.org/10.1016/j.bbalip.2006.04.015

Corbalan-Garcia, S., & Gómez-Fernández, J. C. (2014). Signaling through C2 domains: More than one lipid target. *Biochimica et Biophysica Acta (BBA) - Biomembranes*, *1838*(6), 1536–1547. https://doi.org/10.1016/J.BBAMEM.2014.01.008

Cordes, R., Schuster-Gossler, K., Serth, K., & Gossler, A. (2004). Specification of vertebral identity is coupled to Notch signalling and the segmentation clock. *Development*, *131*(6), 1221–1233. Scopus. https://doi.org/10.1242/dev.01030

Cordle, J., Johnson, S., Zi, J., Tay, Y., Roversi, P., Wilkin, M., Hernandez-Diaz, B., Shimizu, H., Jensen, S., Whiteman, P., Jin, B., Redfield, C., Baron, M., Lea, S. M., & Handford, P. A. (2008). A Conserved Face of the Jagged/Serrate DSL Domain is Involved in Notch Trans-Activation and Cis-Inhibition. *Nature Structural & Molecular Biology*, 849–857. https://doi.org/10.1038/nsmb.1457

Cornell, M., Evans, D. A., Mann, R., Fostier, M., Flasza, M., Monthatong, M., Artavanis-Tsakonas, S., & Baron, M. (1999). The Drosophila melanogaster Suppressor of deltex gene, a regulator of the Notch receptor signaling pathway, is an E3 class ubiquitin ligase. *Genetics*, *152*(2), 567–576. https://doi.org/10.1093/genetics/152.2.567

Daudet, N., & Lewis, J. (2005). Two contrasting roles for Notch activity in chick inner ear development: Specification of prosensory patches and lateral inhibition of hair-cell differentiation. *Development (Cambridge, England)*, *132*(3), 541–551. https://doi.org/10.1242/dev.01589

Davletov, B., Perisic, O., & Williams, R. L. (1998). Calcium-dependent Membrane Penetration Is a Hallmark of the C2 Domain of Cytosolic Phospholipase A2 Whereas the C2A

Domain of Synaptotagmin Binds Membranes Electrostatically. *Journal of Biological Chemistry*, *273*(30), 19093–19096. https://doi.org/10.1074/JBC.273.30.19093

Davletov, B., & Sudhof, T. C. (1993). A single C2domain from synaptotagmin I is sufficient for high affinity Ca2+/phospholipid binding. *Journal of Biological Chemistry*, *268*(35), 26386–26390.

De Celis, J. F., & Bray, S. (1997). Feed-back mechanisms affecting Notch activation at the dorsoventral boundary in the Drosophila wing. *Development (Cambridge, England)*, *124*(17), 3241–3251. https://doi.org/10.1242/dev.124.17.3241

De Celis, J. F., & Garcia-Bellido, A. (1994). Modifications of the Notch function by Abruptex mutations in Drosophila melanogaster. *Genetics*, *136*(1), 183–194. https://doi.org/10.1093/genetics/136.1.183

De Decker, M., Lavaert, M., Roels, J., Tilleman, L., Vandekerckhove, B., Leclercq, G., Van Nieuwerburgh, F., Van Vlierberghe, P., & Taghon, T. (2021). HES1 and HES4 have non-redundant roles downstream of Notch during early human T-cell development. *Haematologica*, *106*(1), 130–141. https://doi.org/10.3324/haematol.2019.226126

Deblandre, G. A., Lai, E. C., & Kintner, C. (2001). Xenopus Neuralized Is a Ubiquitin Ligase that Interacts with XDelta1 and Regulates Notch Signaling. *Developmental Cell*, *1*(6), 795–806. https://doi.org/10.1016/S1534-5807(01)00091-0

DeHaro-Arbona, F. J., Roussos, C., Baloul, S., Townson, J., Gómez Lamarca, M. J., & Bray, S. (2024). Dynamic modes of Notch transcription hubs conferring memory and stochastic activation revealed by live imaging the co-activator Mastermind. *eLife*, *12*. https://doi.org/10.7554/eLife.92083

Del Álamo, D., Rouault, H., & Schweisguth, F. (2011). Mechanism and Significance of cis-Inhibition in Notch Signalling. *Current Biology*, *21*(1), R40–R47. https://doi.org/10.1016/j.cub.2010.10.034

Del Amo, F. F., Smith, D. E., Swiatek, P. J., Gendron-Maguire, M., Greenspan, R. J., McMahon, A. P., & Gridley, T. (1992). Expression pattern of Motch, a mouse homolog of Drosophila Notch, suggests an important role in early postimplantation mouse development. *Development (Cambridge, England)*, *115*(3), 737–744. https://doi.org/10.1242/dev.115.3.737

Dexter, J. S. (1914). The Analysis of a Case of Continuous Variation in Drosophila by a Study of Its Linkage Relations. *The American Naturalist*, *48*(576), 712–758. https://doi.org/10.1086/279446

D'haene, B., Vandesompele, J., & Hellemans, J. (2010). Accurate and objective copy number profiling using real-time quantitative PCR. *Methods (San Diego, Calif.)*, *50*(4), 262–270. https://doi.org/10.1016/j.ymeth.2009.12.007

Dhanesh, S. B., Subashini, C., & James, J. (2016). Hes1: The maestro in neurogenesis. *Cellular and Molecular Life Sciences : CMLS*, *73*(21), 4019–4042. https://doi.org/10.1007/s00018-016-2277-z

Dinchuk, J. E., Focht, R. J., Kelley, J. A., Henderson, N. L., Zolotarjova, N. I., Wynn, R., Neff, N. T., Link, J., Huber, R. M., Burn, T. C., Rupar, M. J., Cunningham, M. R., Selling, B. H., Ma, J., Stern, A. A., Hollis, G. F., Stein, R. B., Friedman, P. A., Dinchuk, J. E., … Friedman, P. A. (2002). Absence of Post-translational Aspartyl-Hydroxylation of Epidermal Growth Factor Domains in Mice Leads to Developmental Defects and an Increased Incidence of Intestinal Neoplasia* Downloaded from. *THE JOURNAL OF BIOLOGICAL CHEMISTRY*, *277*(15), 12970–12977. https://doi.org/10.1074/jbc.M110389200

Dong, Y., Jesse, A. M., Kohn, A., Gunnell, L. M., Honjo, T., Zuscik, M. J., O'Keefe, R. J., & Hilton, M. J. (2010). RBPjkappa-dependent Notch signaling regulates mesenchymal progenitor cell proliferation and differentiation during skeletal development. *Development (Cambridge, England)*, *137*(9), 1461–1471. https://doi.org/10.1242/dev.042911

Downing, A. K., Knott, V., Werner, J. M., Cardy, C. M., Campbell, I. D., & Handford, P. A. (1996). Solution Structure of a Pair of Calcium-Binding Epidermal Growth Factor-like Domains: Implications for the Marfan Syndrome and Other Genetic Disorders. *Cell*, *85*(4), 597–605. https://doi.org/10.1016/S0092-8674(00)81259-3

Dray, N., Mancini, L., Binshtok, U., Cheysson, F., Supatto, W., Mahou, P., Bedu, S., Ortica, S., Than-Trong, E., Krecsmarik, M., Herbert, S., Masson, J.-B., Tinevez, J.-Y., Lang, G., Beaurepaire, E., Sprinzak, D., & Bally-Cuif, L. (2021). Dynamic spatiotemporal coordination of neural stem cell fate decisions occurs through local feedback in the adult vertebrate brain. *Cell Stem Cell*, *28*(8), 1457-1472.e12. https://doi.org/10.1016/j.stem.2021.03.014

D'Souza, B., Meloty-Kapella, L., & Weinmaster, G. (2010). Canonical and non-canonical Notch ligands. *Current Topics in Developmental Biology*, *92*, 73–129. https://doi.org/10.1016/S0070-2153(10)92003-6

D'souza, B., Miyamoto, A., & Weinmaster, G. (2008). The many facets of Notch ligands. *Oncogene*. https://doi.org/10.1038/onc.2008.229

Duran-Romaña, R., Houben, B., De Vleeschouwer, M., Louros, N., Wilson, M. P., Matthijs, G., Schymkowitz, J., & Rousseau, F. (2024). N-glycosylation as a eukaryotic protective mechanism against protein aggregation. *Science Advances*, *10*(5), eadk8173. https://doi.org/10.1126/sciadv.adk8173

Dutta, D., Sharma, V., Mutsuddi, M., & Mukherjee, A. (2022). Regulation of Notch signaling by E3 ubiquitin ligases. *The FEBS Journal*, *289*(4), 937–954. https://doi.org/10.1111/febs.15792

Duvall, K., Crist, L., Perl, A. J., Pode Shakked, N., Chaturvedi, P., & Kopan, R. (2022). Revisiting the role of Notch in nephron segmentation confirms a role for proximal fate selection during mouse and human nephrogenesis. *Development*, *149*(10). https://doi.org/10.1242/dev.200446

Ellisen, L. W., Bird, J., West, D. C., Soreng, A. L., Reynolds, T. C., Smith, S. D., & Sklar, J. (1991). TAN-1, the human homolog of the Drosophila Notch gene, is broken by chromosomal translocations in T lymphoblastic neoplasms. *Cell*, *66*(4), 649–661. https://doi.org/10.1016/0092-8674(91)90111-B

Emery, G., Hutterer, A., Berdnik, D., Mayer, B., Wirtz-Peitz, F., Gaitan, M. G., & Knoblich, J. A. (2005). Asymmetric Rab11 Endosomes Regulate Delta Recycling and Specify Cell Fate in the Drosophila Nervous System. *Cell*, *122*(5), 763–773. https://doi.org/10.1016/j.cell.2005.08.017

Esmail, S., & Manolson, M. F. (2021). Advances in understanding N-glycosylation structure, function, and regulation in health and disease. *European Journal of Cell Biology*, *100*(7), 151186. https://doi.org/10.1016/j.ejcb.2021.151186

Fabris, L., Cadamuro, M., Guido, M., Spirli, C., Fiorotto, R., Colledan, M., Torre, G., Alberti, D., Sonzogni, A., Okolicsanyi, L., & Strazzabosco, M. (2007). Analysis of Liver Repair Mechanisms in Alagille Syndrome and Biliary Atresia Reveals a Role for Notch Signaling. *Am J Pathol*, *171*, 641–653. https://doi.org/10.2353/ajpath.2007.070073

Fabris, L., Fiorotto, R., Spirli, C., Cadamuro, M., Mariotti, V., Perugorria, M. J., Banales, J. M., & Strazzabosco, M. (2019). Pathobiology of inherited biliary diseases: A roadmap to understand acquired liver diseases. *Nature Reviews Gastroenterology & Hepatology*, *16*, 497–511. https://doi.org/10.1038/s41575-019-0156-4

Falo-Sanjuan, J., Lammers, N. C., Garcia, H. G., & Bray, S. J. (2019). Enhancer Priming Enables Fast and Sustained Transcriptional Responses to Notch Signaling. *Developmental Cell*, *50*(4), 411-425.e8. https://doi.org/10.1016/j.devcel.2019.07.002

Fasoulakis, Z., Koutras, A., Ntounis, T., Pergialiotis, V., Chionis, A., Katrachouras, A., Palios, V.-C., Symeonidis, P., Valsamaki, A., Syllaios, A., Diakosavvas, M., Angelou, K., Samara, A. A., Pagkalos, A., Theodora, M., Schizas, D., & Kontomanolis, E. N. (2022). The Prognostic Role and Significance of Dll4 and Toll-like Receptors in Cancer Development. *Cancers*, *14*(7). https://doi.org/10.3390/cancers14071649

Fernandez-Valdivia, R., Takeuchi, H., Samarghandi, A., Lopez, M., Leonardi, J., Haltiwanger, R. S., & Jafar-Nejad, H. (2011). Regulation of mammalian Notch signaling and embryonic development by the protein O-glucosyltransferase Rumi. *Development (Cambridge, England)*, *138*(10), 1925–1934. https://doi.org/10.1242/dev.060020

Finn, J., Sottoriva, K., Pajcini, K. V., Kitajewski, J. K., Chen, C., Zhang, W., Malik, A. B., & Liu, Y. (2019). Dlk1-Mediated Temporal Regulation of Notch Signaling Is Required for

Differentiation of Alveolar Type II to Type I Cells during Repair. *Cell Reports*, *26*(11), 2942-2954.e5. https://doi.org/10.1016/j.celrep.2019.02.046

Fischer-Zirnsak, B., Segebrecht, L., Schubach, M., Charles, P., Alderman, E., Brown, K., Cadieux-Dion, M., Cartwright, T., Chen, Y., Costin, C., Fehr, S., Fitzgerald, K. M., Fleming, E., Foss, K., Ha, T., Hildebrand, G., Horn, D., Liu, S., Marco, E. J., … Ehmke, N. (2019). Haploinsufficiency of the Notch Ligand DLL1 Causes Variable Neurodevelopmental Disorders. *American Journal of Human Genetics*, *105*(3), 631–639. https://doi.org/10.1016/j.ajhg.2019.07.002

Fischetto, R., Palmieri, V. V., Tripaldi, M. E., Gaeta, A., Michelucci, A., Delvecchio, M., Francavilla, R., & Giordano, P. (2019). Alagille Syndrome: A Novel Mutation in JAG1 Gene. *Frontiers in Pediatrics*, *7*, 199. https://doi.org/10.3389/fped.2019.00199

Fleming, R. J. (2020). Ligand-Induced Cis-Inhibition of Notch Signaling: The Role of an Extracellular Region of Serrate. *Advances in Experimental Medicine and Biology*, *1227*, 29–49. https://doi.org/10.1007/978-3-030-36422-9_3

Fleming, R. J., Scottgale, T. N., Diederich, R. J., & Artavanis-Tsakonas, S. (1990). The gene Serrate encodes a putative EGF-like transmembrane protein essential for proper ectodermal development in Drosophila melanogaster. *Genes & Development*, *4*(12A), 2188–2201. https://doi.org/10.1101/gad.4.12a.2188

Forbes, S. A., Beare, D., Boutselakis, H., Bamford, S., Bindal, N., Tate, J., Cole, C. G., Ward, S., Dawson, E., Ponting, L., Stefancsik, R., Harsha, B., Yin Kok, C., Jia, M., Jubb, H., Sondka, Z., Thompson, S., De, T., & Campbell, P. J. (2016). COSMIC: somatic cancer genetics at high-resolution. *Nucleic Acids Research*, *45*, 777–783. https://doi.org/10.1093/nar/gkw1121

Franklin, J. L., Berechid, B. E., Cutting, F. B., Presente, A., Chambers, C. B., Foltz, D. R., Ferreira, A., & Nye, J. S. (1999). Autonomous and non-autonomous regulation of mammalian neurite development by Notch1 and Delta1. *Current Biology*, *9*(24), 1448–1457. Scopus. https://doi.org/10.1016/S0960-9822(00)80114-1

Frenz-Wiessner, S., Fairley, S. D., Buser, M., Goek, I., Salewskij, K., Jonsson, G., Illig, D., zu Putlitz, B., Petersheim, D., Li, Y., Chen, P.-H., Kalauz, M., Conca, R., Sterr, M., Geuder, J., Mizoguchi, Y., Megens, R. T. A., Linder, M. I., Kotlarz, D., … Klein, C. (2024). Generation of complex bone marrow organoids from human induced pluripotent stem cells. *Nature Methods*, *21*(5), 868–881. https://doi.org/10.1038/s41592-024-02172-2

Fryer, C. J., White, J. B., & Jones, K. A. (2004). Mastermind recruits CycC:CDK8 to phosphorylate the Notch ICD and coordinate activation with turnover. *Molecular Cell*, *16*(4), 509–520. https://doi.org/10.1016/j.molcel.2004.10.014

Fukada, S., Yamaguchi, M., Kokubo, H., Ogawa, R., Uezumi, A., Yoneda, T., Matev, M. M., Motohashi, N., Ito, T., Zolkiewska, A., Johnson, R. L., Saga, Y., Miyagoe-Suzuki, Y.,

Tsujikawa, K., Takeda, S., & Yamamoto, H. (2011). Hesr1 and Hesr3 are essential to generate undifferentiated quiescent satellite cells and to maintain satellite cell numbers. *Development (Cambridge, England)*, *138*(21), 4609–4619. https://doi.org/10.1242/dev.067165

Gao, J., Liu, J., Fan, D., Xu, H., Xiong, Y., Wang, Y., Xu, W., Wang, Y., Cheng, Y., & Zheng, G. (2011). Up-regulated expression of Notch1 and Jagged1 in human colon adenocarcinoma. *Pathologie Biologie*, *59*(6), 298–302. https://doi.org/10.1016/J.PATBIO.2010.11.001

García-García, A., Serna, S., Yang, Z., Delso, I., Taleb, V., Hicks, T., Artschwager, R., Vakhrushev, S. Y., Clausen, H., Angulo, J., Corzana, F., Reichardt, N. C., & Hurtado-Guerrero, R. (2021). FUT8-Directed Core Fucosylation of N-glycans Is Regulated by the Glycan Structure and Protein Environment. *ACS Catalysis*, *11*(15), 9052–9065. https://doi.org/10.1021/acscatal.1c01698

Ge, C., & Stanley, P. (2008). The O-fucose glycan in the ligand-binding domain of Notch1 regulates embryogenesis and T cell development. *Proceedings of the National Academy of Sciences of the United States of America*, *105*(5), 1539–1544. https://doi.org/10.1073/pnas.0702846105

Genestine, M., Ambriz, D., Crabtree, G. W., Dummer, P., Molotkova, A., Quintero, M., Mela, A., Biswas, S., Feng, H., Zhang, C., Canoll, P., Hargus, G., Agalliu, D., Gogos, J. A., & Au, E. (2021). Vascular-derived SPARC and SerpinE1 regulate interneuron tangential migration and accelerate functional maturation of human stem cell-derived interneurons. *eLife*, *10*. https://doi.org/10.7554/eLife.56063

Gerber, S. H., Rizo, J., & Südhof, T. C. (2001). The top loops of the C(2) domains from synaptotagmin and phospholipase A(2) control functional specificity. *The Journal of Biological Chemistry*, *276*(34), 32288–32292. https://doi.org/10.1074/jbc.C100108200

Gerhardt, H., Golding, M., Fruttiger, M., Ruhrberg, C., Lundkvist, A., Abramsson, A., Jeltsch, M., Mitchell, C., Alitalo, K., Shima, D., & Betsholtz, C. (2003). VEGF guides angiogenic sprouting utilizing endothelial tip cell filopodia. *The Journal of Cell Biology*, *161*(6), 1163–1177. https://doi.org/10.1083/jcb.200302047

Gerl, M. J., Sampaio, J. L., Urban, S., Kalvodova, L., Verbavatz, J.-M., Binnington, B., Lindemann, D., Lingwood, C. A., Shevchenko, A., Schroeder, C., & Simons, K. (2012). Quantitative analysis of the lipidomes of the influenza virus envelope and MDCK cell apical membrane. *The Journal of Cell Biology*, *196*(2), 213–221. https://doi.org/10.1083/jcb.201108175

Giaimo, B. D., Gagliani, E. K., Kovall, R. A., & Borggrefe, T. (2021). Transcription Factor RBPJ as a Molecular Switch in Regulating the Notch Response. *Advances in*

Experimental Medicine and Biology, *1287*, 9–30. https://doi.org/10.1007/978-3-030-55031-8_2

Gilbert, M. A., Bauer, R. C., Rajagopalan, R., Grochowski, C. M., Chao, G., McEldrew, D., Nassur, J. A., Rand, E. B., Krock, B. L., Kamath, B. M., Krantz, I. D., Piccoli, D. A., Loomes, K. M., & Spinner, N. B. (2019). Alagille syndrome mutation update: Comprehensive overview of JAG1 and NOTCH2 mutation frequencies and insight into missense variant classification. *Human Mutation*, *40*(12), 2197–2220. https://doi.org/10.1002/humu.23879

Gioftsidi, S., Relaix, F., & Mourikis, P. (2022). The Notch signaling network in muscle stem cells during development, homeostasis, and disease. *Skeletal Muscle*, *12*(1), 9. https://doi.org/10.1186/s13395-022-00293-w

Gonzalez-Perez, D., Das, S., Antfolk, D., Ahsan, H. S., Medina, E., Dundes, C. E., Jokhai, R. T., Egan, E. D., Blacklow, S. C., Loh, K. M., Rodriguez, P. C., & Luca, V. C. (2023). Affinity-matured DLL4 ligands as broad-spectrum modulators of Notch signaling. *Nature Chemical Biology*, *19*(1), 9–17. https://doi.org/10.1038/s41589-022-01113-4

Gordon, W. R., Roy, M., Vardar-Ulu, D., Garfinkel, M., Mansour, M. R., Aster, J. C., & Blacklow, S. C. (2009). Structure of the Notch1-negative regulatory region: Implications for normal activation and pathogenic signaling in T-ALL. *Blood*, *113*(18), 4381. https://doi.org/10.1182/BLOOD-2008-08-174748

Gordon, W. R., Vardar-Ulu, D., Histen, G., Sanchez-Irizarry, C., Aster, J. C., & Blacklow, S. C. (2007). Structural basis for autoinhibition of Notch. *Nat Struct Mol Biol*, *14*(4), 295–300. https://doi.org/10.1038/nsmb1227

Gordon, W. R., Zimmerman, B., He, L., Miles, L. J., Huang, J., Tiyanont, K., McArthur, D. G., Aster, J. C., Perrimon, N., Loparo, J. J., & Blacklow, S. C. (2015). Mechanical Allostery: Evidence for a Force Requirement in the Proteolytic Activation of Notch. *Developmental Cell*, *33*(6), 729–736. https://doi.org/10.1016/j.devcel.2015.05.004

Gozlan, O., & Sprinzak, D. (2023). Notch signaling in development and homeostasis. *Development*, *150*(4). https://doi.org/10.1242/dev.201138

Graham, F. L., Smiley, J., Russell, W. C., & Nairn, R. (1977). Characteristics of a human cell line transformed by DNA from human adenovirus type 5. *The Journal of General Virology*, *36*(1), 59–74. https://doi.org/10.1099/0022-1317-36-1-59

Greenwald, I., & Seydoux, G. (1990). Analysis of gain-of-function mutations of the lin-12 gene of Caenorhabditis elegans. *Nature*, *346*(6280), 197–199. https://doi.org/10.1038/346197a0

Grimmer, S., Ying, M., Wälchli, S., van Deurs, B., & Sandvig, K. (2005). Golgi vesiculation induced by cholesterol occurs by a dynamin- and cPLA2-dependent mechanism. *Traffic (Copenhagen, Denmark)*, *6*(2), 144–156. https://doi.org/10.1111/j.1600-0854.2005.00258.x

Grimwade, B. G., Muskavitch, M. A., Welshons, W. J., Yedvobnick, B., & Artavanis-Tsakonas, S. (1985). The molecular genetics of the Notch locus in Drosophila melanogaster. *Developmental Biology*, *107*(2), 503–519. https://doi.org/10.1016/0012-1606(85)90331-8

Grobler, J. A., Essen, L. O., Williams, R. L., & Hurley, J. H. (1996). C2 domain conformational changes in phospholipase C-delta 1. *Nature Structural Biology*, *3*(9), 788–795. https://doi.org/10.1038/nsb0996-788

Groot, A. J., & Vooijs, M. A. (2012). The role of Adams in Notch signaling. *Advances in Experimental Medicine and Biology*, *727*, 15–36. https://doi.org/10.1007/978-1-4614-0899-4_2

Guerrero-Valero, M., Ferrer-Orta, C., Querol-Audí, J., Marin-Vicente, C., Fita, I., Gómez-Fernández, J. C., Verdaguer, N., & Corbalán-García, S. (2009). Structural and mechanistic insights into the association of PKCα-C2 domain to PtdIns(4,5)P2. *Proceedings of the National Academy of Sciences*, *106*(16), 6603–6607. https://doi.org/10.1073/PNAS.0813099106

Guo, D., Ye, J., Li, L., Dai, J., Ma, D., & Ji, C. (2009). Down-regulation of Notch-1 increases co-cultured Jurkat cell sensitivity to chemotherapy. *Https://Doi.Org/10.1080/10428190802553257*, *50*(2), 270–278. https://doi.org/10.1080/10428190802553257

Hainaud, P., Contrerès, J.-O., Villemain, A., Liu, L.-X., Plouët, J., Tobelem, G., & Dupuy, E. (2006). The role of the vascular endothelial growth factor-Delta-like 4 ligand/Notch4-ephrin B2 cascade in tumor vessel remodeling and endothelial cell functions. *Cancer Research*, *66*(17), 8501–8510. https://doi.org/10.1158/0008-5472.CAN-05-4226

Haines, N., & Irvine, K. D. (2003). Glycosylation regulates Notch signalling. *Nature Reviews Molecular Cell Biology*, *4*(10), 786–797. https://doi.org/10.1038/nrm1228

Ham, H., Medlyn, M., & Billadeau, D. D. (2022). Locked and Loaded: Mechanisms Regulating Natural Killer Cell Lytic Granule Biogenesis and Release. *Frontiers in Immunology*, *13*, 871106. https://doi.org/10.3389/fimmu.2022.871106

Hambleton, S., Valeyev, N. V., Muranyi, A., Knott, V., Werner, J. M., McMichael, A. J., Handford, P. A., & Downing, A. K. (2004). Structural and functional properties of the human notch-1 ligand binding region. *Structure (London, England : 1993)*, *12*(12), 2173–2183. https://doi.org/10.1016/j.str.2004.09.012

Hamel, S., Fantini, J., & Schweisguth, F. (2010). Notch ligand activity is modulated by glycosphingolipid membrane composition in Drosophila melanogaster. *The Journal of Cell Biology*, *188*(4), 581–594. https://doi.org/10.1083/jcb.200907116

Hammerman, P. S., Voet, D., Lawrence, M. S., Voet, D., Jing, R., Cibulskis, K., Sivachenko, A., Stojanov, P., McKenna, A., Lander, E. S., Gabriel, S., Getz, G., Imielinski, M., Helman, E., Hernandez, B., Pho, N. H., Meyerson, M., Chu, A., Hye-Chun, J. E., …

Shen, R. (2012). Comprehensive genomic characterization of squamous cell lung cancers. *Nature*, *489*(7417), 519–525. https://doi.org/10.1038/NATURE11404

Handford, P. A., Mayhew, M., Baron, M., Winship, P. R., Campbell, I. D., & Brownlee, G. G. (1991). Key residues involved in calcium-binding motifs in EGF-like domains. *Nature*, *351*(6322), 164–167. https://doi.org/10.1038/351164a0

Hankeova, S., Salplachta, J., Zikmund, T., Kavkova, M., Van Hul, N., Brinek, A., Smekalova, V., Laznovsky, J., Dawit, F., Jaros, J., Bryja, V., Lendahl, U., Ellis, E., Nemeth, A., Fischler, B., Hannezo, E., Kaiser, J., & Andersson, E. R. (2021). DUCT reveals architectural mechanisms contributing to bile duct recovery in a mouse model for Alagille syndrome. *eLife*, *10*. https://doi.org/10.7554/eLife.60916

Hankeova, S., Van Hul, N., Laznovsky, J., Verboven, E., Mangold, K., Hensens, N., Adori, C., Verhoef, E., Zikmund, T., Dawit, F., Kavkova, M., Salplachta, J., Sjöqvist, M., Johansson, B. R., Hassan, M. G., Fredriksson, L., Baumgärtel, K., Bryja, V., Lendahl, U., … Andersson, E. R. (2022). Sex differences and risk factors for bleeding in Alagille syndrome. *EMBO Molecular Medicine*, *14*(12), e15809. https://doi.org/10.15252/emmm.202215809

Haritunians, T., Chow, T., De Lange, R. P. J., Nichols, J. T., Ghavimi, D., Dorrani, N., St Clair, D. M., Weinmaster, G., & Schanen, C. (2005). Functional analysis of a recurrent missense mutation in Notch3 in CADASIL. *Journal of Neurology, Neurosurgery, and Psychiatry*, *76*(9), 1242–1248. https://doi.org/10.1136/jnnp.2004.051854

Hartman, B. H., Reh, T. A., & Bermingham-McDonogh, O. (2010). Notch signaling specifies prosensory domains via lateral induction in the developing mammalian inner ear. *Proceedings of the National Academy of Sciences of the United States of America*, *107*(36), 15792–15797. https://doi.org/10.1073/pnas.1002827107

Harvey, B. M., & Haltiwanger, R. S. (2018). Regulation of Notch Function by O-Glycosylation. *Advances in Experimental Medicine and Biology*, *1066*, 59–78. https://doi.org/10.1007/978-3-319-89512-3_4

Héliès-Toussaint, C., Gambert, S., Roller, P., Tricot, S., Lacour, B., & Grynberg, A. (2006). Lipid metabolism in human endothelial cells. *Biochimica et Biophysica Acta (BBA) - Molecular and Cell Biology of Lipids*, *1761*(7), 765–774. https://doi.org/10.1016/j.bbalip.2006.05.013

Hellström, M., Phng, L.-K., Hofmann, J. J., Wallgard, E., Coultas, L., Lindblom, P., Alva, J., Nilsson, A.-K., Karlsson, L., Gaiano, N., Yoon, K., Rossant, J., Iruela-Arispe, M. L., Kalén, M., Gerhardt, H., & Betsholtz, C. (2007). Dll4 signalling through Notch1 regulates formation of tip cells during angiogenesis. *Nature*, *445*(7129), 776–780. https://doi.org/10.1038/nature05571

Henderson, S. T., Gao, D., Christensen, S., Kimble, J., & ¶#§. (1997). Functional Domains of LAG-2, a Putative Signaling Ligand for LIN-12 and GLP-1 Receptors in Caenorhabditis elegans. In *Molecular Biology of the Cell* (Vol. 8).

Henderson, S. T., Gao, D., Lambie, E. J., & Kimble, J. (1994). Lag-2 may encode a signaling ligand for the GLP-1 and LIN-12 receptors of C. elegans. *Development (Cambridge, England)*, *120*(10), 2913–2924. https://doi.org/10.1242/dev.120.10.2913

Henrique, D., Hirsinger, E., Adam, J., Roux, I. L., Pourquié, O., Ish-Horowicz, D., & Lewis, J. (1997). Maintenance of neuroepithelial progenitor cells by Delta-Notch signalling in the embryonic chick retina. *Current Biology*, *7*(9), 661–670. Scopus. https://doi.org/10.1016/S0960-9822(06)00293-4

Henrique, D., & Schweisguth, F. (2019). Mechanisms of Notch signaling: A simple logic deployed in time and space. *Development*, *146*(3). https://doi.org/10.1242/dev.172148

Herbert, S. P., & Stainier, D. Y. R. (2011). Molecular control of endothelial cell behaviour during blood vessel morphogenesis. *Nature Reviews. Molecular Cell Biology*, *12*(9), 551–564. https://doi.org/10.1038/nrm3176

Herrick, D. Z., Kuo, W., Huang, H., Schwieters, C. D., Ellena, J. F., & Cafiso, D. S. (2009). Solution and Membrane-Bound Conformations of the Tandem C2A and C2B Domains of Synaptotagmin 1: Evidence for Bilayer Bridging. *Journal of Molecular Biology*, *390*(5), 913–923. https://doi.org/10.1016/j.jmb.2009.06.007

Herrick, D. Z., Sterbling, S., Rasch, K. A., Hinderliter, A., & Cafiso, D. S. (2006). Position of Synaptotagmin I at the Membrane Interface: Cooperative Interactions of Tandem C2 Domains. *Biochemistry*, *45*(32), 9668–9674. https://doi.org/10.1021/bi060874j

High, F. A., Lu, M. M., Pear, W. S., Loomes, K. M., Kaestner, K. H., & Epstein, J. A. (2008). Endothelial expression of the Notch ligand Jagged1 is required for vascular smooth muscle development. *Proceedings of the National Academy of Sciences of the United States of America*, *105*(6), 1955–1959. https://doi.org/10.1073/pnas.0709663105

High, F. A., Zhang, M., Proweller, A., Tu, L., Parmacek, M. S., Pear, W. S., & Epstein, J. A. (2007). An essential role for Notch in neural crest during cardiovascular development and smooth muscle differentiation. *The Journal of Clinical Investigation*, *117*(2), 353–363. https://doi.org/10.1172/JCI30070

Hilton, M. J., Tu, X., Wu, X., Bai, S., Zhao, H., Kobayashi, T., Kronenberg, H. M., Teitelbaum, S. L., Ross, F. P., Kopan, R., & Long, F. (2008). Notch signaling maintains bone marrow mesenchymal progenitors by suppressing osteoblast differentiation. *Nature Medicine*, *14*(3), 306–314. https://doi.org/10.1038/nm1716

Hirano, K.-I., Suganami, A., Tamura, Y., Yagita, H., Habu, S., Kitagawa, M., Sato, T., & Hozumi, K. (2020). Delta-like 1 and Delta-like 4 differently require their extracellular

domains for triggering Notch signaling in mice. *Elife*, *9*, e50979. https://doi.org/10.7554/eLife.50979

Hirano, Y., Gao, Y. G., Stephenson, D. J., Vu, N. T., Malinina, L., Simanshu, D. K., Chalfant, C. E., Patel, D. J., & Brown, R. E. (2019). Structural basis of phosphatidylcholine recognition by the C2-domain of cytosolic phospholipase A2α. *eLife*, *8*. https://doi.org/10.7554/eLife.44760

Hirata, H., Yoshiura, S., Ohtsuka, T., Bessho, Y., Harada, T., Yoshikawa, K., & Kageyama, R. (2002). Oscillatory expression of the bHLH factor Hes1 regulated by a negative feedback loop. *Science (New York, N.Y.)*, *298*(5594), 840–843. https://doi.org/10.1126/science.1074560

Ho, A. S., Kannan, K., Roy, D. M., Morris, L. G. T., Ganly, I., Katabi, N., Ramaswami, D., Walsh, L. A., Eng, S., Huse, J. T., Zhang, J., Dolgalev, I., Huberman, K., Heguy, A., Viale, A., Drobnjak, M., Leversha, M. A., Rice, C. E., Singh, B., … Chan, T. A. (2013). The mutational landscape of adenoid cystic carcinoma. *Nature Genetics 2013 45:7*, *45*(7), 791–798. https://doi.org/10.1038/ng.2643

Honigmann, A., van den Bogaart, G., Iraheta, E., Risselada, H. J., Milovanovic, D., Mueller, V., Müllar, S., Diederichsen, U., Fasshauer, D., Grubmüller, H., Hell, S. W., Eggeling, C., Kühnel, K., & Jahn, R. (2013). Phosphatidylinositol 4,5-bisphosphate clusters act as molecular beacons for vesicle recruitment. *Nature Structural & Molecular Biology*, *20*(6), 679–686. https://doi.org/10.1038/nsmb.2570

Hu, W., Lu, C., Dong, H. H., Huang, J., Shen, D., Stone, R. L., Nick, A. M., Shahzad, M. M. K., Mora, E., Jennings, N. B., Lee, S. J., Roh, J.-W., Matsuo, K., Nishimura, M., Goodman, B. W., Jaffe, R. B., Langley, R. R., Deavers, M. T., Lopez-Berestein, G., … Sood, A. K. (2011). Biological roles of the Delta family Notch ligand Dll4 in tumor and endothelial cells in ovarian cancer. *Cancer Research*, *71*(18), 6030–6039. https://doi.org/10.1158/0008-5472.CAN-10-2719

Huppert, S. S., Jacobsen, T. L., & Muskavitch, M. A. (1997). Feedback regulation is central to Delta-Notch signalling required for Drosophila wing vein morphogenesis. *Development (Cambridge, England)*, *124*(17), 3283–3291. https://doi.org/10.1242/dev.124.17.3283

Ikenouchi, J. (2018). Roles of membrane lipids in the organization of epithelial cells: Old and new problems. *Tissue Barriers*, *6*(2), 1–8. https://doi.org/10.1080/21688370.2018.1502531

Ikenouchi, J., Hirata, M., Yonemura, S., & Umeda, M. (2013). Sphingomyelin clustering is essential for the formation of microvilli. *Journal of Cell Science*, *126*(Pt 16), 3585–3592. https://doi.org/10.1242/jcs.122325

Ilagan, M. X. G., Lim, S., Fulbright, M., Piwnica-Worms, D., & Kopan, R. (2011). Real-time imaging of notch activation with a luciferase complementation-based reporter. *Science Signaling*, *4*(181), rs7–rs7. https://doi.org/10.1126/scisignal.2001656

Inada, M., Izawa, G., Kobayashi, W., & Ozawa, M. (2016). 293 cells express both epithelial as well as mesenchymal cell adhesion molecules. *International Journal of Molecular Medicine*, *37*(6), 1521–1527. https://doi.org/10.3892/ijmm.2016.2568

Indraccolo, S., Minuzzo, S., Masiero, M., & Amadori, A. (2010). Ligand-driven activation of the notch pathway in T-ALL and solid tumors: Why Not(ch)? *Cell Cycle (Georgetown, Tex.)*, *9*(1), 80–85. https://doi.org/10.4161/cc.9.1.10346

Irvine, K. D., & Wieschaus, E. (1994). Fringe, a Boundary-specific signaling molecule, mediates interactions between dorsal and ventral cells during Drosophila wing development. *Cell*, *79*(4), 595–606. https://doi.org/10.1016/0092-8674(94)90545-2

Iso, T., Maeno, T., Oike, Y., Yamazaki, M., Doi, H., Arai, M., & Kurabayashi, M. (2006). Dll4-selective Notch signaling induces ephrinB2 gene expression in endothelial cells. *Biochem Biophys Res Commun*, *341*(3), 708–714. https://doi.org/10.1016/j.bbrc.2006.01.020

Itoh, M., Kim, C. H., Palardy, G., Oda, T., Jiang, Y. J., Maust, D., Yeo, S. Y., Lorick, K., Wright, G. J., Ariza-McNaughton, L., Weissman, A. M., Lewis, J., Chandrasekharappa, S. C., & Chitnis, A. B. (2003). Mind bomb is a ubiquitin ligase that is essential for efficient activation of Notch signaling by Delta. *Developmental Cell*, *4*(1), 67–82. https://doi.org/10.1016/s1534-5807(02)00409-4

Jacobsen, T. L., Brennan, K., Arias, A. M., & Muskavitch, M. A. (1998). Cis-interactions between Delta and Notch modulate neurogenic signalling in Drosophila. *Development (Cambridge, England)*, *125*(22), 4531–4540. https://doi.org/10.1242/dev.125.22.4531

Jakobsson, L., Franco, C. A., Bentley, K., Collins, R. T., Ponsioen, B., Aspalter, I. M., Rosewell, I., Busse, M., Thurston, G., Medvinsky, A., Schulte-Merker, S., & Gerhardt, H. (2010). Endothelial cells dynamically compete for the tip cell position during angiogenic sprouting. *Nature Cell Biology*, *12*(10), 943–953. https://doi.org/10.1038/ncb2103

James, A. C., Szot, J. O., Iyer, K., Major, J. A., Pursglove, S. E., Chapman, G., & Dunwoodie, S. L. (2014). Notch4 reveals a novel mechanism regulating Notch signal transduction. *Biochimica et Biophysica Acta*, *1843*(7), 1272–1284. https://doi.org/10.1016/j.bbamcr.2014.03.015

Johansen, K. M., Fehon, R. G., & Artavanis-Tsakonas, S. (1989). The notch gene product is a glycoprotein expressed on the cell surface of both epidermal and neuronal precursor cells during Drosophila development. *The Journal of Cell Biology*, *109*(5), 2427–2440. https://doi.org/10.1083/jcb.109.5.2427

Johnston, S. H., Rauskolb, C., Wilson, R., Prabhakaran, B., Irvine, K. D., & Vogt, T. F. (1997). A family of mammalian Fringe genes implicated in boundary determination and the Notch pathway. *Development (Cambridge, England)*, *124*(11), 2245–2254. https://doi.org/10.1242/dev.124.11.2245

Joutel, A., Corpechot, C., Ducros, A., Vahedi, K., Chabriat, H., Mouton, P., Alamowitch, S., Domenga, V., Cécillion, M., Marechal, E., Maciazek, J., Vayssiere, C., Cruaud, C., Cabanis, E. A., Ruchoux, M. M., Weissenbach, J., Bach, J. F., Bousser, M. G., & Tournier-Lasserve, E. (1996). Notch3 mutations in CADASIL, a hereditary adult-onset condition causing stroke and dementia. *Nature*, *383*(6602), 707–710. https://doi.org/10.1038/383707a0

Jubb, A. M., Browning, L., Campo, L., Turley, H., Steers, G., Thurston, G., Harris, A. L., & Ansorge, O. (2012). Expression of vascular Notch ligands Delta-like 4 and Jagged-1 in glioblastoma. *Histopathology*, *60*(5), 740–747. https://doi.org/10.1111/J.1365-2559.2011.04138.X

Kaether, C., Schmitt, S., Willem, M., & Haass, C. (2006). Amyloid Precursor Protein and Notch Intracellular Domains are Generated after Transport of their Precursors to the Cell Surface. *Traffic*, *7*(4), 408–415. https://doi.org/10.1111/J.1600-0854.2006.00396.X

Kageyama, R., Ohtsuka, T., & Kobayashi, T. (2007). The Hes gene family: Repressors and oscillators that orchestrate embryogenesis. *Development*, *134*(7), 1243–1251. https://doi.org/10.1242/dev.000786

Kakuda, S., & Haltiwanger, R. S. (2017). Deciphering the Fringe-Mediated Notch Code: Identification of Activating and Inhibiting Sites Allowing Discrimination between Ligands. *Developmental Cell*, *40*(2), 193–201. https://doi.org/10.1016/j.devcel.2016.12.013

Kakuda, S., LoPilato, R. K., Ito, A., & Haltiwanger, R. S. (2020). Canonical Notch ligands and Fringes have distinct effects on NOTCH1 and NOTCH2. *Journal of Biological Chemistry*, *295*(43), 14710–14722. https://doi.org/10.1074/jbc.RA120.014407

Kamath, B. M., Spinner, N. B., & Rosenblum, N. D. (2013). Renal involvement and the role of Notch signalling in Alagille syndrome. *Nature Publishing Group*, *9*, 409–418. https://doi.org/10.1038/nrneph.2013.102

Kang, K., Lee, D., Hong, S., Park, S.-G., & Song, M.-R. (2013). The E3 Ligase Mind Bomb-1 (Mib1) Modulates Delta-Notch Signaling to Control Neurogenesis and Gliogenesis in the Developing Spinal Cord*. *Journal of Biological Chemistry*, *288*(4), 2580–2592. https://doi.org/10.1074/jbc.M112.398263

Käsbauer, T., Towb, P., Alexandrova, O., David, C. N., Dall'Armi, E., Staudigl, A., Stiening, B., & Böttger, A. (2007). The Notch signaling pathway in the cnidarian Hydra.

Developmental Biology, *303*(1), 376–390. Scopus. https://doi.org/10.1016/j.ydbio.2006.11.022

Kataoka, T., Togashi, K., Takayama, H., Takaku, K., & Nagai, K. (1997). Inactivation and proteolytic degradation of perforin within lytic granules upon neutralization of acidic pH. *Immunology*, *91*(3), 493–500. https://doi.org/10.1046/j.1365-2567.1997.00257.x

Katic, I., Vallier, L. G., & Greenwald, I. (2005). New Positive Regulators of lin-12 Activity in Caenorhabditis elegans Include the BRE-5/Brainiac Glycosphingolipid Biosynthesis Enzyme. *Genetics*, *171*(4), 1605–1615. https://doi.org/10.1534/GENETICS.105.048041

Kershaw, N. J., Church, N. L., Griffin, M. D. W., Luo, C. S., Adams, T. E., & Burgess, A. W. (2015). Notch ligand delta-like1: X-ray crystal structure and binding affinity. *The Biochemical Journal*, *468*(1), 159–166. https://doi.org/10.1042/BJ20150010

Khan, H. M., He, T., Fuglebakk, E., Grauffel, C., Yang, B., Roberts, M. F., Gershenson, A., & Reuter, N. (2016). A Role for Weak Electrostatic Interactions in Peripheral Membrane Protein Binding. *Biophysical Journal*, *110*(6), 1367–1378. https://doi.org/10.1016/j.bpj.2016.02.020

Khoshamooz, H., Kaviani, S., Atashi, A., & Mirpour Hassankiadeh, S. H. (2020). Combination Effect of Notch1 and PI3K/AKT/mTOR Signaling Pathways Inhibitors on T-ALL Cell Lines. *International Journal of Hematology-Oncology and Stem Cell Research*, *14*(2), 99–109.

Kidd, S., Kelley, M. R., & Young, M. W. (1986). Sequence of the notch locus of Drosophila melanogaster: Relationship of the encoded protein to mammalian clotting and growth factors. *Molecular and Cellular Biology*, *6*(9), 3094–3108. https://doi.org/10.1128/mcb.6.9.3094-3108.1986

Kidd, S., & Lieber, T. (2002). Furin cleavage is not a requirement for Drosophila Notch function. *Mechanisms of Development*, *115*(1–2), 41–51. https://doi.org/10.1016/s0925-4773(02)00120-x

Kim, E. J., Kim, S. O., Jin, X., Ham, S. W., Kim, J., Park, J. B., Lee, J. Y., Kim, S. C., & Kim, H. (2015). Epidermal growth factor receptor variant III renders glioma cancer cells less differentiated by JAGGED1. *Tumor Biology*, *36*(4), 2921–2928. https://doi.org/10.1007/S13277-014-2922-9/FIGURES/4

Kiyota, T., & Kinoshita, T. (2002). Cysteine-rich region of X-Serrate-1 is required for activation of Notch signaling in Xenopus primary neurogenesis. *International Journal of Developmental Biology*, *46*(8), 1057–1060. https://doi.org/10.1387/IJDB.12533029

Klein, T., Brennan, K., & Arias, A. M. (1997). An intrinsic dominant negative activity of serrate that is modulated during wing development in Drosophila. *Developmental Biology*, *189*(1), 123–134. https://doi.org/10.1006/dbio.1997.8564

Klose, R., Berger, C., Moll, I., Adam, M. G., Schwarz, F., Mohr, K., Augustin, H. G., & Fischer, A. (2015). Soluble Notch ligand and receptor peptides act antagonistically during angiogenesis. *Cardiovascular Research*, *107*(1), 153–163. https://doi.org/10.1093/cvr/cvv151

Klueg, K. M., & Muskavitch, M. A. T. (1999). Ligand-receptor interactions and trans-endocytosis of Delta, Serrate and Notch: Members of the Notch signalling pathway in Drosophila. *Journal of Cell Science*, *112 (Pt 1*(19), 3289–3297. https://doi.org/10.1242/JCS.112.19.3289

Kobayashi, T., & Kageyama, R. (2010). Hes1 regulates embryonic stem cell differentiation by suppressing Notch signaling. *Genes to Cells : Devoted to Molecular & Cellular Mechanisms*, *15*(7), 689–698. https://doi.org/10.1111/j.1365-2443.2010.01413.x

Kobia, F. M., Preusse, K., Dai, Q., Weaver, N., Hass, M. R., Chaturvedi, P., Stein, S. J., Pear, W. S., Yuan, Z., Kovall, R. A., Kuang, Y., Eafergen, N., Sprinzak, D., Gebelein, B., Brunskill, E. W., & Kopan, R. (2020). Notch dimerization and gene dosage are important for normal heart development, intestinal stem cell maintenance, and splenic marginal zone B-cell homeostasis during mite infestation. *PLOS Biology*, *18*(10), e3000850. https://doi.org/10.1371/journal.pbio.3000850

Kohsaka, T., Yuan, Z., Guo, S., Tagawa, M., Nakamura, A., Nakano, M., Kawasasaki, H., Inomata, Y., Tanaka, K., & Miyauchi, J. (2002). The significance of human jagged 1 mutations detected in severe cases of extrahepatic biliary atresia. *Hepatology*, *36*(4), 904–912. https://doi.org/10.1053/jhep.2002.35820

Koichi, K., Michiya, F., & Makoto, N. (1974). Lipid components of two different regions of an intestinal epithelial cell membrane of mouse. *Biochimica et Biophysica Acta (BBA) - Lipids and Lipid Metabolism*, *369*(2), 222–233. https://doi.org/10.1016/0005-2760(74)90253-7

Komatsu, H., Chao, M. Y., Larkins-Ford, J., Corkins, M. E., Somers, G. A., Tucey, T., Dionne, H. M., White, J. Q., Wani, K., Boxem, M., & Hart, A. C. (2008). OSM-11 facilitates LIN-12 Notch signaling during Caenorhabditis elegans vulval development. *PLoS Biology*, *6*(8), e196. https://doi.org/10.1371/journal.pbio.0060196

Kopan, R., & Ilagan, M. X. G. (2009). The Canonical Notch Signaling Pathway: Unfolding the Activation Mechanism. In *Cell*. https://doi.org/10.1016/j.cell.2009.03.045

Kosaka, K., Takayama, N., Paul, S. K., Kanashiro, M. A., Oshima, M., Fukuyo, M., Rahmutulla, B., Tajiri, I., Mukai, M., Kubota, Y., Akita, S., Furuyama, N., Kaneda, A., Iwama, A., Eto, K., & Mitsukawa, N. (2024). iPSC-derived megakaryocytes and platelets accelerate wound healing and angiogenesis. *Stem Cell Research & Therapy*, *15*(1), 364. https://doi.org/10.1186/s13287-024-03966-z

Koutelou, E., Sato, S., Tomomori-Sato, C., Florens, L., Swanson, S. K., Washburn, M. P., Kokkinaki, M., Conaway, R. C., Conaway, J. W., & Moschonas, N. K. (2008).

Neuralized-like 1 (Neurl1) targeted to the plasma membrane by N-myristoylation regulates the Notch ligand Jagged1. *J Biol Chem*, *283*(7), 3846–3853. https://doi.org/10.1074/jbc.M706974200

Kuang, Y., Pyo, A., Eafergan, N., Cain, B., Gutzwiller, L. M., Axelrod, O., Gagliani, E. K., Weirauch, M. T., Kopan, R., Kovall, R. A., Sprinzak, D., & Gebelein, B. (2021). Enhancers with cooperative Notch binding sites are more resistant to regulation by the Hairless co-repressor. *PLoS Genetics*, *17*(9), e1009039. https://doi.org/10.1371/journal.pgen.1009039

Kuintzle, R., Santat, L. A., & Elowitz, M. B. (2023). *Diversity in Notch ligand-receptor signaling interactions*. https://doi.org/10.1101/2023.08.24.554677

Kuo, W., Herrick, D. Z., Ellena, J. F., & Cafiso, D. S. (2009). The Calcium-Dependent and Calcium-Independent Membrane Binding of Synaptotagmin 1: Two Modes of C2B Binding. *Journal of Molecular Biology*, *387*(2), 284–294. https://doi.org/10.1016/j.jmb.2009.01.064

Lahmann, I., Bröhl, D., Zyrianova, T., Isomura, A., Czajkowski, M. T., Kapoor, V., Griger, J., Ruffault, P.-L., Mademtzoglou, D., Zammit, P. S., Wunderlich, T., Spuler, S., Kühn, R., Preibisch, S., Wolf, J., Kageyama, R., & Birchmeier, C. (2019). Oscillations of MyoD and Hes1 proteins regulate the maintenance of activated muscle stem cells. *Genes & Development*, *33*(9–10), 524–535. https://doi.org/10.1101/gad.322818.118

Lai, E. C., Deblandre, G. A., Kintner, C., & Rubin, G. M. (2001). Drosophila neuralized is a ubiquitin ligase that promotes the internalization and degradation of delta. *Developmental Cell*, *1*(6), 783–794. https://doi.org/10.1016/s1534-5807(01)00092-2

Lai, E. C., Roegiers, F., Qin, X., Jan, Y. N., & Rubin, G. M. (2005). The ubiquitin ligase Drosophila Mind bomb promotes Notch signaling by regulating the localization and activity of Serrate and Delta. *Development (Cambridge, England)*, *132*(10), 2319–2332. https://doi.org/10.1242/dev.01825

Lai, N., Jayaraman, A., & Lee, K. (2009). Enhanced proliferation of human umbilical vein endothelial cells and differentiation of 3T3-L1 adipocytes in coculture. *Tissue Engineering. Part A*, *15*(5), 1053–1061. https://doi.org/10.1089/ten.tea.2008.0101

Lambie, E. J., & Kimble, J. (1991). Two homologous regulatory genes, lin-12 and glp-1, have overlapping functions. *Development (Cambridge, England)*, *112*(1), 231–240. https://doi.org/10.1242/dev.112.1.231

Lardelli, M., Williams, R., & Lendahl, U. (1995). Notch-related genes in animal development. *Int J Dev Biol*, *39*(5), 769–780.

Larsen, A. H., John, L. H., Sansom, M. S. P., & Corey, R. A. (2022). Specific interactions of peripheral membrane proteins with lipids: What can molecular simulations show us? *Bioscience Reports*, *42*(4). https://doi.org/10.1042/BSR20211406

Larsen, A. H., & Sansom, M. S. P. (2021). Binding of Ca2+-independent C2 domains to lipid membranes: A multi-scale molecular dynamics study. *Structure*. https://doi.org/10.1016/J.STR.2021.05.011

Lau, S., Gossen, M., Lendlein, A., & Jung, F. (2022). Differential sensitivity of assays for determining vein endothelial cell senescence. *Clinical Hemorheology and Microcirculation*, *81*(3), 191–203. https://doi.org/10.3233/CH-211294

Law, R. H. P., Lukoyanova, N., Voskoboinik, I., Caradoc-Davies, T. T., Baran, K., Dunstone, M. A., D'angelo, M. E., Orlova, E. V, Coulibaly, F., Verschoor, S., Browne, K. A., Ciccone, A., Kuiper, M. J., Bird, P. I., Trapani, J. A., Saibil, H. R., & Whisstock, J. C. (2010). The structural basis for membrane binding and pore formation by lymphocyte perforin. *Nature*, *468*. https://doi.org/10.1038/nature09518

Le Borgne, R., Remaud, S., Hamel, S., & Schweisguth, F. (2005). Two Distinct E3 Ubiquitin Ligases Have Complementary Functions in the Regulation of Delta and Serrate Signaling in Drosophila. *PLoS Biology*, *3*(4), e96. https://doi.org/10.1371/journal.pbio.0030096

Le Bras, S., Loyer, N., & Le Borgne, R. (2011). The Multiple Facets of Ubiquitination in the Regulation of Notch Signaling Pathway. *Traffic*, *12*(2), 149–161. https://doi.org/10.1111/j.1600-0854.2010.01126.x

Le Caignec, C., Lefevre, M., Schott, J. J., Chaventre, A., Gayet, M., Calais, C., & Moisan, J. P. (2002). Familial deafness, congenital heart defects, and posterior embryotoxon caused by cysteine substitution in the first epidermal-growth-factor-like domain of jagged 1. *American Journal of Human Genetics*, *71*(1), 180–186. https://doi.org/10.1086/341327

Le Friec, G., Sheppard, D., Whiteman, P., Karsten, C. M., Shamoun, S. A.-T., Laing, A., Bugeon, L., Dallman, M. J., Melchionna, T., Chillakuri, C., Smith, R. A., Drouet, C., Couzi, L., Fremeaux-Bacchi, V., Köhl, J., Waddington, S. N., McDonnell, J. M., Baker, A., Handford, P. A., … Kemper, C. (2012). The CD46-Jagged1 interaction is critical for human TH1 immunity. *Nature Immunology*, *13*(12), 1213–1221. https://doi.org/10.1038/ni.2454

LeBon, L., Lee, T. V., Sprinzak, D., Jafar-Nejad, H., & Elowitz, M. B. (2014). Fringe proteins modulate Notch-ligand cis and trans interactions to specify signaling states. *eLife*, *3*, e02950. https://doi.org/10.7554/eLife.02950

Lee, H. S., Qi, Y., & Im, W. (2015). Effects of N-glycosylation on protein conformation and dynamics: Protein Data Bank analysis and molecular dynamics simulation study. *Scientific Reports*, *5*. Scopus. https://doi.org/10.1038/srep08926

Lee, H.-J., Kim, M.-Y., & Park, H.-S. (2015). Phosphorylation-dependent regulation of Notch1 signaling: The fulcrum of Notch1 signaling. *BMB Reports*, *48*(8), 431–437. https://doi.org/10.5483/bmbrep.2015.48.8.107

Lee, J.-O., Yang, H., Georgescu, M.-M., Di Cristofano, A., Maehama, T., Shi, Y., Dixon, J. E., Pandolfi, P., & Pavletich, N. P. (1999). Crystal Structure of the PTEN Tumor Suppressor: Implications for Its Phosphoinositide Phosphatase Activity and Membrane Association. *Cell*, *99*(3), 323–334. https://doi.org/10.1016/S0092-8674(00)81663-3

Lefevre, G. (1955). Mutation Isoalleles at the Yellow Locus in Drosophila Melanogaster. *Genetics*, *40*(3), 374–387. https://doi.org/10.1093/genetics/40.3.374

Lehmann, R., Jim\simnez, F., Dietrich, U., & Campos-Ortega, J. A. (1983). On the Phenotype and Development of Mutants of Early Neurogenesis in Drosophila melanogaster. In *Arch Dev Biol* (Vol. 192, pp. 62–74). https://link.springer.com/content/pdf/10.1007%2FBF00848482.pdf

Leonardi, J., Fernandez-Valdivia, R., Li, Y.-D., Simcox, A. A., & Jafar-Nejad, H. (2011). Multiple O-glucosylation sites on Notch function as a buffer against temperature-dependent loss of signaling. *Development (Cambridge, England)*, *138*(16), 3569–3578. https://doi.org/10.1242/dev.068361

Li, J. C. (1927). Development in DROSOPHILA MELANOGASTER. *Genetics*, *12*(1), 1–58. https://doi.org/10.1093/genetics/12.1.1

Li, J.-L., Sainson, R. C. A., Shi, W., Leek, R., Harrington, L. S., Preusser, M., Biswas, S., Turley, H., Heikamp, E., Hainfellner, J. A., & Harris, A. L. (2007). Delta-like 4 Notch Ligand Regulates Tumor Angiogenesis, Improves Tumor Vascular Function, and Promotes Tumor Growth In vivo. *Cancer Research*, *67*(23), 11244–11253. https://doi.org/10.1158/0008-5472.CAN-07-0969

Li, L., Krantz, I. D., Deng, Y., Genin, A., Banta, A. B., Collins, C. C., Qi, M., Trask, B. J., Kuo, W. L., Cochran, J., Costa, T., Pierpont, M. E. M., Rand, E. B., Piccoli, D. A., Hood, L., & Spinner, N. B. (1997). Alagille syndrome is caused by mutations in human Jagged1, which encodes a ligand for Notch1. *Nature Genetics*, *16*(3), 243–251. https://doi.org/10.1038/ng0797-243

Li, S.-T., Lu, T.-T., Xu, X.-X., Ding, Y., Li, Z., Kitajima, T., Dean, N., Wang, N., & Gao, X.-D. (2019). Reconstitution of the lipid-linked oligosaccharide pathway for assembly of high-mannose N-glycans. *Nature Communications*, *10*(1), 1813. https://doi.org/10.1038/s41467-019-09752-3

Li, T., Aredo, B., Zhang, K., Zhong, X., Pulido, J. S., Wang, S., He, Y.-G., Huang, X., Brekken, R. A., & Ufret-Vincenty, R. L. (2015). Phosphatidylserine (PS) Is Exposed in Choroidal Neovascular Endothelium: PS-Targeting Antibodies Inhibit Choroidal Angiogenesis In Vivo and Ex Vivo. *Investigative Ophthalmology & Visual Science*, *56*(12), 7137–7145. https://doi.org/10.1167/iovs.15-17302

Liefke, R., Oswald, F., Alvarado, C., Ferres-Marco, D., Mittler, G., Rodriguez, P., Dominguez, M., & Borggrefe, T. (2010). Histone demethylase KDM5A is an integral part of the

core Notch-RBP-J repressor complex. *Genes & Development*, *24*(6), 590–601. https://doi.org/10.1101/gad.563210

Lim, J. S., Ibaseta, A., Fischer, M. M., Cancilla, B., O'Young, G., Cristea, S., Luca, V. C., Yang, D., Jahchan, N. S., Hamard, C., Antoine, M., Wislez, M., Kong, C., Cain, J., Liu, Y.-W., Kapoun, A. M., Garcia, K. C., Hoey, T., Murriel, C. L., & Sage, J. (2017). Intratumoural heterogeneity generated by Notch signalling promotes small-cell lung cancer. *Nature*, *545*(7654), 360–364. https://doi.org/10.1038/nature22323

Lin, S., Shen, H., Jin, B., Gu, Y., Chen, Z., Cao, C., Hu, C., Keller, C., Pear, W. S., & Wu, L. (2013). Brief report: Blockade of Notch signaling in muscle stem cells causes muscular dystrophic phenotype and impaired muscle regeneration. *Stem Cells (Dayton, Ohio)*, *31*(4), 823–828. https://doi.org/10.1002/stem.1319

Lin, Y.-C., Boone, M., Meuris, L., Lemmens, I., Van Roy, N., Soete, A., Reumers, J., Moisse, M., Plaisance, S., Drmanac, R., Chen, J., Speleman, F., Lambrechts, D., Van de Peer, Y., Tavernier, J., & Callewaert, N. (2014). Genome dynamics of the human embryonic kidney 293 lineage in response to cell biology manipulations. *Nature Communications*, *5*(1), 4767. https://doi.org/10.1038/ncomms5767

Livak, K. J., & Schmittgen, T. D. (2001). Analysis of relative gene expression data using real-time quantitative PCR and the 2(-Delta Delta C(T)) Method. *Methods (San Diego, Calif.)*, *25*(4), 402–408. https://doi.org/10.1006/meth.2001.1262

Lobov, I. B., Renard, R. A., Papadopoulos, N., Gale, N. W., Thurston, G., Yancopoulos, G. D., & Wiegand, S. J. (2007). Delta-like ligand 4 (Dll4) is induced by VEGF as a negative regulator of angiogenic sprouting. *Proceedings of the National Academy of Sciences*, *104*(9), 3219–3224. https://doi.org/10.1073/pnas.0611206104

Logeat, F., Bessia, C., Brou, C., LeBail, O., Jarriault, S., Seidah, N. G., & Israël, A. (1998). The Notch1 receptor is cleaved constitutively by a furin-like convertase. *Proceedings of the National Academy of Sciences of the United States of America*, *95*(14), 8108–8112. https://doi.org/10.1073/PNAS.95.14.8108/ASSET/009C6B77-98CE-4BE0-BC51-0E6FB5E43A39/ASSETS/GRAPHIC/PQ1481625005.JPEG

Logeay, R., Géminard, C., Lassus, P., Rodríguez-Vázquez, M., Kantar, D., Heron-Milhavet, L., Fischer, B., Bray, S. J., Colinge, J., & Djiane, A. (2022). Mechanisms underlying the cooperation between loss of epithelial polarity and Notch signaling during neoplastic growth in *Drosophila*. *Development*, *149*(3). https://doi.org/10.1242/dev.200110

Lopez, J. A., Susanto, O., Jenkins, M. R., Lukoyanova, N., Sutton, V. R., Law, R. H. P., Johnston, A., Bird, C. H., Bird, P. I., Whisstock, J. C., Trapani, J. A., Saibil, H. R., & Voskoboinik, I. (2013). Perforin forms transient pores on the target cell plasma membrane to facilitate rapid access of granzymes during killer cell attack. *Blood*, *121*(14), 2659–2668. https://doi.org/10.1182/blood-2012-07-446146

Lopez, P. H. H., & Schnaar, R. L. (2009). Gangliosides in cell recognition and membrane protein regulation. *Current Opinion in Structural Biology*, *19*(5), 549–557. https://doi.org/10.1016/j.sbi.2009.06.001

Lowell, S., Jones, P., Le Roux, I., Dunne, J., & Watt, F. M. (2000). Stimulation of human epidermal differentiation by Delta-Notch signalling at the boundaries of stem-cell clusters. *Current Biology*. https://doi.org/10.1016/S0960-9822(00)00451-6

Lu, F., Morrissette, J. J. D., & Spinner, N. B. (2003). Conditional JAG1 mutation shows the developing heart is more sensitive than developing liver to JAG1 dosage. *American Journal of Human Genetics*, *72*(4), 1065–1070. https://doi.org/10.1086/374386

Luca, V. C., Jude, K. M., Pierce, N. W., Nachury, M. V., Fischer, S., & Garcia, K. C. (2015). Structural basis for Notch1 engagement of Delta-like 4. *Science*, *347*(6224), 847. https://doi.org/10.1126/science.1261093

Luca, V. C., Kim, B. C., Ge, C., Kakuda, S., Wu, D., Roein-Peikar, M., Haltiwanger, R. S., Zhu, C., Ha, T., & Garcia, K. C. (2017). Notch-Jagged complex structure implicates a catch bond in tuning ligand sensitivity. *Science*, *355*(6331), 1320–1324. https://doi.org/10.1126/science.aaf9739

Ma, W., Du, J., Chu, Q., Wang, Y., Liu, L., Song, M., & Wang, W. (2011). hCLP46 regulates U937 cell proliferation via Notch signaling pathway. *Biochemical and Biophysical Research Communications*, *408*(1), 84–88. https://doi.org/10.1016/j.bbrc.2011.03.124

Maeda, Y., Isomura, A., Masaki, T., & Kageyama, R. (2023). Differential cell-cycle control by oscillatory versus sustained Hes1 expression via p21. *Cell Reports*, *42*(5). https://doi.org/10.1016/j.celrep.2023.112520

Manderfield, L. J., High, F. A., Engleka, K. A., Liu, F., Li, L., Rentschler, S., & Epstein, J. A. (2012). Notch activation of Jagged1 contributes to the assembly of the arterial wall. *Circulation*, *125*(2), 314–323. https://doi.org/10.1161/CIRCULATIONAHA.111.047159

Marchetto, N. M., Begum, S., Wu, T., O'Besso, V., Yarborough, C. C., Valero-Pacheco, N., Beaulieu, A. M., Kitajewski, J. K., Shawber, C. J., & Douglas, N. C. (2020). Endothelial Jagged1 Antagonizes Dll4/Notch Signaling in Decidual Angiogenesis during Early Mouse Pregnancy. *International Journal of Molecular Sciences*, *21*(18). https://doi.org/10.3390/ijms21186477

Martin, A. P., Bradshaw, G. A., Eisert, R. J., Egan, E. D., Tveriakhina, L., Rogers, J. M., Dates, A. N., Scanavachi, G., Aster, J. C., Kirchhausen, T., Kalocsay, M., & Blacklow, S. C. (2023). A spatiotemporal Notch interaction map from plasma membrane to nucleus. *Science Signaling*, *16*(796), eadg6474. https://doi.org/10.1126/scisignal.adg6474

Martincorena, I., Fowler, J. C., Wabik, A., Lawson, A. R. J., Abascal, F., Hall, M. W. J., Cagan, A., Murai, K., Mahbubani, K., Stratton, M. R., Fitzgerald, R. C., Handford, P. A.,

Campbell, P. J., Saeb-Parsy, K., & Jones, P. H. (2018). Somatic mutant clones colonize the human esophagus with age. *Science (New York, N.Y.)*, *362*(6417), 911–917. https://doi.org/10.1126/science.aau3879

Martins, T., Meng, Y., Korona, B., Suckling, R., Johnson, S., Handford, P. A., Lea, S. M., & Bray, S. J. (2021). The conserved C2 phospholipid-binding domain in Delta contributes to robust Notch signalling. *EMBO Reports*, *22*(10), e52729. https://doi.org/10.15252/embr.202152729

Masiero, M., Li, D., Whiteman, P., Bentley, C., Greig, J., Hassanali, T., Watts, S., Stribbling, S., Yates, J., Bealing, E., Li, J. L., Chillakuri, C., Sheppard, D., Serres, S., Sarmiento-Soto, M., Larkin, J., Sibson, N. R., Handford, P. A., Harris, A. L., & Banham, A. H. (2019). Development of Therapeutic Anti-JAGGED1 Antibodies for Cancer Therapy. *Molecular Cancer Therapeutics*, *18*(11), 2030–2042. https://doi.org/10.1158/1535-7163.MCT-18-1176

Matsuda, M., & Chitnis, A. B. (2009). Interaction with Notch determines endocytosis of specific Delta ligands in zebrafish neural tissue. *Development (Cambridge, England)*, *136*(2), 197–206. https://doi.org/10.1242/dev.027938

Matsuno, K., Diederich, R. J., Go, M. J., Blaumueller, C. M., & Artavanis-Tsakonas, S. (1995). Deltex acts as a positive regulator of Notch signaling through interactions with the Notch ankyrin repeats. *Development (Cambridge, England)*, *121*(8), 2633–2644.

Maya Kamath, B., Bauer, R. C., Loomes, K. M., Chao, G., Gerfen, J., Hutchinson, A., Hardikar, W., Hirschfield, G., Jara, P., Krantz, I. D., Lapunzina, P., Leonard, L., Ling, S., Lee Ng, V., Le Hoang, P., Piccoli, D. A., & Bettina Spinner, N. (2012). *NOTCH2 mutations in Alagille syndrome*. 138–144. https://doi.org/10.1136/jmedgenet-2011-100544

McLaughlin, S., Wang, J., Gambhir, A., & Murray, D. (2002). PIP(2) and proteins: Interactions, organization, and information flow. *Annual Review of Biophysics and Biomolecular Structure*, *31*, 151–175. https://doi.org/10.1146/annurev.biophys.31.082901.134259

Meester, J. A. N., Southgate, L., Stittrich, A. B., Venselaar, H., Beekmans, S. J., den Hollander, N., Bijlsma, E. K., Helderman-van den Enden, A., Verheij, J. B., Glusman, G., Roach, J. C., Lehman, A., Patel, M. S., de Vries, B. B., Ruivenkamp, C., Itin, P., Prescott, K., Clarke, S., Trembath, R., … Wuyts, W. (2015). Heterozygous Loss-of-Function Mutations in DLL4 Cause Adams-Oliver Syndrome. *American Journal of Human Genetics*, *97*(3), 475–482. https://doi.org/10.1016/j.ajhg.2015.07.015

Meester, J. A. N., Verstraeten, A., Alaerts, M., Schepers, D., Van Laer, L., & Loeys, B. L. (2019). Overlapping but distinct roles for NOTCH receptors in human cardiovascular disease. *Clinical Genetics*, *95*(1), 85–94. https://doi.org/10.1111/cge.13382

Meloty-Kapella, L., Shergill, B., Kuon, J., Botvinick, E., & Weinmaster, G. (2012). Notch ligand endocytosis generates mechanical pulling force dependent on dynamin, epsins, and

actin. *Developmental Cell*, *22*(6), 1299–1312. https://doi.org/10.1016/j.devcel.2012.04.005

Mendonça, L., Trindade, A., Carvalho, C., Correia, J., Badenes, M., Gigante, J., & Duarte, A. (2019). Metastasis is impaired by endothelial-specific Dll4 loss-of-function through inhibition of epithelial-to-mesenchymal transition and reduction of cancer stem cells and circulating tumor cells. *Clinical & Experimental Metastasis*, *36*(4), 365–380. https://doi.org/10.1007/s10585-019-09973-2

Meng, Y., Bo, Z., Feng, X., Yang, X., & Handford, P. A. (2023). The Notch Signaling Pathway: Mechanistic Insights in Health and Disease. *Engineering*. https://doi.org/10.1016/j.eng.2023.11.011

Meng, Y., Sanlidag, S., Jensen, S. A., Burnap, S. A., Struwe, W. B., Larsen, A. H., Feng, X., Mittal, S., Sansom, M. S. P., Sahlgren, C., & Handford, P. A. (2022). An N-glycan on the C2 domain of JAGGED1 is important for Notch activation. *Science Signaling*, *15*(755), eabo3507. https://doi.org/10.1126/scisignal.abo3507

Micchelli, C. A., Rulifson, E. J., & Blair, S. S. (1997). The function and regulation of cut expression on the wing margin of Drosophila: Notch, Wingless and a dominant negative role for Delta and Serrate. *Development (Cambridge, England)*, *124*(8), 1485–1495. https://doi.org/10.1242/dev.124.8.1485

Michaels, Y. S., Edgar, J. M., Major, M. C., Castle, E. L., Zimmerman, C., Yin, T., Hagner, A., Lau, C., Hsu, H. H., Ibañez-Rios, M. I., Durland, L. J., Knapp, D. J. H. F., & Zandstra, P. W. (2022). DLL4 and VCAM1 enhance the emergence of T cell–competent hematopoietic progenitors from human pluripotent stem cells. *Science Advances*, *8*(34), eabn5522. https://doi.org/10.1126/sciadv.abn5522

Miller, A. C., Lyons, E. L., & Herman, T. G. (2009). Cis-Inhibition of Notch by endogenous Delta biases the outcome of lateral inhibition. *Current Biology : CB*, *19*(16), 1378–1383. https://doi.org/10.1016/j.cub.2009.06.042

Minnis-Lyons, S. E., Ferreira-González, S., Aleksieva, N., Man, T. Y., Gadd, V. L., Williams, M. J., Guest, R. V., Lu, W.-Y., Dwyer, B. J., Jamieson, T., Nixon, C., Van Hul, N., Lemaigre, F. P., McCafferty, J., Leclercq, I. A., Sansom, O. J., Boulter, L., & Forbes, S. J. (2021). Notch-IGF1 signaling during liver regeneration drives biliary epithelial cell expansion and inhibits hepatocyte differentiation. *Science Signaling*, *14*(688), eaay9185. https://doi.org/10.1126/scisignal.aay9185

Minuzzo, S., Agnusdei, V., Pusceddu, I., Pinazza, M., Moserle, L., Masiero, M., Rossi, E., Crescenzi, M., Hoey, T., Ponzoni, M., Amadori, A., & Indraccolo, S. (2015). DLL4 regulates NOTCH signaling and growth of T acute lymphoblastic leukemia cells in NOD/SCID mice. *Carcinogenesis*, *36*(1), 115–121. https://doi.org/10.1093/carcin/bgu223

Mo, J.-S., Kim, M.-Y., Han, S.-O., Kim, I.-S., Ann, E.-J., Lee, K. S., Seo, M.-S., Kim, J.-Y., Lee, S.-C., Park, J.-W., Choi, E.-J., Seong, J. Y., Joe, C. O., Faessler, R., & Park, H.-S. (2007). Integrin-linked kinase controls Notch1 signaling by down-regulation of protein stability through Fbw7 ubiquitin ligase. *Molecular and Cellular Biology*, *27*(15), 5565–5574. https://doi.org/10.1128/MCB.02372-06

Moloney, D. J., Panin, V. M., Johnston, S. H., Chen, J., Shao, L., Wilson, R., Wang, Y., Stanley, P., Irvine, K. D., Haltiwanger, R. S., & Vogt, T. F. (2000). Fringe is a glycosyltransferase that modifies Notch. *Nature*, *406*(6794), 369–375. https://doi.org/10.1038/35019000

Moloney, D. J., Shair, L. H., Lu, F. M., Xia, J., Locke, R., Matta, K. L., & Haltiwanger, R. S. (2000). *Mammalian Notch1 Is Modified with Two Unusual Forms of O-Linked Glycosylation Found on Epidermal Growth Factor-like Modules**. http://www.jbc.org/

Monahan, P., Rybak, S., & Raetzman, L. T. (2009). The notch target gene HES1 regulates cell cycle inhibitor expression in the developing pituitary. *Endocrinology*, *150*(9), 4386–4394. https://doi.org/10.1210/en.2009-0206

Monk, N. A. M. (2003). Oscillatory Expression of Hes1, p53, and NF-κB Driven by Transcriptional Time Delays. *Current Biology*, *13*(16), 1409–1413. https://doi.org/10.1016/S0960-9822(03)00494-9

Moretti, J., & Brou, C. (2013). Ubiquitinations in the Notch Signaling Pathway. *International Journal of Molecular Sciences*, *14*(3), 6359–6381.

Morgan, T. H. (1917). The Theory of the Gene. *The American Naturalist*, *51*(609), 513–544. https://doi.org/10.1086/279629

Morgan, T. H., B., C. B. (1923). *The third-chromosome group of mutant characters of Drosophila melanogaster*.

Morrissette, J. J. D., Colliton, R. P., & Spinner, N. B. (2001). Defective intracellular transport and processing of JAG1 missense mutations in Alagille syndrome. *Human Molecular Genetics*, *10*(4), 405–413. https://doi.org/10.1093/HMG/10.4.405

Morsut, L., Roybal, K. T., Xiong, X., Gordley, R. M., Coyle, S. M., Thomson, M., Lim Correspondence, W. A., & Lim, W. A. (2016). Engineering Customized Cell Sensing and Response Behaviors Using Synthetic Notch Receptors. *Cell*, *164*, 780–791. https://doi.org/10.1016/j.cell.2016.01.012

Mourikis, P., Sambasivan, R., Castel, D., Rocheteau, P., Bizzarro, V., & Tajbakhsh, S. (2012). A critical requirement for notch signaling in maintenance of the quiescent skeletal muscle stem cell state. *Stem Cells (Dayton, Ohio)*, *30*(2), 243–252. https://doi.org/10.1002/stem.775

Müller, R., Jenny, A., & Stanley, P. (2013). The EGF repeat-specific O-GlcNAc-transferase Eogt interacts with notch signaling and pyrimidine metabolism pathways in Drosophila. *PloS One*, *8*(5), e62835. https://doi.org/10.1371/journal.pone.0062835

Murphy, E. J., Joseph, L., Stephens, R., & Horrocks, L. A. (1992). Phospholipid composition of cultured human endothelial cells. *Lipids*, *27*(2), 150–153. https://doi.org/10.1007/BF02535816

Murray, D., & Honig, B. (2002). Electrostatic Control of the Membrane Targeting of C2 Domains. *Molecular Cell*, *9*(1), 145–154. https://doi.org/10.1016/S1097-2765(01)00426-9

Nagasaka, M., Taniguchi-Ikeda, M., Inagaki, H., Ouchi, Y., Kurokawa, D., Yamana, K., Harada, R., Nozu, K., Sakai, Y., Mishra, S. K., Yamaguchi, Y., Morioka, I., Toda, T., Kurahashi, H., & Iijima, K. (2017). Novel missense mutation in DLL4 in a Japanese sporadic case of Adams–Oliver syndrome. *Journal of Human Genetics*, *62*(9), 851–855. https://doi.org/10.1038/jhg.2017.48

Nalefski, E. A., Wisner, M. A., Chen, J. Z., Sprang, S. R., Fukuda, M., Mikoshiba, K., & Falke, J. J. (2001). C2 domains from different Ca2+ signaling pathways display functional and mechanistic diversity. *Biochemistry*, *40*(10), 3089–3100. https://doi.org/10.1021/bi001968a

Nandagopal, N., Santat, L. A., & Elowitz, M. B. (2019). Cis-activation in the Notch signaling pathway. *eLife*, *8*. https://doi.org/10.7554/eLife.37880

Nandagopal, N., Santat, L. A., LeBon, L., Sprinzak, D., Bronner, M. E., & Elowitz, M. B. (2018). Dynamic Ligand Discrimination in the Notch Signaling Pathway. *Cell*, *172*(4), 869-880.e19. https://doi.org/10.1016/j.cell.2018.01.002

Narasimhan, S. (1982). Control of glycoprotein synthesis. UDP-GlcNAc:glycopeptide beta 4-N-acetylglucosaminyltransferase III, an enzyme in hen oviduct which adds GlcNAc in beta 1-4 linkage to the beta-linked mannose of the trimannosyl core of N-glycosyl oligosaccharides. *The Journal of Biological Chemistry*, *257*(17), 10235–10242.

Negri, V. A., Logtenberg, M. E. W., Renz, L. M., Oules, B., Walko, G., & Watt, F. M. (2019). Delta-like 1-mediated cis-inhibition of Jagged1/2 signalling inhibits differentiation of human epidermal cells in culture. *Scientific Reports*, *9*(1), 10825. https://doi.org/10.1038/s41598-019-47232-2

Nichols, J. T., Miyamoto, A., Olsen, S. L., D'Souza, B., Yao, C., & Weinmaster, G. (2007). DSL ligand endocytosis physically dissociates Notch1 heterodimers before activating proteolysis can occur. *J Cell Biol*, *176*(4), 445–458. https://doi.org/10.1083/jcb.200609014

Nishikawa, A., Ihara, Y., Hatakeyama, M., Kangawa, K., & Taniguchi, N. (1992). Purification, cDNA cloning, and expression of UDP-N-acetylglucosamine: Beta-D-mannoside beta-1,4N-acetylglucosaminyltransferase III from rat kidney. *The Journal of Biological Chemistry*, *267*(25), 18199–18204.

Nolan, T., Hands, R. E., & Bustin, S. A. (2006). Quantification of mRNA using real-time RT-PCR. *Nature Protocols*, *1*(3), 1559–1582. https://doi.org/10.1038/nprot.2006.236

Noseda, M., Fu, Y., Niessen, K., Wong, F., Chang, L., McLean, G., & Karsan, A. (2006). Smooth Muscle alpha-actin is a direct target of Notch/CSL. *Circulation Research*, *98*(12), 1468–1470. https://doi.org/10.1161/01.RES.0000229683.81357.26

Nowell, C. S., & Radtke, F. (2017). Notch as a tumour suppressor. *Nature Reviews Cancer*, *17*(3), 145–159. https://doi.org/10.1038/nrc.2016.145

Nyenhuis, S. B., Karandikar, N., Kiessling, V., Kreutzberger, A. J. B., Thapa, A., Liang, B., Tamm, L. K., & Cafiso, D. S. (2021). Conserved arginine residues in synaptotagmin 1 regulate fusion pore expansion through membrane contact. *Nature Communications*, *12*(1), 761. https://doi.org/10.1038/s41467-021-21090-x

Ogawa, M., Tashima, Y., Sakaguchi, Y., Takeuchi, H., & Okajima, T. (2020). Contribution of extracellular O-GlcNAc to the stability of folded epidermal growth factor-like domains and Notch1 trafficking. *Biochemical and Biophysical Research Communications*, *526*(1), 184–190. https://doi.org/10.1016/j.bbrc.2020.03.066

Okajima, T., Reddy, B. V. V. G., Matsuda, T., & Irvine, K. D. (2008). Contributions of chaperone and glycosyltransferase activities of O-fucosyltransferase 1 to Notch signaling. *BMC Biology*, *6*. https://doi.org/10.1186/1741-7007-6-1

Okajima, T., Xu, A., & Irvine, K. D. (2003). Modulation of notch-ligand binding by protein O-fucosyltransferase 1 and fringe. *The Journal of Biological Chemistry*, *278*(43), 42340–42345. https://doi.org/10.1074/jbc.M308687200

Okamura, Y., & Saga, Y. (2008). Pofut1 is required for the proper localization of the Notch receptor during mouse development. *Mechanisms of Development*, *125*(8), 663–673. https://doi.org/10.1016/j.mod.2008.04.007

O'Neil, J., Grim, J., Strack, P., Rao, S., Tibbitts, D., Winter, C., Hardwick, J., Welcker, M., Meijerink, J. P., Pieters, R., Draetta, G., Sears, R., Clurman, B. E., & Look, A. T. (2007). FBW7 mutations in leukemic cells mediate NOTCH pathway activation and resistance to gamma-secretase inhibitors. *The Journal of Experimental Medicine*, *204*(8), 1813–1824. https://doi.org/10.1084/jem.20070876

Ong, S. G. M., Chitneni, M., Lee, K. S., Ming, L. C., & Yuen, K. H. (2016). Evaluation of Extrusion Technique for Nanosizing Liposomes. *Pharmaceutics*, *8*(4), 36. https://doi.org/10.3390/pharmaceutics8040036

Oon, C. E., Bridges, E., Sheldon, H., Sainson, R. C. A., Jubb, A., Turley, H., Leek, R., Buffa, F., Harris, A. L., & Li, J.-L. (2017). Role of Delta-like 4 in Jagged1-induced tumour angiogenesis and tumour growth. *Oncotarget*, *8*(25), 40115–40131. https://doi.org/10.18632/oncotarget.16969

Oswald, F., & Kovall, R. A. (2018). CSL-Associated Corepressor and Coactivator Complexes. *Advances in Experimental Medicine and Biology*, *1066*, 279–295. https://doi.org/10.1007/978-3-319-89512-3_14

Palmer, W. H., Jia, D., & Deng, W.-M. (2014). Cis-interactions between Notch and its ligands block ligand-independent Notch activity. *Elife*, *3*, e04415. https://doi.org/10.7554/eLife.04415

Pandey, A., Harvey, B. M., Lopez, M. F., Ito, A., Haltiwanger, R. S., & Jafar-Nejad, H. (2019). Glycosylation of Specific Notch EGF Repeats by O-Fut1 and Fringe Regulates Notch Signaling in Drosophila. *Cell Rep*, *29*(7), 2054-2066.e6. https://doi.org/10.1016/j.celrep.2019.10.027

Pandey, A., Niknejad, N., & Jafar-Nejad, H. (2021). Multifaceted regulation of Notch signaling by glycosylation. *Glycobiology*, *31*(1), 8–28. https://doi.org/10.1093/glycob/cwaa049

Panin, V. M., Papayannopoulos, V., Wilson, R., & Irvine, K. D. (1997). Fringe modulates Notch-ligand interactions. *Nature*, *387*(6636), 908–912. https://doi.org/10.1038/43191

Panin, V. M., Shao, L., Lei, L., Moloney, D. J., Irvine, K. D., & Haltiwanger, R. S. (2002). Notch ligands are substrates for protein O-fucosyltransferase-1 and Fringe. *The Journal of Biological Chemistry*, *277*(33), 29945–29952. https://doi.org/10.1074/jbc.M204445200

Parks, A. L., Klueg, K. M., Stout, J. R., & Muskavitch, M. A. (2000). Ligand endocytosis drives receptor dissociation and activation in the Notch pathway. *Development (Cambridge, England)*, *127*(7), 1373–1385. https://doi.org/10.1242/dev.127.7.1373

Parks, A. L., Stout, J. R., Shepard, S. B., Klueg, K. M., Dos Santos, A. A., Parody, T. R., Vaskova, M., & Muskavitch, M. A. T. (2006). Structure-function analysis of delta trafficking, receptor binding and signaling in Drosophila. *Genetics*, *174*(4), 1947–1961. https://doi.org/10.1534/genetics.106.061630

Patel, N. S., Li, J.-L., Generali, D., Poulsom, R., Cranston, D. W., & Harris, A. L. (2005). Up-regulation of delta-like 4 ligand in human tumor vasculature and the role of basal expression in endothelial cell function. *Cancer Research*, *65*(19), 8690–8697. https://doi.org/10.1158/0008-5472.CAN-05-1208

Pauty, J., Usuba, R., Cheng, I. G., Hespel, L., Takahashi, H., Kato, K., Kobayashi, M., Nakajima, H., Lee, E., Yger, F., Soncin, F., & Matsunaga, Y. T. (2018). A Vascular Endothelial Growth Factor-Dependent Sprouting Angiogenesis Assay Based on an In Vitro Human Blood Vessel Model for the Study of Anti-Angiogenic Drugs. *EBioMedicine*, *27*, 225–236. https://doi.org/10.1016/j.ebiom.2017.12.014

Pennarubia, F., Ito, A., Takeuchi, M., & Haltiwanger, R. S. (2022). Cancer-associated Notch receptor variants lead to O-fucosylation defects that deregulate Notch signaling. *The Journal of Biological Chemistry*, *298*(12), 102616. https://doi.org/10.1016/j.jbc.2022.102616

Penton, A. L., Leonard, L. D., & Spinner, N. B. (2012). Notch signaling in human development and disease. *Semin Cell Dev Biol*, *23*(4), 450–457. https://doi.org/10.1016/j.semcdb.2012.01.010

Pérez-Lara, Á., Thapa, A., Nyenhuis, S. B., Nyenhuis, D. A., Halder, P., Tietzel, M., Tittmann, K., Cafiso, D. S., & Jahn, R. (2016). PtdInsP2 and PtdSer cooperate to trap synaptotagmin-1 to the plasma membrane in the presence of calcium. *eLife*, *5*, e15886. https://doi.org/10.7554/eLife.15886

Perisic, O., Fong, S., Lynch, D. E., Bycroft, M., & Williams, R. L. (1998). Crystal Structure of a Calcium-Phospholipid Binding Domain from Cytosolic Phospholipase A2*. *Journal of Biological Chemistry*, *273*(3), 1596–1604. https://doi.org/10.1074/jbc.273.3.1596

Petrovic, J., Formosa-Jordan, P., Luna-Escalante, J. C., Abelló, G., Ibañes, M., Neves, J., & Giraldez, F. (2014). Ligand-dependent Notch signaling strength orchestrates lateral induction and lateral inhibition in the developing inner ear. *Development (Cambridge, England)*, *141*(11), 2313–2324. https://doi.org/10.1242/dev.108100

Phng, L.-K., & Gerhardt, H. (2009). Angiogenesis: A Team Effort Coordinated by Notch. *Developmental Cell*, *16*(2), 196–208. Scopus. https://doi.org/10.1016/j.devcel.2009.01.015

Pintar, A., De Biasio, A., Popovic, M., Ivanova, N., & Pongor, S. (2007). The intracellular region of Notch ligands: Does the tail make the difference? *Biology Direct*, *2*, 19. https://doi.org/10.1186/1745-6150-2-19

Pittaway, J. F. H., Lipsos, C., Mariniello, K., & Guasti, L. (2021). The role of delta-like non-canonical Notch ligand 1 (DLK1) in cancer. *Endocrine-Related Cancer*, *28*(12), R271–R287. https://doi.org/10.1530/ERC-21-0208

Poodry, C. A. (1990). Shibire, a neurogenic mutant of Drosophila. *Developmental Biology*, *138*, 464–472. https://doi.org/10.1016/0012-1606(90)90212-2

Porcheri, C., Golan, O., Calero-Nieto, F. J., Thambyrajah, R., Ruiz-Herguido, C., Wang, X., Catto, F., Guillén, Y., Sinha, R., González, J., Kinston, S. J., Mariani, S. A., Maglitto, A., Vink, C. S., Dzierzak, E., Charbord, P., Göttgens, B., Espinosa, L., Sprinzak, D., & Bigas, A. (2020). Notch ligand Dll4 impairs cell recruitment to aortic clusters and limits blood stem cell generation. *The EMBO Journal*, *39*(8), e104270. https://doi.org/10.15252/embj.2019104270

Poulson, D. F. (1937). Chromosomal Deficiencies and the Embryonic Development of Drosophila Melanogaster. *Proc Natl Acad Sci U S A*, *23*(3), 133–137. https://doi.org/10.1073/pnas.23.3.133

Poulson, D. F. (1967). Developmental effects of mutants at the Notch locus in Drosophila melanogaster. *Drosophila Information Service*, *42*, 81.

Prexl, A., Münder, S., Loy, B., Kremmer, E., Tischer, S., & Böttger, A. (2011). The putative Notch ligand HyJagged is a transmembrane protein present in all cell types of adult

Hydra and upregulated at the boundary between bud and parent. *BMC Cell Biology*, *12*. Scopus. https://doi.org/10.1186/1471-2121-12-38

Ramkumar, N., Harvey, B. M., Lee, J. D., Alcorn, H. L., Silva-Gagliardi, N. F., McGlade, C. J., Bestor, T. H., Wijnholds, J., Haltiwanger, R. S., & Anderson, K. V. (2015). Protein O-Glucosyltransferase 1 (POGLUT1) Promotes Mouse Gastrulation through Modification of the Apical Polarity Protein CRUMBS2. *PLoS Genetics*, *11*(10), e1005551. https://doi.org/10.1371/journal.pgen.1005551

Ran, S., & Thorpe, P. E. (2002). Phosphatidylserine is a marker of tumor vasculature and a potential target for cancer imaging and therapy. *International Journal of Radiation Oncology, Biology, Physics*, *54*(5), 1479–1484. https://doi.org/10.1016/s0360-3016(02)03928-7

Rand, M. D., Grimm, L. M., Artavanis-Tsakonas, S., Patriub, V., Blacklow, S. C., Sklar, J., & Aster, J. C. (2000). Calcium depletion dissociates and activates heterodimeric notch receptors. *Molecular and Cellular Biology*, *20*(5), 1825–1835. https://doi.org/10.1128/MCB.20.5.1825-1835.2000

Rashid, S., Azeem, S., & Riaz, S. (2022). Adams-Oliver Syndrome: A Rare Congenital Disorder. *Cureus*, *14*(3), e23297. https://doi.org/10.7759/cureus.23297

Rebay, I., Fehon, R. G., & Artavanis-Tsakonas, S. (1993). Specific truncations of Drosophila Notch define dominant activated and dominant negative forms of the receptor. *Cell*, *74*(2), 319–329. https://doi.org/10.1016/0092-8674(93)90423-n

Rebay, I., Fleming, R. J., Fehon, R. G., Cherbas, L., Cherbas, P., & Artavanis-Tsakonas, S. (1991). Specific EGF repeats of Notch mediate interactions with Delta and serrate: Implications for notch as a multifunctional receptor. *Cell*. https://doi.org/10.1016/0092-8674(91)90064-6

Reedijk, M., Odorcic, S., Chang, L., Zhang, H., Miller, N., McCready, D. R., Lockwood, G., & Sean, E. (2005). High-level Coexpression of JAG1 and NOTCH1 Is Observed in Human Breast Cancer and Is Associated with Poor Overall Survival. *Cancer Research*, *65*(18), 8530–8537. https://doi.org/10.1158/0008-5472.CAN-05-1069

Rees, D. J., Jones, I. M., Handford, P. A., Walter, S. J., Esnouf, M. P., Smith, K. J., & Brownlee, G. G. (1988). The role of beta-hydroxyaspartate and adjacent carboxylate residues in the first EGF domain of human factor IX. *The EMBO Journal*, *7*(7), 2053–2061. https://doi.org/10.1002/j.1460-2075.1988.tb03045.x

Reeves, P. J., Callewaert, N., Contreras, R., & Khorana, H. G. (2002). Structure and function in rhodopsin: High-level expression of rhodopsin with restricted and homogeneous N-glycosylation by a tetracycline-inducible N-acetylglucosaminyltransferase I-negative HEK293S stable mammalian cell line. *Proceedings of the National Academy of Sciences*, *99*(21), 13419–13424. https://doi.org/10.1073/pnas.212519299

Reily, C., Stewart, T. J., Renfrow, M. B., & Novak, J. (2019). Glycosylation in health and disease. *Nature Reviews Nephrology*, *15*(6), 346–366. https://doi.org/10.1038/s41581-019-0129-4

Revici, R., Hosseini-Alghaderi, S., Haslam, F., Whiteford, R., & Baron, M. (2022). E3 Ubiquitin Ligase Regulators of Notch Receptor Endocytosis: From Flies to Humans. *Biomolecules*, *12*(2). https://doi.org/10.3390/biom12020224

Rizo, J., & Südhof, T. C. (1998). C2-domains, Structure and Function of a Universal Ca2+-binding Domain*. *Journal of Biological Chemistry*, *273*(26), 15879–15882. https://doi.org/10.1074/jbc.273.26.15879

Rojnueangnit, K., Phawan, T., Khetkham, T., Techasatid, W., & Sirichongkolthong, B. (2022). A novel DLL4 mutation in Adams–Oliver syndrome with absence of the right pulmonary artery in newborn. *American Journal of Medical Genetics Part A*, *188*(2), 658–664. https://doi.org/10.1002/ajmg.a.62562

Ruiz-Villalba, A., Ruijter, J. M., & van den Hoff, M. J. B. (2021). Use and Misuse of C(q) in qPCR Data Analysis and Reporting. *Life (Basel, Switzerland)*, *11*(6). https://doi.org/10.3390/life11060496

Ryan, M. J., Bales, C., Nelson, A., Gonzalez, D. M., Underkoffler, L., Segalov, M., Wilson-Rawls, J., Cole, S. E., Moran, J. L., Russo, P., Spinner, N. B., Kusumi, K., & Loomes, K. M. (2008). Bile duct proliferation in Jag1/fringe heterozygous mice identifies candidate modifiers of the Alagille syndrome hepatic phenotype. *Hepatology (Baltimore, Md.)*, *48*(6), 1989–1997. https://doi.org/10.1002/hep.22538

Sabherwal, N., Rowntree, A., Marinopoulou, E., Pettini, T., Hourihane, S., Thomas, R., Soto, X., Kursawe, J., & Papalopulu, N. (2021). Differential phase register of Hes1 oscillations with mitoses underlies cell-cycle heterogeneity in ER+ breast cancer cells. *Proceedings of the National Academy of Sciences*, *118*(45), e2113527118. https://doi.org/10.1073/pnas.2113527118

Saiki, W., Ma, C., Okajima, T., & Takeuchi, H. (2021). Current Views on the Roles of O-Glycosylation in Controlling Notch-Ligand Interactions. *Biomolecules*, *11*(2). https://doi.org/10.3390/biom11020309

Sampaio, J. L., Gerl, M. J., Klose, C., Ejsing, C. S., Beug, H., Simons, K., & Shevchenko, A. (2011). Membrane lipidome of an epithelial cell line. *Proceedings of the National Academy of Sciences*, *108*(5), 1903–1907. https://doi.org/10.1073/pnas.1019267108

San Pietro, E., Capestrano, M., Polishchuk, E. V., DiPentima, A., Trucco, A., Zizza, P., Mariggiò, S., Pulvirenti, T., Sallese, M., Tete, S., Mironov, A. A., Leslie, C. C., Corda, D., Luini, A., & Polishchuk, R. S. (2009). Group IV phospholipase A(2)alpha controls the formation of inter-cisternal continuities involved in intra-Golgi transport. *PLoS Biology*, *7*(9), e1000194. https://doi.org/10.1371/journal.pbio.1000194

Sanchez-Irizarry, C., Carpenter, A. C., Weng, A. P., Pear, W. S., Aster, J. C., & Blacklow, S. C. (2004). Notch subunit heterodimerization and prevention of ligand-independent proteolytic activation depend, respectively, on a novel domain and the LNR repeats. *Molecular and Cellular Biology*, *24*(21), 9265–9273. https://doi.org/10.1128/MCB.24.21.9265-9273.2004

Santagata, S., Demichelis, F., Riva, A., Varambally, S., Hofer, M. D., Kutok, J. L., Kim, R., Tang, J., Montie, J. E., Chinnaiyan, A. M., Rubin, M. A., & Aster, J. C. (2004). JAGGED1 expression is associated with prostate cancer metastasis and recurrence. *Cancer Research*, *64*(19), 6854–6857. https://doi.org/10.1158/0008-5472.CAN-04-2500

SantaLucia, J. J., & Hicks, D. (2004). The thermodynamics of DNA structural motifs. *Annual Review of Biophysics and Biomolecular Structure*, *33*, 415–440. https://doi.org/10.1146/annurev.biophys.32.110601.141800

Sasamura, T., Sasaki, N., Miyashita, F., Nakao, S., Ishikawa, H. O., Ito, M., Kitagawa, M., Harigaya, K., Spana, E., Bilder, D., Perrimon, N., & Matsuno, K. (2003). Neurotic, a novel maternal neurogenic gene, encodes an O-fucosyltransferase that is essential for Notch-Delta interactions. *Development (Cambridge, England)*, *130*(20), 4785–4795. https://doi.org/10.1242/dev.00679

Sawaguchi, S., Varshney, S., Ogawa, M., Sakaidani, Y., Yagi, H., Takeshita, K., Murohara, T., Kato, K., Sundaram, S., Stanley, P., & Okajima, T. (2017). O-GlcNAc on NOTCH1 EGF repeats regulates ligand-induced Notch signaling and vascular development in mammals. *eLife*, *6*, e24419. https://doi.org/10.7554/eLife.24419

Sawangarun, W., Mandasari, M., Aida, J., Morita, K. ichi, Kayamori, K., Ikeda, T., & Sakamoto, K. (2018). Loss of Notch1 predisposes oro-esophageal epithelium to tumorigenesis. *Experimental Cell Research*, *372*(2), 129–140. https://doi.org/10.1016/J.YEXCR.2018.09.019

Schneider, M., Kumar, V., Nordstrøm, L. U., Feng, L., Takeuchi, H., Hao, H., Luca, V. C., Garcia, K. C., Stanley, P., Wu, P., & Haltiwanger, R. S. (2018). Inhibition of Delta-induced Notch signaling using fucose analogs. *Nature Chemical Biology*, *14*(1), 65–71. https://doi.org/10.1038/nchembio.2520

Schneider, R., Jensen, S. A., Whiteman, P., McCullagh, J. S. O., Redfield, C., & Handford, P. A. (2010). Biophysical characterisation of fibulin-5 proteins associated with disease. *Journal of Molecular Biology*, *401*(4), 605–617. https://doi.org/10.1016/j.jmb.2010.06.039

Schrijver, I., Liu, W., Brenn, T., Furthmayr, H., & Francke, U. (1999). Cysteine substitutions in epidermal growth factor-like domains of fibrillin-1: Distinct effects on biochemical and clinical phenotypes. *American Journal of Human Genetics*, *65*(4), 1007–1020. https://doi.org/10.1086/302582

Schuster-Gossler, K., Cordes, R., & Gossler, A. (2007). Premature myogenic differentiation and depletion of progenitor cells cause severe muscle hypotrophy in Delta1 mutants. *Proceedings of the National Academy of Sciences of the United States of America*, *104*(2), 537–542. https://doi.org/10.1073/pnas.0608281104

Seet, C. S., He, C., Bethune, M. T., Li, S., Chick, B., Gschweng, E. H., Zhu, Y., Kim, K., Kohn, D. B., Baltimore, D., Crooks, G. M., & Montel-Hagen, A. (2017). Generation of mature T cells from human hematopoietic stem and progenitor cells in artificial thymic organoids. *Nature Methods*, *14*(5), 521–530. https://doi.org/10.1038/nmeth.4237

Servián-Morilla, E., Cabrera-Serrano, M., Johnson, K., Pandey, A., Ito, A., Rivas, E., Chamova, T., Muelas, N., Mongini, T., Nafissi, S., Claeys, K. G., Grewal, R. P., Takeuchi, M., Hao, H., Bönnemann, C., Lopes Abath Neto, O., Medne, L., Brandsema, J., Töpf, A., … Paradas, C. (2020). POGLUT1 biallelic mutations cause myopathy with reduced satellite cells, α-dystroglycan hypoglycosylation and a distinctive radiological pattern. *Acta Neuropathologica*, *139*(3), 565–582. https://doi.org/10.1007/s00401-019-02117-6

Servián-Morilla, E., Takeuchi, H., Lee, T. V., Clarimon, J., Mavillard, F., Area-Gómez, E., Rivas, E., Nieto-González, J. L., Rivero, M. C., Cabrera-Serrano, M., Gómez-Sánchez, L., Martínez-López, J. A., Estrada, B., Márquez, C., Morgado, Y., Suárez-Calvet, X., Pita, G., Bigot, A., Gallardo, E., … Paradas, C. (2016). A POGLUT1 mutation causes a muscular dystrophy with reduced Notch signaling and satellite cell loss. *EMBO Molecular Medicine*, *8*(11), 1289–1309. https://doi.org/10.15252/emmm.201505815

Seydoux, G., & Greenwald, I. (1989). Cell autonomy of lin-12 function in a cell fate decision in C. elegans. *Cell*, *57*(7), 1237–1245. https://doi.org/10.1016/0092-8674(89)90060-3

Seymour, P. A., Collin, C. A., Egeskov-Madsen, A. la R., Jørgensen, M. C., Shimojo, H., Imayoshi, I., de Lichtenberg, K. H., Kopan, R., Kageyama, R., & Serup, P. (2020). Jag1 Modulates an Oscillatory Dll1-Notch-Hes1 Signaling Module to Coordinate Growth and Fate of Pancreatic Progenitors. *Developmental Cell*, *52*(6), 731-747.e8. https://doi.org/10.1016/J.DEVCEL.2020.01.015

Shaheen, R., Aglan, M., Keppler-Noreuil, K., Faqeih, E., Ansari, S., Horton, K., Ashour, A., Zaki, M. S., Al-Zahrani, F., Cueto-González, A. M., Abdel-Salam, G., Temtamy, S., & Alkuraya, F. S. (2013). Mutations in EOGT confirm the genetic heterogeneity of autosomal-recessive Adams-Oliver syndrome. *American Journal of Human Genetics*, *92*(4), 598–604. https://doi.org/10.1016/j.ajhg.2013.02.012

Shao, X., Davletov, B. A., Sutton, R. B., Südhof, T. C., & Rizo, J. (1996). Bipartite Ca2+-Binding Motif in C2 Domains of Synaptotagmin and Protein Kinase C. *Science*, *273*(5272), 248–251. https://doi.org/10.1126/science.273.5272.248

Shao, X., Fernandez, I., Südhof, T. C., & Rizo, J. (1998). Solution structures of the Ca2+-free and Ca2+-bound C2A domain of synaptotagmin I: does Ca2+ induce a conformational change? *Biochemistry*, *37*(46), 16106–16115. https://doi.org/10.1021/bi981789h

Shao, X., Li, C., Fernandez, I., Zhang, X., Südhof, T. C., & Rizo, J. (1997). Synaptotagmin-syntaxin interaction: The C2 domain as a Ca2+-dependent electrostatic switch. *Neuron*. https://doi.org/10.1016/S0896-6273(01)80052-0

Shaw, G., Morse, S., Ararat, M., & Graham, F. L. (2002). Preferential transformation of human neuronal cells by human adenoviruses and the origin of HEK 293 cells. *FASEB Journal : Official Publication of the Federation of American Societies for Experimental Biology*, *16*(8), 869–871. https://doi.org/10.1096/fj.01-0995fje

Shelake, R. M., Ito, Y., Masumoto, J., Morita, E. H., & Hayashi, H. (2017). A novel mechanism of 'metal gel-shift' by histidine-rich Ni2+-binding Hpn protein from Helicobacter pylori strain SS1. *PloS One*, *12*(2), e0172182. https://doi.org/10.1371/journal.pone.0172182

Shellenbarger, D. L., & Mohler, J. D. (1975). Temperature-sensitive mutations of the notch locus in Drosophila melanogaster. *Genetics*, *81*(1), 143–162. https://doi.org/10.1093/genetics/81.1.143

Sherwood, D. R., & McClay, D. R. (1997). Identification and localization of a sea urchin Notch homologue: Insights into vegetal plate regionalization and Notch receptor regulation. *Development (Cambridge, England)*, *124*(17), 3363–3374. https://doi.org/10.1242/dev.124.17.3363

Shimizu, H., Woodcock, S. A., Wilkin, M. B., Trubenová, B., Monk, N. A., & Baron, M. (2014). Compensatory flux changes within an endocytic trafficking network maintain thermal robustness of Notch signaling. *Cell*, *157*(5), 1160–1174. https://doi.org/10.1016/j.cell.2014.03.050

Shimizu, K., Chiba, S., Kumano, K., Hosoya, N., Takahashi, T., Kanda, Y., Hamada, Y., Yazaki, Y., & Hirai, H. (1999). Mouse jagged1 physically interacts with notch2 and other notch receptors. Assessment by quantitative methods. *The Journal of Biological Chemistry*, *274*(46), 32961–32969. https://doi.org/10.1074/JBC.274.46.32961

Siebel, C., & Lendahl, U. (2017). Notch signaling in development, tissue homeostasis, and disease. *Physiological Reviews*, *97*(4), 1235–1294. https://doi.org/10.1152/PHYSREV.00005.2017/ASSET/IMAGES/LARGE/Z9J00417 28220006.JPEG

Simons, K., & Ikonen, E. (1997). Functional rafts in cell membranes. *Nature*, *387*(6633), 569–572. https://doi.org/10.1038/42408

Simons, K., & Toomre, D. (2000). Lipid rafts and signal transduction. *Nature Reviews. Molecular Cell Biology*, *1*(1), 31–39. https://doi.org/10.1038/35036052

Simpson, P. (1990). Lateral inhibition and the development of the sensory bristles of the adult peripheral nervous system of Drosophila. *Development*, *109*(3), 509–519. Scopus.

Simpson, P. (1997). Notch signalling in development: On equivalence groups and asymmetric developmental potential. *Current Opinion in Genetics and Development*. https://doi.org/10.1016/S0959-437X(97)80083-4

Smyrlaki, I., Fördős, F., Rocamonde-Lago, I., Wang, Y., Shen, B., Lentini, A., Luca, V. C., Reinius, B., Teixeira, A. I., & Högberg, B. (2024). Soluble and multivalent Jag1 DNA origami nanopatterns activate Notch without pulling force. *Nature Communications*, *15*(1), 465. https://doi.org/10.1038/s41467-023-44059-4

Song, R., Koo, B. K., Yoon, K. J., Yoon, M. J., Yoo, K. W., Kim, H. T., Oh, H. J., Kim, Y. Y., Han, J. K., Kim, C. H., & Kong, Y. Y. (2006). Neuralized-2 regulates a Notch ligand in cooperation with Mind bomb-1. *The Journal of Biological Chemistry*, *281*(47), 36391–36400. https://doi.org/10.1074/JBC.M606601200

Sorensen, E. B., & Conner, S. D. (2010). γ secretase-dependent cleavage initiates Notch signaling from the plasma membrane. *Traffic (Copenhagen, Denmark)*, *11*(9), 1234. https://doi.org/10.1111/J.1600-0854.2010.01090.X

Southgate, L., Sukalo, M., Karountzos, A. S. V., Taylor, E. J., Collinson, C. S., Ruddy, D., Snape, K. M., Dallapiccola, B., Tolmie, J. L., Joss, S., Brancati, F., Digilio, M. C., Graul-Neumann, L. M., Salviati, L., Coerdt, W., Jacquemin, E., Wuyts, W., Zenker, M., Machado, R. D., & Trembath, R. C. (2015). Haploinsufficiency of the NOTCH1 Receptor as a Cause of Adams–Oliver Syndrome With Variable Cardiac Anomalies. *Circulation: Cardiovascular Genetics*, *8*(4), 572–581. https://doi.org/10.1161/CIRCGENETICS.115.001086

Sparks, E. E., Huppert, K. A., Brown, M. A., Washington, M. K., & Huppert, S. S. (2010). Notch signaling regulates formation of the three-dimensional architecture of intrahepatic bile ducts in mice. *Hepatology (Baltimore, Md.)*, *51*(4), 1391–1400. https://doi.org/10.1002/hep.23431

Sparrow, D. B., Chapman, G., Wouters, M. A., Whittock, N. V., Ellard, S., Fatkin, D., Turnpenny, P. D., Kusumi, K., Sillence, D., & Dunwoodie, S. L. (2006). Mutation of the LUNATIC FRINGE gene in humans causes spondylocostal dysostosis with a severe vertebral phenotype. *American Journal of Human Genetics*, *78*(1), 28–37. https://doi.org/10.1086/498879

Sprinzak, D., & Blacklow, S. C. (2021). Biophysics of Notch Signaling. *Annu Rev Biophys*, *50*, 157–189. https://doi.org/10.1146/annurev-biophys-101920-082204

Sprinzak, D., Lakhanpal, A., Lebon, L., Santat, L. A., Fontes, M. E., Anderson, G. A., Garcia-Ojalvo, J., & Elowitz, M. B. (2010). Cis-interactions between Notch and Delta generate mutually exclusive signalling states. *Nature*, *465*(7294), 86–90. https://doi.org/10.1038/nature08959

Spyros Artavanis-Tsakonas. (1988). The molecular biology of the Notch locus and the fine tuning of differentiation in Drosophila. *Trends in Genetics*, *4*(4), 95–100. https://doi.org/10.1016/0168-9525(88)90096-0

Stephens, P. J., Davies, H. R., Mitani, Y., Van Loo, P., Shlien, A., Tarpey, P. S., Papaemmanuil, E., Cheverton, A., Bignell, G. R., Butler, A. P., Gamble, J., Gamble, S., Hardy, C., Hinton, J., Jia, M., Jayakumar, A., Jones, D., Latimer, C., McLaren, S., … Futreal, P. A. (2013). Whole exome sequencing of adenoid cystic carcinoma. *The Journal of Clinical Investigation*, *123*(7), 2965. https://doi.org/10.1172/JCI67201

Stittrich, A.-B., Lehman, A., Bodian, D. L., Ashworth, J., Zong, Z., Li, H., Lam, P., Khromykh, A., Iyer, R. K., Vockley, J. G., Baveja, R., Silva, E. S., Dixon, J., Leon, E. L., Solomon, B. D., Glusman, G., Niederhuber, J. E., Roach, J. C., & Patel, M. S. (2014). Mutations in NOTCH1 cause Adams-Oliver syndrome. *American Journal of Human Genetics*, *95*(3), 275–284. https://doi.org/10.1016/j.ajhg.2014.07.011

Stransky, N., Egloff, A. M., Tward, A. D., Kostic, A. D., Cibulskis, K., Sivachenko, A., Kryukov, G. V., Lawrence, M. S., Sougnez, C., McKenna, A., Shefler, E., Ramos, A. H., Stojanov, P., Carter, S. L., Voet, D., Cortés, M. L., Auclair, D., Berger, M. F., Saksena, G., … Grandis, J. R. (2011). The mutational landscape of head and neck squamous cell carcinoma. *Science (New York, N.Y.)*, *333*(6046), 1157–1160. https://doi.org/10.1126/SCIENCE.1208130

Strati, T. M., Kotoula, V., Kostopoulos, I., Manousou, K., Papadimitriou, C., Lazaridis, G., Lakis, S., Pentheroudakis, G., Pectasides, D., Pazarli, E., Christodoulou, C., Razis, E., Pavlakis, K., Magkou, C., Chrisafi, S., Aravantinos, G., Bafaloukos, D., Papakostas, P., Gogas, H., … Fountzilas, G. (2017). Prognostic Subcellular Notch2, Notch3 and Jagged1 Localization Patterns in Early Triple-negative Breast Cancer. *Anticancer Research*, *37*(5), 2323–2334. https://doi.org/10.21873/ANTICANRES.11570

Struhl, G., Fitzgerald, K., & Greenwald, I. (1993). Intrinsic activity of the Lin-12 and Notch intracellular domains in vivo. *Cell*, *74*(2), 331–345. https://doi.org/10.1016/0092-8674(93)90424-o

Suchting, S., Freitas, C., le Noble, F., Benedito, R., Bréant, C., Duarte, A., & Eichmann, A. (2007). The Notch ligand Delta-like 4 negatively regulates endothelial tip cell formation and vessel branching. *Proceedings of the National Academy of Sciences*, *104*(9), 3225–3230. https://doi.org/10.1073/PNAS.0611177104

Suckling, R. J., Korona, B., Whiteman, P., Chillakuri, C., Holt, L., Handford, P. A., & Lea, S. M. (2017). Structural and functional dissection of the interplay between lipid and Notch binding by human Notch ligands. *The EMBO Journal*, *36*(15), 2204–2215. https://doi.org/10.15252/embj.201796632

Sugiyama, M., Oki, E., Nakaji, Y., Tsutsumi, S., Ono, N., Nakanishi, R., Sugiyama, M., Nakashima, Y., Sonoda, H., Ohgaki, K., Yamashita, N., Saeki, H., Okano, S., Kitao, H., Morita, M., Oda, Y., & Maehara, Y. (2016). High expression of the Notch ligand Jagged-1 is associated with poor prognosis after surgery for colorectal cancer. *Cancer Science*, *107*(11), 1705–1716. https://doi.org/10.1111/CAS.13075

Suh, B.-C., & Hille, B. (2008). PIP2 is a necessary cofactor for ion channel function: How and why? *Annual Review of Biophysics*, *37*, 175–195. https://doi.org/10.1146/annurev.biophys.37.032807.125859

Sullivan, J. M., Motley, W. W., Johnson, J. O., Aisenberg, W. H., Marshall, K. L., Barwick, K. E., Kong, L., Huh, J. S., Saavedra-Rivera, P. C., McEntagart, M. M., Marion, M.-H., Hicklin, L. A., Modarres, H., Baple, E. L., Farah, M. H., Zuberi, A. R., Lutz, C. M., Gaudet, R., Traynor, B. J., … Sumner, C. J. (2020). Dominant mutations of the Notch ligand Jagged1 cause peripheral neuropathy. *The Journal of Clinical Investigation*, *130*(3), 1506–1512. https://doi.org/10.1172/JCI128152

Sun, X., & Artavanis-Tsakonas, S. (1996). The intracellular deletions of Delta and Serrate define dominant negative forms of the Drosophila Notch ligands. *Development*, *122*(8), 2465–2474. https://doi.org/10.1242/DEV.122.8.2465

Sun, X., & Artavanis-Tsakonas, S. (1997). Secreted forms of DELTA and SERRATE define antagonists of Notch signaling in Drosophila. *Development (Cambridge, England)*, *124*(17), 3439–3448. https://doi.org/10.1242/DEV.124.17.3439

Sun, X.-Y., Ju, X.-C., Li, Y., Zeng, P.-M., Wu, J., Zhou, Y.-Y., Shen, L.-B., Dong, J., Chen, Y.-J., & Luo, Z.-G. (2022). Generation of vascularized brain organoids to study neurovascular interactions. *eLife*, *11*, e76707. https://doi.org/10.7554/eLife.76707

Suresh, P., & London, E. (2022). Using cyclodextrin-induced lipid substitution to study membrane lipid and ordered membrane domain (raft) function in cells. *Biochimica et Biophysica Acta. Biomembranes*, *1864*(1), 183774. https://doi.org/10.1016/j.bbamem.2021.183774

Suresh, P., & London, E. (2024). MαCD-based plasma membrane outer leaflet lipid exchange in mammalian cells to study insulin receptor activity. *Methods in Enzymology*, *700*, 485–507. https://doi.org/10.1016/bs.mie.2024.03.027

Takeshita, K., Satoh, M., Ii, M., Silver, M., Limbourg, F. P., Mukai, Y., Rikitake, Y., Radtke, F., Gridley, T., Losordo, D. W., & Liao, J. K. (2007). Critical role of endothelial Notch1 signaling in postnatal angiogenesis. *Circulation Research*, *100*(1), 70–78. https://doi.org/10.1161/01.RES.0000254788.47304.6e

Takeuchi, H., Schneider, M., Williamson, D. B., Ito, A., Takeuchi, M., Handford, P. A., & Haltiwanger, R. S. (2018). Two novel protein O-glucosyltransferases that modify sites distinct from POGLUT1 and affect Notch trafficking and signaling. *Proceedings of the*

National Academy of Sciences of the United States of America, *115*(36), E8395–E8402. https://doi.org/10.1073/pnas.1804005115

Takeuchi, H., Yu, H., Hao, H., Takeuchi, M., Ito, A., Li, H., & Haltiwanger, R. S. (2017). O-Glycosylation modulates the stability of epidermal growth factor-like repeats and thereby regulates Notch trafficking. *The Journal of Biological Chemistry*, *292*(38), 15964–15973. https://doi.org/10.1074/JBC.M117.800102

Tannous, A., Pisoni, G. B., Hebert, D. N., & Molinari, M. (2015). N-linked sugar-regulated protein folding and quality control in the ER. *Seminars in Cell and Developmental Biology*, *41*, 79–89. Scopus. https://doi.org/10.1016/j.semcdb.2014.12.001

Tax, F. E., Yeargers, J. J., & Thomas, J. H. (1994). Sequence of C. elegans lag-2 reveals a cell-signalling domain shared with Delta and Serrate of Drosophila. *Nature*, *368*(6467), 150–154. https://doi.org/10.1038/368150a0

Taylor, P., Takeuchi, H., Sheppard, D., Chillakuri, C., Lea, S. M., Haltiwanger, R. S., & Handford, P. A. (2014). Fringe-mediated extension of O-linked fucose in the ligand-binding region of Notch1 increases binding to mammalian Notch ligands. *Proceedings of the National Academy of Sciences of the United States of America*, *111*(20), 7290–7295. https://doi.org/10.1073/pnas.1319683111

Thakurdas, S. M., Lopez, M. F., Kakuda, S., Fernandez-Valdivia, R., Zarrin-Khameh, N., Haltiwanger, R. S., & Jafar-Nejad, H. (2016). Jagged1 heterozygosity in mice results in a congenital cholangiopathy which is reversed by concomitant deletion of one copy of Poglut1 (Rumi). *Hepatology (Baltimore, Md.)*, *63*(2), 550–565. https://doi.org/10.1002/hep.28024

Thambyrajah, R., Maqueda, M., Neo, W. H., Imbach, K., Guillén, Y., Grases, D., Fadlullah, Z., Gambera, S., Matteini, F., Wang, X., Calero-Nieto, F. J., Esteller, M., Florian, M. C., Porta, E., Benedito, R., Göttgens, B., Lacaud, G., Espinosa, L., & Bigas, A. (2024). Cis inhibition of NOTCH1 through JAGGED1 sustains embryonic hematopoietic stem cell fate. *Nature Communications*, *15*(1), 1604. https://doi.org/10.1038/s41467-024-45716-y

Thompson, B. J., Buonamici, S., Sulis, M. L., Palomero, T., Vilimas, T., Basso, G., Ferrando, A., & Aifantis, I. (2007). The SCFFBW7 ubiquitin ligase complex as a tumor suppressor in T cell leukemia. *The Journal of Experimental Medicine*, *204*(8), 1825–1835. https://doi.org/10.1084/jem.20070872

Tiemeijer, L. A., Frimat, J. P., Stassen, O. M. J. A., Bouten, C. V. C., & Sahlgren, C. M. (2018). Spatial patterning of the Notch ligand Dll4 controls endothelial sprouting in vitro. *Scientific Reports*, *8*(1), 6392. https://doi.org/10.1038/s41598-018-24646-y

Tiemeijer, L. A., Ristori, T., Stassen, O. M. J. A., Ahlberg, J. J., de Bijl, J. J. J., Chen, C. S., Bentley, K., Bouten, C. V. C., & Sahlgren, C. M. (2022). Engineered patterns of Notch

ligands Jag1 and Dll4 elicit differential spatial control of endothelial sprouting. *iScience*, *25*(5), 104306. https://doi.org/10.1016/j.isci.2022.104306

Timmerman, L. A., Grego-Bessa, J., Raya, A., Bertrán, E., Pérez-Pomares, J. M., Díez, J., Aranda, S., Palomo, S., McCormick, F., Izpisúa-Belmonte, J. C., & de la Pompa, J. L. (2004). Notch promotes epithelial-mesenchymal transition during cardiac development and oncogenic transformation. *Genes & Development*, *18*(1), 99–115. https://doi.org/10.1101/gad.276304

Traore, D. A. K., Brennan, A. J., Law, R. H. P., Dogovski, C., Perugini, M. A., Lukoyanova, N., Leung, E. W. W., Norton, R. S., Lopez, J. A., Browne, K. A., Yagita, H., Lloyd, G. J., Ciccone, A., Verschoor, S., Trapani, J. A., Whisstock, J. C., & Voskoboinik, I. (2013). Defining the interaction of perforin with calcium and the phospholipid membrane. *The Biochemical Journal*, *456*(3), 323–335. https://doi.org/10.1042/BJ20130999

Troost, T., Binshtok, U., Sprinzak, D., & Klein, T. (2023). Cis-inhibition suppresses basal Notch signaling during sensory organ precursor selection. *Proceedings of the National Academy of Sciences*, *120*(23). https://doi.org/10.1073/pnas.2214535120

Trotman-Grant, A. C., Mohtashami, M., De Sousa Casal, J., Martinez, E. C., Lee, D., Teichman, S., Brauer, P. M., Han, J., Anderson, M. K., & Zúñiga-Pflücker, J. C. (2021). DL4-µbeads induce T cell lineage differentiation from stem cells in a stromal cell-free system. *Nature Communications*, *12*(1), 5023. https://doi.org/10.1038/s41467-021-25245-8

Vaccari, T., Lu, H., Kanwar, R., Fortini, M. E., & Bilder, D. (2008). Endosomal entry regulates Notch receptor activation in Drosophila melanogaster. *The Journal of Cell Biology*, *180*(4), 755. https://doi.org/10.1083/JCB.200708127

Vaish, V., Kim, J., & Shim, M. (2017). Jagged-2 (JAG2) enhances tumorigenicity and chemoresistance of colorectal cancer cells. *Oncotarget*, *8*(32), 53262. https://doi.org/10.18632/ONCOTARGET.18391

Valapala, M., Hose, S., Gongora, C., Dong, L., Wawrousek, E. F., Samuel Zigler, J., & Sinha, D. (2013). Impaired endolysosomal function disrupts Notch signalling in optic nerve astrocytes. *Nature Communications 2013 4:1*, *4*(1), 1–12. https://doi.org/10.1038/ncomms2624

Van Beest, M., Robben, J. H., Savelkoul, P. J. M., Hendriks, G., Devonald, M. A. J., Konings, I. B. M., Lagendijk, A. K., Karet, F., & Deen, P. M. T. (2006). Polarisation, key to good localisation. *Aquaporins*, *1758*(8), 1126–1133. https://doi.org/10.1016/j.bbamem.2006.03.007

Van Guilder, H. D., Vrana, K. E., & Freeman, W. M. (2008). Twenty-Five Years of Quantitative PCR for Gene Expression Analysis. *BioTechniques*, *44*(5), 619–626. https://doi.org/10.2144/000112776

Varshney, S., & Stanley, P. (2018). Multiple roles for O-glycans in Notch signalling. *FEBS Letters*, *592*(23), 3819–3834. https://doi.org/10.1002/1873-3468.13251

Varshney, S., Wei, H. X., Batista, F., Nauman, M., Sundaram, S., Siminovitch, K., Tanwar, A., & Stanley, P. (2019). A modifier in the 129S2/SvPasCrl genome is responsible for the viability of Notch1[12f/12f] mice. *BMC Dev Biol*, *19*(1), 19. https://doi.org/10.1186/s12861-019-0199-3

Vässin, H., & Campos-Ortega, J. A. (1987). Genetic Analysis of Delta, a Neurogenic Gene of Drosophila melanogaster. *Genetics*, *116*(3), 433–445. https://doi.org/10.1093/genetics/116.3.433

Verdaguer, N., Corbalan-Garcia, S., Ochoa, W. F., Fita, I., & Gómez-Fernández, J. C. (1999). Ca2+ bridges the C2 membrane-binding domain of protein kinase Cα directly to phosphatidylserine. *The EMBO Journal*, *18*(22), 6329–6338. https://doi.org/10.1093/emboj/18.22.6329

Viaud, J., Mansour, R., Antkowiak, A., Mujalli, A., Valet, C., Chicanne, G., Xuereb, J.-M., Terrisse, A.-D., Séverin, S., Gratacap, M.-P., Gaits-Iacovoni, F., & Payrastre, B. (2016). Phosphoinositides: Important lipids in the coordination of cell dynamics. *Biochimie*, *125*, 250–258. https://doi.org/10.1016/j.biochi.2015.09.005

Vishwakarma, R. A., Vehring, S., Mehta, A., Sinha, A., Pomorski, T., Herrmann, A., & Menon, A. K. (2005). New fluorescent probes reveal that flippase-mediated flip-flop of phosphatidylinositol across the endoplasmic reticulum membrane does not depend on the stereochemistry of the lipid. *Organic & Biomolecular Chemistry*, *3*(7), 1275–1283. https://doi.org/10.1039/b500300h

Wang, N. J., Sanborn, Z., Arnett, K. L., Bayston, L. J., Liao, W., Proby, C. M., Leigh, I. M., Collisson, E. A., Gordon, P. B., Jakkula, L., Pennypacker, S., Zou, Y., Sharma, M., North, J. P., Vemula, S. S., Mauro, T. M., Neuhaus, I. M., LeBoit, P. E., Hur, J. S., … Cho, R. J. (2011). Loss-of-function mutations in Notch receptors in cutaneous and lung squamous cell carcinoma. *Proceedings of the National Academy of Sciences of the United States of America*, *108*(43), 17761–17766. https://doi.org/10.1073/PNAS.1114669108/-/DCSUPPLEMENTAL

Wang, W., & Struhl, G. (2004). Drosophila Epsin mediates a select endocytic pathway that DSL ligands must enter to activate Notch. *Development*, *131*(21). https://doi.org/10.1242/dev.01413

Wang, W., & Struhl, G. (2005). Distinct roles for Mind bomb, Neuralized and Epsin in mediating DSL endocytosis and signaling in Drosophila. *Development (Cambridge, England)*, *132*(12), 2883–2894. https://doi.org/10.1242/DEV.01860

Wang, X., & Ha, T. (2013). Defining Single Molecular Forces Required to Activate Integrin and Notch Signaling. *Science*, *340*(6135), 991–994. https://doi.org/doi:10.1126/science.1231041

Wang, X.-M., Yao, M., Liu, S.-X., Hao, J., Liu, Q.-J., & Gao, F. (2014). Interplay between the Notch and PI3K/Akt pathways in high glucose-induced podocyte apoptosis. *American Journal of Physiology. Renal Physiology*, *306*(2), F205-213. https://doi.org/10.1152/ajprenal.90005.2013

Wang, Y., Lee, G. F., Kelley, R. F., & Spellman, M. W. (1996). Identification of a GDP-L-fucose:polypeptide fucosyltransferase and enzymatic addition of O-linked fucose to EGF domains. *Glycobiology*, *6*(8), 837–842. https://doi.org/10.1093/glycob/6.8.837

Wang, Y., Shao, L., Shi, S., Harris, R. J., Spellman, M. W., Stanley, P., & Haltiwanger, R. S. (2001). Modification of epidermal growth factor-like repeats with O-fucose. Molecular cloning and expression of a novel GDP-fucose protein O-fucosyltransferase. *The Journal of Biological Chemistry*, *276*(43), 40338–40345. https://doi.org/10.1074/jbc.M107849200

Ward, K. E., Ropa, J. P., Adu-Gyamfi, E., & Stahelin, R. V. (2012). C2 domain membrane penetration by group IVA cytosolic phospholipase A_2 induces membrane curvature changes. *Journal of Lipid Research*, *53*(12), 2656–2666. https://doi.org/10.1194/jlr.M030718

Ward, K. E., Sengupta, R., Ropa, J. P., Amiar, S., & Stahelin, R. V. (2020). The Cytosolic Phospholipase A(2)α N-terminal C2 Domain Binds and Oligomerizes on Membranes with Positive Curvature. *Biomolecules*, *10*(4). https://doi.org/10.3390/biom10040647

Weinmaster, G., Roberts, V. J., & Lemke, G. (1991). A homolog of Drosophila Notch expressed during mammalian development. *Development (Cambridge, England)*, *113*(1), 199–205. https://doi.org/10.1242/dev.113.1.199

Weisshuhn, P. C., Sheppard, D., Taylor, P., Whiteman, P., Lea, S. M., Handford, P. A., & Redfield, C. (2016). Non-Linear and Flexible Regions of the Human Notch1 Extracellular Domain Revealed by High-Resolution Structural Studies. *Structure (London, England : 1993)*, *24*(4), 555–566. https://doi.org/10.1016/j.str.2016.02.010

Welshons, W. J. (1958a). A PRELIMINARY INVESTIGATION OF PSEUDOALLELISM AT THE NOTCH LOCUS OF Drosophila Melanogaster. *Proceedings of the National Academy of Sciences of the United States of America*, *44*(3), 254–258. https://doi.org/10.1073/pnas.44.3.254

Welshons, W. J. (1958b). The analysis of a pseudoallelic recessive lethal system at the notch locus of Drosophila melanogaster. *Cold Spring Harbor Symposia on Quantitative Biology*, *23*, 171–176. https://doi.org/10.1101/sqb.1958.023.01.021

Welshons, W. J. (1965). Analysis of a Gene in Drosophila. *Science*, *150*(3700), 1122–1129. https://doi.org/1122

Welshons, W. J., & Von Halle, E. S. (1962). Pseudoallelism at the notch locus in drosophila. *Genetics*, *47*(6), 743–759. https://doi.org/10.1093/genetics/47.6.743

Weng, A. P., Ferrando, A. A., Lee, W., Morris IV, J. P., Silverman, L. B., Sanchez-Irizarry, C., Blacklow, S. C., Look, A. T., & Aster, J. C. (2004). Activating mutations of NOTCH1 in human T cell acute lymphoblastic leukemia. *Science*, *306*(5694), 269–271. https://doi.org/10.1126/SCIENCE.1102160/SUPPL_FILE/WENG_SOM.PDF

Westhoff, B., Colaluca, I. N., D'Ario, G., Donzelli, M., Tosoni, D., Volorio, S., Pelosi, G., Spaggiari, L., Mazzarol, G., Viale, G., Pece, S., & Di Fiore, P. P. (2009). Alterations of the Notch pathway in lung cancer. *Proceedings of the National Academy of Sciences of the United States of America*, *106*(52), 22293. https://doi.org/10.1073/PNAS.0907781106

Wharton, K. A., Johansen, K. M., Xu, T., & Artavanis-Tsakonas, S. (1985). Nucleotide sequence from the neurogenic locus notch implies a gene product that shares homology with proteins containing EGF-like repeats. *Cell*, *43*(3 Pt 2), 567–581. https://doi.org/10.1016/0092-8674(85)90229-6

Whiteman, P., & Handford, P. A. (2003). Defective secretion of recombinant fragments of fibrillin-1: Implications of protein misfolding for the pathogenesis of Marfan syndrome and related disorders. *Human Molecular Genetics*, *12*(7), 727–737. https://doi.org/10.1093/HMG/DDG081

Wilkin, M., Carbery, A.-M., Fostier, M., Aslam, H., Mazaleyrat, S. L., Higgs, J., Myat, A., Evans, D. A. P., Cornell, M., & Baron, M. (2004). Regulation of Notch Endosomal Sorting and Signaling by Drosophila Nedd4 Family Proteins. *Current Biology*, *14*(24), 2237–2244. https://doi.org/10.1016/j.cub.2004.11.030

Wilkin, M., Tongngok, P., Gensch, N., Clemence, S., Motoki, M., Yamada, K., Hori, K., Taniguchi-Kanai, M., Franklin, E., Matsuno, K., & Baron, M. (2008). Drosophila HOPS and AP-3 complex genes are required for a Deltex-regulated activation of notch in the endosomal trafficking pathway. *Developmental Cell*, *15*(5), 762–772. https://doi.org/10.1016/j.devcel.2008.09.002

Wimmer, R. A., Leopoldi, A., Aichinger, M., Wick, N., Hantusch, B., Novatchkova, M., Taubenschmid, J., Hämmerle, M., Esk, C., Bagley, J. A., Lindenhofer, D., Chen, G., Boehm, M., Agu, C. A., Yang, F., Fu, B., Zuber, J., Knoblich, J. A., Kerjaschki, D., & Penninger, J. M. (2019). Human blood vessel organoids as a model of diabetic vasculopathy. *Nature*, *565*(7740), 505–510. https://doi.org/10.1038/s41586-018-0858-8

Xie, X., Cho, B., & Fischer, J. A. (2012). Drosophila Epsin's role in Notch ligand cells requires three Epsin protein functions: The lipid binding function of the ENTH domain, a single Ubiquitin interaction motif, and a subset of the C-terminal protein binding modules. *Developmental Biology*, *363*(2). https://doi.org/10.1016/j.ydbio.2012.01.004

Xu, A., Haines, N., Dlugosz, M., Rana, N. A., Takeuchi, H., Haltiwanger, R. S., & Irvine, K. D. (2007). In vitro reconstitution of the modulation of Drosophila Notch-ligand binding

by Fringe. *The Journal of Biological Chemistry*, *282*(48), 35153–35162. https://doi.org/10.1074/jbc.M707040200

Xu, C., & Ng, D. T. W. (2015). Glycosylation-directed quality control of protein folding. *Nature Reviews Molecular Cell Biology*, *16*(12), 742–752. Scopus. https://doi.org/10.1038/nrm4073

Xu, T., Rebay, I., Fleming, R. J., Scottgale, T. N., & Artavanis-Tsakonas, S. (1990). *The Notch locus and the genetic circuitry involved in early Drosophila neurogenesis*. http://genesdev.cshlp.org/content/4/3/464.full.pdf

Xue, M., Ma, C., Craig, T. K., Rosenmund, C., & Rizo, J. (2008). The Janus-faced nature of the C2B domain is fundamental for synaptotagmin-1 function. *Nature Structural & Molecular Biology*, *15*(11), 1160–1168. https://doi.org/10.1038/nsmb.1508

Yagi, H., Conroy, P. J., Leung, E. W. W., Law, R. H. P., Trapani, J. A., Voskoboinik, I., Whisstock, J. C., & Norton, R. S. (2015). Structural Basis for Ca2+-mediated Interaction of the Perforin C2 Domain with Lipid Membranes. *J Biol Chem*, *290*(42), 25213–25226. https://doi.org/10.1074/jbc.M115.668384

Yamamoto, E., Kalli, A. C., Yasuoka, K., & Sansom, M. S. P. (2016). Interactions of Pleckstrin Homology Domains with Membranes: Adding Back the Bilayer via High-Throughput Molecular Dynamics. *Structure (London, England : 1993)*, *24*(8), 1421–1431. https://doi.org/10.1016/j.str.2016.06.002

Yamamoto, S., Charng, W. L., Rana, N. A., Kakuda, S., Jaiswal, M., Bayat, V., Xiong, B., Zhang, K., Sandoval, H., David, G., Wang, H., Haltiwanger, R. S., & Bellen, H. J. (2012). A mutation in EGF repeat-8 of notch discriminates between serrate/jagged and delta family ligands. *Science*, *338*(6111), 1229–1232. https://doi.org/10.1126/science.1228745

Yan, S., Zhang, J., Zhang, T., Li, Y., & Li, X. (2024). Advances in endothelial cell lipid metabolism and tumor angiogenesis. *Results in Chemistry*, *7*, 101467. https://doi.org/10.1016/j.rechem.2024.101467

Yan, Y., Denef, N., & Schüpbach, T. (2009). The vacuolar proton pump, V-ATPase, is required for notch signaling and endosomal trafficking in Drosophila. *Developmental Cell*, *17*(3), 387–402. https://doi.org/10.1016/J.DEVCEL.2009.07.001

Yang, J., Kemps-Mols, B., Spruyt-Gerritse, M., Anholts, J., Claas, F., & Eikmans, M. (2016). The source of SYBR green master mix determines outcome of nucleic acid amplification reactions. *BMC Research Notes*, *9*, 292. https://doi.org/10.1186/s13104-016-2093-4

Yang, L.-T., Nichols, J. T., Yao, C., Manilay, J. O., Robey, E. A., & Weinmaster, G. (2005). Fringe glycosyltransferases differentially modulate Notch1 proteolysis induced by Delta1 and Jagged1. *Molecular Biology of the Cell*, *16*(2), 927–942. https://doi.org/10.1091/mbc.e04-07-0614

Yao, D., Huang, Y., Huang, X., Wang, W., Yan, Q., Wei, L., Xin, W., Gerson, S., Stanley, P., Lowe, J. B., & Zhou, L. (2011). Protein O-fucosyltransferase 1 (Pofut1) regulates lymphoid and myeloid homeostasis through modulation of Notch receptor ligand interactions. *Blood*, *117*(21), 5652–5662. https://doi.org/10.1182/blood-2010-12-326074

Yartseva, V., Goldstein, L. D., Rodman, J., Kates, L., Chen, M. Z., Chen, Y.-J. J., Foreman, O., Siebel, C. W., Modrusan, Z., Peterson, A. S., & Jovičić, A. (2020). Heterogeneity of Satellite Cells Implicates DELTA1/NOTCH2 Signaling in Self-Renewal. *Cell Reports*, *30*(5), 1491-1503.e6. https://doi.org/10.1016/j.celrep.2019.12.100

Yen, W.-C., Fischer, M. M., Hynes, M., Wu, J., Kim, E., Beviglia, L., Yeung, V. P., Song, X., Kapoun, A. M., Lewicki, J., Gurney, A., Simeone, D. M., & Hoey, T. (2012). Anti-DLL4 has broad spectrum activity in pancreatic cancer dependent on targeting DLL4-notch signaling in both tumor and vasculature cells. *Clinical Cancer Research*, *18*(19), 5374–5386. Scopus. https://doi.org/10.1158/1078-0432.CCR-12-0736

Yochem, J., Weston, K., & Greenwald, I. (1988). The Caenorhabditis elegans lin-12 gene encodes a transmembrane protein with overall similarity to Drosophila Notch. *Nature*, *335*(6190), 547–550. https://doi.org/10.1038/335547a0

Yokoi, Y., & Nishimura, S. I. (2020). Effect of Site-Specific O-Glycosylation on the Structural Behavior of NOTCH1 Receptor Extracellular EGF-like Domains 11 and 10. *Chemistry - A European Journal*, *26*(54). https://doi.org/10.1002/chem.202002652

Yuan, X., Wu, H., Xu, H., Han, N., Chu, Q., Yu, S., Chen, Y., & Wu, K. (2015). Meta-analysis reveals the correlation of Notch signaling with non-small cell lung cancer progression and prognosis. *Scientific Reports*, *5*. https://doi.org/10.1038/SREP10338

Zeronian, M. R., Klykov, O., Portell i de Montserrat, J., Konijnenberg, M. J., Gaur, A., Scheltema, R. A., & Janssen, B. J. C. (2021). Notch–Jagged signaling complex defined by an interaction mosaic. *Proceedings of the National Academy of Sciences*, *118*(30), e2102502118. https://doi.org/10.1073/pnas.2102502118

Zhang, D., & Aravind, L. (2010). Identification of novel families and classification of the C2 domain superfamily elucidate the origin and evolution of membrane targeting activities in eukaryotes. *Gene*, *469*(1–2), 18–30. https://doi.org/10.1016/j.gene.2010.08.006

Zhang, K., Wu, S., Wu, H., Liu, L., & Zhou, J. (2021). Effect of the Notch1-mediated PI3K-Akt-mTOR pathway in human osteosarcoma. *Aging*, *13*(17), 21090–21101. https://doi.org/10.18632/aging.203261

Zhang, K., Zhang, Y.-Q., Ai, W.-B., Hu, Q.-T., Zhang, Q.-J., Wan, L.-Y., Wang, X.-L., Liu, C.-B., & Wu, J.-F. (2015). Hes1, an important gene for activation of hepatic stellate cells, is regulated by Notch1 and TGF-β/BMP signaling. *World Journal of Gastroenterology*, *21*(3), 878–887. https://doi.org/10.3748/wjg.v21.i3.878

Zhang, Y., Baycin-Hizal, D., Kumar, A., Priola, J., Bahri, M., Heffner, K. M., Wang, M., Han, X., Bowen, M. A., & Betenbaugh, M. J. (2017). High-Throughput Lipidomic and Transcriptomic Analysis To Compare SP2/0, CHO, and HEK-293 Mammalian Cell Lines. *Analytical Chemistry*, *89*(3), 1477–1485. https://doi.org/10.1021/acs.analchem.6b02984

Zhang, Y., Lahmann, I., Baum, K., Shimojo, H., Mourikis, P., Wolf, J., Kageyama, R., & Birchmeier, C. (2021). Oscillations of Delta-like1 regulate the balance between differentiation and maintenance of muscle stem cells. *Nature Communications*, *12*(1), 1318. https://doi.org/10.1038/s41467-021-21631-4

Zhang, Y.-Z., Qin, F., Han, Z.-G., Liu, Q., Zhou, L., & Wang, Y.-W. (2015). Prognostic significance of DLL4 expression in papillary thyroid cancer. *European Review for Medical and Pharmacological Sciences*, *19*(15), 2901–2905. Scopus.

Zhao, Y., Yang, R., Bousraou, Z., Richardson, K., & Wang, S. (2022). Probing Notch1-Dll4 signaling in regulating osteogenic differentiation of human mesenchymal stem cells using single cell nanobiosensor. *Scientific Reports*, *12*(1), 10315. https://doi.org/10.1038/s41598-022-14437-x

Zheng, C. G., Chen, R., Xie, J. B., Liu, C. B., Jin, Z., & Jin, C. (2015). Immunohistochemical expression of Notch1, Jagged1, NF-κB and MMP-9 in colorectal cancer patients and the relationship to clinicopathological parameters. *Cancer Biomarkers*, *15*(6), 889–897. https://doi.org/10.3233/CBM-150533

Zhu, C., Ho, Y.-J., Salomao, M. A., Dapito, D. H., Bartolome, A., Schwabe, R. F., Lee, J.-S., Lowe, S. W., & Pajvani, U. B. (2021). Notch activity characterizes a common hepatocellular carcinoma subtype with unique molecular and clinicopathologic features. *Journal of Hepatology*, *74*(3), 613–626. https://doi.org/10.1016/j.jhep.2020.09.032

Zong, Y., Panikkar, A., Xu, J., Antoniou, A., Raynaud, P., Lemaigre, F., & Stanger, B. Z. (2009). Notch signaling controls liver development by regulating biliary differentiation. *Development (Cambridge, England)*, *136*(10), 1727–1739. https://doi.org/10.1242/dev.029140